SUPERCONDUCTIVITY IN MAGNETIC AND PROXIMITY EFFECT SYSTEMS

By

© WALTER HUGO STEPHAN, B.Sc.(Hon.), M.Sc.

A Thesis

Submitted to the Faculty of Graduate Studies

in Partial Fulfillment of the Requirements

for the Degree

Doctor of Philosophy

McMaster University

March, 1987

ISBN 0-315-35899-8

SUPERCONDUCTIVITY IN MAGNETIC AND PROXIMITY EFFECT SYSTEMS

DOCTOR OF PHILOSOPHY (1987)
(Physics)

McMASTER UNIVERSITY
Hamilton.Ontario

TITLE: SUPERCONDUCTIVITY IN MAGNETIC AND PROXIMITY EFFECT SYSTEMS

AUTHOR: WALTER HUGO STEPHAN.
B.Sc.(Honours) (University of Manitoba)
M.Sc. (McMaster University)

SUPERVISOR: PROFESSOR JULES P. CARBOTTE

NUMBER OF PAGES: xii. 228

ABSTRACT

Some aspects of the theory of superconductors containing paramagnetic impurities in the model of Shiba and Rusinov (SR) are examined. The critical magnetic field deviation function is shown to be very sensitive to the SR scattering parameter ϵ_0, with the behavior of D(t) correlated with the zero frequency density of states, and improved agreement is found with experiment for Zn-Mn, as compared to the predictions of the theory of Abrikosov and Gor'Kov (AG).

Optical absorption and thermal conductivity experiments involving a variety of transition metal alloys are reanalyzed including up to three scattering phase shifts, with no significant improvement found over the agreement obtained with only a single phase shift. The electromagnetic coherence length with SR impurities is also considered.

Model calculations for superconducting spin-glasses show that systems such as $Gd_xCe_{1-x}Ru_2$, which exhibit significant deviations from the AG prediction for the reduction of the critical temperature with impurity concentration, are also expected to exhibit significant deviations from AG behavior for the temperature variation of properties such as the thermodynamic critical field and the electromagnetic penetration depth.

The model of Lee for reentrant ferromagnetic superconductors is shown to be only in qualitative agreement with the temperature

dependence of the free energy difference and thermal conductivity determined experimentally for $ErRh_4B_4$. This model is not in agreement with the measured peak in ultrasonic attenuation at higher temperature.

A variety of properties of proximity effect junctions are considered within the McMillan model. The free energy difference is shown to be given by the standard Bardeen-Stephen result applied to both sides of the junction. The temperature dependence of the free energy difference differs significantly from that of a BCS superconductor, with the deviation function becoming much more negative than the BCS prediction. Both the free energy difference and the specific heat jump are suppressed by increasing normal film thickness or the addition of paramagnetic impurities, and this behavior is relatively insensitive to the details of scattering as described by the SR scattering parameter ϵ_0.

The optical absorption of the normal side of a proximity effect junction is found to have a small structure associated with the two peaked structure of the density of states predicted by the McMillan model, with the effect of SR model impurities qualitatively the same as in the intrinsic case. The electromagnetic penetration depth at low temperature is found to be quite sensitive to the addition of paramagnetic impurities, as well as to the SR scattering parameter ϵ_0.

Finally, the temperature dependence of the zero bias tunneling conductance of a proximity effect induced superconducting spin-glass is calculated and shown to be in reasonable agreement with experiments involving Ag-Mn.

ACKNOWLEDGEMENTS

I would like to thank first and foremost my supervisor, Dr. Jules P. Carbotte, whose enthusiasm for new ideas often helped to revive my own interest when it seemed that things were going nowhere. The other members of our group here: Mike Coombes, Frank Marsiglio, Michael Schossmann, Jeff Blezius, Peter Williams, and of course Dr. Ewald Schachinger (whose periodic appearances here never failed to stir up a flurry of activity) also deserve my thanks for all of the interesting discussions we have had over the years, and more importantly for simply being friends. Mike Coombes deserves special mention for all of his help with the cosmetic aspects of the thesis, things like proofreading and figuring out how to convince the word processor to use the appropriate page formats, and of course for slaving over the photocopier.

There were others who made significant contributions to my years here at McMaster, in particular Dr. Mahboob Ashraf, who showed how useful a fresh post-doc. can be to a new graduate student taking graduate courses (and of course taught me how to make his mother's chicken curry). The entire membership of the Liquid State softball team, with special mention for Dr. Michiaki Nishimura, a decent first

baseman, patient ski instructor and good friend, also deserve mention for their contributions to the development of my feeling for classical projectile motion, as well as their appreciation of the necessity for relaxation (spelled beer) after a hard days' slaving over a computer terminal. NSERC should also be mentioned for this agency's contribution to my ability to buy the aforementioned beer.

Speaking of computers, I should mention something of the passing of our Cyber here at Mac, since, as luck (or my own slow writing) would have it, the beast was decommissioned as I was nearing the end of writing this thesis, but was still trying to plot graphs! Spending the afternoon/evening of Dec. 31 frantically transferring files from Cyber to Vax was not a lot of fun. On the bright side, being forced to switch over to the Vax did end up helping in the plotting of figures, as I was able to use our new laser printer, which greatly reduced the turnaround time for the excising of extraneous wiggles.

On a more serious note, I would like to end by dedicating this thesis to the memory of Dr. P. Franchesco Fracassi, a good friend, oenophile, music lover, and physicist, who is dearly missed, and without whom my earlier years here would have been much poorer.

TABLE OF CONTENTS

LIST OF ILLUSTATIONS

CHAPTER I

INTRODUCTION

Historically, the apparent antagonism between superconductivity and magnetism was an experimentally observed fact long before the microscopic theory of Bardeen, Cooper and Schrieffer[1] (BCS) could allow one to claim that superconductivity itself was well understood. The pioneering work of Matthias *et al.*[2], which investigated the effects of magnetic impurities on the transition temperature of superconductors, demonstrated that the transition temperature T_c is strongly depressed by small concentrations of paramagnetic impurities. Concentrations of the order of only a few atomic percent are required to suppress superconductivity entirely. A successful model for the depression of T_c by exchange scattering of conduction electrons from paramagnetic impurities was proposed by Abrikosov and Gor'Kov[3] (AG) only briefly after the development of BCS theory. Although throughout the body of this thesis a certain amount of background knowledge will be assumed, a brief introduction to the necessary physical concepts may be appropriate here.

It is now understood, on the basis of the microscopic theory of BCS, that superconductivity will be suppressed with the application of any perturbation which breaks the time reversal invariance of the conduction electrons. This is a consequence of the symmetry of the superconducting state. According to BCS theory, the ground state of a

superconductor cannot be described in terms of quasi-free electrons filling available energy levels up to the Fermi level, as is commonly done for normal metals. The interaction between electrons near the Fermi energy, which is a combination of the screened Coulomb repulsion and the attractive electron-phonon interaction, is most strongly attractive for electrons of opposite momentum and spin (Cooper pairs), and results in the formation of a new many-body ground state. This many-body state may be thought of as being built of a coherent superposition of these Cooper pairs. The presence of a magnetic impurity which may scatter conduction electrons with a change in spin as well as momentum makes it less energetically favorable for the formation of Cooper pairs, and pairs acquire a finite lifetime, resulting in a reduction of the superconducting critical temperature.

The above ideas were first formulated mathematically within the framework of BCS theory by Abrikosov and Gor'kov (AG)[3]. The AG theory assumes that one may describe the interaction between conduction electrons and an isolated localized magnetic moment due to an impurity using the well known *s-d* exchange interaction (or *s-f* in the case of a rare earth impurity)[4]. It is assumed that the interaction is weak enough that it may be treated in the Born approximation, and that the impurities are dilute enough so that an electron interacts with one impurity at a time, and that the impurities do not interact significantly with one another. Using these assumptions, AG were able to produce a theory which at least qualitatively explains many experimentally observed results. The AG theory predicts an initially linear depression of the critical temperature with impurity

concentration, in agreement with experiment for many alloy systems[5]. A variety of thermodynamic, transport, and electromagnetic properties have also been calculated within AG theory and found to be in reasonable agreement with experiment for some alloys.

There are, however, some systems which were found to differ significantly from the predictions of AG theory. For example, in the first infrared absorption experiment designed to test the predicted change in the superconducting density of states, Dick and Reif[6] found that lead-gadolinium (Pb-Gd) alloys were consistent with AG theory, while lead-manganese (Pb-Mn) alloys were not. Similar differences had previously been found by Woolf and Reif[7] in tunneling experiments.

Of the various approximations made in the derivation of AG theory, it was recognized quite early that a likely candidate to explain this difference between rare-earth (Gd) and transition metal (Mn) impurities is the restriction to weak scattering implied by the use of the Born approximation for the scattering. Because the magnetic moment of Gd is due to the partially filled $4f$ shell, which is spatially more localised than the $3d$ shell of Mn, one would expect that the screened exchange interaction with a conduction electron would be significantly stronger in the case of Mn. This means that while the Born approximation may be good for Gd, it may not be appropriate for Mn.

The extension of AG theory to include strong scattering was carried out independently by Shiba[8] and Rusinov[9] (SR) in 1969. Many physical properties have since been calculated within this theory, with significantly improved agreement with experiment than is found

with AG theory. The most notable difference between SR and AG theory is the prediction of possible impurity bands within the energy gap in SR theory. This difference in the density of states then shows up in other physical properties.

Chapter II of this thesis is concerned with some aspects of SR theory, in particular the consequences of inclusion of more than one channel for the scattering amplitude.

One other approximation made in the derivation of both AG and SR theory is the restriction to noninteracting spins. While this is a valid approximation in the extreme dilute limit, many experiments have seen indications of significant deviations from SR and AG theory at concentrations still well below the critical value which sends the critical temperature to zero. Evidence exists[10] for significant inter-impurity interaction even in the concentration range of approximately 0.1-at.% in similar non-superconducting systems such as Cu-Mn, which display spin-glass behaviour. Chapter III, the second major part of this thesis, is concerned with this phenomenon as well as with even more concentrated systems such as $ErRh_4B_4$ which order ferromagnetically.

Finally, the range of magnetic systems which may be studied through their influence on superconductivity may be greatly expanded through the use of the superconducting proximity effect to induce superconductivity in otherwise nonsuperconducting metals. These proximity effect junctions typically consist of a thin film of a normal metal, which may or may not be magnetic, deposited on another film of a relatively high critical temperature superconductor such as lead. The

existence of superconductivity throughout the entire sample if the films are sufficiently thin may then be described in a very rough way as the leakage of Cooper pairs from the superconductor into the normal metal. This phenomenon is reasonably well described by a theory due to McMillan[11]. Extended versions of McMillan's model will be used in Chapter IV to calculate some properties of proximity effect bilayers in the thin film limit, both with and without the inclusion of magnetic effects in the normal metal side of the junction.

CHAPTER II

SOME ASPECTS OF THE THEORY OF SHIBA AND RUSINOV

2.1 Basic Notation and Formalism

All of the results presented in this work are in the weak-coupling or BCS limit for the pairing interaction which produces superconductivity. The basic Hamiltonian in this limit may be written in the form

$$H_0 = \sum_{\underline{k}\sigma} \epsilon_{\underline{k}} c^{\dagger}_{\underline{k}\sigma} c_{\underline{k}\sigma} - \frac{1}{2} \sum_{\underline{k}\underline{q}\sigma} V_{\underline{k}\underline{q}} c^{\dagger}_{\underline{k}\sigma} c^{\dagger}_{-\underline{k}-\sigma} c_{-\underline{q}-\sigma} c_{\underline{k}\sigma} . \qquad (2.1)$$

Here $c_{\underline{k}\sigma}$ ($c^{\dagger}_{\underline{k}\sigma}$) annihilates (creates) an electron of quasi-momentum $\underline{k}$ and spin σ, where underlined characters such as $\underline{k}$ will be understood to be vectors. The pairing interaction $V_{\underline{k}\underline{q}}$ is chosen to be positive; hence the minus sign in front of the two body term.

The basic interaction between conduction electrons and impurities at positions $\underline{R}_n$ may be described in a standard way by the interaction Hamiltonian

$$H_I = \sum_{n\alpha\beta} \int d^3r \; c^{\dagger}_{\alpha}(\underline{r}) \; U_{\alpha\beta}(\underline{r}-\underline{R}_n) \; c_{\beta}(\underline{r}) . \qquad (2.2)$$

The operator $c_\alpha(\underline{r})$ is the annihilation operator for an electron at position $\underline{r}$ with spin α, and is related to the momentum space operator $c_{\underline{k}\alpha}$ by the standard Fourier relation

$$c_\alpha(\underline{r}) = \sum_{\underline{k}} e^{i\underline{k}\cdot\underline{r}} \varphi_{\underline{k}\alpha} \quad . \tag{2.3}$$

Here the volume of the system has been set to unity.

The impurity-conduction electron scattering potential $U_{\alpha\beta}(\underline{r}-\underline{R}_n)$ has the form

$$U_{\alpha\beta}(\underline{r}) = U_1(\underline{r}) + \underline{\sigma}_{\alpha\beta} \cdot \underline{S}\, J(\underline{r}) \quad , \tag{2.4}$$

where U_1 is the spin independent part of the potential, $J(\underline{r})$ is the exchange term, and the matrices $\underline{\sigma}$ are the standard 2x2 Pauli spin matrices.

It is conventional to rewrite the Hamiltonian in a 4-component spinor Nambu[12] notation, as used by Ambegaokar and Griffin[13]. This allows the interaction Hamiltonian in the case of spin dependent forces to be written in the form of a one-body operator. This then allows ordinary diagram techniques to be used for the corresponding 4x4 matrix Green's functions. The spinor field operator is defined as

$$\varphi_{\underline{k}} = \begin{bmatrix} c_{\underline{k}\uparrow} \\ c_{\underline{k}\downarrow} \\ c^{\dagger}_{-\underline{k}\uparrow} \\ c^{\dagger}_{-\underline{k}\downarrow} \end{bmatrix} \quad . \tag{2.5a}$$

together with the Hermitian conjugate

$$\Psi_{\underline{k}}^{\dagger} = (c_{\underline{k}\uparrow}^{\dagger} \cdot c_{\underline{k}\downarrow}^{\dagger} \cdot c_{-\underline{k}\uparrow} \cdot c_{-\underline{k}\downarrow}). \qquad (2.5b)$$

The Hamiltonian, equation (2.1), may then be written in the form

$$H_0 = \frac{1}{2} \sum_{\underline{k}} \epsilon_{\underline{k}} \Psi_{\underline{k}}^{\dagger} \rho_3 \Psi_{\underline{k}} - \frac{1}{8} \sum_{\underline{kq}} V_{\underline{kq}} (\Psi_{\underline{k}}^{\dagger} \rho_3 \Psi_{\underline{q}}) (\Psi_{-\underline{k}}^{\dagger} \rho_3 \Psi_{-\underline{q}}^{\dagger}) . \qquad (2.6)$$

All quantities such as $\rho_3\sigma_0$ are the direct product of two Pauli matrices, with the ρ matrices acting in particle-hole space, and the σ matrices acting in spin space. For example, one has

$$\rho_3\sigma_0 = \begin{bmatrix} \sigma_0 & 0 \\ 0 & -\sigma_0 \end{bmatrix} = \begin{bmatrix} 1 & 0 & 0 & 0 \\ 0 & 1 & 0 & 0 \\ 0 & 0 & -1 & 0 \\ 0 & 0 & 0 & -1 \end{bmatrix}. \qquad (2.7)$$

Note that ρ_3 in (2.6) actually means $\rho_3\sigma_0$, the direct product of two Pauli matrices, with σ_0 the 2×2 identity matrix. When the meaning is clear from context, the identity matrices ρ_0 and σ_0 will often not be written out explicitly.

The factor of $\frac{1}{2}$ associated with each factor of $(\Psi^{\dagger}\rho_3\Psi)$ in (2.6) arises from the redundancy of the 4-component notation. These factors may be removed if one notes that in the application of Wick's Theorem[14] to these operators, terms of the form $\Psi\Psi$ or $\Psi^{\dagger}\Psi^{\dagger}$ contain normal ordered pairs of operators $cc^{\dagger}$. In fact these terms contribute

exactly the same amount as does $\Psi\Psi^\dagger$. This means that if a generalized Wick's Theorem is used, where contractions like $\langle\Psi\Psi\rangle$ or $\langle\Psi^\dagger\Psi^\dagger\rangle$ are set to zero, keeping only $\langle\Psi\Psi^\dagger\rangle$, then the factors of $\frac{1}{2}$ in the Hamiltonian may be removed, and the perturbation theory for the matrix Green's function in terms of the spinor field operators Ψ will be identical with that for the conventional Green's function in terms of the c-operators (see Vonsovsky *et al.*[14] pp.70-75 for more on this point). The same conclusion may also be reached without introducing Wick's theorem by following Gor'kov[15], for example, and deriving the equations of motion for the matrix Green's function directly from the equations of motion for the conventional and anomalous Green's functions, which correspond to the diagonal and off diagonal components of the matrix Green's function.

The net result is that if one uses the Hamiltonian

$$H_0 = \sum_{\underline{k}} \epsilon_{\underline{k}} \Psi^\dagger_{\underline{k}} \rho_3 \Psi_{\underline{k}} - \frac{1}{2} \sum_{\underline{kq}} V_{\underline{kq}} (\Psi^\dagger_{\underline{k}} \rho_3 \Psi_{\underline{q}})(\Psi^\dagger_{-\underline{k}} \rho_3 \Psi^\dagger_{-\underline{q}}) \qquad (2.8)$$

then conventional diagram techniques apply to a matrix temperature Green's function defined by

$$\mathcal{G}_{\alpha\beta}(\underline{k},\tau) = -\langle T_\tau \Psi_\alpha(\underline{k},\tau) \Psi^\dagger_\beta(\underline{k},0)\rangle \ . \qquad (2.9)$$

Here $\tau = it$ is the imaginary time variable, and T_τ is the time ordering operator, which orders τ-dependent operators in order of decreasing τ. The brackets $\langle \ldots \rangle$ denote the statistical average over a Grand

canonical ensemble. Note also that script characters such as $\mathcal{G}$ will be used for 4x4 matrices.

Considering first the case of the normal state, that is if the pairing interaction is turned off momentarily, then it can immediately be seen that the Green's function $\mathcal{G}$ will be diagonal. In fact, directly from the definition one has

$$\mathcal{G}^{00}(\underline{k},\tau) = \begin{bmatrix} G^0(\underline{k},\tau) & 0 & 0 & 0 \\ 0 & G^0(\underline{k},\tau) & 0 & 0 \\ 0 & 0 & -G^0(-\underline{k},-\tau) & 0 \\ 0 & 0 & 0 & -G^0(-\underline{k},-\tau) \end{bmatrix} . \qquad (2.10)$$

where $G^0(k,\tau) = \langle T_\tau c_{\underline{k}}(\tau) c^\dagger_{\underline{k}}(0) \rangle$. The two superscript 0's on $\mathcal{G}^{00}$ in (2.10) indicate the non-interacting and non-superconducting state; the notation $\mathcal{G}^0$ will later be used for the Green's function of the pure superconductor. The Fourier coefficient of the function G^0 has the form

$$G^0(\underline{k}, i\omega_n) = (i\omega_n - \epsilon_{\underline{k}})^{-1} . \qquad (2.11)$$

and if a spherical Fermi surface is assumed, so that $\epsilon_{\underline{k}} = \epsilon_{-\underline{k}}$, this means that equation (2.10) may be rewritten as

$$\mathcal{G}^{00}(\underline{k}, i\omega_n) = (i\omega_n \rho_0\sigma_0 - \epsilon_{\underline{k}}\rho_3\sigma_0)^{-1} = \frac{i\omega_n + \epsilon_{\underline{k}}\rho_3}{(i\omega_n)^2 - \epsilon^2_{\underline{k}}} \qquad (2.12)$$

The Matsubara frequencies are defined by

$$i\omega_n = i(2n-1)\pi T \ , \qquad (2.13)$$

where T is absolute temperature, and Boltzmann's constant has been set to one.

Next consider the case of a pure superconductor, described by the Hamiltonian (2.8). Self-consistent perturbation theory is used to construct the BCS superconductor from the normal state. Dyson's equation is used with the self-energy shown in Fig. 2.1(a). The theory is made self-consistent by replacing the bare propagator $\mathcal{G}^{00}$ in the self-energy with the full propagator $\mathcal{G}^{0}$. In practice an ansatz is made for $\mathcal{G}^{0}$, and the coefficients are determined self-consistently.

The ansatz for $\mathcal{G}^{0}$ is

$$\mathcal{G}^{0}(\underline{k},i\omega_n) = [Zi\omega_n - \tilde{\epsilon}_{\underline{k}}\rho_3 - \Delta\rho_2\sigma_2]^{-1}. \qquad (2.14)$$

Eq.(2.14) must be inserted in the Dyson equation

$$\mathcal{G}^{0}(\underline{k},i\omega_n)^{-1} = \mathcal{G}^{00}(\underline{k},i\omega_n)^{-1} - \Sigma(\underline{k},i\omega_n) \ . \qquad (2.15)$$

where Fig. 2.1(a) gives

$$\Sigma(\underline{k},i\omega_n) = T \sum_{m=-\infty}^{\infty} \int \frac{d^3q}{(2\pi)^3} \rho_3 \, \mathcal{G}^{0}(\underline{k}-\underline{q},i\omega_m) \, V_{\underline{k}\underline{k}-\underline{q}} \, \rho_3 \ . \qquad (2.16)$$

The two factors of ρ_3 on either side of the Green's function in (2.16)

arise from the two interaction vertices. Upon substituting (2.14) into (2.16) one obtains

$$\Sigma(\underline{k},i\omega_n) = (1-Z)i\omega_n + (\tilde{\epsilon}_{\underline{k}}-\epsilon_{\underline{k}})\rho_3 + \Delta\rho_2\sigma_2$$

$$+ T\sum_{m=-\infty}^{\infty}\int\frac{d^3q}{(2\pi)^3}\, V_{\underline{k}\underline{k}-\underline{q}}\left[\frac{Zi\omega_m + \tilde{\epsilon}_{\underline{k}-\underline{q}}\rho_3 - \Delta\rho_2\sigma_2}{Z^2(i\omega_m)^2 - (\tilde{\epsilon}^2_{\underline{k}-\underline{q}} + \Delta^2)}\right]. \quad (2.17)$$

Note that Z=1 is consistent with (2.17), since the sum over m for the term proportional to $\rho_0\sigma_0$ vanishes by symmetry. The term proportional to $\rho_3\sigma_0$ also vanishes to a very good approximation if the electronic density of states may be taken to be constant in the vicinity of the Fermi energy. The remaining totally off diagonal term proportional to $\rho_2\sigma_2$ is also proportional to the superconducting gap function Δ and may be written in the form

$$\Delta = -T\sum_{m=-\infty}^{\infty}\int\frac{d^3q}{(2\pi)^3}\, V_{\underline{k}\underline{k}-\underline{q}}\left[\frac{\Delta}{(i\omega_m)^2 - (\epsilon^2_{\underline{k}-\underline{q}} + \Delta^2)}\right]. \quad (2.18)$$

The identity[16]

$$-T\sum_{m=-\infty}^{\infty}\frac{1}{(i\omega_m)^2 - E^2} = \frac{1}{2E}\tanh[E/(2T)] \quad (2.19)$$

may be used in order to write (2.18) in the form

$$1 = \int \frac{d^3q}{(2\pi)^3} V_{\underline{k}\,\underline{k}-\underline{q}} \left[\frac{1}{2E_{\underline{k}-\underline{q}}} \right] \tanh\left[\frac{E_{\underline{k}-\underline{q}}}{2T}\right] . \qquad (2.20)$$

where

$$E_{\underline{k}-\underline{q}} = \left[\epsilon^2_{\underline{k}-\underline{q}} + \Delta^2\right]^{1/2} \qquad (2.21)$$

is the new quasiparticle energy. Changing from an integral over $\underline{q}$ to an integral over energy $\epsilon_{\underline{q}}$ and introducing the BCS model of a constant pairing interaction within an energy range of $\pm\omega_D$ (ω_D being roughly the Debye frequency) about the Fermi energy, equation (2.20) becomes the standard BCS gap equation,

$$1 = N_0 V \int_0^{\omega_D} \frac{d\epsilon}{E} \tanh\left[\frac{E}{2T}\right] . \qquad (2.22)$$

In (2.22) N_0 is the single spin density of electronic states at the Fermi energy in the normal state, and $E = \left[\epsilon^2 + \Delta^2\right]^{1/2}$, as initially defined in (2.21).

Referring back to the ansatz made for $\mathcal{G}^0$ in (2.14), the superconducting Green's function may now be written as

$$\mathcal{G}^0(\underline{k}, i\omega_n) = \left[i\omega_n - \epsilon_k \rho_3 - \Delta\rho_2\sigma_2\right]^{-1} =$$

$$= -\frac{i\omega_n + \epsilon_k\rho_3 + \Delta\rho_2\sigma_2}{(\omega_n^2 + \epsilon^2_{\underline{k}} + \Delta^2)^{1/2}} . \qquad (2.23)$$

2.2 The Impurity Self-Energy and SR Theory

In this section, the effect of a single paramagnetic impurity on an otherwise pure superconductor will be considered. Following Rusinov[9], the scattering of conduction electrons by the impurity will not be considered to be weak, so that the Born approximation will not be used to describe the scattering. This will be essential in order to allow the possibility of the formation of bound states at the impurity site. To begin with, the interaction Hamiltonian (2.2) should be written in the 4x4 Nambu notation.

Note that to within an additive constant factor

$$\sum_{\alpha\beta} c_\alpha^\dagger \underline{\sigma}_{\alpha\beta} c_\beta = \frac{1}{2} \Psi^\dagger \underline{\alpha} \Psi , \tag{2.24a}$$

with the vector matrix $\underline{\alpha}$ defined as

$$\underline{\alpha} = (\rho_3\sigma_1 , \rho_0\sigma_2 , \rho_3\sigma_3). \tag{2.24b}$$

The factor of $\frac{1}{2}$ in (2.24a), due to the redundancy of the matrix notation, can be removed for exactly the same reason as in going from (2.6) to (2.8). The result is that the impurity Hamiltonian may be written in the form

$$H_I = \sum_n \int d^3r \, \Psi^\dagger(\underline{r}) [\rho_3 U_1(\underline{r}-\underline{R}_n) + \underline{\alpha} \cdot \underline{S} J(\underline{r}-\underline{R}_n)] \Psi(\underline{r}), \tag{2.25}$$

where for a single impurity there is only one term in the summation over n.

In the case of a single impurity the Green's function is no longer translationally invariant, and the momentum space Green's function therefore is a function of two momenta. This Green's function is given by

$$\mathcal{G}(\underline{k},\underline{q}) = \mathcal{G}^0(\underline{k})\delta_{\underline{k},\underline{q}} + \mathcal{G}^0(\underline{k})\mathcal{T}^0_{\underline{k}\underline{q}}\mathcal{G}^0(\underline{q}) \ . \tag{2.26}$$

where the T-matrix is given by

$$\mathcal{T}^0_{\underline{k}\underline{q}} = \mathcal{V}_{\underline{k}\underline{q}} + \int \frac{d^3p}{(2\pi)^3} \mathcal{V}_{\underline{k}\underline{p}} \mathcal{G}^0(\underline{p}) \mathcal{T}^0_{\underline{p}\underline{q}} \ . \tag{2.27}$$

In (2.26) and (2.27) the frequency argument $i\omega_n$ of $\mathcal{G}^0$ and $\mathcal{T}^0$ has been suppressed, the superscript on $\mathcal{T}^0$ signifies the single impurity case, and $\mathcal{G}^0$ is the Green's function for the pure superconductor, given in (2.23). It can easily be verified by iteration in powers of the interaction $\mathcal{V}$, that (2.26,27) corresponds to the summation of the diagrams in Fig. 2.1(b).

Now the solution of (2.27) for the T-matrix is facilitated by the introduction of yet another scattering amplitude f, which involves the principal value Green's function[17]. This allows the T-matrix to be determined solely from the properties of the principal value scattering amplitude f on the Fermi surface, whereas (2.27) in terms of $\mathcal{T}$ involves scattering events off the Fermi surface as well.

The principal value scattering amplitude is defined by[18]

$$\ell_{\underline{k}\underline{q}} = \frac{m}{2\pi} \gamma_{\underline{k}\underline{q}} + P\int \frac{d^3p}{(2\pi)^3} \gamma_{\underline{k}\underline{p}} \frac{1}{-\epsilon_{\underline{p}}} \ell_{\underline{p}\underline{q}} . \qquad (2.28)$$

where P means principal value of the integral. The T-matrix is related to ℓ by

$$\tau^0_{\underline{k}\underline{q}}(i\omega_n) = \frac{2\pi}{m} \ell_{\underline{k}\underline{q}} + p_F \int \frac{d\Omega_{\underline{p}}}{4\pi} \ell_{\underline{k}\underline{p}} \bar{\varsigma}^0_{\underline{p}}(i\omega_n) \tau^0_{\underline{p}\underline{q}}(i\omega_n) . \qquad (2.29)$$

where the integral is over the angles of $\underline{p}$ on the Fermi surface, p_F is the Fermi momentum, and the function $\bar{\varsigma}^0$ is defined by

$$\bar{\varsigma}^0(i\omega_n) = \frac{1}{\pi}\int_{-\infty}^{\infty} d\epsilon_{\underline{p}} \, \varsigma^0_{\underline{p}}(i\omega_n) = -\frac{1}{(\omega_n^2 + \Delta^2)^{1/2}} (i\omega_n + \Delta\rho_2\sigma_2). \qquad (2.30)$$

Equation (2.29) may be solved for τ^0 by using (2.30) and expanding ℓ and τ^0 in series of Legendre polynomials. That is, use

$$\gamma_{\underline{k}\underline{q}} = \sum_{\ell=0}^{\infty} (2\ell+1) \, \gamma_\ell \, P_\ell(\hat{k}.\hat{q}) \qquad (2.31a)$$

and

$$\ell_{\underline{k}\underline{q}} = \sum_{\ell=0}^{\infty} (2\ell+1) \, \ell_\ell \, P_\ell(\hat{k}.\hat{q}) . \qquad (2.31b)$$

where the Legendre polynomials P_ℓ depend on the cosine of the angle

between the unit vectors $\hat{k}$ and $\hat{q}$. The P_ℓ satisfy the orthogonality relation[19]

$$\int \frac{d\Omega_p}{4\pi} P_\ell(\hat{k},\hat{p})\, P_m(\hat{p},\hat{q}) = (2\ell+1)^{-1}\, \delta_{\ell m}\, P_\ell(\hat{k},\hat{q}) \,. \qquad (2.32)$$

Using (2.32) the partial wave components of (2.29) are easily found to be

$$\mathcal{T}_\ell^0 = \frac{2\pi}{m}\, \ell_\ell + p_F \ell_\ell \bar{\mathcal{G}}^0 \mathcal{T}_\ell^0 \,. \qquad (2.33)$$

or

$$\mathcal{T}_\ell^0 = \frac{2\pi}{m}\, \mathcal{S}^{-1}\, \ell_\ell \,. \qquad (2.34)$$

In (2.34), $\mathcal{S}^{-1}$ is the matrix inverse of the matrix

$$\mathcal{S} = 1 - p_F \ell_\ell \bar{\mathcal{G}}^0 \,. \qquad (2.35)$$

Choosing the z-axis to be defined by the direction of the impurity spin, from (2.28) the matrix ℓ_ℓ must have the form

$$\ell_\ell = \begin{pmatrix} f_\ell^- & 0 & 0 & 0 \\ 0 & f_\ell^- & 0 & 0 \\ 0 & 0 & -f_\ell^+ & 0 \\ 0 & 0 & 0 & -f_\ell^- \end{pmatrix} . \qquad (2.36)$$

Using (2.30) for $\bar{\mathcal{G}}^0$ and (2.36) for ℓ_ℓ one finds

$$\mathcal{G} = \rho_0\sigma_0 + \frac{p_F}{2(\omega_n^2+\Delta^2)^{1/2}} \left[i\omega_n \{(f_\ell^+ + f_\ell^-)\rho_3\sigma_0 + (f_\ell^+ - f_\ell^-)\rho_3\sigma_3\} \right.$$
$$\left. - \Delta \{(f_\ell^+ + f_\ell^-)i\rho_1\sigma_2 + (f_\ell^+ - f_\ell^-)\rho_1\sigma_1\} \right] . \qquad (2.37)$$

Defining

$$A^\pm = 1 + i\omega_n p_F f_\ell^\pm/(\omega_n^2 + \Delta^2)^{1/2} , \qquad (2.38a)$$

$$B^\pm = \Delta p_F f_\ell^\pm/(\omega_n^2 + \Delta^2)^{1/2} , \qquad (2.38b)$$

and

$$D^\pm = A^\pm(A^\mp)^* + B^+B^- . \qquad (2.38c)$$

the inverse $\mathcal{G}^{-1}$ may be written in the form

$$\mathcal{G}^{-1} = \begin{pmatrix} A^{-*}/D^+ & 0 & 0 & B^+/D^+ \\ 0 & A^{+*}/D^- & -B^-/D^- & 0 \\ 0 & B^+/D^- & A^-/D^- & 0 \\ -B^-/D^+ & 0 & 0 & A^+/D^+ \end{pmatrix} . \qquad (2.39)$$

Substituting (2.39) and (2.36) into (2.34) then gives

$$\mathcal{G}_\ell^0 = \begin{pmatrix} T_1^+ & 0 & 0 & -T_2 \\ 0 & T_1^- & T_2^* & 0 \\ 0 & T_2^* & -T_1^{+*} & 0 \\ -T_2 & 0 & 0 & -T_1^{-*} \end{pmatrix} , \qquad (2.40)$$

with

$$T_1^\pm = \frac{2\pi}{m} A^\mp f^\pm/D^\pm , \qquad (2.41a)$$

and

$$T_2 = \frac{2\pi}{m} B^- f^+/D^+ . \qquad (2.41b)$$

Introducing the definitions

$$R_\ell = [(1+p_F^2 f_\ell^+ f_\ell^-)^2 + p_F^2 (f_\ell^+ - f_\ell^-)^2]^{1/2} , \tag{2.42a}$$

and

$$\epsilon_\ell = 1 + p_F^2 f_\ell^+ f_\ell^- . \tag{2.42b}$$

equation (2.41) may be written in the form

$$T_1^\pm = \frac{2\pi}{m} \frac{f_\ell^\pm}{R_\ell} [(\omega_n^2+\Delta^2)^{1/2} - i\omega_n p_F f_\ell^\pm] / [\epsilon_\ell (\omega_n^2+\Delta^2)^{1/2} \pm i\omega_n (1-\epsilon_\ell^2)^{1/2}] , \tag{2.43a}$$

and

$$T_2 = \frac{2\pi}{m} \frac{p_F f_\ell^+ f_\ell^- \Delta}{R_\ell} / [\epsilon_\ell (\omega_n^2+\Delta^2)^{1/2} + i\omega_n (1-\epsilon_\ell^2)^{1/2}] . \tag{2.43b}$$

Upon analytic continuation to the real frequency axis, the T-matrix (2.42) is found to have poles at frequencies $\omega + i\eta = \pm\epsilon_\ell \Delta$, giving bound states at these energies localized at the impurity site.

2.3 Finite Impurity Concentrations

In order to treat the case of a small concentration of randomly distributed impurities the ensemble averaging method first used in the paramagnetic impurity problem by Abrikosov and Gor'kov[3] (AG) is conventionally applied. In this approximation an average is performed over all possible impurity positions for all impurities, and then only

those terms which correspond to independent scattering events from one impurity at a time are retained. Due to the positional averaging the electron Green's function recovers translational invariance, and the momentum space propagator has only a single momentum label (see Doniach and Sondheimer[20] pp 98-109 for an introduction for the application of this technique in the case of normal impurities in a normal metal). One should note that the impurity spin is being treated as a classical vector; even in the previous section (2.2) the non-commutivity of spin operators restricts the T-matrix calculated to a classical approximation. However, an approximate solution of the single impurity problem including the Kondo effect was carried out by Muller-Hartmann and Zittartz[21] (MHZ) using a decoupling scheme due to Nagaoko[22]. The MHZ result shows that the SR classical approximation contains much of the important physics; to a good approximation the MHZ result reduces to that of SR, with the parameter ϵ_ℓ acquiring temperature dependence.

In Rusinov's approximation the Dyson equation for the Green's function is

$$\mathcal{G}_{\underline{k}}(i\omega_n) = \mathcal{G}^0_{\underline{k}}(i\omega_n) + n\mathcal{G}^0_{\underline{k}}(i\omega_n)\mathcal{T}_{\underline{k}\underline{k}}(i\omega_n)\mathcal{G}_{\underline{k}}(i\omega_n) \quad , \tag{2.44}$$

where n is the concentration of impurities. The T-matrix in (2.44) satisfies the equation

$$\mathcal{T}_{\underline{k}\underline{q}}(i\omega_n) = \mathcal{V}_{\underline{k}\underline{q}} + \int \frac{d^3p}{(2\pi)^3} \mathcal{V}_{\underline{k}\underline{p}} \mathcal{G}_{\underline{p}}(i\omega_n) \mathcal{T}_{\underline{p}\underline{q}}(i\omega_n) \quad . \tag{2.45}$$

Note that in (2.44) $\mathcal{T}$ is assumed to be averaged over spin orientations, so that the spin up and down components of $\mathcal{G}$ are equivalent. However, in (2.45) the T-matrix $\mathcal{T}$ is found for a particular spin direction, that is along the positive z-axis. Once $\mathcal{T}$ has been calculated then it should be averaged over spin directions before being substituted into (2.44). Note that the similarity of the equation for $\mathcal{T}$ (2.45) to that for $\mathcal{T}^0$ (2.27) implies that if $\bar{\mathcal{G}}$ has the same structure as $\bar{\mathcal{G}}^0$, then $\mathcal{T}$ will have the same structure as $\mathcal{T}^0$. The strategy therefore is to make the ansatz

$$\mathcal{G}(\underline{k}, i\omega_n) = \left[i\tilde{\omega}_n - \tilde{\epsilon}_k\rho_3 - \tilde{\Delta}\rho_2\sigma_2\right]^{-1}$$

$$= -\frac{i\tilde{\omega}_n + \tilde{\epsilon}_k\rho_3 + \tilde{\Delta}\rho_2\sigma_2}{(\tilde{\omega}_n^2 + \tilde{\epsilon}_{\underline{k}}^2 + \tilde{\Delta}^2)^{1/2}} \qquad (2.46)$$

for $\mathcal{G}$, together with a choice for $\mathcal{T}$ motivated by the structure of $\mathcal{T}^0$ given in (2.40) for the single impurity case.

$$\mathcal{T} = \begin{pmatrix} T_1 & 0 & 0 & -T_2 \\ 0 & T_1 & T_2 & 0 \\ 0 & T_2 & -T_1^* & 0 \\ -T_2 & 0 & 0 & -T_1^* \end{pmatrix} \qquad (2.47)$$

The form of (2.47) follows from (2.40) upon averaging over spin up and spin down directions for the impurity spin.

The Dyson equation for $\mathcal{G}$ (2.44) may be written in the form

$$\mathcal{G}_{\underline{k}}(i\omega_n)^{-1} = \mathcal{G}^0_{\underline{k}}(i\omega_n)^{-1} - \Sigma_{\underline{k}}(i\omega_n) \quad . \tag{2.48}$$

where the matrix Σ is given by

$$\Sigma_{\underline{k}}(i\omega_n) = n\, \mathcal{T}_{\underline{k}\underline{k}}(i\omega_n) \quad . \tag{2.49}$$

Substituting (2.49) into (2.48) and using (2.47), (2.46) and (2.23) the gap equations become

$$\tilde{\Delta} = \Delta + nT_2 \quad , \tag{2.50a}$$

$$\tilde{\omega}_n = \omega_n - n\mathrm{Im}(T_1) \quad , \tag{2.50b}$$

$$\tilde{\epsilon}_{\underline{k}} = \epsilon_{\underline{k}} + n\mathrm{Re}(T_1) \quad . \tag{2.50c}$$

Returning for the moment to (2.45) and (2.29), note that the only difference between the equation for $\mathcal{T}$ and that for $\mathcal{T}^0$ is the replacement of $\mathcal{G}$ by $\mathcal{G}^0$. This means that before averaging over impurity directions the only difference between $\mathcal{T}^0$ and $\mathcal{T}$ is the replacement of ω_n by $\tilde{\omega}_n$, and of Δ by $\tilde{\Delta}$. Therefore, the functions T_1 and T_2 in (2.50) may be found by substituting the renormalized frequencies and gap function into (2.43) and performing the average over spin directions. That is, use

$$T_1 = \frac{1}{2}\,(T_1^+ + T_1^-) \quad . \tag{2.51a}$$

and

$$T_2 = \frac{1}{2}(T_2 + T_2^*) \quad . \tag{2.51b}$$

Recalling the definitions (2.42) and noting that the partial wave components of the principal value scattering amplitude satisfy[17]

$$p_F f_\ell^\pm = \tan\delta_\ell^\pm \quad , \tag{2.52}$$

where $\delta_\ell^\pm$ is the phase shift for scattering of an electron of orbital angular momentum ℓ and spin projection $\pm\frac{1}{2}$, one finds

$$\mathrm{Im}(T_1) = -\frac{\pi}{mp_F}\frac{\tilde{\omega}_n(\tilde{\omega}_n^2+\tilde{\Delta}^2)^{1/2}}{\tilde{\omega}_n^2+\epsilon_\ell^2\tilde{\Delta}^2}(\sin^2\delta_\ell^+ + \sin^2\delta_\ell^-) \quad , \tag{2.53a}$$

$$T_2 = \frac{2\pi}{mp_F}\frac{\epsilon_\ell\tilde{\Delta}(\tilde{\omega}_n^2+\tilde{\Delta}^2)^{1/2}}{\tilde{\omega}_n^2+\epsilon_\ell^2\tilde{\Delta}^2}\sin\delta_\ell^+\sin\delta_\ell^- \quad . \tag{2.53b}$$

Using the fact that the Legendre polynomials satisfy the identity

$$P_\ell(\underline{k}.\underline{k}) = P_\ell(\cos\theta=1) = 1 \quad , \tag{2.54a}$$

so that

$$T_{\underline{k}\underline{k}} = \sum_{\ell=0}^{\infty}(2\ell+1)\,T_\ell \quad . \tag{2.54b}$$

the gap equations which follow from substitution of (2.53) into (2.51) are

$$\tilde{\omega}_n = \omega_n + \frac{n\pi}{mp_F} \sum_{\ell=0}^{\infty} (2\ell+1) \frac{\tilde{\omega}_n (\tilde{\omega}_n^2 + \tilde{\Delta}^2)^{1/2}}{\tilde{\omega}_n^2 + \epsilon_\ell^2 \tilde{\Delta}^2} (\sin^2\delta_\ell^+ + \sin^2\delta_\ell^-), \quad (2.55a)$$

and

$$\tilde{\Delta} = \Delta + \frac{2\pi n}{mp_F} \sum_{\ell=0}^{\infty} (2\ell+1) \frac{\epsilon_\ell \tilde{\Delta} (\tilde{\omega}_n^2 + \tilde{\Delta}^2)^{1/2}}{\tilde{\omega}_n^2 + \epsilon_\ell^2 \tilde{\Delta}^2} \sin\delta_\ell^+ \sin\delta_\ell^- . \quad (2.55b)$$

Introducing the definition

$$u_n = \tilde{\omega}_n / \tilde{\Delta} , \quad (2.56)$$

the two equations (2.55) may be combined into one equation for u_n of the form

$$\omega_n/\Delta - u_n \left[1 - \sum_{\ell=0}^{\infty} (2\ell+1) \frac{\alpha_\ell}{\Delta} \frac{(1+u_n^2)^{1/2}}{(\epsilon_\ell^2 + u_n^2)^{1/2}} \right] . \quad (2.57a)$$

with the definition

$$\alpha_\ell = n (1-\epsilon_\ell^2)/(2\pi N_0) . \quad (2.57b)$$

Going back to section 2.1 and considering the effect of including both the pairing self-energy and the impurity self-energy at the same time, the equation for the order parameter (2.22) becomes

$$\Delta = N_0 V \int_0^{\omega_D} d\omega \, \mathrm{Re}\left[\frac{1}{\{u^2(\omega)-1\}^{1/2}} \right] \tanh[\omega/(2T)] . \quad (2.58)$$

The function $u(\omega)$ in (2.58) is the analytic continuation to real frequencies $\omega+i\eta$ (η a positive infinitesimal) of the function u_n defined in (2.56). The derivation of (2.58) requires the use of the spectral representation for the temperature Green's function[14]

$$\mathcal{G}_{\underline{k}}(i\omega_n) = \int_{-\infty}^{\infty} \frac{d\omega}{2\pi} \frac{-2\ \mathrm{Im}\{\mathcal{G}^R_{\underline{k}}(\omega+i\eta)\}}{i\omega_n - \omega} , \tag{2.59}$$

where $\mathcal{G}^R(\omega+i\eta)$ is the real-axis limit of the Fourier transform of the retarded Green's function.

Finally, performing the analytic continuation to real frequency of the equation for u_n (2.57), one obtains the form of the real-axis SR equation applied to various properties in the following sections:

$$\omega/\Delta = u(\omega)\left[1 - i\frac{u(\omega)}{[u^2(\omega)-1]^{1/2}} \sum_{\ell=0}^{\infty} (2\ell+1)\ \frac{\alpha_\ell}{\Delta} \frac{[u^2(\omega)-1]}{[u^2(\omega)-\epsilon_\ell^2]^{1/2}}\right] . \tag{2.60}$$

which must be solved self-consistently together with (2.58) to determine Δ and $u(\omega)$. In (2.60) the square roots must be chosen to have a positive real part for ω greater than zero.

2.4 SR Free Energy Difference and D(t)[23]

The free energy difference between the superconducting and

normal states of a superconductor is strongly influenced by the introduction of paramagnetic impurities. The free energy of the superconducting state is increased as impurities are added, the most obvious manifestation of which is the reduction of the critical temperature. However, the temperature dependence of the free energy difference is also altered. This was investigated for Th-Gd alloys by Decker and Finnemore[24], who found good agreement with AG theory for concentrations of Gd of up to 60 percent of the critical concentration. This agreement with AG theory for Th-Gd alloys is consistent with the agreement found for other properties of Gd alloys[6]. On the other hand, Smith[25] found critical magnetic fields for Zn-Mn alloys to be inconsistent with AG theory. These deviations from AG theory were believed to be due to the existence of states within the superconducting energy gap, but no comparison was made with a theory which allows this effect to be included. Although Chaba and Nagi[26] have calculated the free energy difference within the SR model at zero temperature, as well as the jump in the specific heat at the critical temperature, they did not examine the full temperature dependence of the free energy difference. Shiba[27] has found that his model with $\epsilon_0=0.25$ gives much better agreement with Smith's low temperature critical field data than does AG theory. Zarate and Carbotte[28] have used the free energy formula due to Yamamoto and Nagi[29] to calculate free energies at finite temperature for Pb alloys with SR impurities, but the strong-coupling nature of Pb makes it impossible to draw any conclusions about the temperature dependence of the free energy difference for Zn alloys from this work. It is therefore of some

interest to re-examine Smith's[25] results using SR theory, and at the same time make some general observations about the effect of SR model impurities on the free energy difference of weak-coupling superconductors.

The difference in free energy between the superconducting and normal states of a weak-coupling alloy with paramagnetic impurities has been calculated by Skalski *et al.*[30], who found

$$\frac{F_{N-S}}{N_0} = \int_0^{\omega_D'} \left[\frac{N(\omega)}{N_0} - 1 \right] \left[2\omega \tanh\left\{\frac{\beta\omega}{2}\right\} + \frac{4}{\beta}\left\{ \ell n(1+e^{-\beta\omega}) + \frac{\beta\omega}{1+e^{\beta\omega}} \right\} \right] + \Delta^2 \left[1 - \frac{1}{N_0 V} \right] . \tag{2.61}$$

where

$$\frac{N(\omega)}{N_0} = \mathrm{Re}\left[\frac{u(\omega)}{[u^2(\omega)-1]^{1/2}} \right] \tag{2.62}$$

is the quasiparticle density of states in the superconductor normalized to the normal state value N_0, and $\beta = 1/T$. The thermodynamic critical field is given by

$$H_c^2/(8\pi) = F_{N-S} . \tag{2.63}$$

and the deviation function is defined by

$$D(t) = [H_c(t)/H_c(0)] - (1-t^2) , \tag{2.64}$$

where $t = T/T_c$. One conventionally plots $D(t)$ versus t^2 rather than

the critical field directly.

Note that in the derivation[30] of (2.61) no assumption is made about the strength of the impurity scattering. This formula for the free energy difference is valid in the SR case as well as in the AG limit for weak-coupling superconductors. The strong-coupling free energy formula derived by Yamamoto and Nagi[29] for the SR case contains a correction to the usual Bardeen-Stephen[31] strong coupling formula. This corrected formula will be used in Chapter IV for proximity effect systems, where the simpler Skalski formula (2.61) cannot be applied directly. Although they are not obviously identical, in the present case both formulae have been found numerically to give the same result to an accuracy of approximately 0.1%.

Figure 2.2 shows the two extreme cases possible in SR theory. Figure 2.2(a) demonstrates the variation of $D(t)$ with impurity concentration in the AG limit, $\epsilon_0=1$ (the value actually used was $\epsilon_0 = 0.995$ for reasons of programming expediency). Decker and Finnemore[24] have previously shown such curves for values of the reduced pair-breaking parameter α/α_c between 0 and approximately 0.75. Their measured results for Th-Gd alloys agree well with AG theory for concentrations of up to 0.2 at.% Gd, corresponding to $\alpha/\alpha_c=0.6$. They were however, not able to examine higher Gd concentrations, particularly the predicted onset of gaplessness at $\alpha/\alpha_c=0.91$.

In agreement with the results of Decker and Finnemore[24], the minimum of $D(t)$ decreases to roughly -0.07 for $\alpha/\alpha_c=0.85$. However, for still higher concentrations the minimum of the curve rapidly increases toward zero. This interesting behavior coincides approximately with

the onset of gaplessness at zero temperature, which occurs for α/α_c=0.91 in AG theory. It will be established later in this section that a nonzero density of states at zero frequency is always correlated in SR theory with the minimum of $D(t)$ being an increasing function of impurity concentration.

The other extreme case possible within SR theory is illustrated in Fig. 2.2(b), which is a set of $D(t)$ curves for ϵ_0=0.001. In this case the minimum of $D(t)$ is a monotonically increasing function of impurity concentration, in striking contrast with the AG results. In this limit the density of states at zero frequency is always nonzero for any finite impurity concentration; that is, the material is always gapless.

Next the deviation function for different scattering parameters in SR theory will be considered, including both S- and P-wave scattering as well as the S-wave results already described. The general behavior may be seen more readily by plotting the value of $D(t)$ at one particular reduced temperature t as a function of impurity concentration, rather than plotting full $D(t)$ curves. The temperature t=0.7 was arbitrarily chosen because the minimum of the curves is generally found near t^2=0.5. Figure 2.3(a) contains several curves of $D(0.7)$ versus α/α_c for different scattering parameters. The corresponding densities of states at zero frequency, $N(0)/N_0$, are plotted in Fig. 2.3(b).

Several general observations may be made upon examination of Fig. 2.3. Perhaps the most interesting and important observation concerns a correlation between the slope of $D(0.7)$ versus α/α_c in Fig.

2.3(a) and the slope of $N(0)/N_0$ versus α/α_c in Fig. 2.3(b). While $N(0)$ is zero $D(0.7)$ is a decreasing function of impurity concentration. However when $N(0)/N_0$ increases rapidly, $D(0.7)$ also has a large positive slope as a function of α/α_c.

Note that when two partial waves are included, both the $D(0.7)$ and $N(0)$ curves in Fig. 2.3 lie between the curves which result when the same numerical values ϵ_0, ϵ_1 are used for S-wave scattering only. Futhermore, although this is not shown in Fig. 2.3, these curves are quite insensitive to the interchange of scattering parameters. For example, the curves for $\epsilon_0=0.6, \epsilon_1=0.01$ and those for $\epsilon_0=0.01, \epsilon_1=0.6$ are nearly indistinguishable.

Turning now to the particular case of Zn-Mn alloys, note that recently Terris and Ginsberg[32] have analyzed the tunneling characteristics of Zn-Mn films in terms of SR theory. They extracted two sets of parameters ϵ_ℓ, $\ell=0,1,2$ which fit their experimental conductances reasonably well. The $D(t)$ curves calculated for these two sets of parameters shown in Fig 2.4 are at least in qualitative agreement with Smith's[25] data. The most notable feature of these curves is the fact that for both sets of parameters the curves initially become more negative as the Mn concentration increases, followed by an increase toward zero at higher concentrations. Figure 2.4(a) shows some $D(t)$ curves for parameter set I, in future called Zn-Mn I: $\epsilon_0=1.00$, $\epsilon_1=0.53$, $\epsilon_2=0.94$. In this case the minimum of $D(t)$ remains between -0.03 and -0.04 for impurity concentrations between 0% and more than 60% of the critical concentration.

Figure 2.4(b) consists of $D(t)$ curves for the second set of

parameters, Zn-Mn II, which is ϵ_0=0.25, ϵ_1=0.50, and ϵ_2=1.00. In this case the minimum of $D(t)$ remains between -0.02 and -0.04 for concentrations between 0% and more than 50% of the critical concentration. Although the amount of scatter in the data of Smith[25] makes detailed comparison difficult, both sets of parameters give $D(t)$ curves which agree at least qualitatively with the experimental results. The same thing cannot be said for AG theory; the $D(t)$ curves of Smith do not become sufficiently negative to agree at all with the AG results of Fig. 2.2(a).

Another comparison may be made by examining the relationship between $H_c(0)$ and T_c through the quantity $\tilde{H}^2=H_c^2(0)/\gamma T_c^2$. Here γ is the coefficient of the linear term in the electronic specific heat for the pure material. Figure 2.5 shows the AG prediction to be significantly different from Smith's results, while the SR results using Ginsberg's parameters Zn-Mn I and II are at least in qualitative agreement with the experimental results. Also included in Fig. 2.5 is a curve for a set of scattering parameters calculated by Kunz and Ginsberg[33]: ϵ_0=0.951, ϵ_1=0.842, and ϵ_2=0.998. Terris and Ginsberg[32] found that these parameters give significantly worse agreement with their measured tunneling characteristics than do Zn-Mn I and Zn-Mn II. The present calculation shows that these calculated parameters also give critical fields which are in worse agreement with the measurements of Smith than Zn-Mn I and Zn-Mn II. Also note that Shiba[27] has previously shown that Smith's low temperature critical field measurements are consistent with the single scattering parameter ϵ_0=0.25, which gives a critical field curve very similar to that shown for Zn-Mn II in Fig. 2.5.

In conclusion, the deviation function has been found to be very sensitive to the location of the impurity levels inside the energy gap predicted by SR theory. The change in $D(t)$ is correlated with the zero frequency density of states N(0). While N(0) is zero, the minimum of $D(t)$ decreases with increasing impurity concentration. When N(0) is nonzero, the minimum of $D(t)$ increases with increasing impurity concentration. Furthermore, the more rapid the increase in N(0), the more rapid the rise of the minimum of $D(t)$ toward zero with increasing impurity concentration.

The zero temperature critical fields of Zn-Mn alloys have also been found to be consistent with the set of scattering parameters Zn-Mn I, with the same degree of agreement as was found for the single scattering parameter $\epsilon_0=0.25$ by Shiba[27].

2.5 SR Electromagnetic Absorption[34]

The absorption of electromagnetic radiation is one of the more direct probes of the quasiparticle density of states of a superconductor and provides the same type of information as the more common tunneling experiments. The far-infrared study by Dick and Reif[6] of Pb-Gd alloy films provided corroboration of the applicability of the theory of Abrikosov and Gor'kov[3] (AG) to these alloys, in agreement with the results of tunneling experiments by Woolf and Reif[7]. These same experiments also showed convincingly that Pb-Mn films are not well described by AG theory.

Chaba and Nagi[26] have reexamined the tunneling conductance of these Pb-Mn alloys using SR theory, and found that ϵ_0=0.55 gives significantly better agreement than does AG theory (ϵ_0=1.0). More recently Bauriedl *et al.*[35] measured tunneling characterstics of Pb-Mn alloys and concluded that the set of parameters ϵ_0=0.23, ϵ_1=0.79 gives a good fit to the location of conductance peaks observed inside the gap. On the other hand, Machida[36] has observed that ϵ_0=0.5 gives significantly better agreement with the electromagnetic absorption experiments of Dick and Reif[6] than does AG theory. It may therefore be of some interest to compare the predictions of the absorption for some of these different scattering parameters with the experimental results.

At this point it should be noted that an earlier published version of this section[34] is deficient in several respects. Most importantly, the predicted finite temperature structure associated with the excitation of thermally excited quasiparticles, of which more will be said later, was greatly exaggerated in magnitude by an error in the computer code. The error was discovered when the previous results were compared with some nonproximity runs of the SR-McMillan model proximity effect program which was used to calculate most of the results in Chapter IV (this check was ostensibly carried out as a check of the proximity program, then under development). The resulting erratum[34] pointed out that the earlier prediction of a significant peak in the absorption should be downgraded to a small peak or kink. The second point is one of omission. After publication of the paper[34], D.M. Ginsberg helpfully pointed out the existence of the set of scattering

parameters determined by Bauriedl *et al.*[35] from tunneling experiments. These parameters were not used to calculate absorption curves in the earlier paper.

Turning now to the calculation of the electromagnetic absorption, this has been found by Nam[37] for the AG case, and by Machida[36] for the SR model. The absorption, normalised to the normal state value is given by

$$\frac{\sigma_1(\omega)}{\sigma_N} = \frac{1}{\omega}\int_{\omega_g-\omega}^{\omega_g} d\nu\ [n(\nu)n(\omega+\nu)+p(\nu)p(\omega+\nu)]\ \tanh\left\{\frac{\beta}{2}(\omega+\nu)\right\}$$

$$+ \frac{1}{\omega}\int_{\omega_g}^{\infty} d\nu\ [n(\nu)n(\omega+\nu)+p(\nu)p(\omega+\nu)]\ \left[\tanh\left\{\frac{\beta}{2}(\omega+\nu)\right\} - \tanh\left\{\frac{\beta\nu}{2}\right\}\right]. \quad (2.65)$$

Here

$$n(\nu) = \mathrm{Re}\left[\frac{u(\nu)}{\{u^2(\nu)-1\}^{1/2}}\right] \quad (2.66a)$$

is the single particle density of states, and

$$p(\nu) = \mathrm{Re}\left[\frac{1}{\{u^2(\nu)-1\}^{1/2}}\right] \quad (2.66b)$$

is the pair density of states. The normal state conductivity σ_N is assumed to be frequency independent in the frequency range of interest. The frequency ω_g is defined as the lowest frequency where the density of states becomes non-zero.

Some well-known properties of the electromagnetic absorption of superconductors will be reviewed next. Recall that in BCS theory at

zero temperature there is no absorption for $\omega<\omega_g$, where $\omega_g=\Delta$. At finite temperature there is some absorption at all frequencies, but for relatively low temperature ($T/T_c\lesssim 0.2$) $\sigma_1(\omega)$ is negligibly small in the "gap" when compared with the absorption at higher frequencies. The absorption does increase at low frequencies, however, and diverges at zero frequency. The singular behavior at zero frequency arises from the square-root singularity in the density of states at $\omega=\Delta$. Qualitatively, one might say that some states above the Fermi level are thermally occupied, and these quasiparticles have an infinite density of states to scatter into with the absorption of a photon of vanishingly small energy.

With paramagnetic impurities in the AG model, the situation is qualitatively very similar. At zero temperature there is no absorption for $\omega<2\omega_g$, but in this case $\omega_g<\Delta$. In fact, as the impurity concentration increases ω_g approaches zero (gapless region). At nonzero temperature there is finite absorption at all frequencies, with a peak at zero frequency. In contrast to the pure BCS case the peak at zero frequency is finite, which may be attributed to the disappearance of the singularity in the density of states with the addition of paramagnetic impurities .

In SR theory the addition of regions of nonzero density of states within the gap results in extra structure in the zero temperature absorption shown in Fig. 2.6(a). This can be understood qualitatively by examining the density of states, Fig. 2.6(b). At finite temperature the same mechanism which is involved in the AG case gives rise to a finite peak at zero frequency. In addition, there may

be a structure between $\omega=0$ and $\omega=\Delta$, which is not seen at zero temperature. This peak, which may appear as a shoulder on the zero frequency peak at higher temperatures, is located at a frequency which may not coincide with any of the zero temperature peaks. Figure 2.7a shows an example of this behavior.

To help explain this effect recall Eq. (2.65) for the absorption in terms of the density of states:

$$\frac{\sigma_1(\omega)}{\sigma_N} = \frac{1}{\omega}\int_{\omega_g-\omega}^{\omega_g} d\nu\ [n(\nu)n(\omega+\nu)+p(\nu)p(\omega+\nu)]\ \tanh\left\{\frac{\beta}{2}(\omega+\nu)\right\}$$
$$+\frac{2}{\omega}\int_{\omega_g}^{\infty} d\nu\left\{[n(\nu)n(\omega+\nu)+p(\nu)p(\omega+\nu)]\right.$$
$$\left.\left[f\{\beta\nu\}\left[1-f\{\beta(\omega+\nu)\}\right]-f\{\beta(\omega+\nu)\}\left[1-f\{\beta\nu\}\right]\right]\right\}. \qquad (2.67)$$

The identity $\tanh(x/2)=1-2f(x)$ was used in rewriting the second integral in (2.67). Note that the first integral contributes at all temperatures, and does not change dramatically on going from zero to finite temperatures. It is the second integral which gives rise to the structure in question.

The second integral in (2.67) was written in this form to emphasize the similarity to tunneling I-V characteristics, and to allow qualitative identification of the various contributions. The first occupation factor $f\{\beta\nu\}\left[1-f\{\beta(\omega+\nu)\}\right]$ indicates absorption of a photon of frequency ω, with a quasiparticle scattering from ν to $\nu+\omega$. The subtracted term $-f\{\beta(\omega+\nu)\}\left[1-f\{\beta\nu\}\right]$ corresponds to stimulated emission

of a photon ω, with a quasiparticle dropping from $\nu+\omega$ to ν. The absorption will be maximized when the first contribution is large and the subtracted term is relatively small.

Figure 2.7(b) illustrates the qualitatively distinct scattering processes which contribute only at finite temperatures. The arrows labeled E represent the absorption processes and those labeled e the emission processes which give rise to the peak in question, labeled E in Fig. 2.7(a). Looking in the positive energy region (above the Fermi level) of Fig. 2.7(b), one can see that while the number of occupied states in the impurity levels (roughly $0.2<\omega/\Delta<0.8$) is comparable to the number of occupied states just above the main rise ($1.0<\omega/\Delta\lesssim 1.8$), this is not true for the unoccupied states. There are many more unoccupied states available above $\omega/\Delta=1.0$, which means that the phase space for absorption events at $\omega/\Delta=0.8$ is much larger than that for stimulated emission. For frequencies larger or smaller than this optimum value this lack of balance between the phase space available for absorption and emission decreases, resulting in a smaller contribution to the absorption from these types of processes.

In general, this peak or shoulder in the absorption can be expected to occur near the frequency $\Delta-\omega_g$ as long as the impurity concentration is small enough so that a well defined peak still exists in the density of states near $\omega=\Delta$. Note also that as the AG limit ($\epsilon_0=1.0$) is approached this structure moves toward zero frequency and merges with the peak which always exists there.

Turning now to the electromagnetic absorption for Pb-Mn alloys, Figs. 2.8-2.10 show a comparison of the experimental measurements of

Dick and Reif[6] to three different sets of scattering parameters. In all cases an approximate strong-coupling correction was made using the equation

$$\frac{\omega}{\Delta} = \frac{\omega}{T_c^0}\left[\frac{T_c^0}{\Delta_0}\right]\left[\frac{\Delta_0}{\Delta}\right] \tag{2.68}$$

to manipulate the data of Dick and Reif[6]. Here the experimental value of $\Delta_0/T_c^0=2.31$ has been used, along with the ratio Δ/Δ_0 determined from our weak-coupling calculation. Also, because the absolute value of σ_1/σ_N was not determined directly in the experiment, the normalization of this axis is somewhat model dependent. This has simply been adjusted slightly from model to model so that the last few points are close to the theoretical curves. All curves have also been calculated for the experimental temperature of 1.5 K.

Figure 2.8 shows the results for the model Pb-Mn I[33]: $\epsilon_0=0.985$, $\epsilon_1=0.967$, and $\epsilon_2=0.970$. Clearly there is much more absorption at low frequencies than is predicted by this model. Noting that all of the scattering parameters (ϵ_ℓ's) are quite near 1.0, it is reasonable that this model should give results which are similar to the AG results, which were found to be in disagreement with experiment by Dick and Reif[6].

Figure 2.9 shows a comparison of the experimental measurements with the predictions of the model Pb-Mn II from the band-structure calculation of Kunz and Ginsberg[33]: $\epsilon_0=0.959$, $\epsilon_1=-0.680$, and $\epsilon_2=0.990$. The agreement in this case is slightly better than that

shown in Fig. 2.8, but there is still more absorption observed at low frequencies than is predicted by this model.

Figure 2.10 shows a comparison of the experimental results with calculations using a set of scattering parameters determined by Bauriedl, Ziemann, and Buckel[35] from tunneling experiments: ϵ_0=0.23, and ϵ_1=0.79. The agreement in this case is significantly better than that displayed by either of the other two models. One might note as well the more complicated structure within the "gap" for the low concentration curve (T_c/T_c^0=0.95) in this case; this is a reflection of the fact that for this concentration there are two distinct bands in the "gap" separated by a region of zero density of states. Although the other two models have three scattering parameters, even for the lowest concentration shown there is only one distinct band in the gap (for Pb-Mn II) or none at all (for Pb-Mn I), which results in a smoother absorption curve at low frequencies.

In this section, the electromagnetic absorption of superconductors with SR model paramagnetic impurities has been examined. The finite temperature absorption has been shown to exhibit a small peak or shoulder which is not found at zero temperature. Finally, of the various sets of scattering parameters considered, the set of parameters determined by Bauriedl *et al.*[35] from tunneling experiments give the best agreement with the optical absorption measurements of Dick and Reif[6].

2.6 SR Electromagnetic Coherence Length

The electromagnetic coherence length of a superconductor is of major importance in determining the response of the material to applied electromagnetic fields. The coherence length describes the extent to which the response of a superconductor is non-local, that is it gives the spatial range of the kernal $K_{\mu\upsilon}(\underline{r}-\underline{r}')$ which relates the current density $j_\mu(\underline{r})$ to the vector potential $A_\upsilon(\underline{r}')$. The penetration depths for a given material in different situations, for example with varying purity, may be related to one another through the use of the coherence length[38].

The electromagnetic coherence length has been calculated by Lemberger, Ginsberg, and Rickayzen[39] (LGR) for weak coupling superconductors containing SR model impurities with a single scattering parameter. Although the coherence length is of some importance, it was not felt to be of much interest to check the influence of including multiple scattering channels. In the course of checking the current computer code by comparing calculated results with previously published work, however, it became clear that the results were not consistent with the numerical results presented by LGR. Upon further investigation of the calculation of LGR[39], it became apparent that their equations (3-4) are not exactly the same as the conventional SR gap equations. The discrepency in question arises from the spin-flip scattering rate α in their (3) and (4). Comparing this with equation (33) in Rusinov's[9] derivation, (2.55) here, it can be seen that they differ significantly. The point is that in the case $\epsilon_0 \neq 1$ the

contribution of exchange scattering to the ω and Δ channels (2.55a and b respectively) is not equal and opposite, as it is in AG theory. While the resulting density of states from (6) in LGR is correct, the renormalized gap function $\tilde{\Delta}_n$ is not consistent with SR theory when the same values of ϵ_0 and α are used in their equation (4). This would not be important for most properties, such as thermodynamics for example, since they do not depend explicitly on the renormalization function Z. However, the coherence length as calculated by LGR[39] depends explicitly on $\tilde{\Delta}_n = Z_n \Delta_n$.

The gap equations (2.55) may be written in the form

$$\tilde{\omega}_n = \omega_n + \frac{1}{2\tau_1} \frac{u_n(1+u_n^2)^{1/2}}{\epsilon_0^2 + u_n^2} \tag{2.68a}$$

$$\tilde{\Delta}_n = \Delta + \frac{1}{2\tau_2} \frac{(1+u_n^2)^{1/2}}{\epsilon_0^2 + u_n^2} \tag{2.68b}$$

where

$$\frac{1}{2\tau_1} = \frac{\pi n_I}{m p_F} (\sin^2\delta_0^+ + \sin^2\delta_0^-) = \frac{\pi n_I}{m p_F} (1-\epsilon_0\eta_0) \tag{2.69a}$$

$$\frac{1}{2\tau_2} = \frac{\pi n_I}{m p_F} 2 \sin\delta_0^+ \sin\delta_0^- \cos(\delta_0^+-\delta_0^-) = - \frac{\pi n_I}{m p_F} \epsilon_0(\eta_0-\epsilon_0) \tag{2.69b}$$

and

$$\epsilon_0 = \cos(\delta_0^+-\delta_0^-) \tag{2.70a}$$

$$\eta_0 = \cos(\delta_0^++\delta_0^-) \tag{2.70b}$$

Here the limit of only a single scattering channel has been taken, and the new quantity η_0 describes the non-exchange scattering from the SR impurities. In the limit where only exchange scattering is considered one has $\eta_0 = 1$. Exactly as in Section 2.3, the gap equations (2.68) may be combined into a single equation for the function u_n, resulting in

$$\omega_n/\Delta = u_n \left[1 - \frac{\alpha}{\Delta} \frac{(1 + u_n^2)^{1/2}}{(\epsilon_0^2 + u_n^2)^{1/2}} \right] . \qquad (2.71a)$$

where

$$\alpha = \frac{\pi n_I}{m p_F} (1-\epsilon_0^2) , \qquad (2.71b)$$

which is exactly equation (6) in LGR.

The rest of the calculation by LGR still holds, so that the coherence length is given by their equation (18)

$$\xi = \frac{v_F}{2} \sum_n \frac{1}{\tilde{\Delta}_n (1+u_n^2)^{3/2}} \Big/ \sum_n \frac{1}{(1+u_n^2)} , \qquad (2.72)$$

where $\tilde{\Delta}_n$ is given by (2.68b) and u_n by (2.71a), with v_F the Fermi velocity. Standard techniques[16] may now be used to rewrite (2.72) in terms of real frequency axis integrals. While the real axis equations are actually more difficult and time consuming to solve numerically than the corresponding imaginary axis versions, the existence of a working real axis computer program puts the bias in favor of this

approach. By representing the summations in (2.72) in terms of contour integrals, and deforming the contours to the real-axis, these results become

$$I = \pi T \sum_n \frac{1}{(1+u_n^2)} = \mathrm{Im} \int_0^\infty \frac{d\omega}{[1-u^2(\omega)]} \tanh(\beta\omega/2) \quad , \quad (2.73a)$$

and

$$K = \pi T \sum_n \frac{1}{\tilde{\Delta}_n (1+u_n^2)^{3/2}} = -\mathrm{Re} \int_0^\infty \frac{d\omega}{\tilde{\Delta}(\omega)[u^2(\omega)-1]^{3/2}} \tanh(\beta\omega/2) \quad (2.73b)$$

with the coherence length given by

$$\xi = \frac{v_F K}{2 I} \quad . \quad (2.73c)$$

The square root in (2.73b) must be chosen to have a positive real part.

Figure 2.11 shows the zero temperature coherence length ξ_0 normalised to the value for the pure material $\xi_{00} = \frac{v_F}{\pi\Delta_0}$ and mutiplied by T_c/T_c^0 , which is predicted to be one by the BCS law of corresponding states, for several different reduced critical temperatures as a function of the scattering parameter ϵ_0. The dashed curves in Fig. 2.11 were calculated with the same program but with the substitutions $\frac{1}{2\tau_1} = \alpha/2$ and $\frac{1}{2\tau_2} = -\alpha/2$, which corresponds to the R-∞ limit of LGR[39]. These curves agree with those shown in Fig. 1 of LGR.

Figure 2.12 shows the normalised zero temperature coherence length as a function of normalised inpurity concentration α/α_c for

various values of the scattering parameter ϵ_0. The fact that the coherence length always increases with increasing impurity concentration simply reflects the fact that the weakening of the pairing correlations is much stronger than the reduction of mean free path associated with the impurities. Also note that at high concentrations, near the critical value, the coherence length is a monotonically increasing function of the scattering parameter ϵ_0.

Figure 2.13 shows the temperature dependence of the coherence length for several values of ϵ_0 and a given reduced critical temperature T_c/T_c^0=0.63, corresponding to α/α_c=0.5. Note that although the zero temperature value is non-monotonic as a function of ϵ_0 for this concentration of impurities, as may also be seen in Fig. 2.12, the coherence length at the critical temperature decreases monotonically with decreasing ϵ_0.

From the LGR results, the effect of including the normal scattering from the SR impurities would be expected to be a reduction of the coherence length for all concentrations and temperatures. An example is shown in Fig. 2.14(a), where the zero temperature coherence length is shown as a function of reduced paramagnetic impurity concentration α/α_c with no normal scattering (η_0=1.0) and with the maximum allowed amount (η_0=-0.5 for ϵ_0=0.5). The trends are just what would be expected; with increasing normal scattering associated with the paramagnetic impurities the enhancement of the coherence length caused by the pair-breaking exchange scattering is decreased, so that in the extreme limit where the the normal scattering takes on the maximum allowed value the zero temperature coherence length is only

very weakly dependent on impurity concentration.

The effect of including normal scattering from the SR impurities on the temperature dependence of the coherence length for a concentration which is half of the critical value is shown in Fig. 2.14(b). The most important feature of this figure is the fact that with increasing normal scattering (decreasing η_0) the coherence length is most strongly suppressed at low temperatures, resulting in an overall reduction in the magnitude of the temperature dependence with increasing normal scattering.

2.7 SR Thermal Conductivity

The thermal conductivity for a superconducting alloy with SR model impurities has been calculated by Leon and Nagi[40]. Although a significant dependence on ϵ_0, the single scattering parameter used, is predicted, the variations are largest in the region of large impurity concentration and low temperature, a very difficult regime to explore experimentally. A practical difficulty is that the effects of interactions between impurities, which are ignored in SR theory, tend to become important in exactly this situation. This must be kept in mind when analyzing experimental results.

Despite the difficulties, a fair number of experimental investigations have been made of alloys which may possibly be described by SR theory. Sánchez[41] has investigated the thermal conductivity of Zn-Mn alloys, and has found reasonably good agreement with AG theory

for concentrations of Mn less than 10.0 ppm. Lemberger and Ginsberg[42] later analysed Sánchez' results using SR theory and concluded that while the parameter $\epsilon_0=0.7$ seemed to give best agreement, no value of ϵ_0 in the range from 0.0 to 1.0 could be ruled out entirely. This inconclusiveness may be attributed to a large extent to the limited temperature range of the experiment, which had a minimum temperature of 0.36 K, compared with the critical temperature of pure Zn films of 0.857 K. This means that for the higher concentration samples only a very narrow temperature range near T_c could be investigated.

In light of the above, it should not be surprising that the inclusion of multiple scattering channels within SR theory does not significantly alter the conclusions. The thermal conductivity is given by[40]

$$\frac{K_S}{K_N} = \frac{3\beta^3}{2\pi^2} \int_0^{\omega_D} d\omega\, \omega^2\, \mathrm{sech}^2(\beta\omega/2)\, h(\omega) \,, \tag{2.74}$$

where

$$h(\omega) = \left[\mathrm{Re}\, \frac{u(\omega)}{[u^2(\omega)-1]^{1/2}}\right]^2 - \left[\mathrm{Re}\, \frac{1}{[u^2(\omega)-1]^{1/2}}\right]^2$$

$$= \frac{1}{2}\left[1 + \frac{|u(\omega)|^2-1}{|u^2(\omega)-1|}\right] . \tag{2.75}$$

The function $u(\omega)$ is given by the expression (2.60), which differs from the expression used by Leon and Nagi[40] only in the inclusion of the sum over partial wave indices ℓ.

The results obtained for the two models previously introduced

in Section 2.4, Zn-Mn I and II, are shown in Fig. 2.15 for an intermediate impurity concentration case of 6.0 ppm. Mn, along with a curve for ϵ_0=0.7. Calculated results for the other samples with 8.4 ppm. Mn or less show identical agreement with experiment. Note that because T_c was determined from the thermal conductivity measurements there is some freedom for small adjustments to T_c when using different parameters. This was not done in Fig. 2.15 in order to illustrate the differences which result when the same reduced critical temperature T_c/T_c^0 is used. Noting that Sánchez'[41] estimated uncertainty in T_c is more than ±2%, one realizes that the curves for Zn-Mn I or II in Fig. 2.15 could quite easily be made to fit the experimental points just as well as that for ϵ_0=0.7. As a result, the type of fit which may be obtained with the multiple scattering parameter models is virtually identical to that found by Lemberger and Ginsberg[42] using only a single scattering parameter. Note also that throughout the comparison with measurements on Zn alloys an approximate correction should be made for the fact that the ratio $2\Delta_0/T_c^0 = 3.4$[41] for Zn, compared to the BCS value of 3.53. This is simply done by multiplying the numerically converged order parameter Δ for arbitrary temperature and impurity concentration by the ratio $3.4/3.53 \simeq 0.96$, and therefore scaling the frequency dependence of the gap function $\Delta(\omega)$ and the auxiliary function $u(\omega)$ by the same amount.

At this point it may be mentioned that the two highest concentrations examined by Sánchez are in significant disagreement with SR theory for any choice of parameters. As pointed out by Lemberger and Ginsberg[42], the measured thermal conductivity is much larger than

the calculated value for any parameters. This problem has also been considered by Matsui and Masuda[43], who used an approximate version of the MHZ[21] theory, in which the parameter ϵ_0 satisfies

$$\epsilon_0 = \left[\frac{\ell n(T/T_K)}{\ell n^2(T/T_K)+\pi^2 S(S+1)}\right] . \qquad (2.76)$$

where T_K is the Kondo[44] temperature, which results in an increasing exchange scattering rate as T_K is approached from above. They found, however, that for parameters presumably suitable for Zn-Mn the increase is not at all large enough to explain Sánchez'[41] high concentration data. For the lower concentrations their model gave similar agreement with experiment as may be achieved in SR theory.

Sánchez suggested that this deviation from AG (and SR) theory for the two high concentration samples might be due to inter-impurity interactions, and attempted to correct for this phenomenologically by correcting the normal state values to what they would have been in the absence of interaction. While this correction moved the data down toward the theoretical predictions, no correction was made to the superconducting state thermal conductivity, and significant disagreement remains.

Another phenomenological approach which suggests itself immediately is to note that within the present approximations the normal state thermal conductivity is given by Eq. (22) in Leon and Nagi[40]

$$K_N = \frac{n_e \pi^2 T}{3m} \tau_1 \quad . \qquad (2.77)$$

where τ_1 is the lifetime due to both spin-flip and normal scattering processes. In the SR model, where the Kondo effect and inter-impurity interactions are neglected, this lifetime is found to be temperature independent. Note that the normal state values of K_N/T displayed by Sánchez in his Fig. (3) are consistent with a constant τ_1 only for pure Zn and the 2.7 ppm. Mn sample. All higher Mn concentration samples show a significant deviation from a constant temperature independent value for K_N/T. The decrease in this ratio with decreasing temperature is consistent with τ_1 decreasing due to the Kondo effect. Using Mathiessen's rule[45] in order to subtract out the residual temperature independent part of τ_1 due to non-magnetic scattering sources, one might attempt to use the resulting temperature dependent scattering time in the calculation of the superconducting gap function. A simple linear regression of $(K_N/T)^{-1}$ at T=1 K versus n_I from Sánchez' data in his Fig. 3 yields

$$(K_N/T)^{-1} = .071 + .073\, n_I \quad . \qquad (2.78)$$

with n_I in ppm., and K_N/T in $W/(cm\text{-}K^2)$. Note that according to (2.77) $(K_N/T)^{-1} \propto 1/\tau_1$, so that if it is assumed that Mathiessen's rule applies here, one might simply subtract off the intercept at $n_I=0$, that is 0.071, in order to extract the contribution of the magnetic impurities to $1/\tau_1$. If it is further assumed that the temperature

dependence of the spin-flip scattering time is the same as the temperature dependence of the resulting magnetic impurity contribution to τ_1 then one might try using this temperature dependent spin-flip scattering rate in the gap equation for calculation of the thermal conductivity. The temperature dependence which results for the scattering rate in the two highest impurity concentration cases Fig.3 (e) and 3 (f) of Sánchez[41] is shown in Fig. 2.16. Here the scattering rate $1/\tau_1$ normalized to the value for the highest experimental temperature has been plotted as a function of temperature. Note that the correction produced by subtracting off the non-magnetic contribution to $(K_N/T)^{-1}$ has only a very small influence on these curves. Using this temperature dependence for the pair-breaking parameter α, with the overall normalization chosen to fit T_c/T_c^0 the thermal conductivity curves shown in Fig. 2.17 are obtained, where the curves for a constant temperature independent α have also been shown for the sake of comparison. It is readily seen that the corrected curves are significantly closer to the experimental points, although both curves still display somewhat lower thermal conductivity than is observed experimentally.

Of the assumptions made in this phenomenological correction, the one which springs immediately to mind is the assumption that the temperature dependence of the spin-flip contribution to the scattering rate is the same as the temperature dependence of the total contribution from the Mn impurities. It might be more reasonable to assume a temperature independent direct contribution together with a temperature dependent exchange contribution. In this case the

estimated temperature dependence shown in Fig. 2.16 would merely be a lower bound on the size of the temperature variation of the pair-breaking parameter α. With this in mind, the 10.0 and 11.7 ppm. Zn-Mn samples of Sánchez may well be consistent with the conventional thermal conductivity equation (2.74-75), but with a temperature dependendent scattering time τ_1, which affects the temperature dependence of both the normal and superconducting state thermal conductivities. The proper calculation of this scattering time, however, requires the treatment of both the Kondo effect and inter-impurity interactions simultaneously, which is still an unsolved problem at this point.

Returning to the question of the effect of including multiple scattering channels on the calculated thermal conductivity, Fig. 2.18 shows a comparison of values calculated for a Pb-Mn alloy using two sets of scattering parameters from the band structure calculation of Kunz and Ginsberg[33]: for Pb-Mn I, ϵ_0=0.985, ϵ_1=0.967, and ϵ_2=0.970, and for Pb-Mn II, ϵ_0=0.959, ϵ_1=-0.680, and ϵ_2=0.990. In this case the necessary strong-coupling correction was made by renormalising the order parameter and therfore the frequency scale of the gap function by the ratio $(2\Delta_0/T_c^0)_{Pb}/(2\Delta_0/T_c^0)_{BCS}$=4.32/3.53=1.22. The experimental results are from Przybysz and Ginsberg[46], who compared their results to AG theory as well as SR theory with ϵ_0= 0 and ϵ_0=0.55. They concluded that ϵ_0=0.55, a value previously suggested to fit tunneling characteristics[26], was consistent with their measurements. However, the existing discrepencies are such that a large variety of scattering parameters could be used with essentially identical agreement. For

example, in their Fig. 2 the curves for samples D and E seem to be fit best by ϵ_0=1.00, while sample C seems to be most consistent with ϵ_0=0.55. This discrepancy at low temperatures may be due to difficulties in the proper subtraction of the phonon contribution to the thermal conductivity which was necessary in this case; the normal state thermal conductivity was not measured below T_c, rather it was extrapolated from a fit to the measurements above T_c. Finally, note that although the results are not shown here, for the other samples examined by Przybysz and Ginsberg[46] the model Pb-Mn I is very close to the AG limit (ϵ_0=1) in all cases, and the Pb-Mn II model is similar to the case ϵ_0=.55 shown in their Figs 1-3.

In the case of the In-Mn alloy measured by Przybysz and Ginsberg[46] the agreement between theory and experiment is much better. Przybysz and Ginsberg found very good agreement between their measurements and SR theory with the parameter ϵ_0=0.85. This is unchanged by the inclusion of more scattering channels in the calculation; shown in Fig. 2.19 is a calculated curve for the set of scattering parameters ϵ_0=0.962, ϵ_1=0.840, and ϵ_2=0.991 from the band structure calculation of Kunz and Ginsberg[33]. The renormalisation for the gap of In was $(2\Delta_0/T_c^0)_{In}/(2\Delta_0/T_c^0)_{BCS}$=3.88/3.53=1.10. The fit here is virtually identical to that obtained with the single scattering parameter ϵ_0=0.85.

The case of the In-Cr alloy measured by Przybysz and Ginsberg[47] is also very similar. They found good agreement with SR theory for the parameter ϵ_0=0.7. Terris and Ginsberg[48] later found that these results are also consistent with the parameters ϵ_0=0.894.

ϵ_1=0.729. and ϵ_2=0.989 from the band structure calculation of Kunz and Ginsberg.[33]

To summarize the results of this section, one can say that while the thermal conductivity of alloys containing magnetic transition metal impurities is often well described by SR theory, these measurements, at least so far , have not been a very discriminating tool for the identification of the location of the states in the energy gap. In cases where several samples were studied the discrepencies are such that a large range of scattering parameters can give a reasonable fit. Leon and Nagi's[40] calculation of the thermal conductivity in the SR model shows that for moderate concentrations of impurities, strong dependence on the location of the states in the gap exists mainly at the lowest temperatures. It is in this regime that the experiments are most difficult to carry out and in which the largest uncertainties are expected.

Fig. 2.1 a) BCS self-energy diagram

b) Shiba-Rusinov impurity self-enegry diagram

(a) $\Sigma_{\mathrm{BCS}} =$ 

(b) $\Sigma_{\mathrm{SR}} =$ 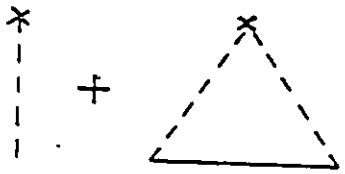

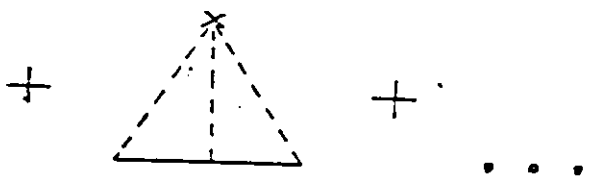

Fig. 2.2 a) Deviation Function for several differnt impurity concentrations with scattering parameter ϵ_0=0.995 (the AG limit). The curves are labeled by reduced impurity concentration α/α_c, where α_c is the critical value of the pair-breaking parameter.

b) Deviation function for several impurity concentrations for ϵ_0=0.001 .

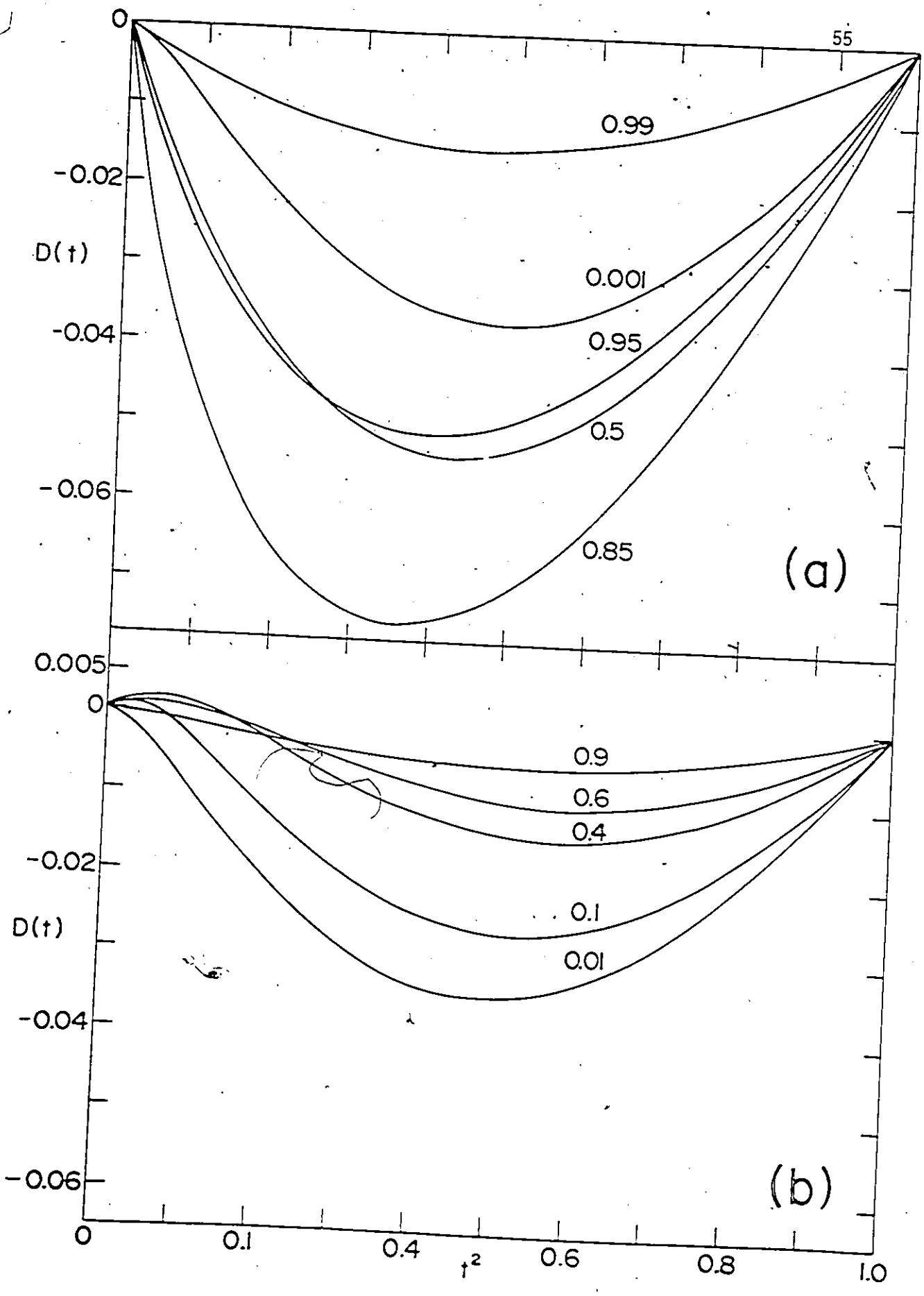
0
-0.02
-0.04
-0.06
D(t)
0.99
0.001
0.95
0.5
0.85
(a)
0.005
0
-0.02
-0.04
-0.06
D(t)
0.9
0.6
0.4
0.1
0.01
(b)
0
0.1
0.4
0.6
0.8
1.0
t²

Fig. 2.3 a) Deviation function at reduced temperature t=0.7 as a function of reduced impurity concentration α/α_c. The curves are labeled by the scattering parameters. The single number c implies $\epsilon_0=c$, and a pair (c,d) implies $\epsilon_0=c$, $\epsilon_1=d$.

b) Density of states at zero frequency as a function of reduced impurity concentration for the same set of parameters as in a).

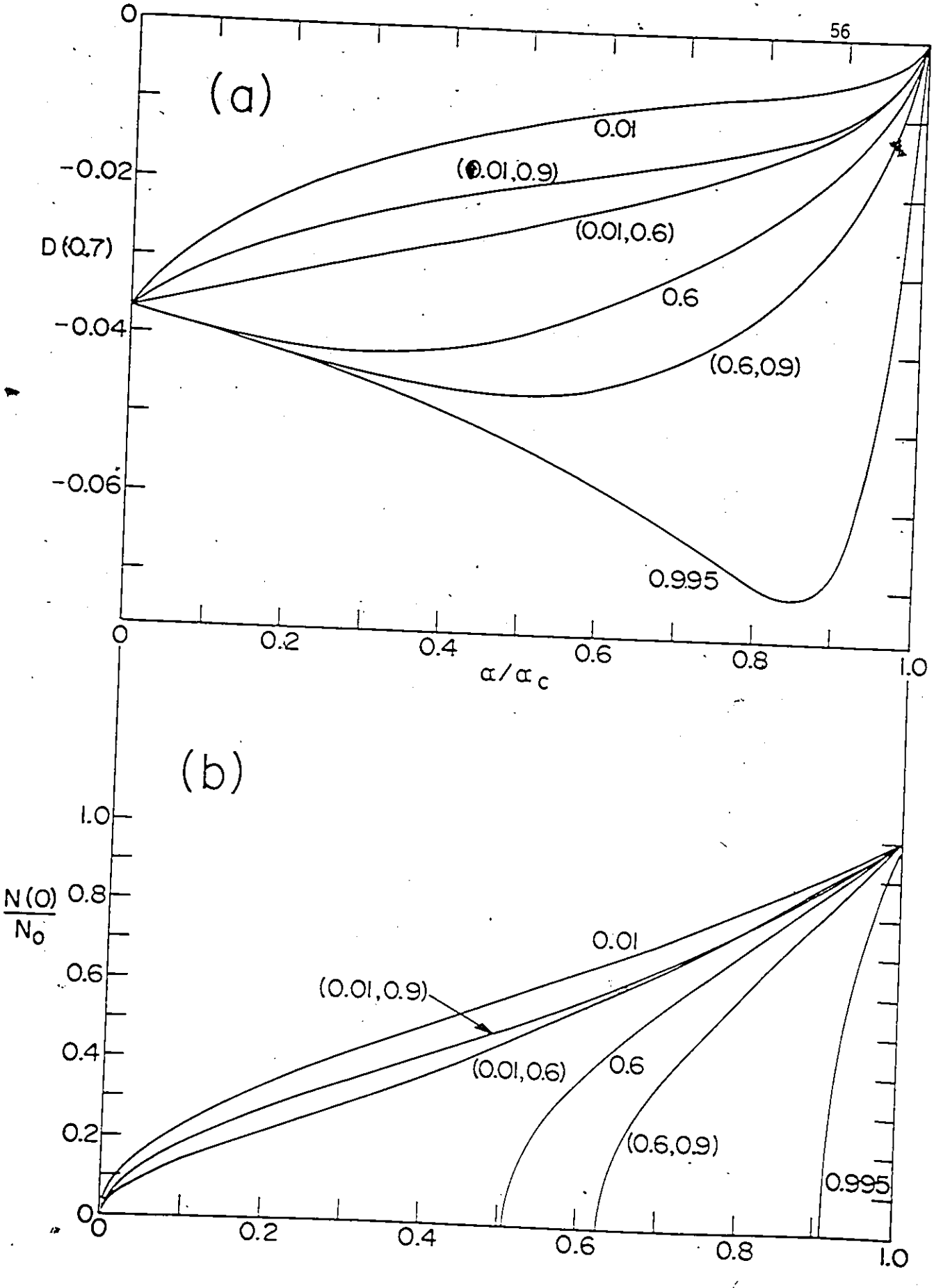
(a)
0
-0.02
-0.04
-0.06
D(0.7)
0.01
(0.01,0.9)
(0.01,0.6)
0.6
(0.6,0.9)
0.995
0
0.2
0.4
0.6
0.8
1.0
α/α_c
(b)
1.0
0.8
0.6
0.4
0.2
0
N(0)/N_0
0.01
(0.01,0.9)
(0.01,0.6)
0.6
(0.6,0.9)
0.995
0
0.2
0.4
0.6
0.8
1.0

Fig. 2.4 a) Several D(t) curves for the set of scattering DOS I (ϵ_0=1.00, ϵ_1=0.53, ϵ_2=0.94). The curves are labeled by reduced impurity concentration, α/α_c.

b) Some D(t) curves for the scattering parameters DOS II (ϵ_0=0.25, ϵ_1=0.50, ϵ_2=1.0), labeled as in a).

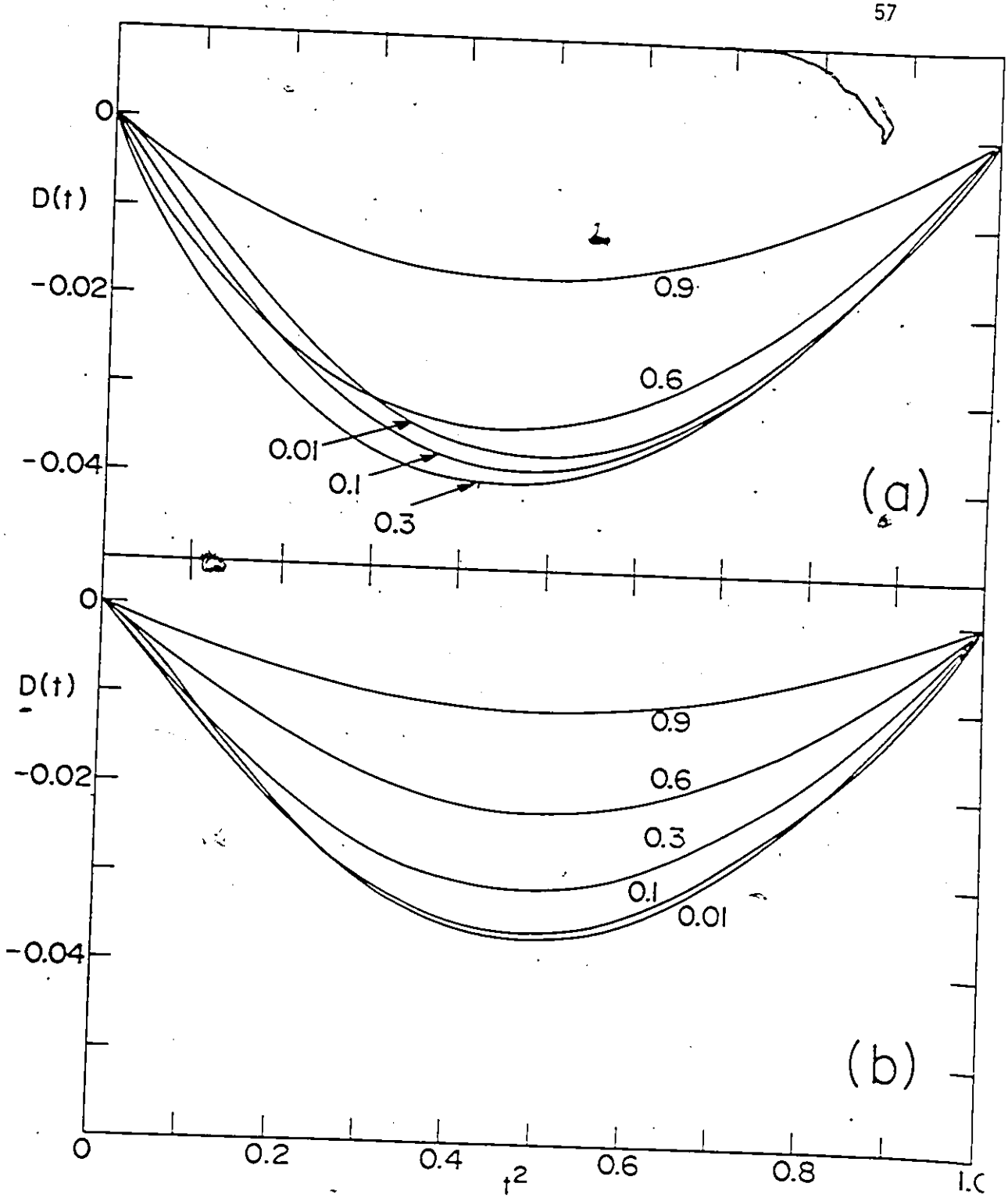
0
D(t)
-0.02
-0.04
0.9
0.6
0.01
0.1
0.3
(a)
0
D(t)
-0.02
-0.04
0.9
0.6
0.3
0.1
0.01
(b)
0
0.2
0.4
t²
0.6
0.8
1.0

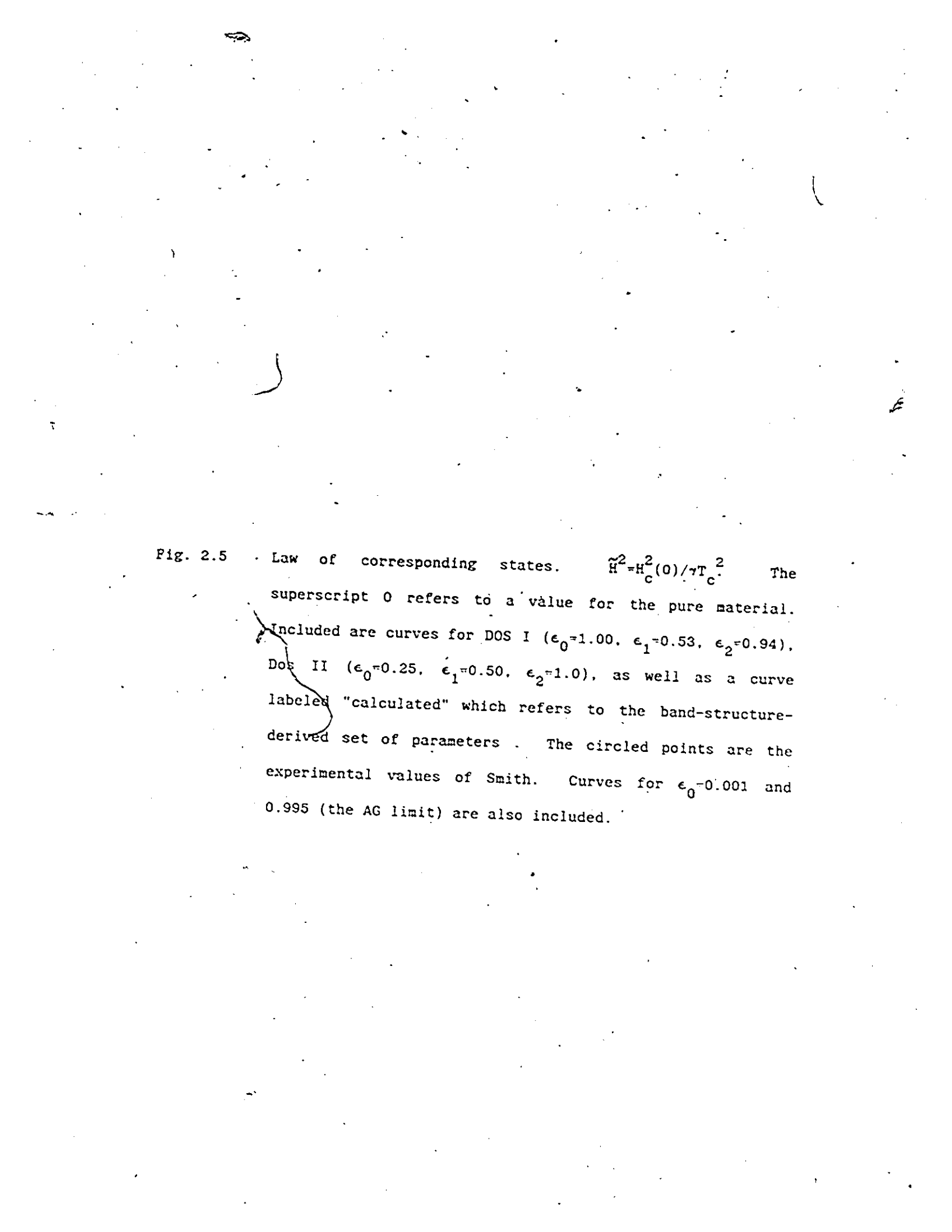

Fig. 2.5 Law of corresponding states. $\tilde{H}^2 = H_c^2(0)/\gamma T_c^2$. The superscript 0 refers to a value for the pure material. Included are curves for DOS I (ϵ_0=1.00, ϵ_1=0.53, ϵ_2=0.94), Dos II (ϵ_0=0.25, ϵ_1=0.50, ϵ_2=1.0), as well as a curve labeled "calculated" which refers to the band-structure-derived set of parameters . The circled points are the experimental values of Smith. Curves for ϵ_0=0.001 and 0.995 (the AG limit) are also included.

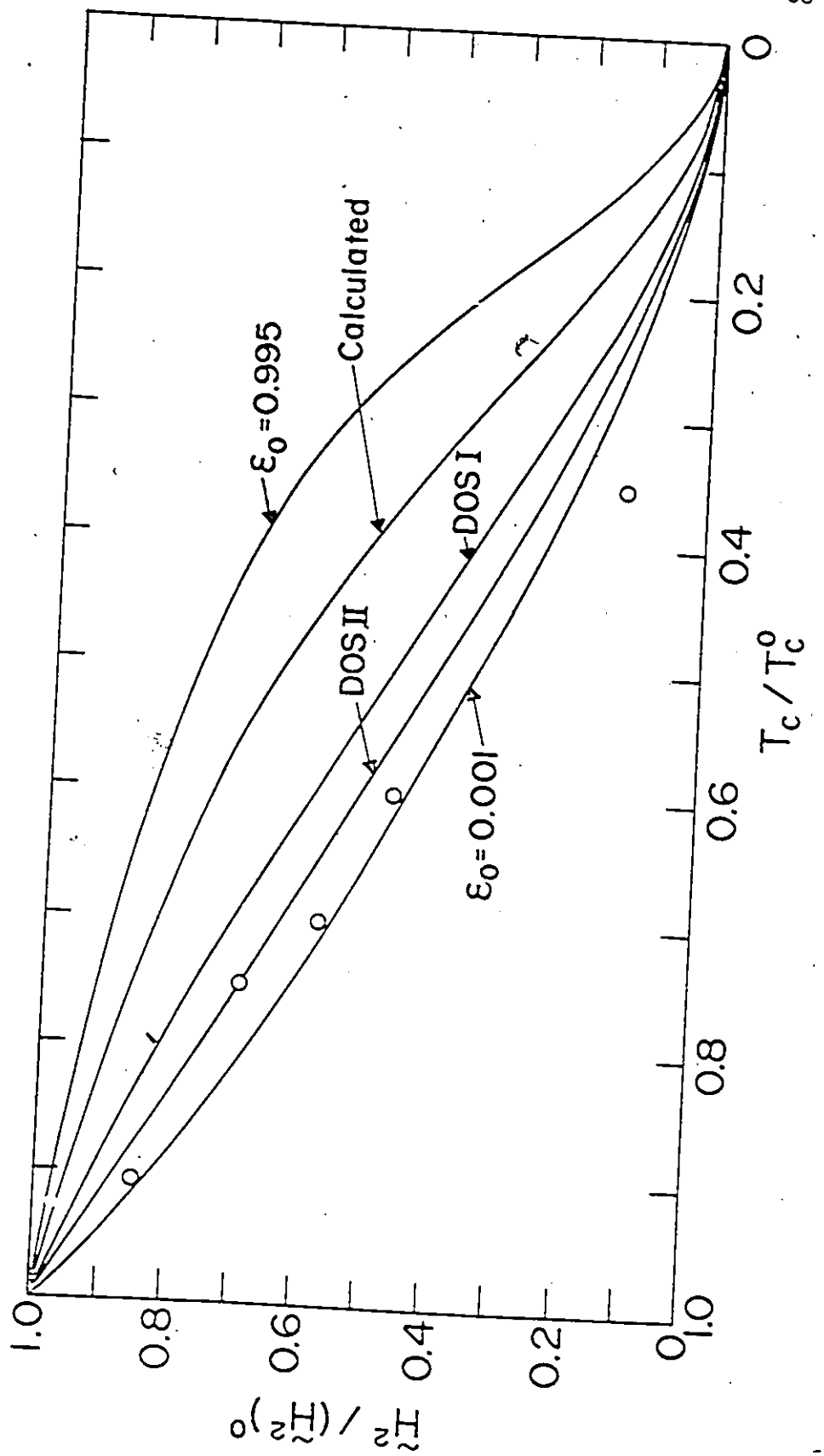
$\tilde{H}^2 / (\tilde{H}^2)^0$
1.0
0.8
0.6
0.4
0.2
0
T_c / T_c^0
0
0.2
0.4
0.6
0.8
1.0
$\varepsilon_0 = 0.995$
Calculated
DOS II
DOS I
$\varepsilon_0 = 0.001$

Fig. 2.6 a) Typical electromagnetic absorption curve for a single phase shift (ϵ_0=0.5) for an impurity concentration, α, of 10% of the critical value, α_c, at T=0. The features labeled A-C arise from the qualitatively distinct quasiparticle scattering processes indicated in b).

b) Density of states $N(\omega)/N_0$ for the same parameters as in a). The arrows labeled A-C represents the quasiparticle scatterng processes responsible for the similarly labeled features of the absorption curve in a).

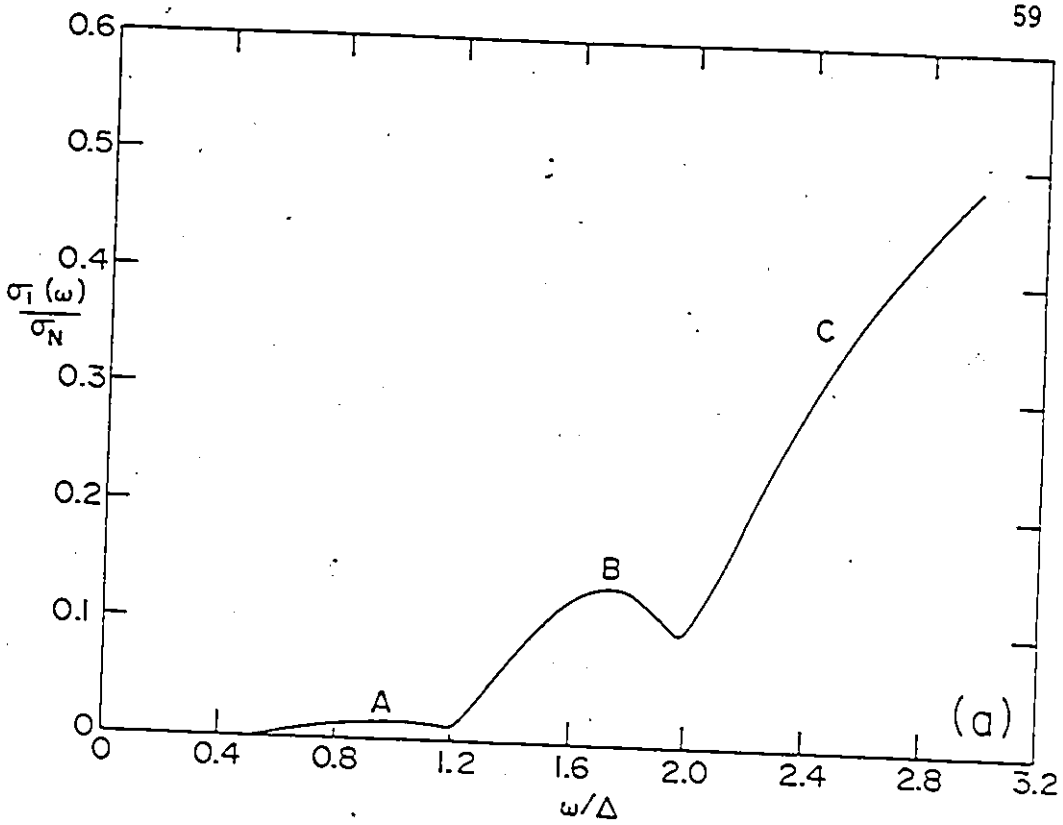
0.6
0.5
0.4
0.3
0.2
0.1
0
$\frac{\sigma_1(\omega)}{\sigma_N}$
A
B
C
(a)
0
0.4
0.8
1.2
1.6
2.0
2.4
2.8
3.2
ω/Δ

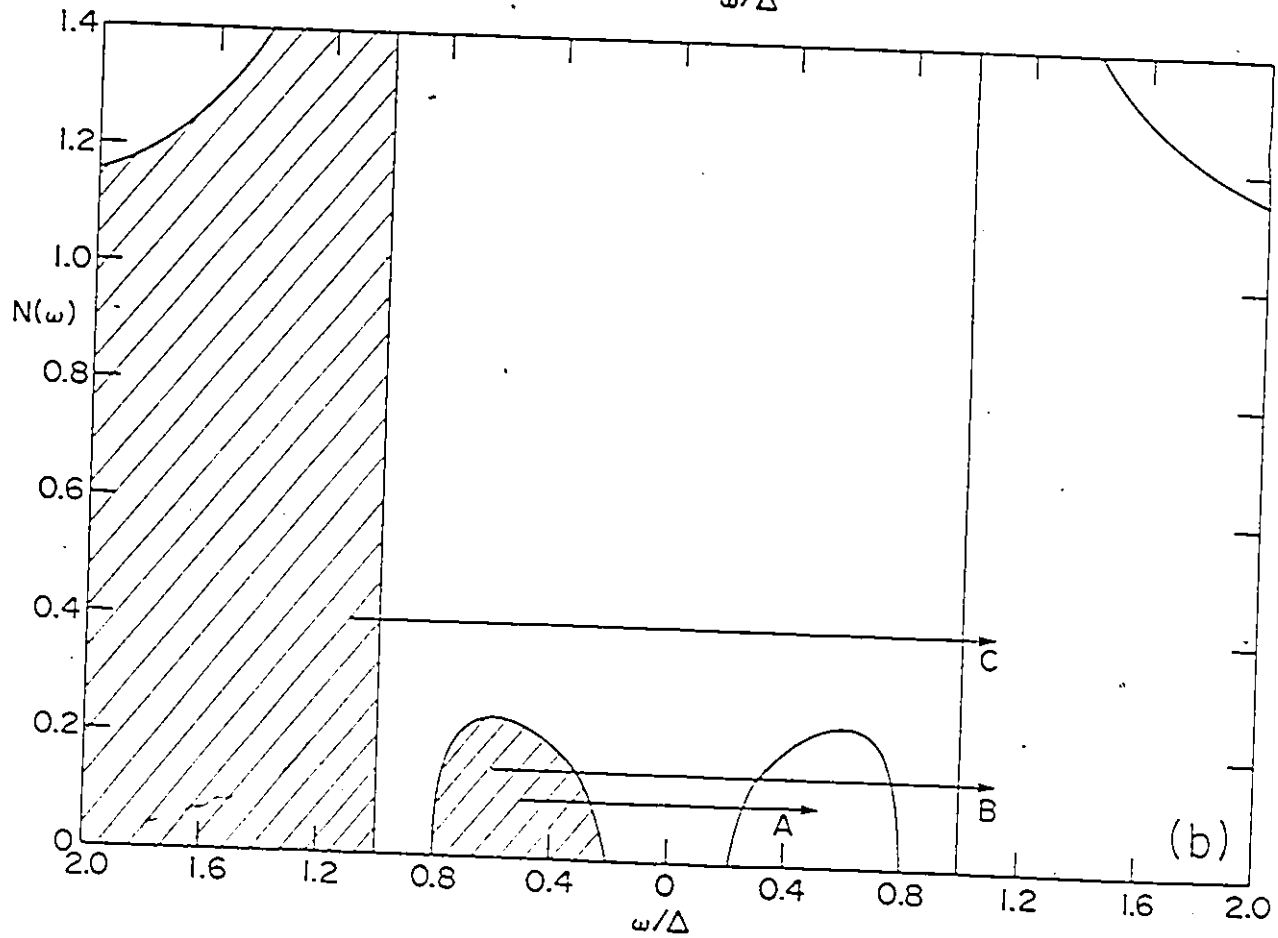
1.4
1.2
1.0
N(ω)
0.8
0.6
0.4
0.2
0
C
B
A
(b)
2.0
1.6
1.2
0.8
0.4
0
0.4
0.8
1.2
1.6
2.0
ω/Δ

Fig. 2.7 a) Electromagnetic absorption curves for the scattering parameter ϵ_0=0.5, reduced impurity concentration α/α_c=0.1, and various temperatures. The curves are labeled by reduced temperature $t=T/T_c$:

t=0.0 (————),

t=0.2 (.......),

t=0.5 (-------),

t=0.8 (-.-.-.-).

b) Density of states $N(\omega)/N_0$ for ϵ_0=0.5, α/α_c=0.1, and T/T_c=0.5 . The shaded areas represent occupied states and unshaded regions indicate unoccupied states. The arrows labeled D and D' represent the low-energy absorption processes which give rise to the peak at zero frequency labeled D in a). The corresponding stimulated emission processes have not been indicated in order to minimize the clutter. The arrows labeled E represent the absorption processes and those labeled e the stimulated emission processes which lead to the peak in the absorption labeled E in a). Of course events of the types labeled A-C in Fig. 2.6b) also contribute at finite temperature.

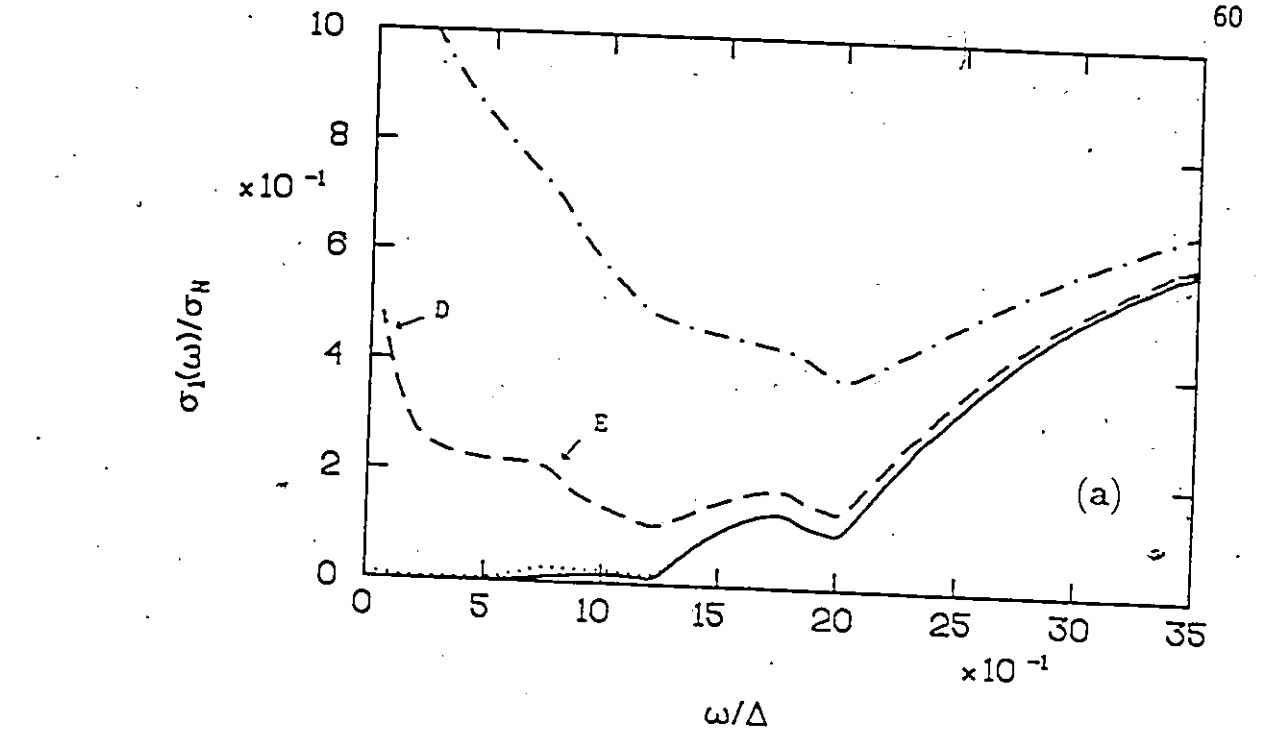
10
8
×10⁻¹
6
4
2
0
σ1(ω)/σN
D
E
(a)
0
5
10
15
20
25
30
35
60
×10⁻¹
ω/Δ

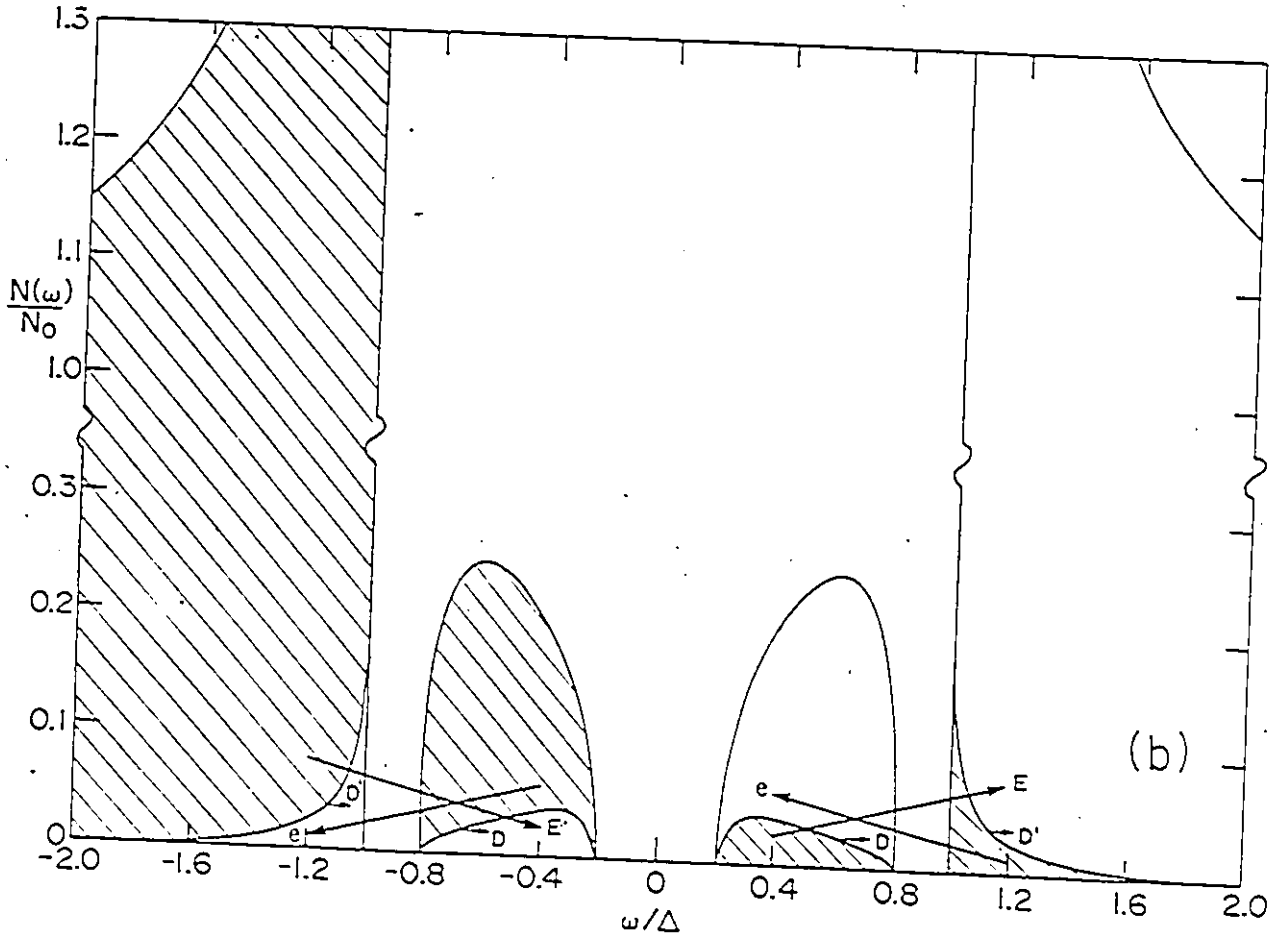
1.3
1.2
1.1
N(ω)/N0
1.0
0.3
0.2
0.1
0
-2.0
-1.6
-1.2
-0.8
-0.4
0
0.4
0.8
1.2
1.6
2.0
ω/Δ
D
e
D
E
e
D
E
D'
(b)

Fig. 2.8 The electromagnetic absorption of Pb-Mn alloys using the scattering parameter set I: ϵ_0=0.985, ϵ_1=0.967, and ϵ_2=0.970 . The curves are labeled by reduced critical temperature T_c/T_c^0:

T_c/T_c^0=0.95 (————),

T_c/T_c^0=0.86 (.....),

T_c/T_c^0=0.76 (-------),

and are all for an absolute temperature of T=1.5 K. The experimental points are due to Dick and Reif[7], and were rescaled as described in the text.

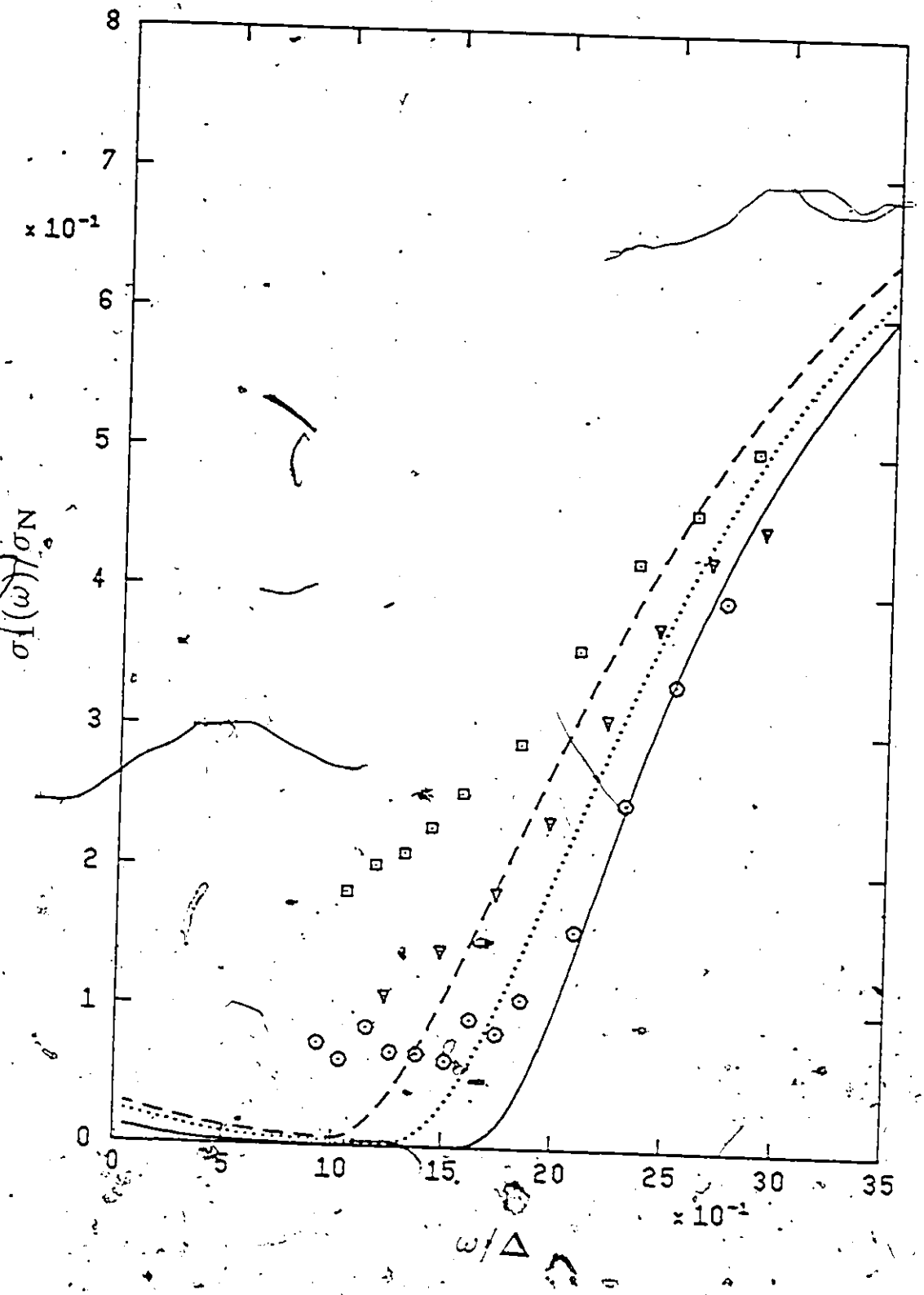
8
7
x 10⁻¹
6
5
4
3
2
1
0
σ1(ω)/σN
0
5
10
15
20
25
30
35
x 10⁻¹
ω/Δ

Fig. 2.9 The electromagnetic absorption of Pb-Mn alloys using the scattering parameter set II: ϵ_0=0.959, ϵ_1=-0.680, and ϵ_2=0.990 . The curves are labeled by reduced critical temperature T_c/T_c^0 as in Fig. 2.8 and are all for an absolute temperature of T=1.5 K. The experimental points are due to Dick and Reif[7] and were rescaled as described in the text.

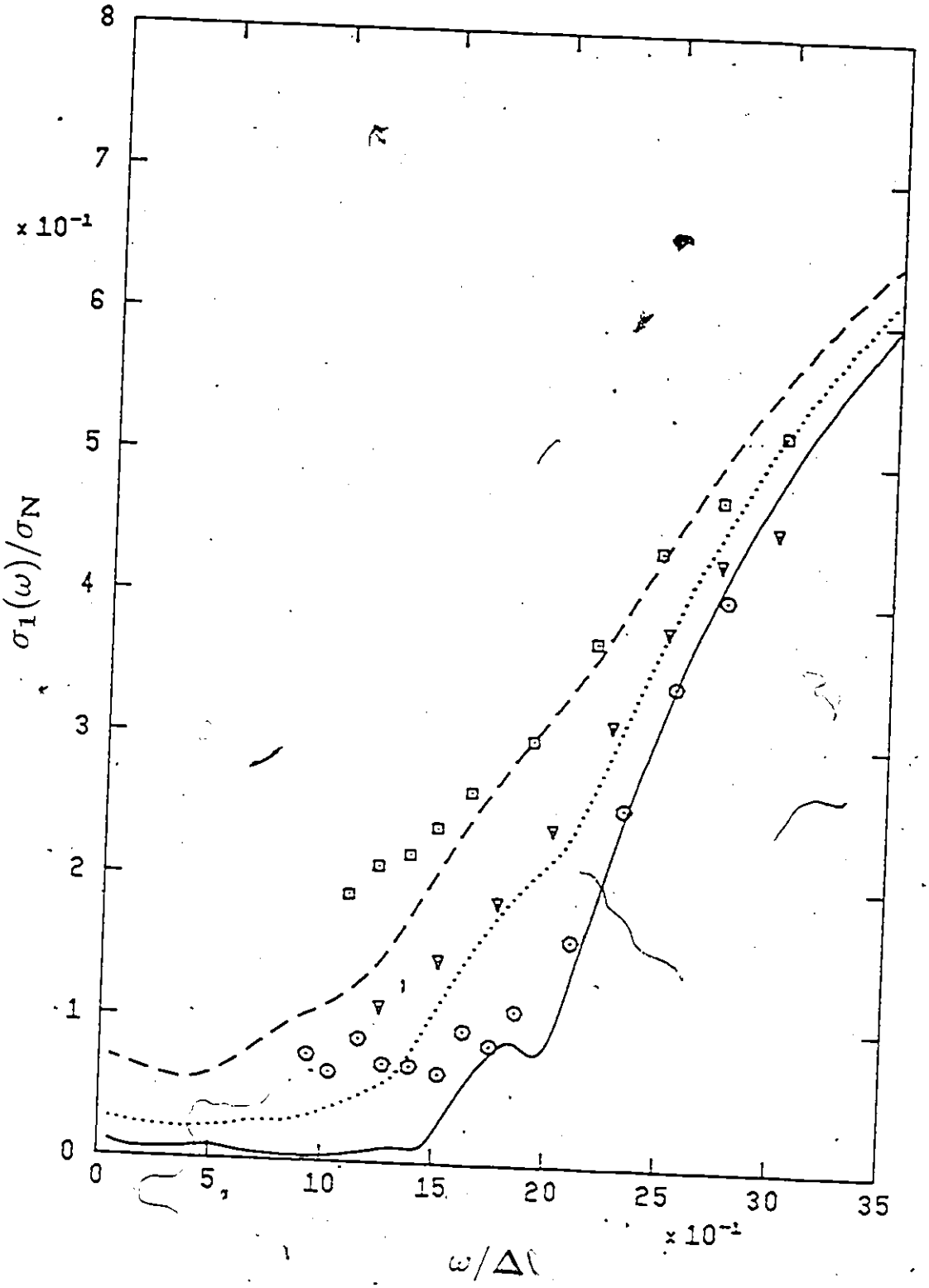
8
7
x 10⁻¹
6
5
4
3
2
1
0
σ1(ω)/σN
0
5
10
15
20
25
30
35
x 10⁻¹
ω/Δ(

Fig. 2.10 The electromagnetic absorption of Pb-Mn alloys using the scattering parameter set of Bauriedl *et al.*[35]: $\epsilon_0=0.23$ and $\epsilon_1=0.79$. The curves are labeled by reduced critical temperature T_c/T_c^0 as in Fig. 2.8 and are all for an absolute temperature of T=1.5 K. The experimental points are due to Dick and Reif[7], and were rescaled as described in the text.

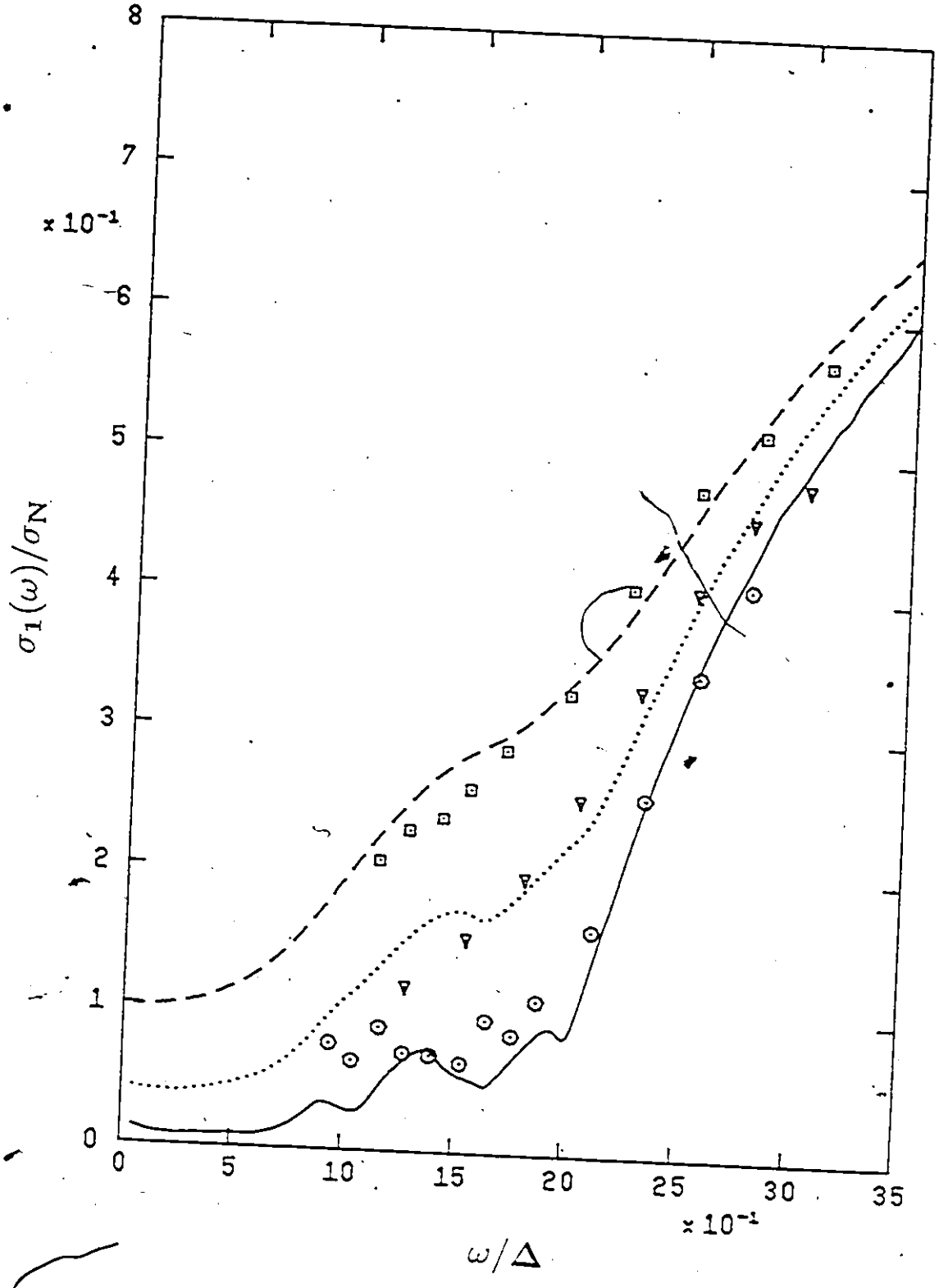
8
7
x 10⁻¹
6
5
4
3
2
1
0
σ1(ω)/σN
0
5
10
15
20
25
30
35
x 10⁻¹
ω/Δ

Fig. 2.11 The zero temperature electromagnetic coherence length ξ_0 normalized to the value for the pure material ξ_{00} and multiplied by the reduced critical temperature T_c/T_c^0 as a function of the SR scattering paramter ϵ_0. This quantity is predicted to be unity by the BCS law of corresponding states. The solid curves were calculated from (2.60), (2.68), and (2.73); the dashed curves used equation (4) of Ref. 39 instead of (2.68b). The curves are labeled by reduced critical temperature T_c/T_c^0.

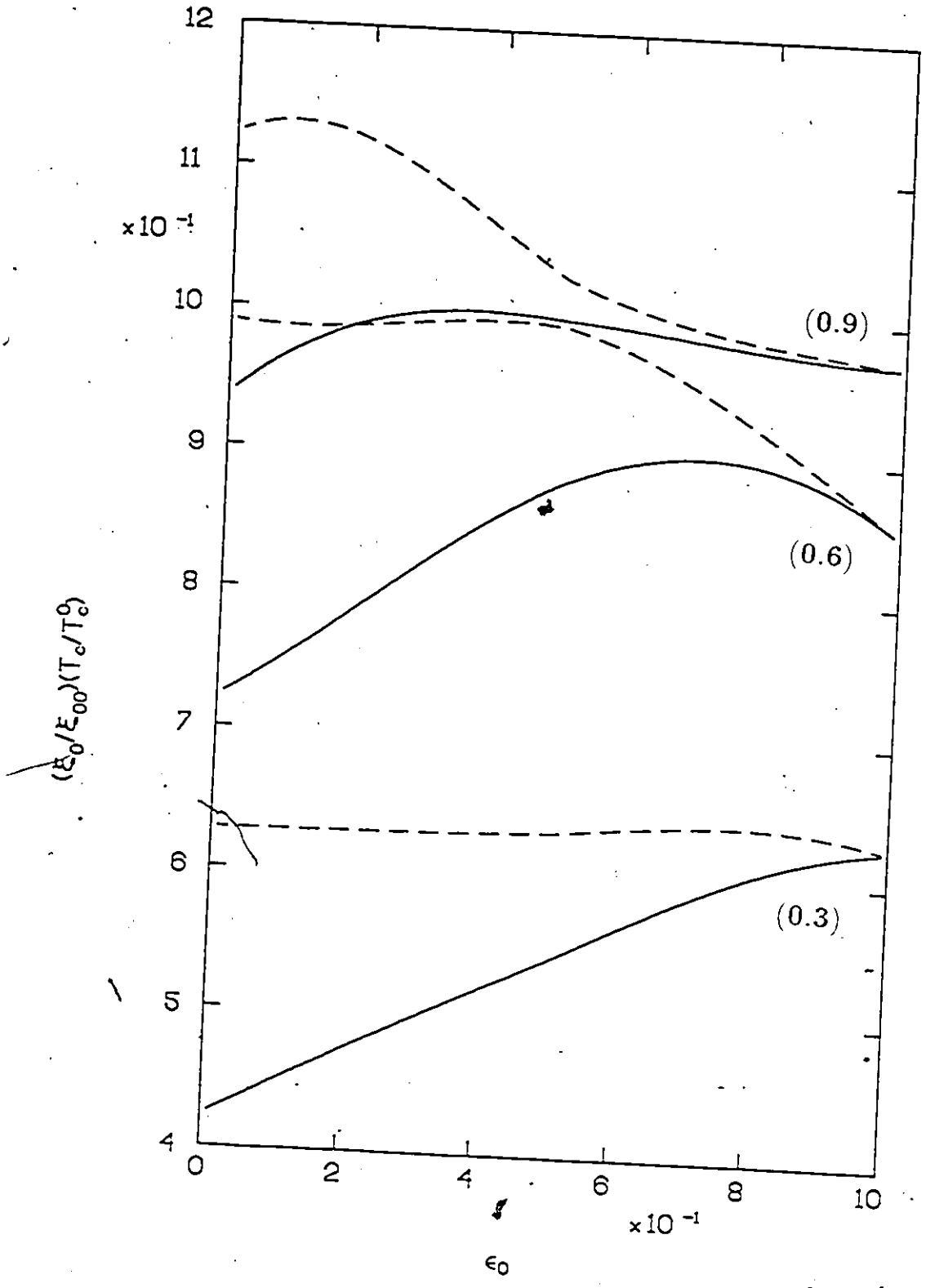
12
11
×10⁻¹
10
9
8
7
6
5
4
0
2
4
6
8
10
×10⁻¹
(0.9)
(0.6)
(0.3)
(ξ0/ξ00)(Tc/Tc0)
ε0

Fig. 2.12 : The reduced zero temperature coherence length ξ_0/ξ_{00} as a function of reduced SR paramagnetic impurity concentration α/α_c for the scattering parameter $\eta_0=1.0$ with ϵ_0 as follows:

$\epsilon_0=0.99$ (————),

$\epsilon_0=0.75$ (.....),

$\epsilon_0=0.50$ (-------),

$\epsilon_0=0.25$ (-.-.-.-),

$\epsilon_0=0.01$ (-..-..-).

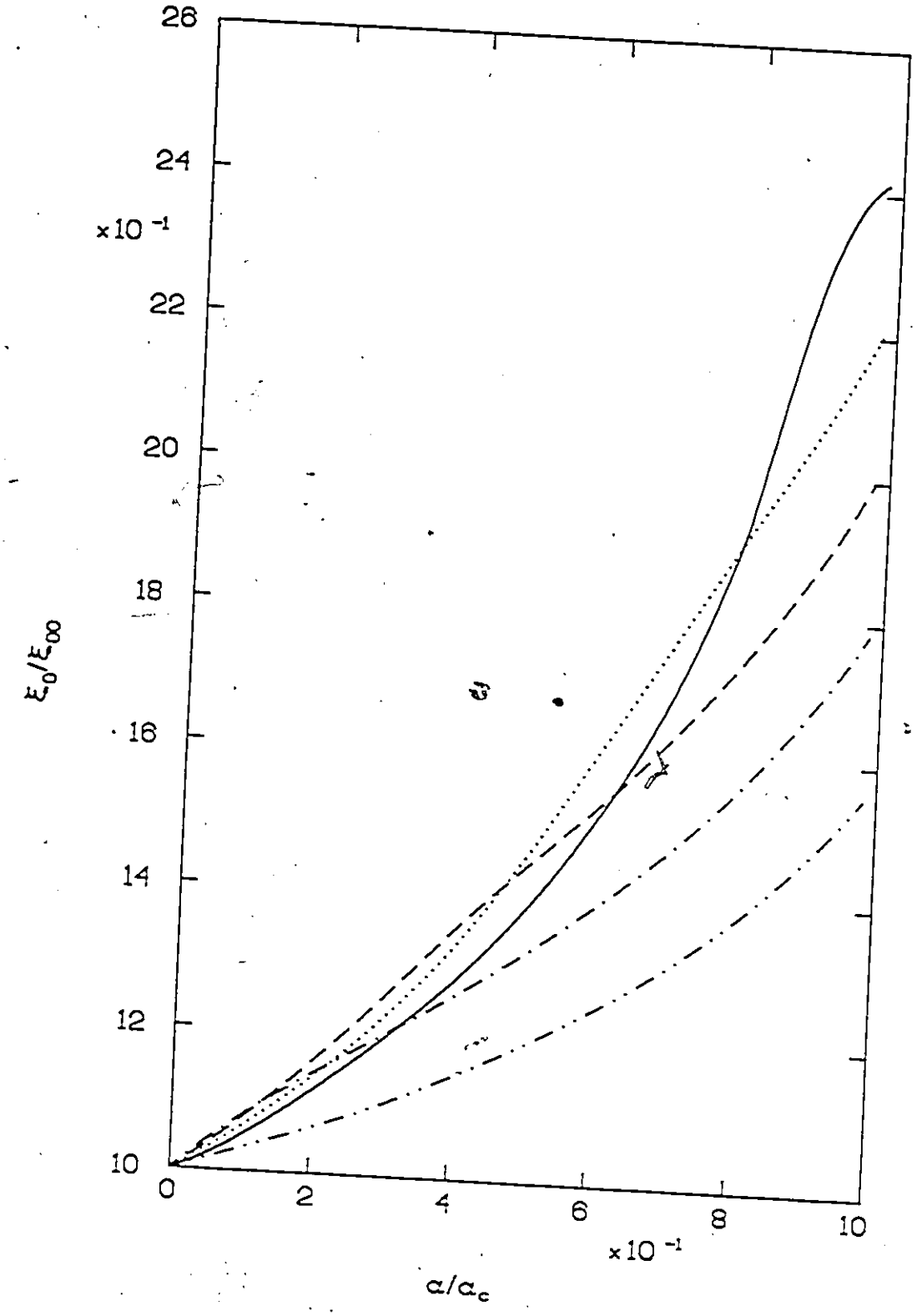
26
24
x10 -1
22
20
18
16
14
12
10
0
2
4
6
8
10
x10 -1
ξ0/ξ∞
α/αc

Fig. 2.13 The temperature dependence of the reduced electromagnetic coherence length $\xi(T)/\xi_{00}$ as a function of reduced temperature T/T_c for a concentration of SR impurities $\alpha/\alpha_c=0.5$ ($T_c/T_c^0\simeq 0.63$) and scattering parameter $\eta_0=1.0$ with ϵ_0 as follows:

$\epsilon_0=0.99$ (———).

$\epsilon_0=0.75$ (.....).

$\epsilon_0=0.50$ (-------).

$\epsilon_0=0.25$ (-.-.-.-).

$\epsilon_0=0.01$ (-..-..-).

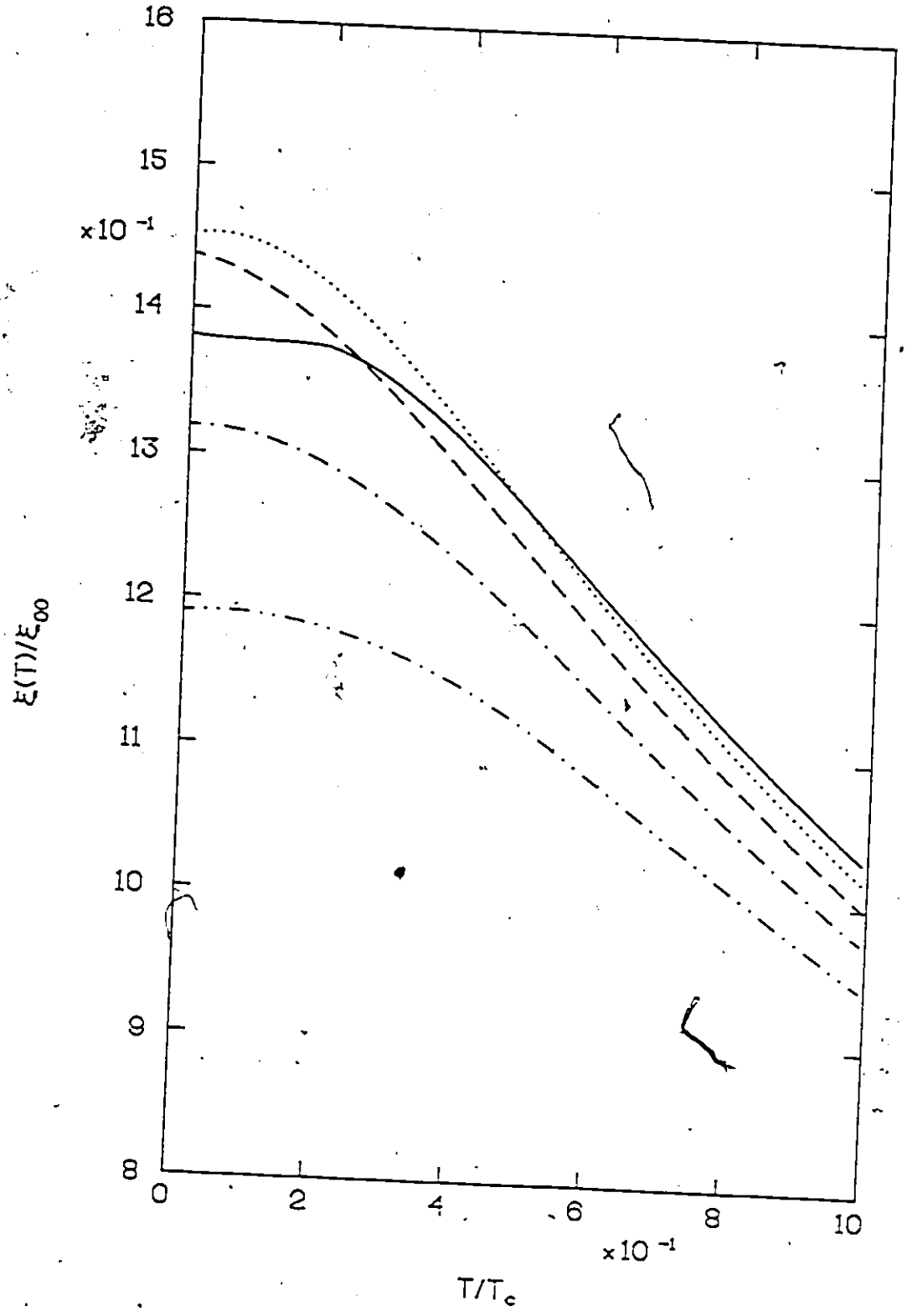
16
15
x10 -1
14
13
12
11
10
9
8
ξ(T)/ξ∞
0
2
4
6
8
10
x10 -1
T/Tc

Fig. 2.14 a) The reduced zero temperature electromagnetic coherence length as a function of reduced SR impurity concentration α/α_c for ϵ_0=0.5 and η_0=1.0 (———) corresponding to no normal scattering, and η_0=-0.5 (.....) corresponding to the maximum amount of normal scattering consistent with this value of ϵ_0.

b) The temperature dependence of the electromagnetic coherence length for α/α_c=0.5, ϵ_0=0.5 and the following scattering paramters:

η_0=1.0 (———).

η_0=0.7071 (. . . . . .).

η_0=0.0 (- - - - - -).

η_0=-0.5 (-.-.-.-).

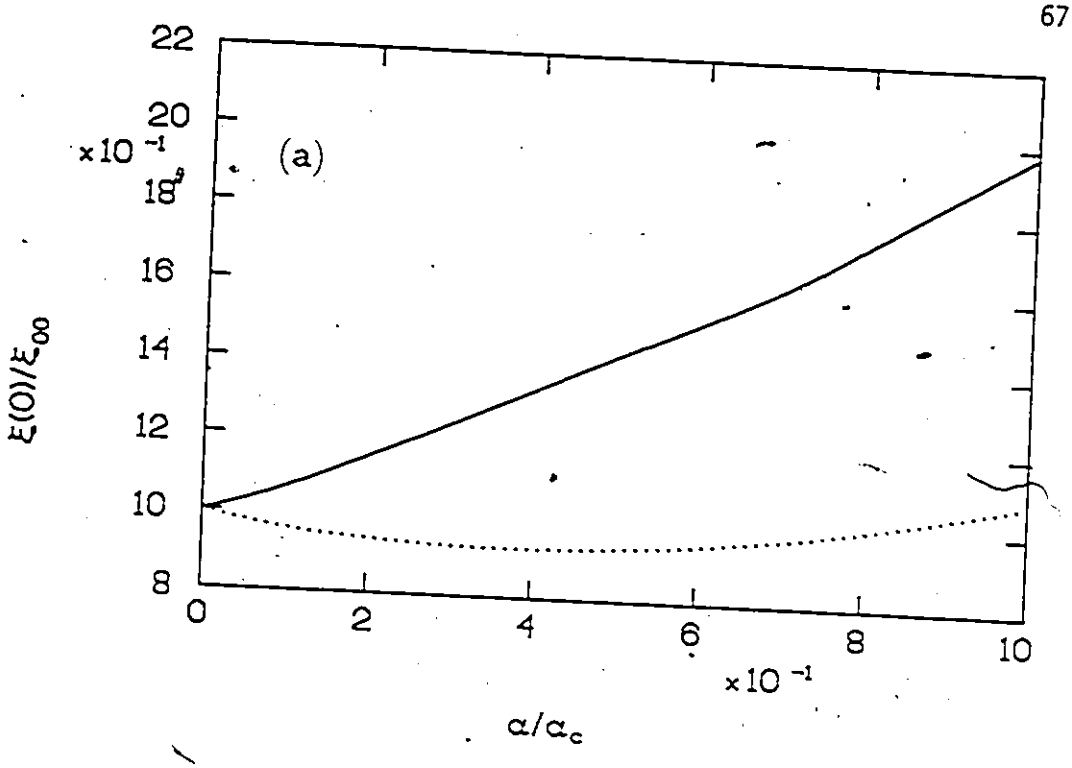
22
20
18
16
14
12
10
8
x10 -1
(a)
ξ(0)/ξ∞
0
2
4
6
8
10
x10 -1
α/αc

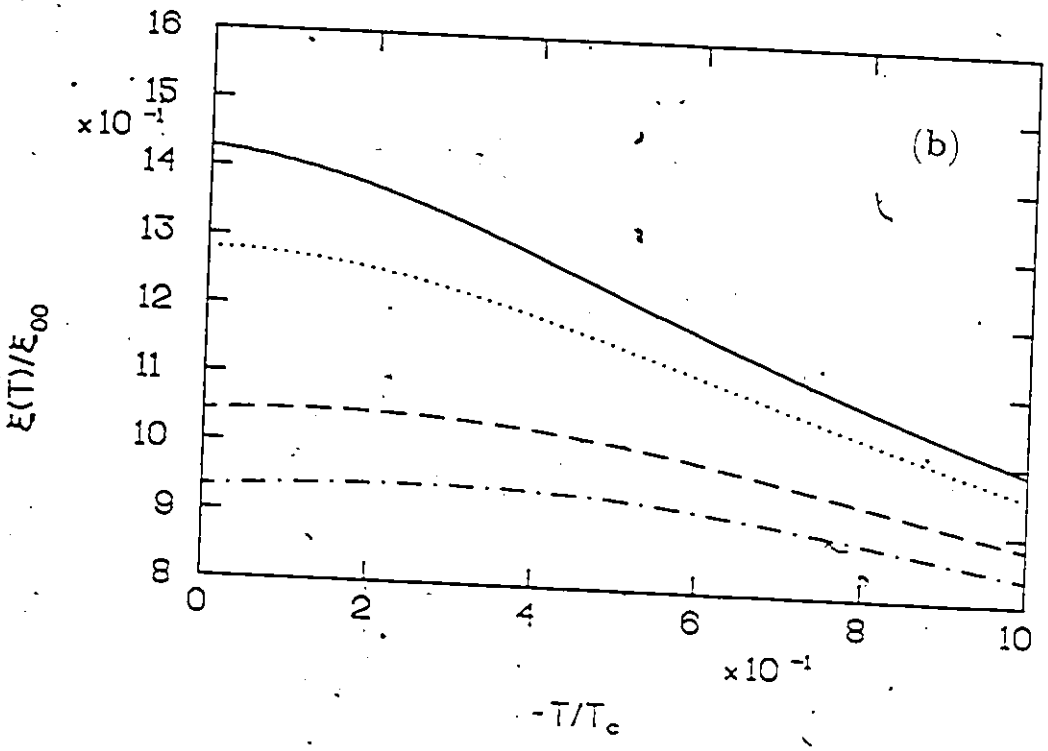
16
15
14
13
12
11
10
9
8
x10 -1
(b)
ξ(T)/ξ∞
0
2
4
6
8
10
x10 -1
-T/Tc

Fig. 2.15 The electronic contribution to the thermal conductivity κ_S divided by the normal state value κ_N as a function of reduced temperature T/T_c for Zn-Mn. The curves were calculated using $2\Delta_0/T_c^0=3.4$, $T_c/T_c^0=0.794$ and various SR scattering parameters:

(————) $\epsilon_0=0.7$,

(.....) Zn-Mn I, $\epsilon_0=1.00$, $\epsilon_1=0.53$, $\epsilon_2=0.94$, and

(-------) Zn-Mn II, $\epsilon_0=0.25$, $\epsilon_1=0.50$, $\epsilon_2=1.00$. The experimental points are from Ref. 41.

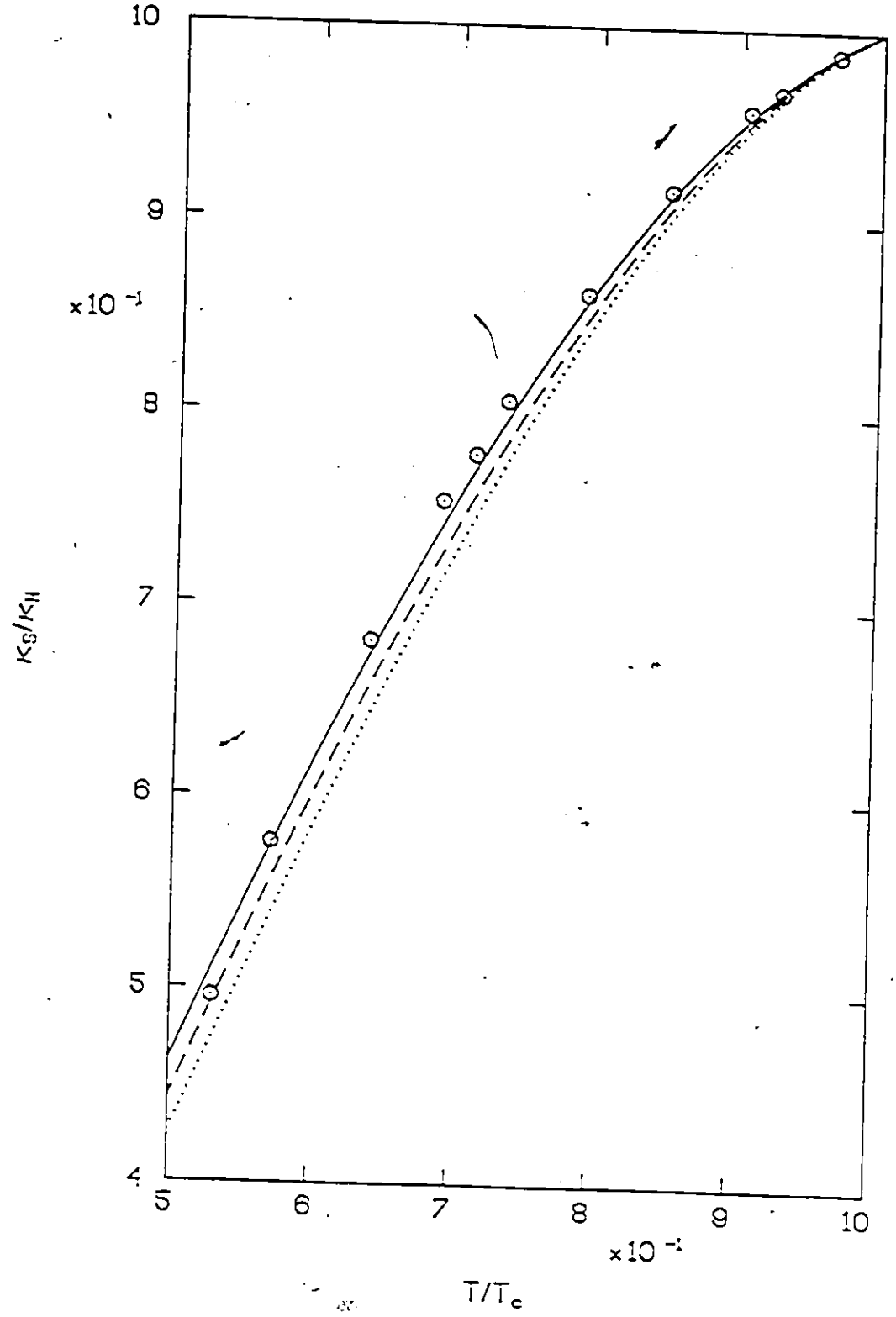
10
9
8
7
6
5
4
$\times 10^{-1}$
K_S/K_N
5
6
7
8
9
10
$\times 10^{-1}$
T/T_c

Fig. 2.16 The total quasiparticle scattering rate $\frac{1}{\tau_1(T)}$ normalized to the value at the highest experimental temperature $\left[\frac{1}{\tau_1(1)}\right]$ as a function of temperature. The points were calculated from (2.77-78) and the normal state thermal conductivity data from Ref. 41, with the circles corresponding to the 11.7 ppm sample and the squares to the 10.0 ppm sample. The lines through the points are merely guides for the eye and were not calculated from any theory.

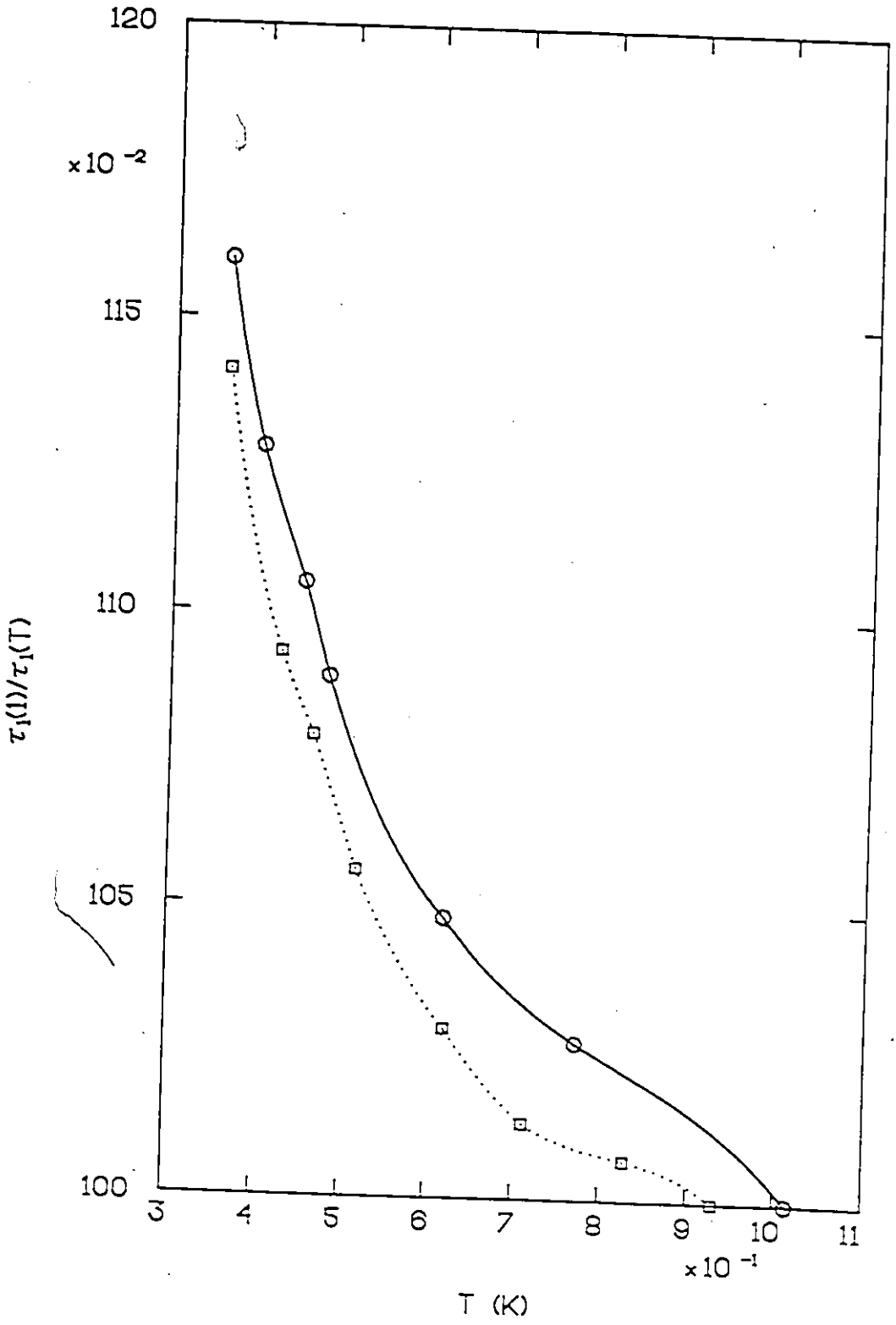
120
x10 -2
115
110
105
100
$\tau_1(1)/\tau_1(T)$
3
4
5
6
7
8
9
10
11
x10 -1
T (K)

Fig. 2.17 The electronic thermal conductivity in the superconducting state κ_S for Zn-Mn divided by the normal state value κ_N as a function of temperature for T_c/T_c^0=0.630 and the scattering set Zn-Mn II. The solid line was calculated using the temperature dependent scattering rate $\frac{1}{\tau_1(T)}$ shown in Fig. 2.16 as squares, the dotted line with a temperature independent scattering rate. The experimental points are from the 10.0 ppm sample (Fig. 5(e)) of Ref. 41.

b) As in a) except with T_c/T_c^0=0.540 and with the temperature dependence of the scattering rate used in the calculation of the solid curve given by the circles of Fig. 2.16. The experimental points are from the 11.7 ppm sample (Fig. 5(f)) of Ref. 41.

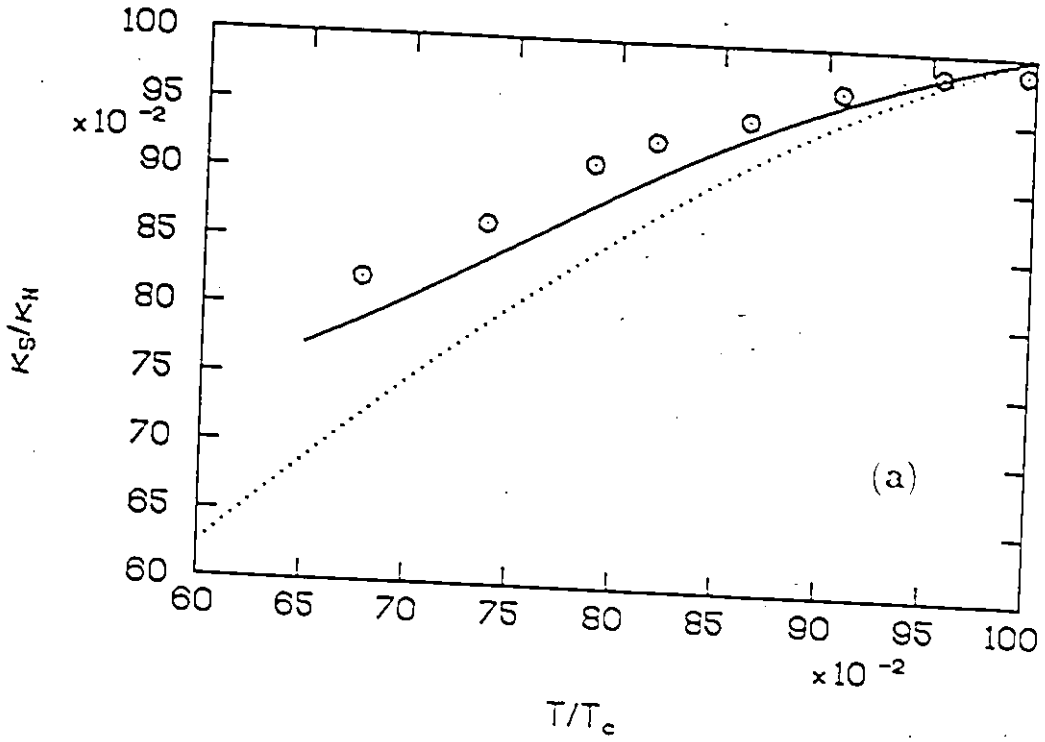
100
95
x10 -2
90
85
80
75
70
65
60
60 65 70 75 80 85 90 95 100
x10 -2
κ_S/κ_N
T/T_c
(a)

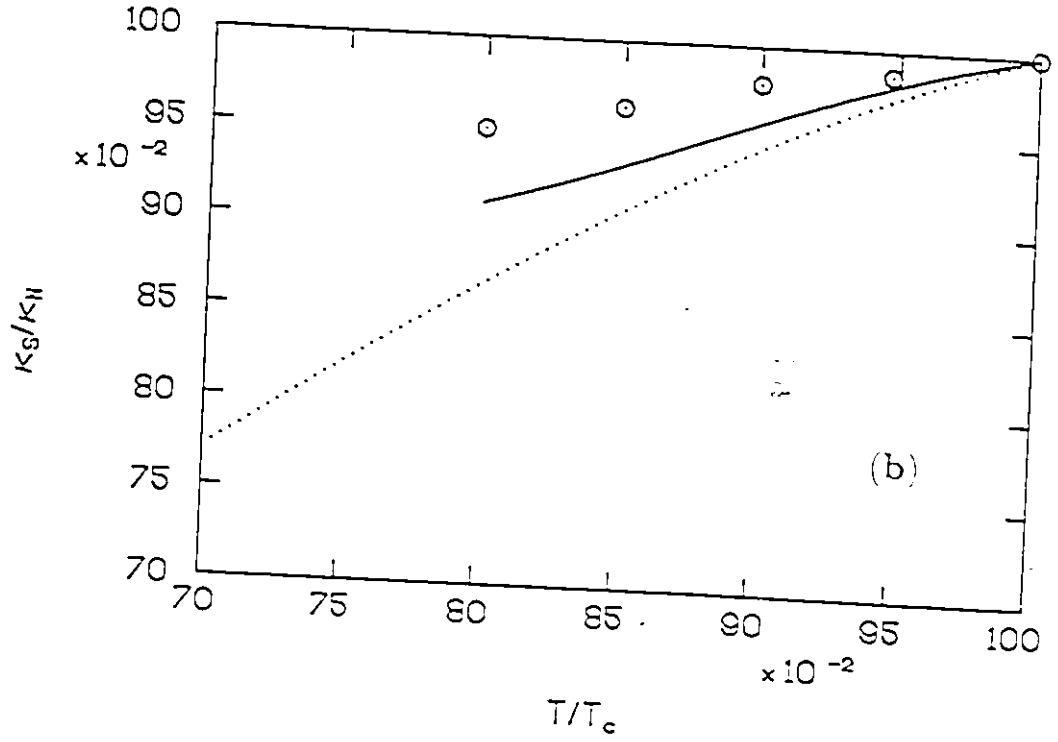
100
95
x10 -2
90
85
80
75
70
70 75 80 85 90 95 100
x10 -2
κ_S/κ_N
T/T_c
(b)

Fig. 2.18 The electronic thermal conductivity κ_S/κ_N for Pb-Mn as a function of the reduced temperature for T_c/T_c^0=0.766, with $2\Delta_0/T_c^0$=4.32 and the scattering parameters:

(————) Pb-Mn I, ϵ_0=0.985, ϵ_1=0.967, ϵ_2=0.970,

(.....) Pb-Mn II, ϵ_0=0.959, ϵ_1=-0.680, ϵ_2=0.970. The experimental data are of Sample B from Fig. 1 of Ref. 41.

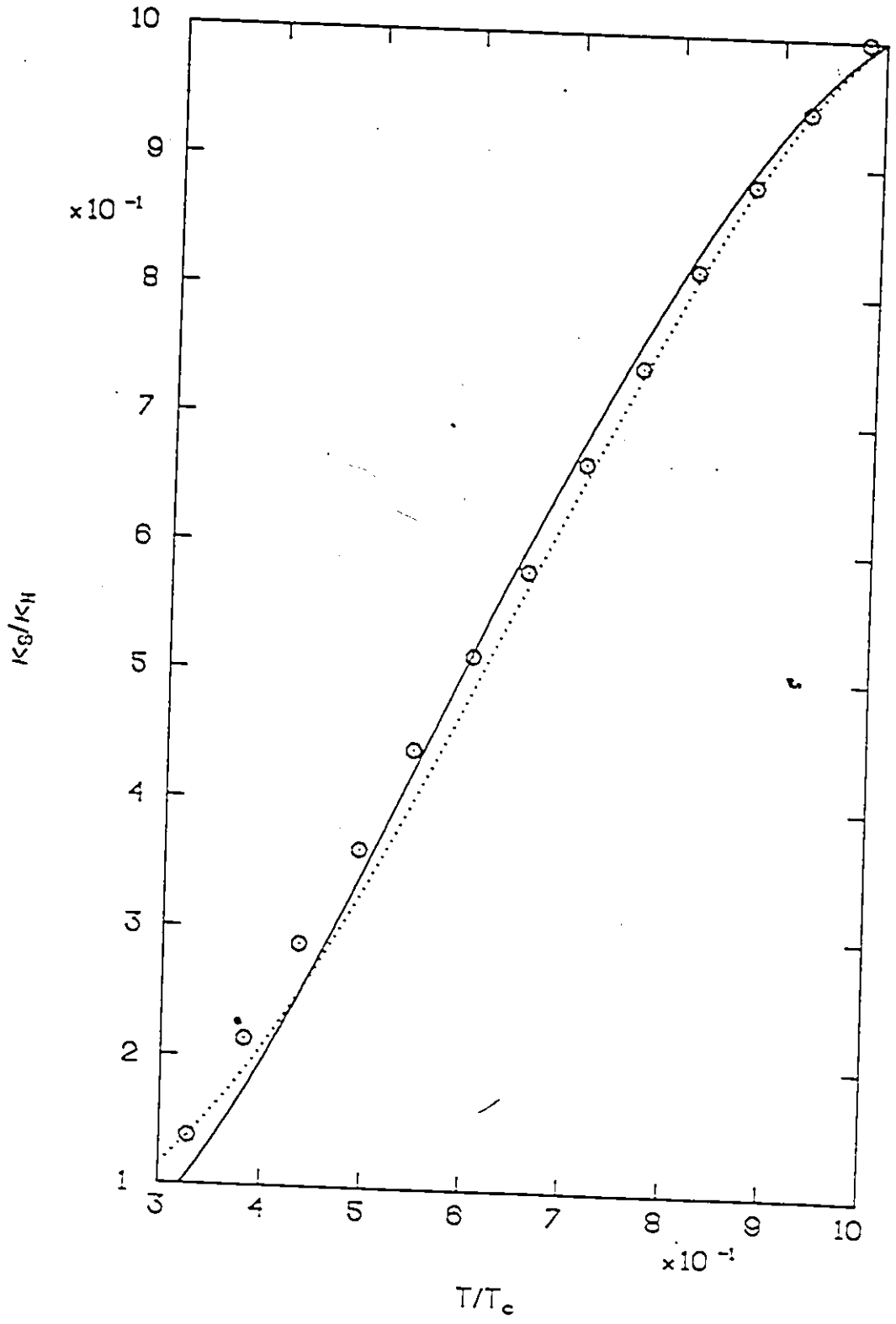
10
9
x10 -1
8
7
6
5
4
3
2
1
3
4
5
6
7
8
9
10
x10 -1
K_S/K_H
T/T_c

Fig. 2.19 The electronic thermal conductivity κ_S/κ_N for In-Mn. The reduced critical temperature was T_c/T_c^0=0.614, with $2\Delta_0/T_c^0$=3.88 and the scattering parameters ϵ_0=0.962, ϵ_1=0.840, ϵ_2=0.991 . The experimental points are from Fig. 4 of Ref. 46.

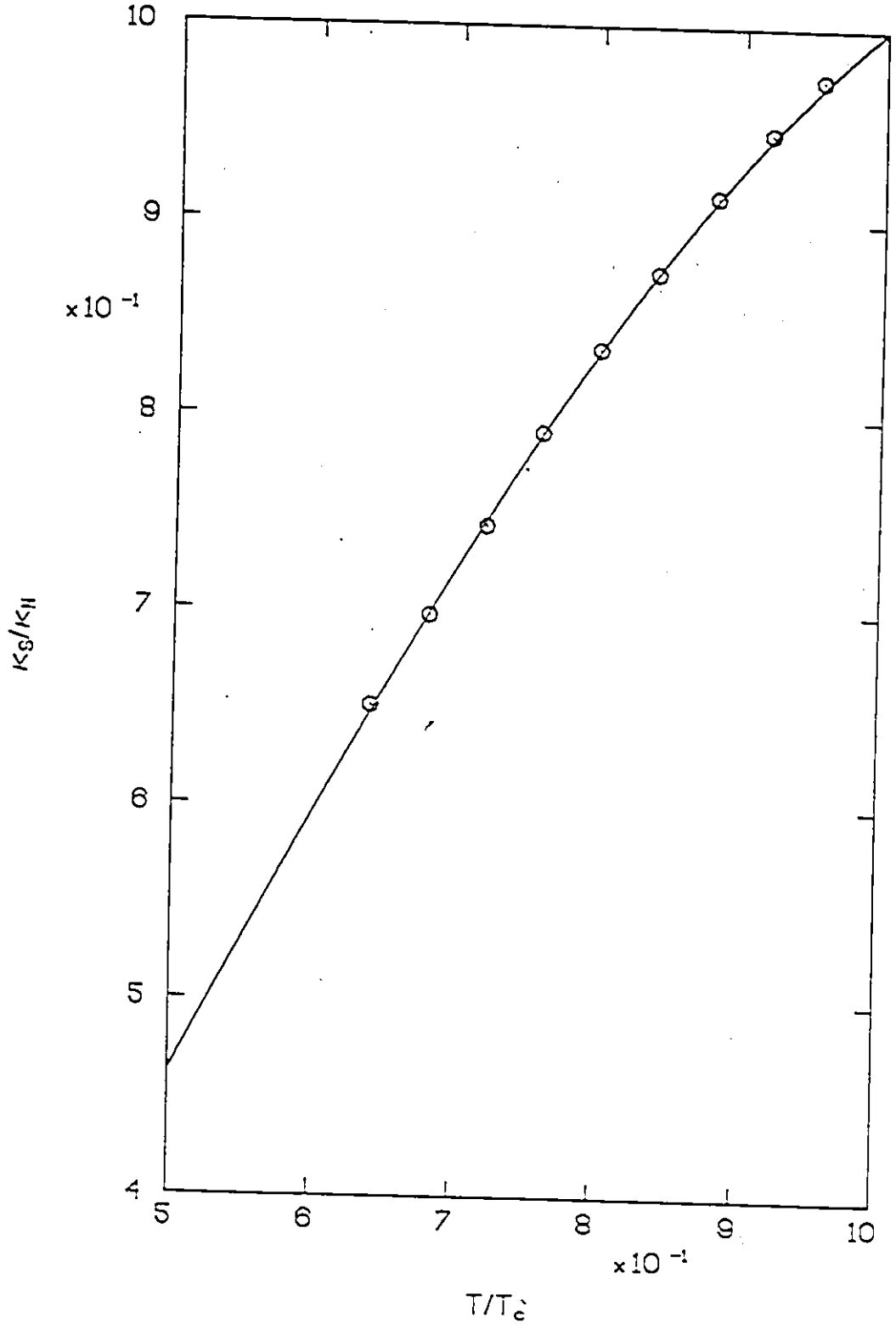
10
9
x10 -1
8
7
6
5
4
κ_s/κ_{11}
5
6
7
8
9
10
x10 -1
T/T_c

CHAPTER III

INTERACTING MAGNETIC SYSTEMS

3.1 Introduction

The results presented in Chapter II were restricted to the case of a dilute concentration of paramagnetic impurities in a superconducting host. It was recognized quite early in the development of both AG and SR theories that while the approximation of noninteracting spins may be good for some alloy systems, some type of magnetic ordering may occur in other cases. At that time, the possible types of order were generally postulated to be either ferromagnetic or antiferromagnetic, the kinds of order most commonly seen in stoichiometric magnetic compounds.

Ferromagnetic order and conventional superconductivity are quite antagonistic, and are generally believed to be incompatible. Stated simply, the macroscopic exchange field associated with ferromagnetically ordered ions results in splitting of the spin-up and -down conduction electron bands, and the formation of Cooper pairs is no longer energetically favorable. On the other hand, in the antiferromagnetic case there is no macroscopic exchange field, and this type of order has recently been found to coexist with superconductivity in some ternary compounds (see Maple and Fischer in Ref. (49) for an introduction and further references).

Other ternary compounds such as $ErRh_4B_4$[50] and $HoMo_6S_8$[51] have been found to be reentrant ferromagnets: that is superconductivity exists in a temperature range $T_{c2}<T<T_{c1}$, and below T_{c2} the superconductivity is quenched by a transition to a ferromagnetic phase. The situation is further complicated by the existence of another ordered magnetic phase above the ferromagnetic one, which apparently coexists with superconductivity[52]. This does not contradict the statement that ferromagnetism and superconductivity are incompatible, since this phase is a spiral or helical one. The basic idea here, due to Anderson and Suhl[53], is that if a magnetically ordered phase has no moment upon averaging over length scales of the order of the superconducting coherence length, then superconductivity is not necessarily ruled out. One special case of this picture is the previously mentioned compatability of superconductivity and antiferromagnetism.

The last part of this chapter will be concerned with calculations of some properties of reentrant ferromagnetic superconductors in the paramagnetic region. A simplified version of a model due to Lee[54] will be used to include the effect of the interacting spin system on the superconducting electrons.

It has also become apparent within the last fifteen to twenty years that some dilute substitutional magnetic alloys (eg. Ag-Mn, and Cu-Mn) undergo a cooperative magnetic transition of a new kind, which has been called spin-glass ordering (see Binder and Young[55], Fischer[56] or the book by Moorjani and Coey[57] for a recent review of theoretical and experimental aspects of spin-glasses). Experimentally,

spin-glasses are characterised by a cusp in the magnetic susceptibility at a freezing temperature T_f, which at first glance appears similar to that of an antiferromagnet at the Néel temperature. Spin-glasses, however, display only a broad maximum in the magnetic contribution to the specific heat centred slightly above T_f, with no sharp anomaly at T_f. Also, the spin glass transition is not accompanied by the appearance of the characteristic magnetic Bragg peaks in neutron scattering experiments which would indicate the presence of long-range magnetic order.

The coexistence of spin-glass freezing and superconductivity has been observed in a variety of alloy systems. For example, Davidov *et al.*[58] have measured the magnetic susceptibility of $Gd_xTh_{1-x}Ru_2$ for x between 0.0 and approximately 0.14, and have found a Curie-like rise in susceptibility above the superconducting transition for a range of Gd concentrations. In yet higher concentration samples a well defined cusp is seen at a concentration dependent temperature T_m, which when extrapolated to lower concentrations yields a finite ordering temperature below the superconducting T_c for samples where the cusp cannot be observed directly due to the diamagnetism of the superconducting state. These same authors[58] point out that susceptibility measurements on $Gd_xCe_{1-x}Ru_2$ alloys are also indicative of spin-glass ordering, and that $Gd_xLa_{3-x}In$, $La_{1-x}Gd_x$, and $Gd_xLa_{1-x}Al_2$ show typical spin-glass effects for certain concentrations of Gd.

Current theoretical attempts to understand spin-glasses tend to stress the importance of frustration and competing interactions. In the canonical spin-glasses such as dilute Ag-Mn, the spins interact via

the indirect Rudermann-Kittel-Kasuya-Yosida (RKKY) interaction (see for example pp. 239-242 of Ref. (4)). which is mediated via conduction electrons. This interaction oscillates in sign with the separation between spins, and is also of long range. In this case frustration arises due to the positional disorder of the magnetic ions and the oscillation in sign of the exchange interaction with distance. The result is a large number of possible spin configurations with essentially the same energy separated by high energy barriers. At low temperatures these different configurations become inaccessible on a laboratory time scale so that the spins seem frozen in one apparently random configuration.

This spin freezing was first described mathematically by Edwards and Anderson[59] (EA). who introduced their now famous order parameter for the spin-glass as

$$q = \lim_{t\to\infty} \langle \underline{S}_i(t)\cdot\underline{S}_i(0)\rangle \ . \qquad (3.1)$$

which is proportional to the probability that a given spin which has a particular direction at t=0 will still "point" in that direction an infinite time later. This is quite different from the order parameters previously seen in ferromagnetic or antiferromagnetic systems (magnetization or sublattice magnetization) which reflect spatial as well as time correlations. Note that in the absence of a magnetic field, although each spin is essentially fixed in direction, upon averaging over all spins the total spin is zero at all temperatures. Also, although this definition of "spin freezing" has an attractive

conceptual simplicity, the practical application of this idea turns out to be quite complex. For example, in the original approach of EA the randomness of the exchange interaction is modeled by introducing a probability distribution, and then averaging over this distribution. In order to carry out the averaging of the free energy over this distribution of exchange interactions, EA used a novel "replica" approach, and succeeded in finding a new order parameter defined as the configurational average of the equal time spin operators at a given site in different replicas of the system

$$q = \langle\langle \underline{S}_i^{\alpha} \cdot \underline{S}_i^{\beta} \rangle\rangle_J \ . \tag{3.2}$$

Here the superscripts α and β indicate which replica the spin belongs to, and the outer brackets $\langle\ \rangle_J$ represent the configurational average over the distribution of exchange integrals J. The connection between this inter-replica order parameter and the original physically motivated order parameter defined in terms of a long time correlation function is not at all obvious at first glance, and they are in fact not identical (see Fischer[56]).

Significant progress has been made in extending these ideas, both in clarifying the concept of replicas as well as in avoiding the introduction of replicas altogether. However, another approach which explains many properties of spin-glasses regards the freezing as an inherently dynamical process. From this point of view the spin-glass is a metastable nonequilibrium state. It is therefore appropriate to close this brief introduction by pointing out that even now, twelve

years after the work of EA and after a much longer period of experimental observation, there is still no consensus as to whether or not real spin-glasses undergo a phase transition in the conventional sense. From the dynamical point of view the transition to the frozen state is not a conventional phase transition.

Due to the great sensitivity of the superconducting state to all kinds of magnetic effects, the existence of spin glass freezing in a superconducting alloy would be expected to be reflected in superconducting properties. Therefore, in the first half of this Chapter a model of spin-glass superconductors due to Nass, Levin and Grest[60] will be used to calculate some of the effects expected to occur in these systems.

3.2. Gap Equations with Interacting Impurities

The gap equations for a superconductor containing magnetic ions which interact with one another have been given by Nass *et al.*[60], Keller and Benda[61], Maekawa and Tachiki[62] and many others (see Vonsovsky *et al.*[14] for a detailed derivation). Assuming a weak exchange interaction J between conduction electrons and the local moments, the contribution of this scattering may be included to second order in terms of the self-energy

$$\underline{\Sigma}_{\underline{p}}(i\omega_n) = -\frac{J^2}{\beta}\sum_m \int \frac{d^3k}{(2\pi)^3}\, \underline{\underline{\alpha}}\, \underline{\underline{g}}_{\underline{k}}(i\omega_m)\, \underline{\underline{\alpha}}\, \underline{\underline{D}}_{\underline{p}-\underline{k}}(i\omega_n - i\omega_m) \,. \qquad (3.3)$$

Here the notation is the same as that used in Chapter II, with the addition of the spin-fluctuation propagator, which has the spectral representation

$$D_{\underline{q}}(i\nu_n) = \int_0^\infty \frac{d\Omega}{\pi} B(\underline{q},\Omega) \frac{2\Omega}{(i\nu_n)^2 - \Omega^2} . \qquad (3.4)$$

In (3.4) the frequencies $i\nu_n$ are even Matsubara frequencies, and the spectral density B is given as usual in terms of the Fourier transform of the spin-spin correlation function

$$B(\underline{q},\Omega) = \frac{1-e^{-\beta\omega}}{2} [S(\underline{q},\Omega) + \pi <\underline{S}(\underline{q})>\cdot<\underline{S}(-q)>\delta(\Omega)] , \qquad (3.5)$$

where

$$S(\underline{q},\Omega) = \int_{-\infty}^{\infty} dt \int \frac{d^3r}{V} e^{i(\Omega t - \underline{k}\cdot\underline{r})} S(\underline{r},t) ,$$

$$= \int_{-\infty}^{\infty} dt\, e^{i\Omega t} [<\underline{S}(\underline{q},t)\cdot\underline{S}(-\underline{q},0)> - <\underline{S}(\underline{q},0)>\cdot<\underline{S}(-\underline{q},0)>] \qquad (3.6)$$

is the spin-spin correlation function. This correlation function will later be approximated by a hydrodynamic model.

Now the derivation of the gap equations follows from the self energy (3.3) and Dyson's equation (2.15) in much the same manner as the derivation in Chapter II. On the imaginary frequency axis

$$\tilde{\omega}_n = \omega_n + \pi T \sum_m \lambda_{sf}(n-m) \frac{\tilde{\omega}_m}{(\tilde{\omega}_m^2+\tilde{\Delta}_m^2)^{1/2}} \quad . \tag{3.7a}$$

and

$$\tilde{\Delta}_n = \Delta_n - \pi T \sum_m \lambda_{sf}(n-m) \frac{\tilde{\Delta}_m}{(\tilde{\omega}_m^2+\tilde{\Delta}_m^2)^{1/2}} \quad . \tag{3.7b}$$

Here the spin-fluctuation mass enhancement function λ_{sf} is related to the spectral density B by

$$\lambda_{sf}(n-m) = 2 \int_0^\infty d\Omega \frac{\Omega P_{sf}(\Omega)}{\Omega^2 + (\omega_n - \omega_m)^2} \quad . \tag{3.8}$$

with the new spectral density P_{sf} given by

$$P_{sf}(\Omega) = N_0 J^2 \int_0^{2k_F} \frac{q\, dq}{2\, k_F^2} B(q,\Omega) \quad . \tag{3.9}$$

Given a spectral density B, the equations (3.7) may be solved self-consistently using (3.8-9). It has been found by Keller[63], however, in the case of a ferromagnet, for a wide range of parameters, that the inclusion of dynamic effects, that is terms for $n \neq m$ in Eq.(3.7), does not alter the critical temperature or specific heat jump significantly. In this case as well, it may be verified that $\lambda_{sf}(n-m)$ for $n-m \neq 0$ is negligible compared to $\lambda_{sf}(0)$ by inserting the model spectral density (to be defined in (3.11-12)) into (3.8-9). Therefore, to a very good approximation the $n \neq m$ terms in the frequency sums in

(3.7) may be neglected. In this static limit these equations are the same as the AG equations, with the exception that the exchange scattering rate is proportional to $T\lambda_0$ ($\lambda_0 - \lambda_{sf}(0)$), which is in general temperature dependent. This means that if only these terms are kept, and the analytic continuation to the real frequency axis is performed, one arrives at exactly the same gap equations as in Chapter II, with a temperature dependent effective exchange scattering rate, and of course the limit $\epsilon_0 \to 1$, the weak scattering limit. In this case exactly the same computer program as was used in calculating the results for Chapter II can be used, with minor changes to handle the temperature dependence of the scattering rate. This will be the approach taken here.

The real axis gap equations within this approximation then have the form

$$\Delta = N_0 V \int_0^{\omega_D} d\omega \, \mathrm{Re}\left[\frac{1}{(u^2(\omega)-1)^{1/2}}\right] \tanh[\beta\omega/2] \, . \qquad (3.10a)$$

where

$$\omega/\Delta = u(\omega)\left[1 - i\,\alpha(T)\,\frac{u(\omega)}{[u^2(\omega)-1]^{1/2}}\right] . \qquad (3.10b)$$

which must be solved self-consistently. In (3.10) the square roots must be chosen to have a positive real part. The pair-breaking parameter α is given by $\alpha = n_I 2\pi T\lambda_0(T)$, with n_I the impurity concentration and λ_0 given by (3.8-9).

Now consider the spectral density which is needed in order to calculate α. Nass *et al.*[60] have used a model for the spin-glass due

to Dzyaloshinskii and Volovik[64] in which the correlation function consists of one part which is identical to the hydrodynamic limit of a paramagnet, together with a term which is proportional to a Dirac delta function in frequency which represents the effect of the spin freezing. A similar approach has been used by Fischer[65] in his calculation of the electrical resistivity of a spin-glass. The parameters which appear in this correlation function are not entirely free, as sum-rule constraints are considered, and in particular the contributions from the dynamic and static parts must be consistent in order to preserve the magnitude of the spin.

The dynamic part of the spectral density used by Nass *et al.*[60] is the same as that of a Heisenberg paramagnet, which has been calculated by many workers, in particular Bennett and Martin[66] and Halperin and Hohenberg[67]. A detailed introduction may be found in the book by Forster[68]. A similar result for spin-glasses has been given by Fischer[65]. This term will be called B_d (d for dynamic) and is given by

$$B_d(q,\omega) = \frac{Dx\omega q^2}{\omega^2+(Dq^2-\omega^2\tau)^2} . \qquad (3.11)$$

where D is the spin diffusion constant and the static susceptibility x is taken to be independent of q for simplicity. The parameter τ is a phenomenological frequency cutoff which allows the sum-rule constraints to be applied. This form for the spectral density is only valid in the limit $q,\omega \to 0$, but the hope is that the required momentum and frequency

integrals will yield a reasonable electronic lifetime.

The static contribution to the spectral density which arises from the spin freezing is given by

$$B_s(q,\omega) = \pi(1-e^{-\beta\omega})\tilde{Q}(T)\ \delta(\omega) \ . \qquad (3.12)$$

The function $\tilde{Q}(T)$ should be related to the EA order parameter, and varies from zero for T greater than T_f to a value of S^2 at zero temperature. As discussed by Nass *et al.*[60], the fact that this term does not go to S(S+1) at zero temperature is a reflection of the non-ergodicity of the EA theory, that is of the fact that the order parameter defined as the infinite time limit of the correlation function is not the same as that defined in terms of the configurational average. This same low temperature limit has also been used by Fischer[65] in his calculation of the electrical resistivity of a spin-glass.

The model used by Nass *et al.* for the temperature dependence of this EA order parameter contribution to the spectral density is

$$\tilde{Q}(t) = S^2(1-\bar{t}^2) \ . \qquad (3.13)$$

where $\bar{t}=T/T_f$. Other models will also be examined, in particular one which will be called $\tilde{Q}_1(\bar{t})$ and is given by

$$\tilde{Q}_1(\bar{t}) = S^2(1-\bar{t}) \ . \qquad (3.14)$$

which has a temperature dependence motivated by the mean-field solution of the EA model, which is nearly linear in $\bar{t}$, both in the classical and quantum limits.

As pointed out by Nass *et al.*[60], and by Keller[63] for the ferromagnetic case, if all of the parameters in the spectral density are varied freely unphysical results may be obtained. One sum-rule which can be used in order to establish relationships between the parameters follows directly from the definition of the spectral density in terms of the time correlation function and is

$$\int_{BZ} d^3q \int_{-\infty}^{\infty} d\omega \, \frac{2}{1-e^{-\beta\omega}} B(q,\omega) = 2\pi S(S+1) \int_{BZ} d^3q \, . \qquad (3.15)$$

where the integrals over q are taken over a Brillouin zone of radius $2k_F$.

The second sum-rule is the f-sum rule, equations (3.4-5) in Nass *et al.*[60], which takes the form

$$\int_{-\infty}^{\infty} \frac{d\omega}{\pi} \, \omega B(q,\omega) = \frac{\rho_s}{2\kappa} q^2 \, . \qquad (3.16)$$

where ρ_s is the spin stiffness constant and κ relates the frustration current density to the Yang-Mills fields introduced by Dzyaloshinskii and Volovik[64]. Using (3.16) together with (3.11) the sum-rule becomes

$$D\chi = \frac{\rho_s}{2\kappa}\tau \ . \qquad (3.17)$$

Following Nass *et al.* the product $D\chi$ will be taken to be a temperature independent constant, that is any temperature variation of ρ_s and κ is neglected. The cutoff parameter τ will also be assumed to be temperature independent.

The general trend of Nass *et al.* for the fixing of parameters is also followed. First a value of τ is chosen. As pointed out by Nass *et al.*, this immediately restricts the possibilities for the product $D\chi$, as only a narrow range of values for $D\chi$ allows the sum-rules to be satisfied for all temperatures in the vicinity of and below the freezing temperature and also yields a temperature dependent susceptibility in reasonable agreement with experiment. A chosen value for the diffusion constant at the freezing temperature then determines D and χ for all temperatures.

Note that the momentum integral which occurs in the sum-rule (3.15) may be performed analytically. It will also be convenient to introduce dimensionless reduced parameters for the application of the sum-rule and subsequent calculation of λ_0. These new parameters are

$$\bar{\omega} = \omega/T_f, \qquad \bar{D} = D(2k_F)^2/T_f \ ,$$

$$\bar{\chi}=T_f\chi, \qquad \bar{\tau}=T_f\tau \qquad \text{and} \quad \bar{t}=T/T_f. \qquad (3.18)$$

Using the definitions (3.18) and the spectral density $B=B_d+B_s$ from

(3.11) and (3.12), the sum-rule (3.15) may be written in the form

$$\bar{D}\bar{x}\int_0^\infty d\bar{\omega}\;\bar{\omega}\coth[\bar{\omega}/(2\bar{t})]\;A(\bar{\omega}) = \frac{\pi}{3}\left[S(S+1) - \tilde{Q}(\bar{t})\right] . \qquad (3.19)$$

where the function $A(\bar{\omega})$ results from performing the momentum integral in the sum-rule (3.15), and may be written in the form

$$A(\bar{\omega}) = \int_0^1 dx\,\frac{x^4}{\bar{\omega}^2+(\bar{D}x^2-\bar{\omega}^2\bar{\tau})^2}$$

$$= \left[1 + \frac{\bar{\omega}^2\bar{\tau}}{\bar{D}}\mathrm{Re}\{L(\bar{\omega})\} + \frac{\bar{\omega}}{2\bar{D}}\,(\bar{\omega}^2\bar{\tau}^2-1)\;\mathrm{Im}\{L(\bar{\omega})\}\right]/\bar{D}^2 , \qquad (3.20)$$

where

$$L(\bar{\omega}) = C^{-1/2}\,\ell n\left[\frac{C-C^{1/2}}{C+C^{1/2}}\right] \qquad (3.21)$$

with

$$C = \bar{\omega}^2\bar{\tau}/\bar{D} + i\bar{\omega}/\bar{D} . \qquad (3.22)$$

In (3.21) the square roots are defined to have a positive real part, and the principal branch of the logarithm is taken. Note that the function $A(\bar{\omega})$ depends explicitly only on $\bar{D}$ and $\bar{\tau}$, not on $\bar{x}$. Therefore the approach taken to determining the parameters is to fix $\bar{\tau}$ and the value of $\bar{D}$ at the freezing temperature, $\bar{D}(T_f)$. Then (3.19) may be used to determine $\bar{x}(T_f)$, which in turn fixes the value of the product $\bar{D}\bar{x}$ for all temperatures when the assumption of temperature independence for this product is recalled. With this product determined, (3.19) may once again be used at arbitrary temperatures to find $\bar{D}$ and therfore

also $\bar{\chi}$.

The calculation of the effective spin-flip scattering rate from the spectral density B is slightly simpler than the performance of the integration for the sum-rule. The major difference is that in the calculation of λ_0 there is no thermal factor of the form $1-e^{-\beta\omega}$ in the dynamic term B_d, so that in this case one is faced with a double integral of a rational function, which may be performed entirely analytically. The result is (see App. A)

$$\lambda_d(0) = N_0 J^2 \int_{-\infty}^{\infty} \frac{d\omega}{\omega} \int_0^{2k_F} \frac{q\, dq}{2\, k_F^2} B_d(q,\omega)$$

$$= N_0 J^2 \frac{2\bar{\chi}\bar{D}}{\bar{T}_f} \int_{-\infty}^{\infty} d\bar{\omega} \int_0^1 \frac{dx\, x^3}{\bar{\omega}^2 + (\bar{D}x^2 - \bar{\omega}^2\bar{\tau})^2}$$

$$= N_0 J^2 \frac{\pi\bar{\chi}}{\bar{T}_f} = N_0 J^2 \pi\chi \,. \tag{3.23}$$

The perhaps surprisingly simple result that this contribution to the scattering rate depends only on χ, and not explicitly on D and τ is exactly what is trivially found in the limit $\tau=0$, $D\to 0$, in which case the spectral density B_d approaches $\pi\chi\delta(\omega)$. When the EA order parameter term (3.12) is included the total spin-flip scattering rate is found to be proportional to

$$T\lambda_0 = N_0 J^2 \pi[T\chi + \tilde{Q}(\bar{t})] \,. \tag{3.24}$$

The implications of this very simple result will be examined in the next section, along with an exploration of the consequences of the sum-rule (3.19-22) for the temperature variation of the model χ.

3.3 $\bar{D}$, $\bar{\chi}$ and λ for the Spin-Glass Model

In this section the properties of the spin-glass models will be examined. Motivated by application to the case of Ag-Mn in Chapter IV, the value S=5/2 for the spin will be used, and it will soon become clear that it is the ratio $S^2/[S(S+1)]$ which determines the scale of variation of the temperature dependence of the spin-flip scattering rate α. This arises essentially from the fact that the zero temperature value of the static (EA order parameter) contribution to the scattering rate is proportional to S^2, while the high temperature dynamic contribution saturates at a value proportional to S(S+1) for T much greater than T_f.

Following Nass *et al.*[60], consider first the case of the cutoff parameter $\bar{\tau} = \tau T_f = 0.2$, with the model $\tilde{Q}(\bar{t}) = S^2(1-\bar{t}^2)$ for the EA order parameter contribution. Figures 3.1(a-b) show the variation of the dimensionless parameters $\bar{D}$ and $\bar{\chi}$ for this cutoff and for several different choices of the value $\bar{D}(\bar{t}=1)$, and therefore for the temperature independent product $\bar{D}\bar{\chi}$. Note, for $\bar{t}$ greater than one, that the diffusion constant shown in Fig. 3.1(b) increases linearly with $\bar{t}$. Since the product $\bar{D}\bar{\chi}$ is taken to be temperature independent, this

implies that $(\bar{\chi})^{-1}$ is linear in $\bar{t}$. Therefore this model with the two sum-rules (3.15-16) correctly gives a Curie-Weiss susceptiblity at high temperatures, with a Curie-Weiss temperature in the range $\Theta \simeq -0.1T_f$ to $-0.5T_f$ which is somewhat model dependent. In Fig. 3.1(c) the temperature variations of the exchange scattering rate α ($\propto T\lambda_0$) for the same sets of parameters are shown. As $\bar{D}(1)$ decreases the temperature range over which α varies becomes smaller.

These results may be compared with those for the other model for the "frozen" spin contribution, $\tilde{Q}_1(\bar{t})=S^2(1-\bar{t})$, shown in Fig. 3.2. The same trends as a function of $\bar{D}(1)$ may be seen, with the further observation that for small $\bar{D}(1)$ the two models give almost identical scattering rates. Note also that the model $\tilde{Q}_1$ shown in Figure 3.2(c) has a more pronounced minimum in $\alpha(t)$ for large $\bar{D}(1)$ than occurs in the t^2 model. This will later be shown to allow the possibility of reentrant effects for the critical temperature.

Considering next the effect of varying the cutoff parameter $\bar{\tau}$. Fig. 3.3 shows that the effect on the scattering rate is very similar to that which can be achieved by varying $\bar{D}(1)$ for a given $\bar{\tau}$. Essentially the same family of curves may be reproduced by varying only $\bar{D}(1)$, so that variations of $\bar{\tau}$ will not be considered further.

Finally, in some cases it will be useful to have a model for the concentration dependence of the spin-glass freezing temperature T_f. While this is in general a complicated problem, at least in the dilute limit a linear dependence is often observed (see, for example page 301 of Ref. 57) and may be understood in terms of the $1/r^3$ spatial dependence of the strength of the RKKY interation. Therefore a simple

model of the form

$$T_f \sim \frac{n_I}{n_c} R T_c^0 \qquad (3.25)$$

may be appropriate. Here n_I is the magnetic impurity concentration, n_c is the critical concentration, T_c^0 is the superconducting critical temperature of the pure superconductor, and R is a dimensionless parameter between zero and approximately one.

3.4 Some Results for the Spin-Glass Models

In this section some of the predictions of the spin-glass models described in the previous section will be examined. Since all properties of superconductors are sensitive to some extent to the exchange scattering rate of the conduction electrons, and the model predicts a temperature dependent scattering rate, one would expect significant deviations from the temperature dependence of a given physical property as predicted by the Abrikosov-Gor'kov[3] (AG) theory.

3.4.i Concentration Dependence of the Critical Temperature

Considering first the dependence of the superconducting critical temperature on impurity concentration, one quickly sees that

the suppression of the exchange scattering rate below the freezing temperature will result in an enhancement of T_c near the critical concentration when compared with the AG result, as shown in Fig. 3.4. Similar results have been reported by Soukoulis and Grest[69] from a slightly different evaluation of the exchange scattering rate of a spin-glass. Roshen and Ruvalds[70] have also reported a similar effect in the case of antiferromagnetic dynamic correlations between pairs of RKKY coupled spins without, however, including the spin "freezing" in any way. This is a familiar result, as many workers (see Fulde and Keller in Ref. 49) have found within a variety of models that antiferromagnetic spin correlations reduce the pair-breaking effect of magnetic ions in a superconductor.

Figure 3.4 shows the reduced critical temperature T_c/T_c^0 as a function of magnetic impurity concentration for the model $\bar{D}(1)=1$, $\tilde{Q} = S^2(1-t^2)$, and for various values of the ratio R defined in (3.25). Note that the maximum deviation from the AG curve is governed by the ratio $[S(S+1)]/S^2 = (S+1)/S$, while the point of departure is determined by R, which fixes the relationship between the freezing temperature T_f and the impurity concentration.

The enhancement of the critical concentration by the factor of $(S+1)/S$ over the AG case is exactly the result predicted by Bennemann[71] for a model of antiferromagnetic ordering. This result was later questioned by Keller and Benda[61], who showed that Bennemann's result would only hold in the limit of very strong exchange fields (energies of the order of the Debye frequency) acting on the local moments. This was considered to be quite unlikely by Keller and

Benda[61]. In the case of the spin-glass model considered here, the suppression of the exchange scattering rate arises from the assumption that at zero temperature the local moments are entirely frozen, so that inelastic scattering is impossible.

Figure 3.5 illustrates the dependence of T_c on concentration predicted for the case of the EA order parameter contribution $\tilde{Q}_1 = S^2(1-\bar{t})$ with a larger diffusion constant $\bar{D}(1) = 2.0$. In this case there is a significant reentrant region, which is qualitatively different from the results in Fig. 3.4. This reentrant behavior will occur for any model which displays a minimum in the exchange scattering rate at a finite temperature. Note that from Figs. 3.1-2 for both models of the EA order parameter contribution large values of the diffusion constant $\bar{D}(1)$ result in minima in the scattering rate $\alpha(\bar{t})$, which in turn results in the appearance of reentrant behaviour. Reentrance has been observed in the $La_{1-x}Gd_xRu_2$ system for $x \gtrsim 4.0$ at.% by Jones et al.[72], with qualitative agreement with the dashed curve of Fig. 3.5. As an aside, note that similar reentrant behaviour is predicted to occur in dilute Kondo[21] alloys, where the logarithmic increase in the exchange scattering rate as the Kondo temperature is approached from above may lead to quenching of superconductivity as the temperature is reduced.

3.4.ii The Free Energy Difference

The difference in free energy between the superconducting and

normal states of a superconducting spin-glass can easily be calculated within the present model. The free energy formula due to Skalski *et al.*[30], (2.61) here, can be employed directly, requiring only the substitution of the appropriate density of states and order parameter which reflect the temperature dependence of the exchange scattering rate.

Considering the deviation function $D(t) = \frac{H_c(t)}{H_c(0)} - [1-t^2]$ as defined in (2.64), one can see immediately that the spin-glass model results will be very different from AG theory. As shown in Fig. 3.6, the deviation function becomes much more negative than the prediction of AG theory (Fig. 2.2(a)), which gives a minimum of approximately -0.07. This large effect is due predominantly to the fact that $H_c(0)$ is enhanced significantly from the AG value due to the suppression of the exhange scattering rate at low temperatures.

This behavior is illustrated in Fig. 3.7, where the thermodynamic critical magnetic field is plotted as a function of temperature for the same parameters as in Fig. 3.6. It is the upturn in H_c at low temperature which results in $D(t)$ being much more negative than the AG prediction for the entire temperature range.

Next consider D(t) for a case which displays reentrance at high concentrations, for example the model $\bar{D}(1) = 2.0$, $\tilde{Q}_1 = S^2(1-\bar{t})$ shown in Fig. 3.8. For intermediate concentrations D(t) for this model does not decrease as rapidly as the previous case, followed by the appearance of an S-shape at high concentrations. This S-shape results from the appearance of a maximum of $H_c(t)$ at a finite temperature, as shown in

Fig. 3.9 for the same parameters.

3.4.iii Transport Properties

Transport properties such as electronic thermal conductivity and ultrasonic attenuation would be expected to be sensitive to variations of the exchange scattering rate. The suppression of exchange scattering below the spin-glass freezing temperature, which leads to enhanced superconductivity compared to the noninteracting case, should result in reduced ultrasonic attenuation and thermal conductivity at low temperatures compared to the AG prediction.

The electronic contribution to the thermal conductivity has previously been calculated in the Shiba-Rusinov (SR)[8.9] limit in section 2.8. Within the present approximations, the spin-glass case may be handled using the same expression in terms of the gap function, equations (2.74-75), with the gap function given by the solution of equations (3.10). This results from the fact that the derivation of this result really depends only on the analytic structure of the Green's function, which is the same in both cases.

The electronic contribution to the thermal conductivity, normalized to the normal state value, is given by

$$\frac{K_S}{K_N} = \frac{3\beta^3}{2\pi^2} \int_0^{\omega_D} d\omega\, \omega^2\, \mathrm{sech}^2(\beta\omega/2)\, h(\omega) \,. \qquad (3.26)$$

where

$$h(\omega) = \left[\mathrm{Re}\ \frac{u(\omega)}{[u^2(\omega)-1]^{1/2}}\right]^2 - \left[\mathrm{Re}\ \frac{1}{[u^2(\omega)-1]^{1/2}}\right]^2$$

$$= \frac{1}{2}\left[1 + \frac{|u(\omega)|^2-1}{|u^2(\omega)-1|}\right] . \qquad (3.27)$$

The function $u(\omega)$ in (3.27) is given by the solution of equation (3.10) at a given temperature and exchange scattering rate $\alpha(T)$.

Figure 3.10 illustrates graphically some of the behavior predicted within this model. This figure shows sets of thermal conductivity curves for the AG model (solid lines) as well as two spin-glass models for various reduced critical temperatures T_c/T_c^0. In all cases the reduction in exchange scattering in the spin-glass models at low temperatures results in decreased thermal conductivity compared to the AG prediction.

The ultrasonic attenuation for a superconductor with SR model paramagnetic impurities has been given by Shukla and Nagi[73], and as in the case of the thermal conductivity, this result also applies here. The ultrasonic attenuation, normalized to the normal state value is therefore given by

$$\frac{\alpha_S}{\alpha_N} = \frac{\beta}{2}\int_0^{\omega_D} d\omega\ \mathrm{sech}^2(\beta\omega/2)\ h(\omega) . \qquad (3.28)$$

where the function $h(\omega)$ is given by (3.27). In (3.28) the frequency of the ultrasound is assumed to be small compared to the superconducting order parameter Δ, so that these phonons cannot cause pair-breaking.

Some results for ultrasonic attenuation for two spin-glass models as well as AG theory are shown in Fig. 3.11. As in the case of the thermal conductivity, the spin-glass model results are reduced from the AG value at low temperatures.

3.4.iv Local Limit Penetration Depth

The electromagnetic response function for a superconductor with paramagnetic impurities has been calculated in the AG limit by Nam[37]. As in the previous sections, this derivation also applies to the present model, and Nam's[37] results may therefore be used here. The only alteration required is the substitution of the AG gap function by the gap function with the appropriate temperature dependence.

One quantity of interest is the magnetic penetration depth, as this may be measured as a function of temperature quite directly experimentally. Again, because of the suppression of the exchange scattering rate below the spin-glass freezing temperature, it is expected that the penetration depth at low temperatures would be reduced from the AG prediction for the same reduced critical temperature. This intuitive prediction will be born out by the results calculated in this section.

The electromagnetic penetration depth as calculated by Nam[37] within the AG theory and Thomasson and Ginsberg[74] in SR theory is given in the local limit ($\lambda_\ell << \xi_{00}$, where $\xi_{00} = \frac{v_F}{\pi\Delta_0}$ is the BCS coherence

length) by

$$\lambda_\ell = (4\pi Q)^{-1/2} , \tag{3.29}$$

where

$$Q = 2\sigma_N \, \mathrm{Im} \int_0^\infty d\omega \, \frac{1}{1-u^2(\omega)} \tanh(\beta\omega/2). \tag{3.30}$$

In (3.30) the function $u(\omega)$ is as defined in (3.10) and σ_N is the normal state conductivity.

The dependence of the local limit penetration depth on temperature for two spin-glass models and AG theory is shown in Fig. 3.12. where the largest part of the temperature dependence is removed through the factor $(1-t^4)^{1/2}$, which is the temperature dependence of $1/\lambda$ predicted by the two-fluid model. The deviations from AG theory are quite evident in this figure. At low temperature both spin-glass models exhibit reduced penetration depth compared with the AG prediction for the same reduced critical temperature. The details of the temperature dependence of the exchange scattering rate also appear in the penetration depth, with the minimum in the scattering rate (dashed lines) showing up as a minimum in the penetration depth at higher concentrations. Furthermore, the divergence of the penetration depth at T_c at high concentration is qualitatively different in the spin-glass models compared to the AG prediction. This arises from the fact that the strong temperature dependence of the exchange scattering rate alters the temperature dependence of the superconducting order parameter. It is easily shown that the local limit penetration depth

diverges as the inverse of the order parameter as T approaches T_c, so that the temperature dependence of the exchange scattering rate influences the penetration depth directly.

3.5. Reentrant Ferromagnetic Superconductors

3.5.i Introduction

The discovery of the reentrant ferromagnetic superconducting compounds $ErRh_4B_4$ and $HoMo_6S_8$ (see Ref.49 for reviews) helped spark renewed interest in the problem of the possible coexistence of magnetic and superconducting order. These materials undergo a normal-superconducting phase transition of the conventional type at a critical temperature T_{c1}, together with a reentrant transition to a non-superconducting, ferromagnetic state at a lower temperature T_{c2}. The situation is made even more interesting by the existence of a correlated magnetic phase at temperatures just above T_{c2} which coexists with superconductivity. This cryptoferromagnetic phase exhibits oscillatory magnetization with a wavelength of approximately 20 nm in the case of $HoMo_6S_8$ and approximately 10 nm in $ErRh_4B_4$ [52], so that when averaged over the superconducting coherence length there is no net magnetization. It is this vanishing average magnetization which is believed to allow the coexistence with superconductivity.

The phase diagram for systems which may show both magnetic and superconducting order has long been studied theoretically (see Fulde

and Keller in Ref. 49). Various approaches have been taken, including the use of Ginzburg-Landau theory in the vicinity of the multicritical point as well as more microscopic methods. However, the aspect of this large problem considered here will not be the phase diagram, but rather some superconducting properties in the paramagnetic phase above T_{c2}, and the cryptomagnetic phase will not be considered at all. A model due to Lee[54] for the effective exchange scattering rate due to paramagnetic spin fluctuations will be used. This model is very similar in spirit to the spin-glass model considered previously in this chapter. Lee[54] considers only the effect of elastic scattering of conduction electrons from the spin fluctuations, which is the same (static) approximation made in the spin-glass case in this chapter.

In Lee's[54] model the static susceptibility of the local moment system is given by the mean-field Ornstein-Zernike form

$$\chi(\underline{p}) = \frac{S(S+1)}{T-T_m+\zeta_0^2\underline{p}^2}. \tag{3.31}$$

where T_m is the ferromagnetic ordering temperature, and ζ_0 is a correlation length for spin diffusion. The self-energy is formally identical to (3.3) of the spin-glass case, with the simplification that only elastic scattering is considered right from the beginning, so that there is no need to introduce the spectral representation (3.4). The imaginary-axis gap equations then become

$$\tilde{\omega}_n = \omega_n + \frac{1}{2}\left[\frac{1}{\tau_N} + \frac{\eta(T)}{\tau_S}\right] \frac{\tilde{\omega}_n}{(\tilde{\omega}_n^2+\tilde{\Delta}_n^2)^{1/2}} \qquad (3.32a)$$

and

$$\tilde{\Delta}_n = \Delta_n + \frac{1}{2}\left[\frac{1}{\tau_N} - \frac{\eta(T)}{\tau_S}\right] \frac{\tilde{\Delta}_n}{(\tilde{\omega}_n^2+\tilde{\Delta}_n^2)^{1/2}} \qquad (3.32b)$$

Here τ_N is the lifetime for scattering from non-magnetic impurities, $\frac{1}{\tau_S} = 2\pi J^2 S(S+1)N_0$ is the lifetime for exchange scattering in the absence of magnetic fluctuations and

$$\eta(T) = \frac{T}{T_m}\mu^{-1} \ln\left[\frac{\frac{T}{T_m} - 1 + \mu}{\left[\frac{T}{T_m} - 1\right]^{1/2} + \left[\frac{\mu}{16E_F^2}\left(\tilde{\omega}_n^2+\tilde{\Delta}_n^2\right)\right]^{1/2}}\right] \qquad (3.33)$$

with

$$\mu = \frac{4\zeta_0^2 k_F^2}{T_m} \qquad (3.34)$$

The function $\eta(T)$ in (3.34) arises from the integration of the self energy contribution over momentum. Note that the term $\frac{\mu}{16E_F^2}\left[\tilde{\omega}_n^2 + \tilde{\Delta}_n^2\right]$ inside the logarithm in (3.33), which arises from the integration of the susceptibility over energy, is only significant very near the magnetic ordering temperature, since the parameter μ is expected to be of order one, and $\tilde{\omega}_n/E_F \ll 1$ for cases of interest in superconductivity.

As pointed out by Lee[54], in the dirty limit ($\frac{1}{\tau_N} \gg T_c^0$) to a

very good approximation

$$\tilde{\omega}_n = \frac{1}{2\tau_N} \operatorname{sign}(\omega_n) \ . \tag{3.35}$$

which gives

$$\eta(T) = \frac{T}{T_m} \mu^{-1} \ln \left[\frac{\frac{T}{T_m} - 1 + \mu}{\left[\frac{T}{T_m} - 1\right]^{1/2} + \frac{\mu^{1/2}}{4k_F \ell}} \right] \tag{3.36}$$

with $\ell = v_F \tau_N$.

Equation (3.36) is the form which will be used in this thesis, even when not in the extreme dirty limit. This approximation is well justified, since in the region where it could possibly become significant ($T \to T_m$) the original mean-field ansatz for the susceptibility (3.31) is questionable in any case. Also, since no provision is made to allow for the coexistant cryptomagnetic phase which is observed experimentally in the temperature region just above the reentrant ferromagnetic transition, one cannot realistically expect to compare the predictions of this model with any known material very near T_{c2}.

The gap equations may now be continued to the real frequency axis to arrive at the pair of equations formally identical to the spin-glass case (3.10a-b):

$$\Delta = N_0 V \int_0^{\omega_D} d\omega \ \mathrm{Re}\left[\frac{1}{\{u^2(\omega)-1\}^{1/2}} \right] \tanh[\beta\omega/2] \ . \tag{3.37a}$$

and

$$\omega/\Delta = u(\omega)\left[1 - i\,\frac{\eta(T)}{\tau_S}\,\frac{u(\omega)}{[u^2(\omega)-1]^{1/2}}\right]. \qquad (3.37b)$$

The only difference between (3.10) and (3.37) is the replacement of $\alpha(\bar{t})$ by the appropriate scattering rate $\frac{\eta(T)}{\tau_S}$, where $\eta(T)$ is given by (3.36).

3.5.ii The Free Energy Difference

The difference in free energy between the normal and superconducting states of $ErRh_4B_4$ in the paramagnetic phase has been determined by Behroozi *et al.*[75] through measurements of magnetization curves at various temperatures. They compared their results with the predictions of Ginzburg-Landau (GL) theory, with only limited success. They point out that one factor which may be contributing to the discrepancy is the application of GL theory at temperatures well below T_c, which is not expected to be quantitatively correct. Therefore, it is of some interest to calculate the free energy difference as a function of temperature within the present microscopic model and compare these results with the measurements of Behroozi *et al.*[75].

As in the spin-glass case, one may use the free energy formula due to Skalski *et al.*[30] (2.61), derived in the AG limit. The difference in free energy between the superconducting and normal states is then given by

$$\frac{F_{N-S}}{N_0} = \int_0^{\omega_D'} \left[\frac{N(\omega)}{N_0} - 1 \right] \left[2\omega \tanh\left\{\frac{\beta\omega}{2}\right\} + \frac{4}{\beta}\left\{ \ell n(1+e^{-\beta\omega}) + \frac{\beta\omega}{1+e^{\beta\omega}} \right\}\right] + \Delta^2 \left[1 - \frac{1}{N_0 V} \right] . \tag{3.38}$$

where

$$\frac{N(\omega)}{N_0} = \mathrm{Re}\left[\frac{u(\omega)}{[u^2(\omega)-1]^{1/2}} \right] , \tag{3.39}$$

is the quasiparticle density of states in the superconductor normalized to the normal state value N_0, and $\beta = 1/T$. The thermodynamic critical field is then given by

$$H_c^2/(8\pi) = F_{N-S} . \tag{3.40}$$

Shown in Fig. 3.13 is the predicted temperature dependence of the free energy difference for parameters roughly appropriate to $ErRh_4B_4$: T_c^0=12 K, T_c=8.7 K, T_m=.93 K, and various values of μ and $\frac{1}{k_F\ell}$. The general trends which may be seen are that as μ decreases the suppression of superconductivity above T_m increases, and that for a given μ as $\frac{1}{k_F\ell}$ increases the deviation from AG theory also increases. Further, note that the experimental peak in free energy difference at approximately 3.8 K or T/T_c=0.44 can only be matched with a rather extreme choice of parameters. That is, if one attempts to put the peak in free energy difference at T/T_c=0.44 a very small value of μ must be

used, which results in a reentrant $T_{c2} >> T_m$, in disagreement with experiment. Note that the inclusion of dynamic spin-fluctuation effects (the inclusion of $\lambda_s(n-m)$ for $n \neq m$ in (3.7)) would not be expected to introduce qualitative changes from the static approximation used here. For example, the calculation by Schossmann and Carbotte[76] of the upper critical field H_{c2} including dynamic spin-fluctuations showed that although the dynamic effects may be significant for large ζ_0 ($\mu \gtrsim 1$), similar effects may be produced within the static model simply by varying ζ_0. In a certain sense, one might consider the dynamic effects as approximately renormalizing ζ_0 (note that Keller[63] and Dupont *et al.*[77] have also found dynamic effects to be not very important in the determination of the phase diagram). One is therefore lead to suspect that in this case as well, dynamic effects would not change the qualitative predictions, and that the discrepancy in the location of the peak in the free energy difference would remain even with the inclusion of dynamics.

One possible source for this discrepancy is that crystal field effects have not been included in any way. The specific heat measurements of Woolf *et al.*[78] provide strong evidence for crystal field splittings of the same order of magnitude as the superconducting transition temperature T_{c1}. Coffey *et al.*[79] have performed a dynamic calculation of the tunneling characteristics of a reentrant superconductor, and have estimated the exchange scattering rate at low temperatures (near T_{c2}) to be suppressed by a factor of two from the value calculated neglecting the crystal field splitting. Such effects have been included microscopically by Fulde *et al.*[80] in the case of

superconductors containing uncorrelated spins, but there is apparently no such treatment in the literature for interacting systems.

If this possibility is checked by simply reducing $\frac{1}{\tau_s}$ by a factor of $\frac{1}{2}$ near T_m, it quickly becomes apparent that although the changes are in the right direction, such a correction will not lead to agreement with the measurements of Berhoozi *et al.*[75]. Stated simply, the reduction of pair-breaking associated with this suppression of the exchange scattering rate will result in a shift of the peak in the free energy difference to lower temperature, offsetting to some extent the desired reduction of T_{c2} toward T_m. To conclude this section, it seems that a model of this type is not quantitatively consistent with the temperature dependence of the free energy difference of $ErRh_4B_4$ as extracted by Berhoozi *et al.*[75]

3.5.iii Transport Properties

Within the present model the behavior expected of such properties as ultrasonic attenuation and thermal conductivity is easily predicted. The rapid increase in the exchange scattering rate as T_m is approached from above should result in increasing ultrasonic attenuation and thermal conductivity.

The thermal conductivity of $ErRh_4B_4$ as measured by Odoni and Ott[81] does in fact show a rapid upturn, rising from a minimum value at T≈1.2 K to a maximum near the ferromagnetic ordering temperature of

approximately 0.9 K. Below 0.9 K the thermal conductivity is found to be linear in temperature, consistent with a predominantly electronic contribution. However, between 1.3 K and 2.5 K the behavior is more consistent with a T^3 dependence, which would be predicted for the phonon contribution. In this case it is difficult to unambiguously extract the separate electronic and phonon contributions, so that only a narrow temperature range near T_m will be considered here.

The thermal conductivity is once again given by (3.26-27)

$$\frac{K_S}{K_N} = \frac{3\beta^3}{2\pi^2} \int_0^{\omega_D} d\omega\, \omega^2\, \mathrm{sech}^2(\beta\omega/2)\, h(\omega) \,, \tag{3.41}$$

where

$$h(\omega) = \left[\mathrm{Re}\, \frac{u(\omega)}{[u^2(\omega)-1]^{1/2}}\right]^2 - \left[\mathrm{Re}\, \frac{1}{[u^2(\omega)-1]^{1/2}}\right]^2$$

$$= \frac{1}{2}\left[1 + \frac{|u(\omega)|^2-1}{|u^2(\omega)-1|}\right] . \tag{3.42}$$

The function $u(\omega)$ in (3.42) is given by the solution of (3.37) at a given temperature and exchange scattering rate $\frac{\eta(T)}{\tau_S}$.

Some results for the temperature dependence of the thermal conductivity predicted within this model are shown in Fig. 3.14. Note that rather than plotting the ratio of the superconducting state thermal conductivity at a given temperature to the normal state value at that same temperature, the curve has been normalized to the normal state value at T_{c1}, $\kappa_N(1)$. This should provide a reasonable estimate

of the actual temperature dependence in the neighborhood of T_m. as the experiment of Odoni and Ott[81] showed that the normal state thermal conductivity at T_{c1} does not deviate markedly from an extrapolation of the linear temperature dependence observed below T_m. The results for intermediate parameters ($\mu \simeq 1.0$) are in qualitative agreement with experiment, although the rise as T_m is approached is more rapid than is observed experimentally.

The ultrasonic attenuation may also be calculated using the same formula as in the spin-glass case, (3.28). This calculation was performed, although the results are not shown here. The results for the attenuation are qualitatively identical to the thermal conductivity shown in Fig. 3.14; the behavior at high temperature is similar to the AG model predictions, with a rapid rise in attenuation very near the reentrant transition temperature T_{c2}.

These results bear little resemblance to the measurements on polycrystalline samples by Schneider *et al.*[82]. They found a broad peak in the attenuation centred at roughly 5 K, together with a complicated dependence on applied external magnetic fields. While the magnetic field dependence predicted by a theory due to Tachiki *et al.*[83] is in qualitative agreement with the experiment of Schneider *et al.*[82] at higher applied fields, this theory predicts no attenuation at all in the absence of an applied field well above the magnetic ordering temperature. Note that the increase in attenuation predicted within the present model occurs only quite near the magnetic ordering temperature, so that the lowest experimental temperature of Schneider *et al.* of 1.5 K is still too large to show any sign of this increase

(recall that the observed[81] minimum in the thermal conductivity occurs at approximately 1.2 K). One may therefore conclude that the anomalous temperature dependent attenuation observed by Schneider *et al.*[82] in the absence of an applied magnetic field and well above the magnetic ordering temperature is not understood at the present time.

Fig. 3.1 The spin-glass model with $\tilde{Q}(\bar{t})=S^2(1-\bar{t}^2)$, and $\bar{\tau}=0.2$.

a) The dimensionless spin diffusion constant $\bar{D}(\bar{t})$ versus reduced temperature $\bar{t}=T/T_f$ for

$\bar{D}(1)=0.5$ (———),

$\bar{D}(1)=1.0$ (.....),

$\bar{D}(1)=2.0$ (------).

b) The dimensionless susceptibility $\bar{\chi} = T_f\chi$ for the same parameters as in a).

c) The exchange scattering rate $\alpha(\bar{t})/\alpha(\infty)$ versus reduced temperature for the same parameters as in a).

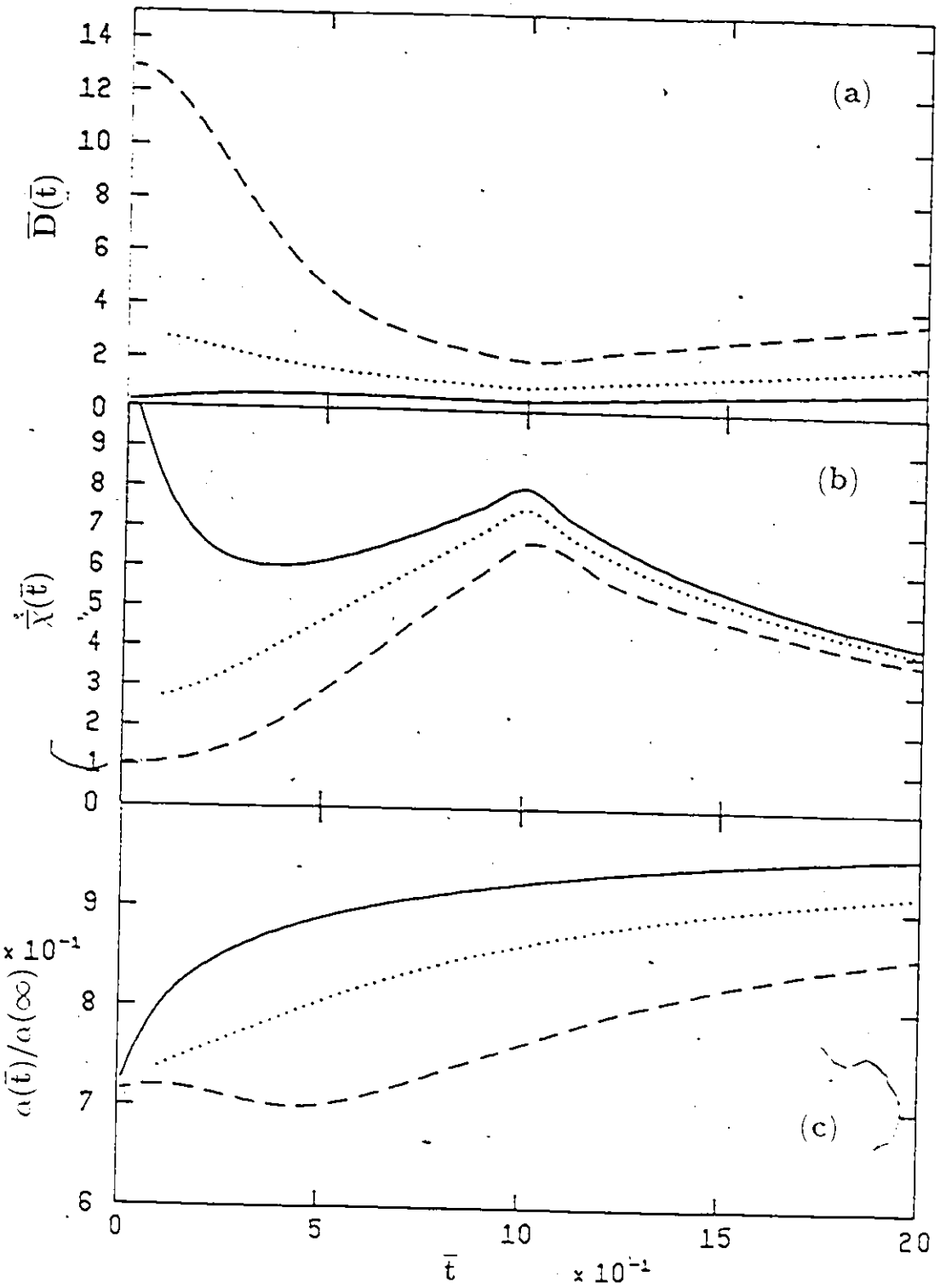
(a)
(b)
(c)
$\overline{D}(\bar{t})$
$\overline{\chi}^{s}(\bar{t})$
$a(\bar{t})/a(\infty)$
x 10^{-1}
$\bar{t}$
x 10^{-1}
0
5
10
15
20
6
7
8
9
0
1
2
3
4
5
6
7
8
9
0
2
4
6
8
10
12
14

Fig. 3.2 The spin-glass model with $\tilde{Q}_1(\bar{t})=S^2(1-\bar{t})$, and $\bar{\tau}=0.2$.

a) The dimensionless spin diffusion constant $\bar{D}(\bar{t})$ versus reduced temperature $\bar{t}=T/T_f$ for

$\bar{D}(1)=0.5$ (———),

$\bar{D}(1)=1.0$ (.....),

$\bar{D}(1)=2.0$ (------).

b) The dimensionless susceptibility $\bar{\chi} = T_f\chi$ for the same parameters as in a).

c) The exchange scattering rate $\alpha(\bar{t})/\alpha(\infty)$ versus reduced temperature for the same parameters as in a).

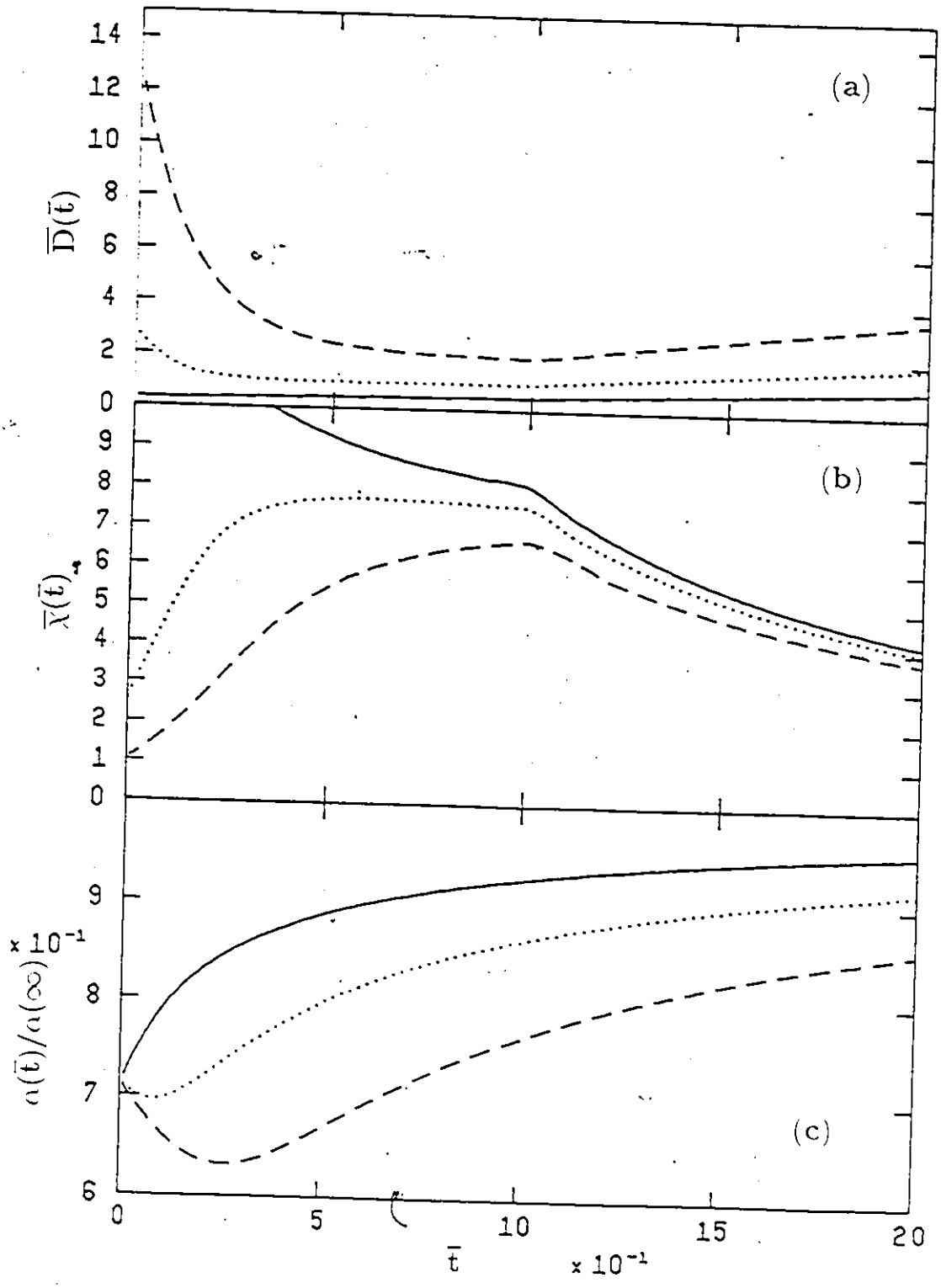
(a)
$\overline{D}(\bar{t})$
14
12
10
8
6
4
2
0
(b)
$\overline{\chi}(\bar{t})$
9
8
7
6
5
4
3
2
1
0
(c)
$\alpha(\bar{t})/\alpha(\infty)$
$\times 10^{-1}$
9
8
7
6
0
5
10
15
20
$\bar{t}$
$\times 10^{-1}$

Fig. 3.3 The dependence of the spin-glass model on the cutoff $\bar{\tau}$ for the model $\tilde{Q}_1(\bar{t}) = s^2(1-\bar{t})$.

a) The dimensionless spin diffusion constant $\bar{D}(\bar{t})$ versus reduced temperature $\bar{t} = T/T_f$ for

$\bar{\tau} = 0.2$, $\bar{D}(1) = 2.0$ (———),

$\bar{\tau} = 0.4$, $\bar{D}(1) = 2.0$ (.....),

$\bar{\tau} = 0.2$, $\bar{D}(1) = 1.0$ (- - - - -),

$\bar{\tau} = 0.4$, $\bar{D}(1) = 1.0$ (-·-·-·-)

b) The dimensionless susceptibility $\bar{\chi} = T_f \chi$ for the same parameters as in a).

c) The exchange scattering rate $\alpha(\bar{t})/\alpha(\infty)$ versus reduced temperature for the same parameters as in a).

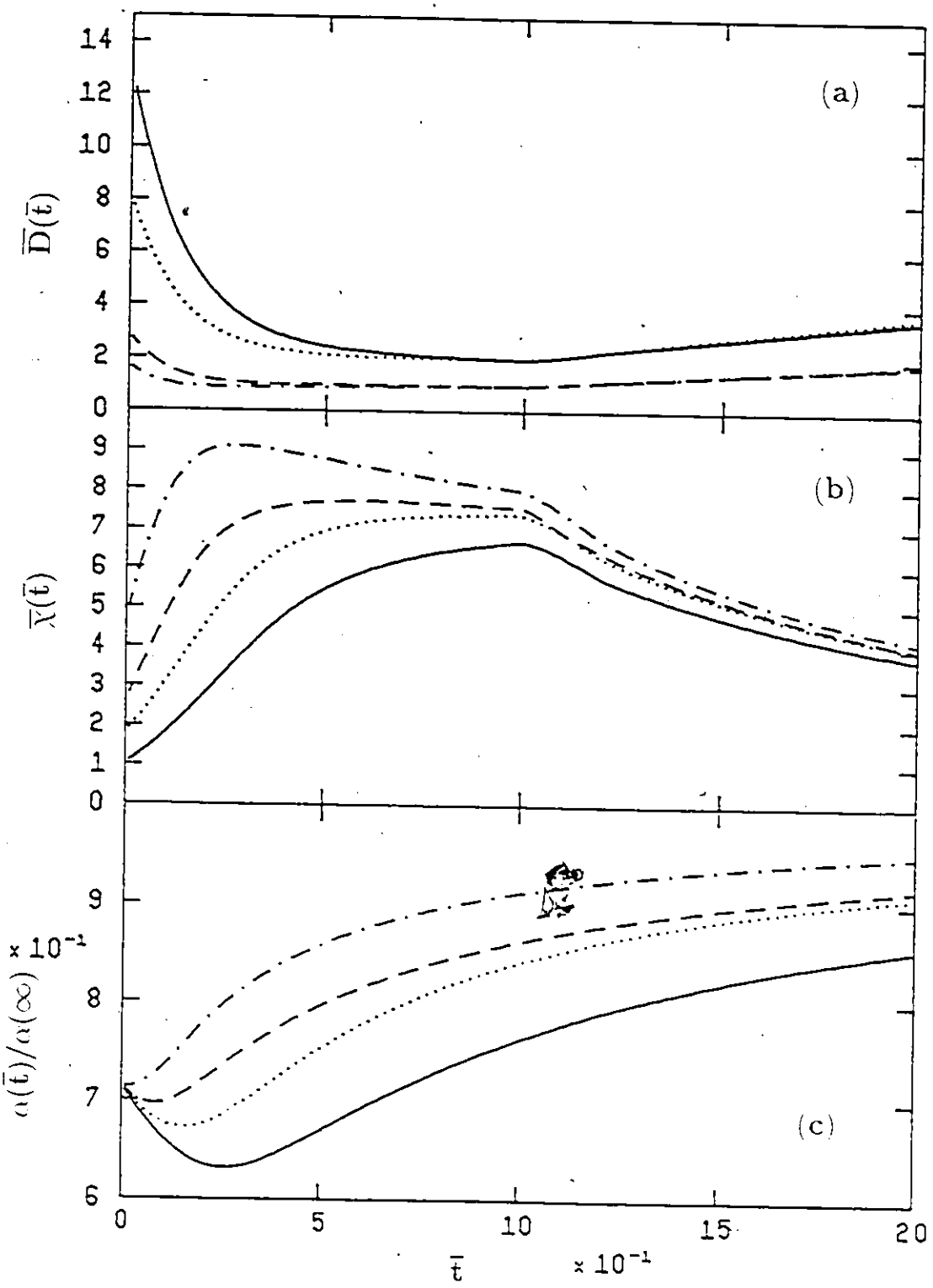
(a)
(b)
(c)
$\overline{D}(\bar{t})$
$\overline{\chi}(\bar{t})$
$\alpha(\bar{t})/\alpha(\infty)$
$\times 10^{-1}$
$\bar{t}$
$\times 10^{-1}$
0
5
10
15
20

Fig. 3.4 The reduced critical temperature T_c/T_c^0 versus impurity concentration $\alpha(\infty)/\alpha_c$ for the spin-glass model $\bar{r}=0.2$, $\bar{D}(1)=1.0$, $\tilde{Q}(\bar{t})=S^2(1-\bar{t}^2)$ and $T_f = R\left[\frac{n}{n_c}I\right]T_c^0$, where

$R=0.1$ (———)

$R=0.4$ (------).

Also included is the AG critical temperature curve (.....).

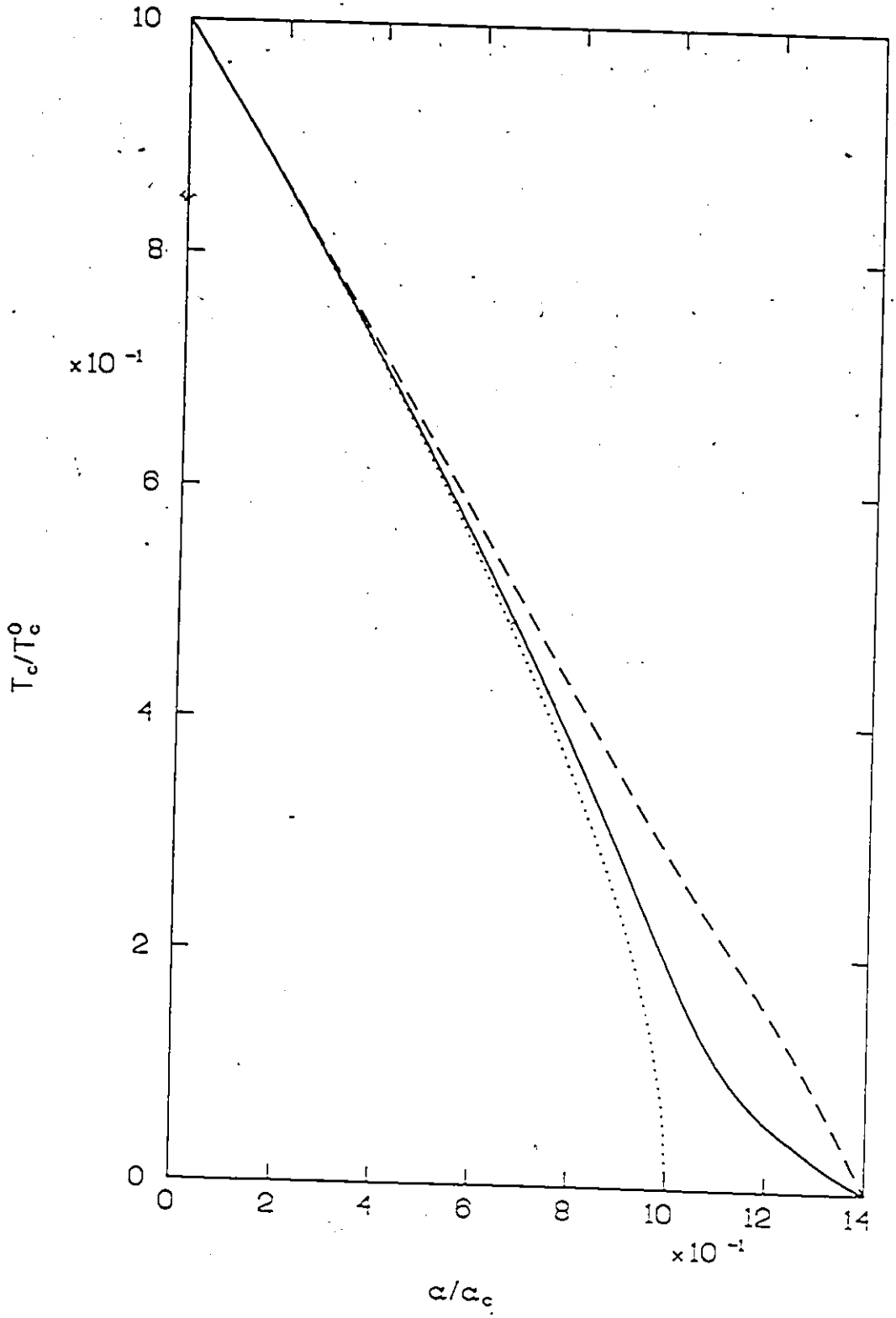
10
8
x10 -1
6
4
2
0
0
2
4
6
8
10
12
14
x10 -1
Tc/Tc0
α/αc

Fig. 3.5 The reduced critical temperature T_c/T_c^0 versus impurity concentration $\alpha(\infty)/\alpha_c$ for the spin-glass model $\bar{\tau}=0.2$, $\bar{D}(1)=2.0$, $\tilde{Q}_1(\bar{t})=S^2(1-\bar{t})$ and $T_f = R\left[\frac{n}{n_c}\right]T_c^0$, where

$R=0.1$ (———)

$R=0.2$ (.....),

$R=0.4$ (------).

Also included is the AG critical temperature curve (-·-·-·).

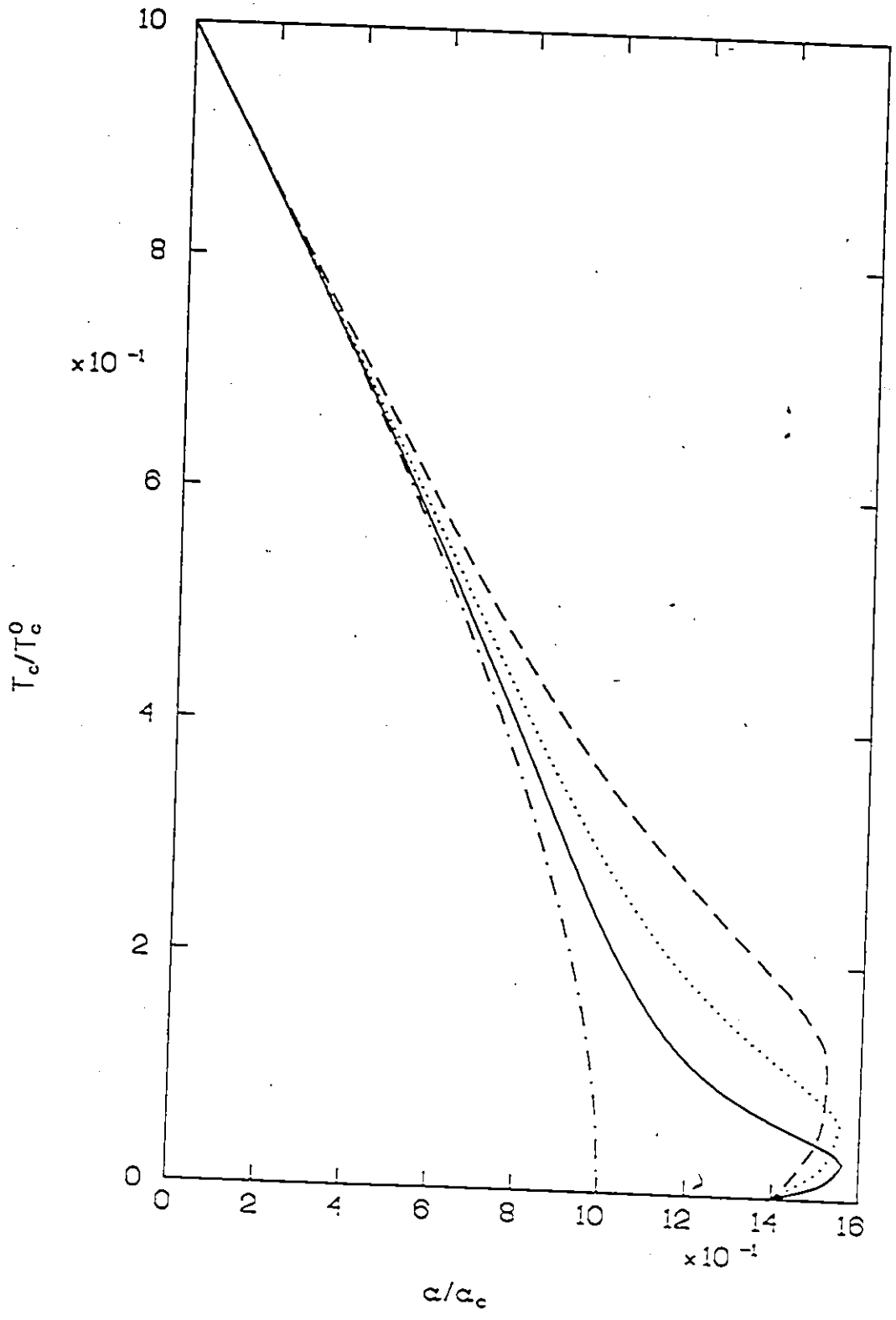
10
8
x10⁻¹
6
4
2
0
0
2
4
6
8
10
12
14
16
x10⁻¹
T_c/T_c^0
α/α_c

Fig. 3.6 The critical magnetic field deviation function D(t) versus t^2 for the spin-glass model $\bar{D}(1)=1.0$, $\tilde{Q}(\tilde{t})=S^2(1-\tilde{t}^2)$ and $R=0.1$ for the reduced critical temperatures

$T_c/T_c^0=0.95$, $T_f/T_c=0.0053$ (———),

$T_c/T_c^0=0.80$, $T_f/T_c=0.025$ (.....),

$T_c/T_c^0=0.58$, $T_f/T_c=0.068$ (------),

$T_c/T_c^0=0.34$, $T_f/T_c=0.18$ (-·-·-·),

$T_c/T_c^0=0.094$, $T_f/T_c=0.85$ (-··-··),

$T_c/T_c^0=0.02$, $T_f/T_c=4.6$ (-···-).

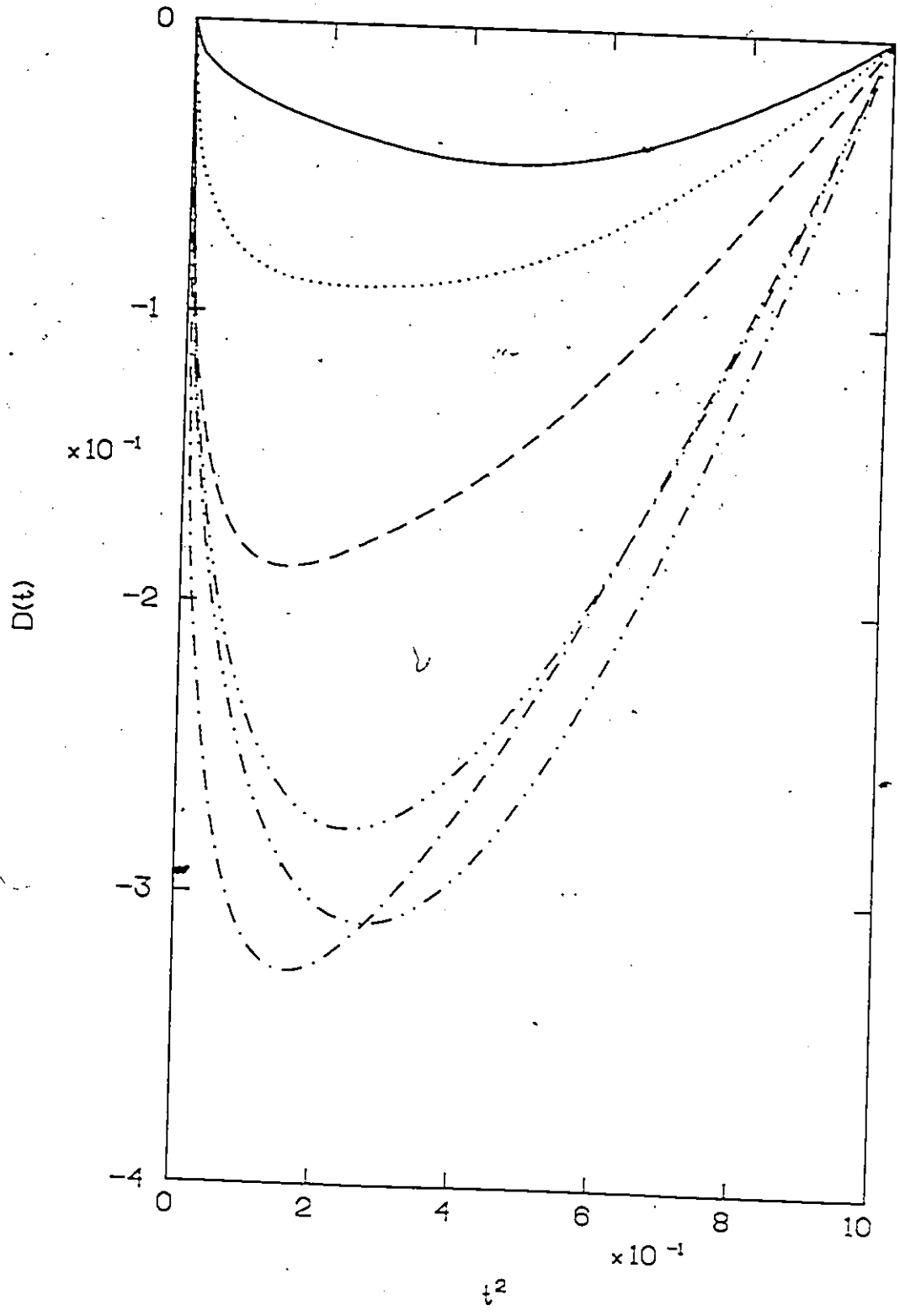
0
−1
−2
−3
−4
x10 −1
D(t)
0
2
4
6
8
10
x10 −1
t²

Fig. 3.7 The temperature dependence of the critical magnetic $H_c(t)$ for the same parameters as in Fig. 3.6: spin-glass model $\tilde{D}(1)=1.0$, $\tilde{Q}(\tilde{t})=S^2(1-\tilde{t}^2)$ and $R=0.1$ for the reduced critical temperatures

$T_c/T_c^0=0.95$, $T_f/T_c=0.0053$ (———),

$T_c/T_c^0=0.80$, $T_f/T_c=0.025$ (.....),

$T_c/T_c^0=0.58$, $T_f/T_c=0.068$ (------),

$T_c/T_c^0=0.34$, $T_f/T_c=0.18$ (—·—·—·),

$T_c/T_c^0=0.094$, $T_f/T_c=0.85$ (—··—··),

$T_c/T_c^0=0.02$, $T_f/T_c=4.6$ (—····—).

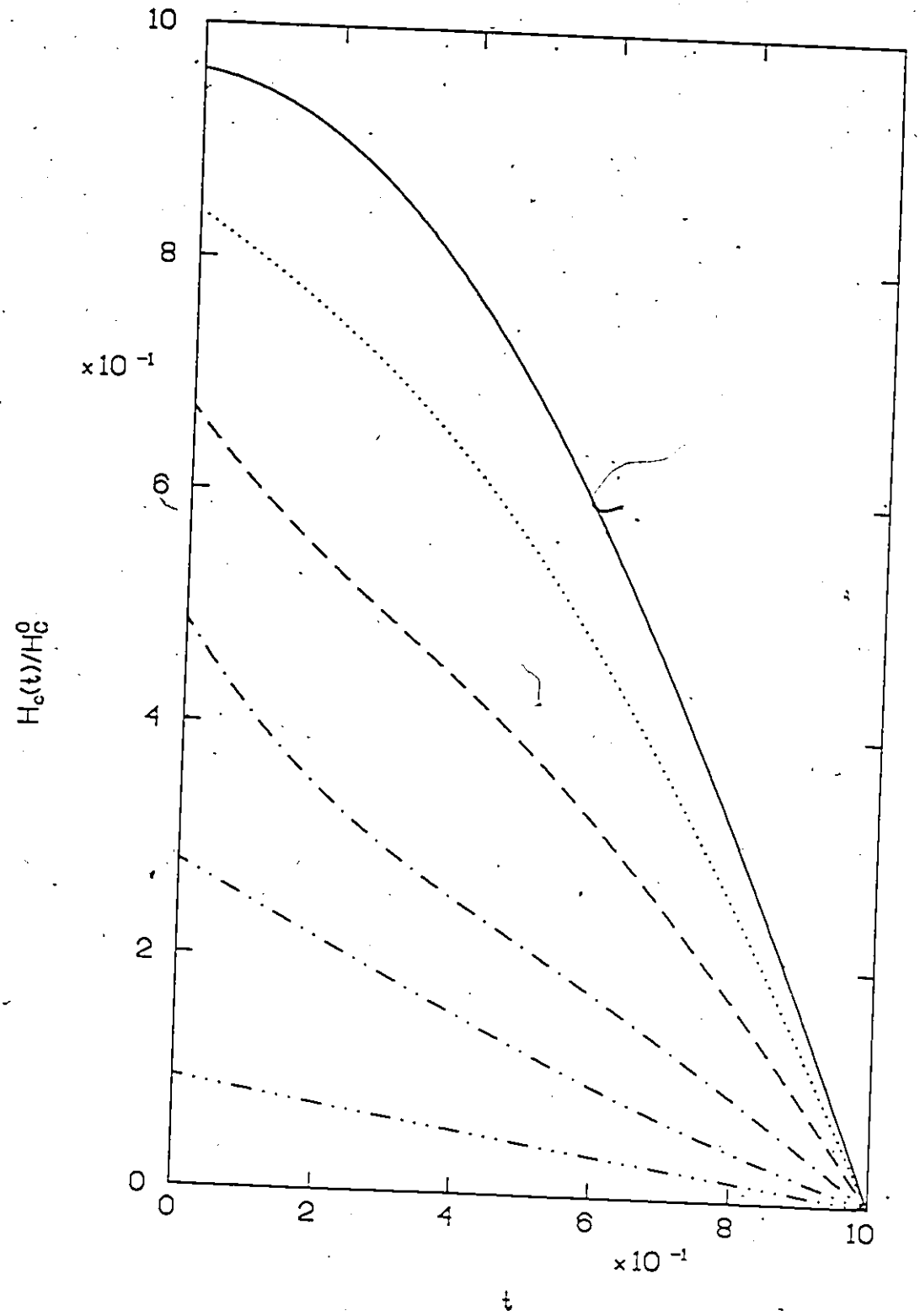
10
8
6
4
2
0
x10 -1
$H_c(t)/H_c^0$
0
2
4
6
8
10
x10 -1
t

Fig. 3.8 The critical magnetic field deviation function $D(\bar{t})$ versus t^2 for the spin-glass model $\tilde{D}(1)=2.0$, $\tilde{Q}_1(\bar{t})=S^2(1-\bar{t})$ and $R=0.2$ for the reduced critical temperatures

$T_c/T_c^0=0.95$, $T_f/T_c=0.0085$ (———),

$T_c/T_c^0=0.80$, $T_f/T_c=0.050$ (.....),

$T_c/T_c^0=0.58$, $T_f/T_c=0.14$ (------),

$T_c/T_c^0=0.34$, $T_f/T_c=0.38$ (—·—·—·).

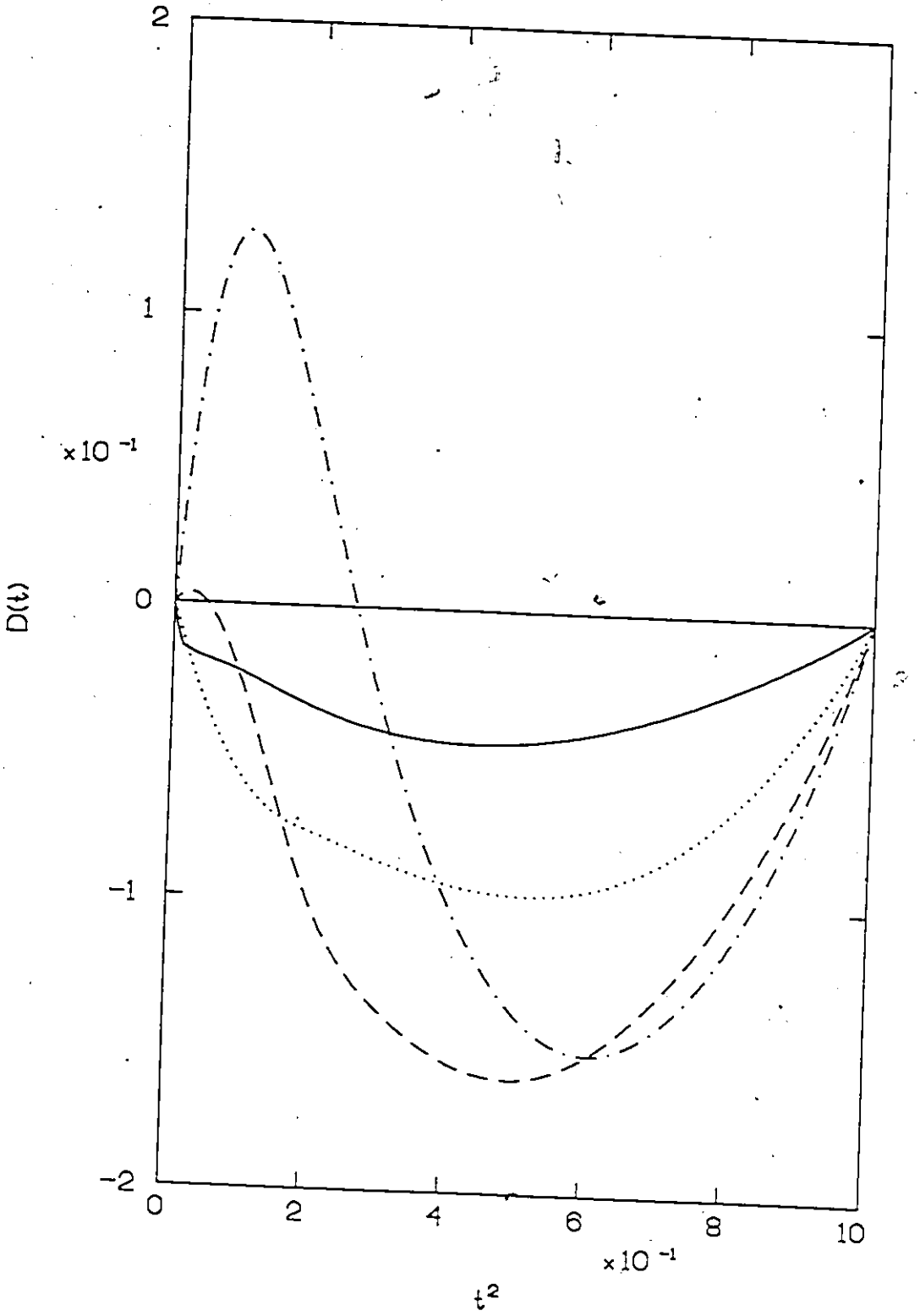
2
1
0
−1
−2
D(t)
×10 −1
0
2
4
6
8
10
×10 −1
t²

Fig. 3.9 The temperature dependence of the critical magnetic $H_c(t)$ for the same parameters as in Fig. 3.8: spin-glass model $\bar{D}(1)=2.0$, $\tilde{Q}_1(\bar{t})=S^2(1-\bar{t})$ and $R=0.2$ for the reduced critical temperatures

$T_c/T_c^0=0.95$, $T_f/T_c=0.0085$ (———),

$T_c/T_c^0=0.80$, $T_f/T_c=0.050$ (.....),

$T_c/T_c^0=0.58$, $T_f/T_c=0.14$ (------),

$T_c/T_c^0=0.34$, $T_f/T_c=0.38$ (—·—·—·).

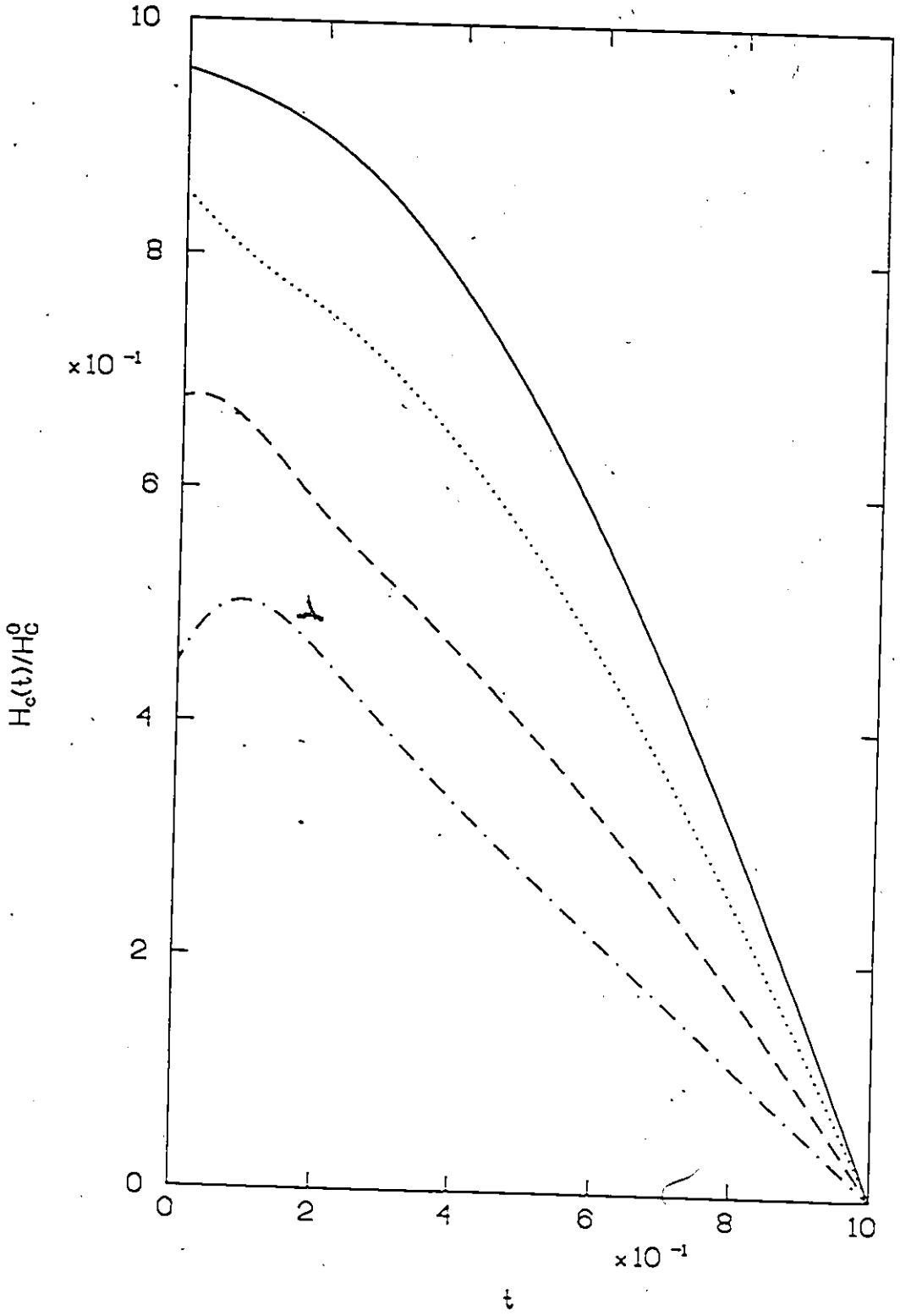
10
8
6
4
2
0
0
2
4
6
8
10
x10 -1
x10 -1
$H_c(t)/H_c^0$
t

Fig. 3.10 The electronic contribution to the thermal conductivity of a superconducting spin-glass for the models $\bar{\tau}=0.2$, $R=0.2$, $\bar{D}(1)=1.0$, $\tilde{Q}(\bar{t})=S^2(1-\bar{t}^2)$ (.....), $\bar{\tau}=0.2$, $R=0.2$, $\bar{D}(1)=2.0$, $\tilde{Q}_1(\bar{t})=S^2(1-\bar{t})$ (------), and AG theory (———). The curves are labeled by reduced critical temperature T_c/T_c^0, and successive curves have been shifted up by 0.2 for clarity. The spin-glass freezing temperatures corresponding to the given reduced critical temperatures are $T_c/T_c^0=0.80 \rightarrow T_f/T_c=0.050$, $T_c/T_c^0=0.60 \rightarrow T_f/T_c=0.14$, and $T_c/T_c^0=0.35 \rightarrow T_f/T_c=0.33$.

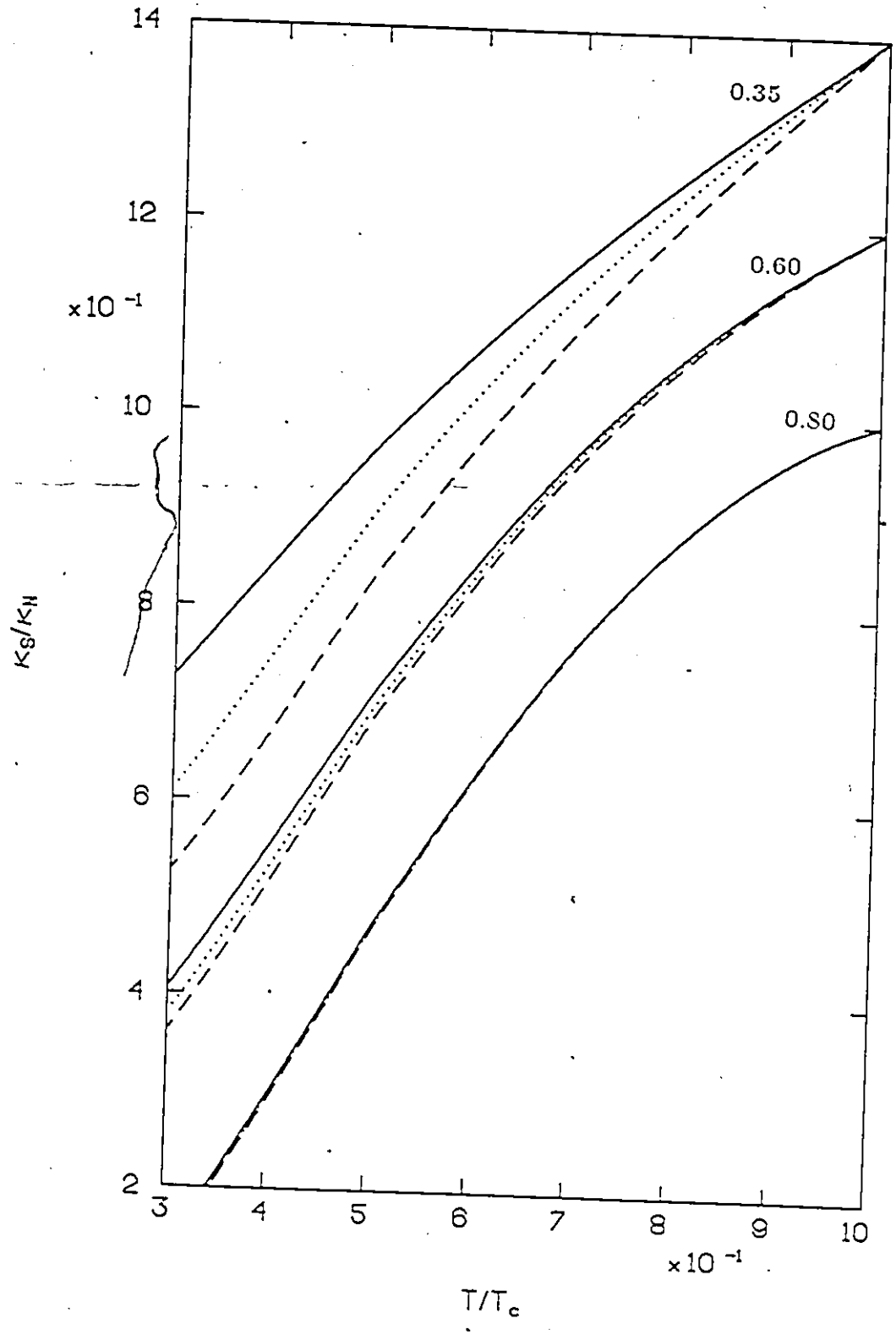
14
12
10
8
6
4
2
x10 -1
κS/κN
0.35
0.60
0.80
3
4
5
6
7
8
9
10
x10 -1
T/Tc

Fig. 3.11 The utrasonic attenuation of a superconducting spin-glass for the models

$\bar{\tau}=0.2$, $R=0.2$, $\bar{D}(1)=1.0$, $\tilde{Q}(\bar{t})=S^2(1-\bar{t}^2)$ (.....),

$\bar{\tau}=0.2$, $R=0.2$, $\bar{D}(1)=2.0$, $\tilde{Q}_1(\bar{t})=S^2(1-\bar{t})$ (------),

and AG theory (———).

The curves are labeled by reduced critical temperature T_c/T_c^0, and successive curves have been shifted up by 0.2 for clarity. The spin-glass freezing temperatures corresponding to the given reduced critical temperatures are $T_c/T_c^0=0.80 \rightarrow T_f/T_c=0.050$,

$T_c/T_c^0=0.60 \rightarrow T_f/T_c=0.14$,

and $T_c/T_c^0=0.35 \rightarrow T_f/T_c=0.33$.

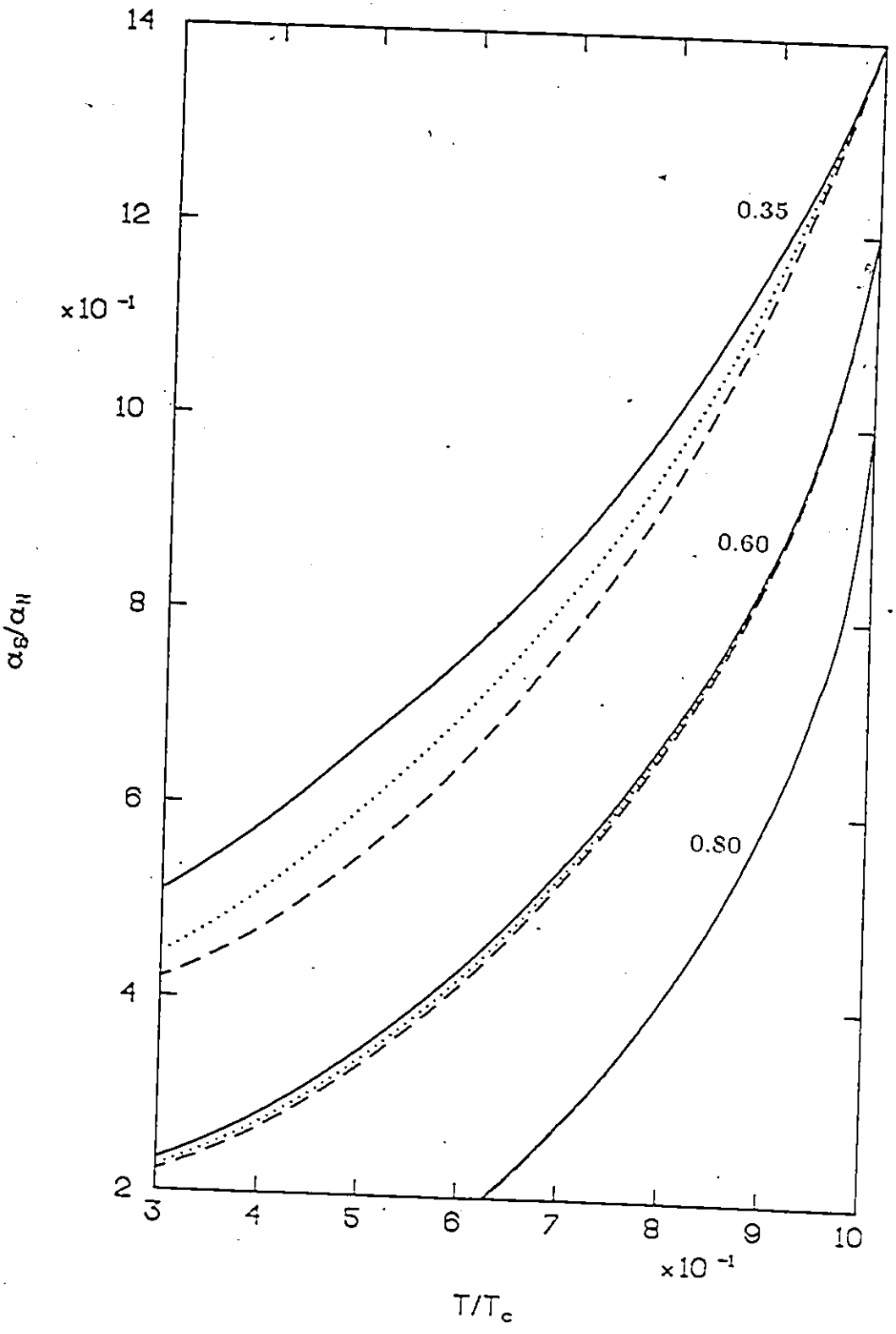
14
12
10
8
6
4
2
x10 -1
αs/αll
0.35
0.60
0.80
3
4
5
6
7
8
9
10
x10 -1
T/Tc

Fig. 3.12 The temperature dependence of the local limit penetration depth for a superconducting spin-glass. Plotted on the ordinate is $\lambda_\ell \left[4\pi\sigma_N[1-t^4]\right]^{1/2}$, where the temperature dependent factor extracts a major part of the temperature variation, and in particular removes the divergence at T_c. The models used are AG (———),

$\bar{r}=0.2$, $\bar{D}(1)=1.0$, $\tilde{Q}(\bar{t})=S^2(1-\bar{t}^2)$, $R=0.2$ (.....),

$\bar{r}=0.2$, $\bar{D}(1)=2.0$, $\tilde{Q}_1(\bar{t})=S^2(1-\bar{t})$, $R=0.2$ (------),

and the curves labeled (1-3) are for the reduced critical and freezing temperatures :

1 $T_c/T_c^0=0.80$, $T_f/T_c=0.050$,

2 $T_c/T_c^0=0.60$, $T_f/T_c=0.14$,

3 $T_c/T_c^0=0.35$, $T_f/T_c=0.33$.

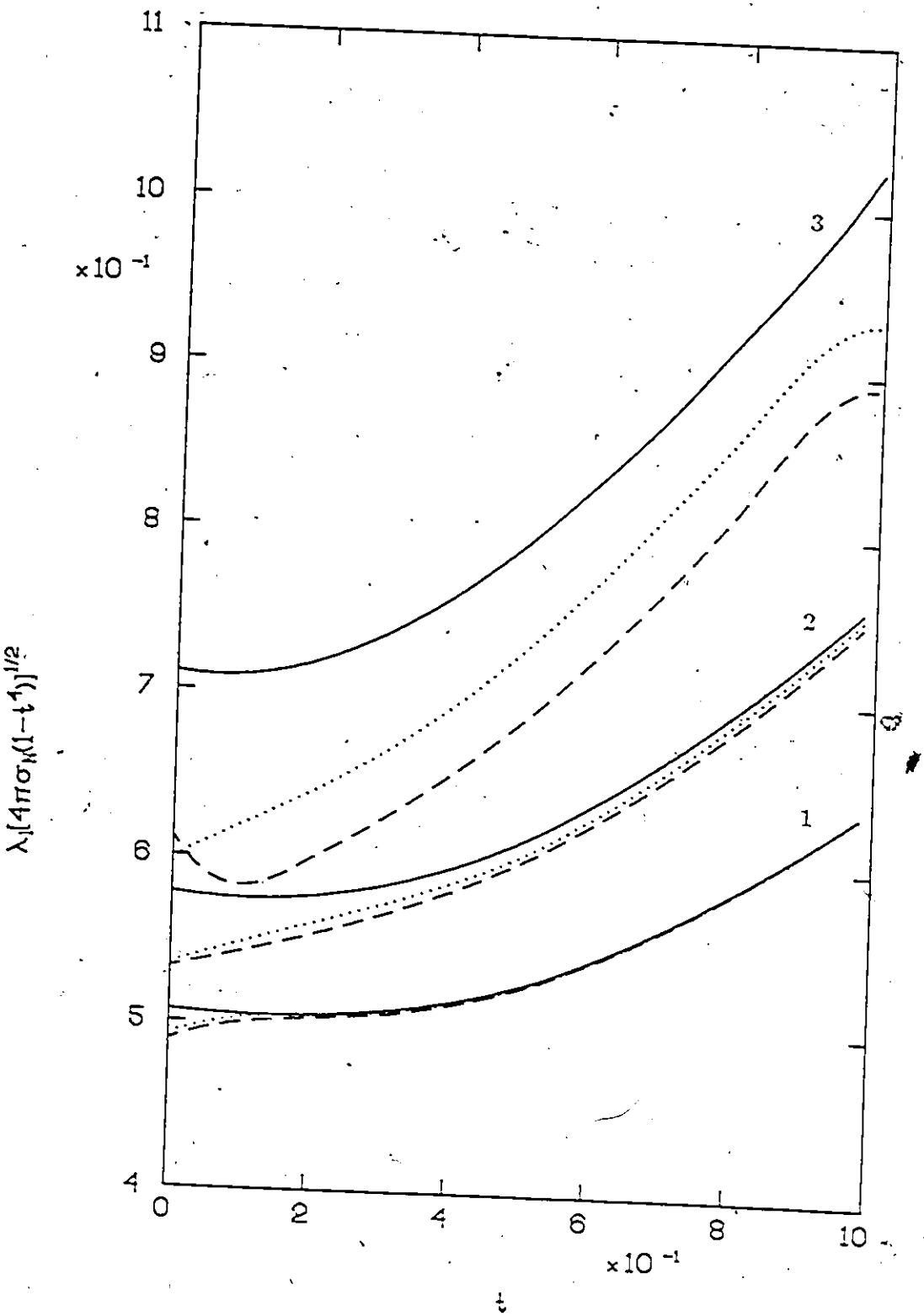
11
10
9
8
7
6
5
4
0
2
4
6
8
10
x10 -1
x10 -1
3
2
1
t
$\lambda_{\parallel}[4\pi\sigma_N(1-t^4)]^{1/2}$

Fig. 3.13 The temperature dependence of the free energy difference of a reentrant ferromagnetic superconductor with exchange scattering rate given by the model of Lee[54]. Here $t=T/T_{c1}$, where T_{c1} is the upper critical temperature, and ΔF_0 is the zero temperature free energy difference which the material would have in the absense of magnetic effects. All curves were calculated with $T_c^0=12$ K, $T_{c1}=8.7$ K, and $T_m=0.93$ K.

a) The temperature dependence of the free energy difference with $1/(4k_F\ell)=0.001$ for different values of the parameter $\mu = 4\varsigma_0^2 k_F^2/T_m$, with: $\mu = 8.0$ (———), $\mu = 2.0$ (.....), $\mu = 0.1$ (------), and $\mu = 0.01$ (-·-·-·).

b) The temperature dependence of the free energy difference for $\mu=1.0$, all critical temperatures as in a), and $1/(4k_F\ell)=0.001$ (———), $1/(4k_F\ell)=0.010$ (.....), and $1/(4k_F\ell)=0.100$ (------).

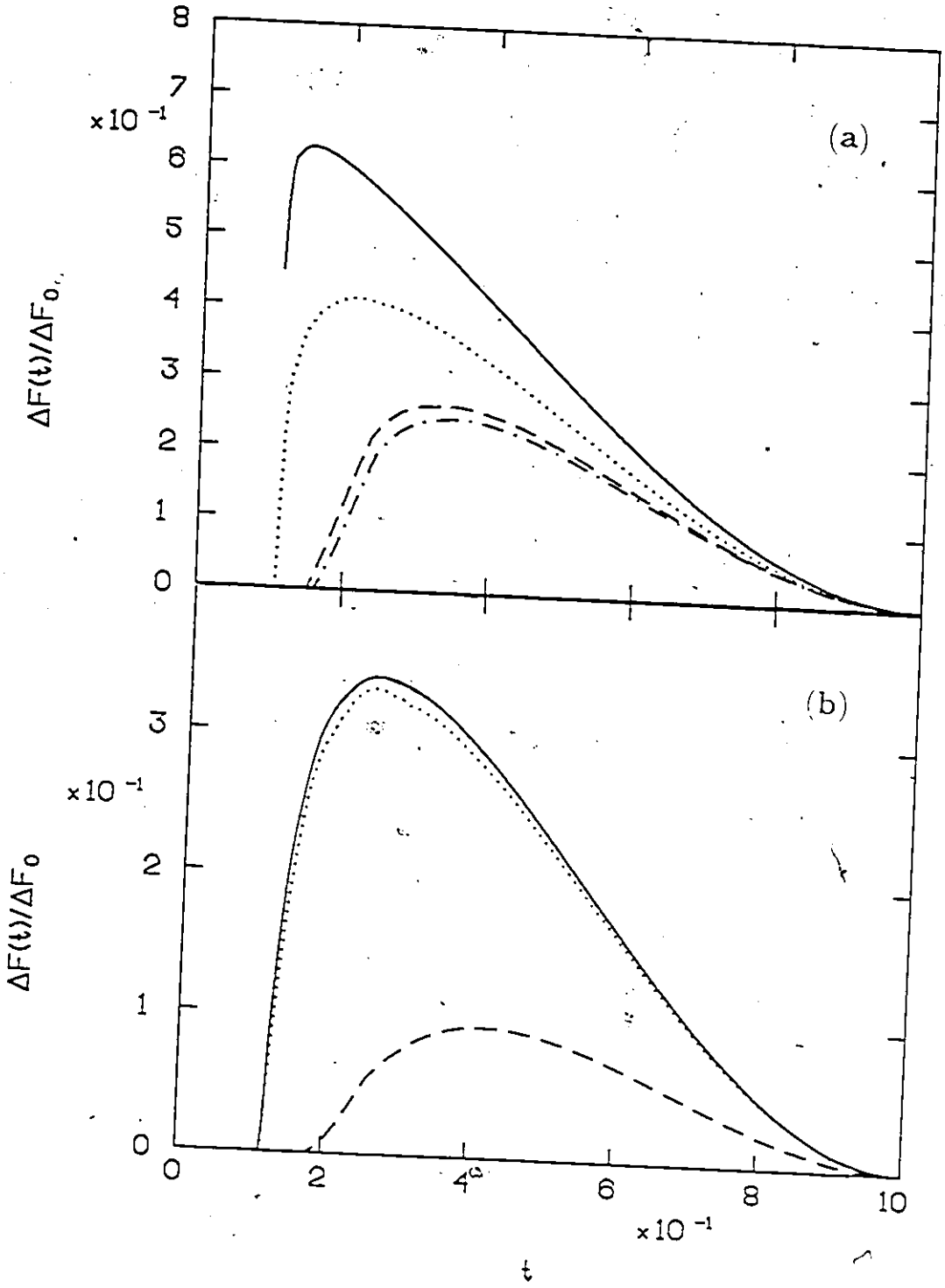
(a)
(b)
$\Delta F(t)/\Delta F_0$
$\times 10^{-1}$
t
$\times 10^{-1}$

Fig. 3.14 The temperature dependence of the thermal conductivity of a reentrant ferromagnetic superconductor $\kappa_S(t)$, normalized to the normal state value at t=1, $\kappa_N(1)$. The parameters of the models are T_c=8.7 K, T_c^0=12 K, T_m=0.93 K, $1/(4k_F\ell)$=0.001, and

μ = 8.0 (———),

μ = 2.0 (.....),

μ = 1.0 (------),

μ = 0.1 (-·-·-·).

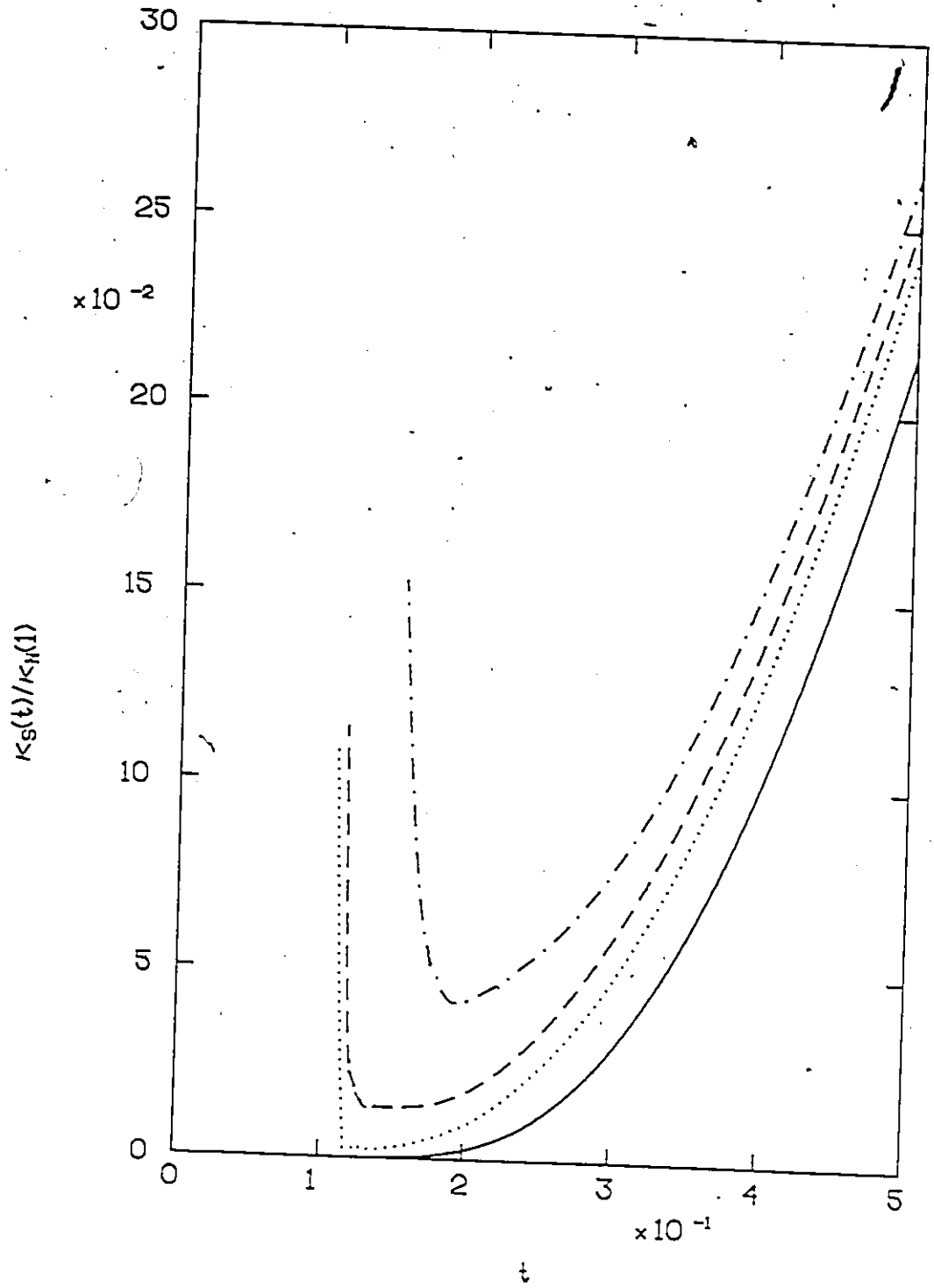
30
25
x10 -2
20
15
10
5
0
0
1
2
3
4
5
x10 -1
t
κS(t)/κH(1)

CHAPTER IV

PROXIMITY EFFECT SYSTEMS

4.1 Introduction

The proximity effect between different metals might be described as the "leakage" of the properties of one metal into another. In the particular case of an interface between a superconductor (S) and a normal metal (N) the superconductivity may be described as "leaking" into the normal metal. This can be understood qualitatively to result from the long range coherence of the superconducting state: the superconducting coherence length is a measure of the spatial range of the special correlations which distinguish the superconducting state from a normal metal. In a rough way this coherence length may be said to reflect the spatial extent of the Cooper pair wavefunction. The superconducting correlations may vary only on length scales greater than, or of the order of, the coherence length, so that on the atomic length scale which is appropriate for a clean interface the superconducting order parameter cannot drop discontinuously to zero on the normal side of a junction.

If there is a thin insulating film (I) between the normal and superconducting metals (S-I-N junction) with a finite probability for electron tunneling through the insulating barrier, then the amplitude of the superconducting correlations near the barrier on the N side will

be reduced compared to that on the S side, but there will still be a finite Cooper pair amplitude, and this will decay in the normal metal on a length scale determined by the coherence length on the N side.

In general the spatial variation of the superconducting order parameter in a junction greatly increases the complexity of the theoretical treatment[84], with the exception of one special limit. It was first realized by McMillan[11] that if both S and N films are thinner than their respective coherence lengths, then to a very good approximation the superconducting order parameter will be constant in amplitude within each film. Within this approximation the spatial dependence of the order parameter is then replaced by two order parameters Δ_S and Δ_N, which are determined self-consistently in terms of the tunneling probability through the barrier. This approximation greatly reduces the computational complexity of the proximity effect problem, and is the model which will be used in this thesis.

Following McMillan[11], and Kaiser and Zuckermann[85], who extended McMillan's model to include paramagnetic impurities on the N side, the thicknesses of the films will be denoted by d_S and d_N for the superconducting and normal sides respectively. One main assumption of the McMillan model is that both N and S films are thinner than their respective coherence lengths, so that the superconducting properties may be treated as being independent of position within a given film. This typically restricts the validity of the McMillan model to films with thicknesses of the order of hundreds of Angstroms or less, despite this it is often applied when this condition is not satisfied. In fact agreement may be essentially identical with experiment in both

cases[86]. A second crucial assumption is that the effect of the interface between the N and S films may be treated in terms of tunneling through a thin insulating layer. This is described mathematically in terms of the tunneling Hamiltonian

$$H_T = \sum_{nm} T_{nm}\left[a^{\dagger}_{n\uparrow}b_{m\uparrow}+b^{\dagger}_{-m\downarrow}a_{-n\downarrow}+b^{\dagger}_{m\uparrow}a_{n\uparrow}+a^{\dagger}_{-n\downarrow}b_{-m\downarrow}\right]. \qquad (4.1)$$

Here the operator $a^{\dagger}_{n\sigma}$ creates an electron in the one-electron state ψ_n with spin σ on the normal metal side of the junction, and the operator $b^{\dagger}_{m\sigma}$ creates an electron in the one-electron state ψ_m with spin σ on the superconducting side. The Hamiltonian (4.1) therefore describes processes involving the transfer of electrons from one side of the insulating barrier to the other, with the matrix element T_{nm}. One further simplifying assumption made by McMillan is that the transfer matrix element T_{nm} is independent of the indices n and m, which means that all states on opposite sides of the barrier are coupled equally. This is obviously not true if the states ψ_n are Bloch states, in which case states with wavevectors parallel or perpendicular to the plane of the boundary would not be expected to have equal tunneling probabilities. However, as pointed out by McMillan[11], if the films are "dirty" in the sense first discussed by Anderson[87], then the appropriate states ψ_n are no longer Bloch states, but rather linear combinations of Bloch states with contributions from all regions of the Fermi surface. In this case the transfer matrix element is, to a very good approximation, independent of the states involved.

The approach as taken by McMillan is to include the contributions from the transfer Hamiltonian H_T to the self energies on either side of the barrier within second order self-consistent perturbation theory. The lowest order contribution to the electronic self-energy on the normal side is then given by

$$\Sigma_N(i\omega_m) = T^2 \sum_n \rho_3 \mathcal{G}_S(n,i\omega_m)\rho_3 \,. \tag{4.2}$$

where $\mathcal{G}_S(n,i\omega_m)$ is the matrix Green's function previously defined in (2.9). The sum over states n in (4.2) is readily performed when the ansatz (2.23) is inserted for $\mathcal{G}(n,i\omega_m)$ (see for example (2.30)). The self-energy contribution then takes the form

$$\Sigma_N(i\omega_m) = T^2 \sum_n \left[\frac{i\omega_m Z_S + \epsilon_n \rho_3 - \tilde{\Delta}_S \rho_2 \sigma_2}{(i\omega_m)^2 Z_S^2 - (\epsilon_n^2 + \tilde{\Delta}_S^2)} \right],$$

$$= \pi T^2 A d_N N_{NO} \frac{i\omega_m Z_S - \tilde{\Delta}_S \rho_2 \sigma_2}{[\tilde{\Delta}_S^2 + \omega_m^2 Z_S^2]^{1/2}} \,. \tag{4.3}$$

where the area of the junction is A, and the one-electron density of states per unit volume at the Fermi level on the normal side is denoted N_{NO}. Note that the frequency argument $i\omega_m$ of Z_S and $\tilde{\Delta}_S$ has been suppressed in (4.3). There is obviously a similar contribution to the self energy of the superconducting side of the junction, which is given by the interchange of the labels N and S.

To include magnetic impurities or the model spin-glass on the

normal side of the junction the appropriate self-energy as considered in Chapters II or III may simply be added to the proximity effect contribution (4.3). This has been carried out for the AG case by Kaiser and Zuckermann[85]. The strong scattering limit has been investigated by Machida[88] within a model which treats the paramagnetic impurity scattering within an approximation which is equivalent to the Shiba[8]-Rusinov[9] (SR) model previously considered in Chapter II of this thesis. Kaiser[89] has also considered the strong scattering limit, and has attempted to include the Kondo effect by using an approximate form of the theory of Müller-Hartmann and Zittartz[21] (MZ). The approximation to the MZ theory results in a Green's function identical in structure to that of the SR model, with the Kondo effect resulting in the scattering parameter ϵ_0 acquiring a temperature dependence. Mori[90] has calculated some transport properties for these models, both with and without including the approximate treatment of the Kondo effect.

If the pairing interaction on the superconducting side of the junction is treated within the BCS approximation, and the normal side is assumed to have no pairing interaction, then the gap equations which result in the SR case are those given by Machida[88]. There are two equations from the two matrix components of the Green's function on both sides of the junction, resulting in four coupled equations for the four functions $\tilde{\Delta}_{S(N)}$ and $Z_{S(N)}$. On the real frequency axis they are

$$\tilde{\Delta}_S(\omega) = \Delta_{Ph} + \Gamma_S \tilde{\Delta}_N(\omega)/D_N(\omega) \qquad (4.4a)$$

$$Z_S(\omega) = 1 + \Gamma_S Z_N(\omega)/D_N(\omega) \tag{4.4b}$$

$$\tilde{\Delta}_N(\omega) = \Gamma_N \tilde{\Delta}_S(\omega)/D_S(\omega) + \Gamma_2(\omega)\tilde{\Delta}_N(\omega)/D_N(\omega) \tag{4.4c}$$

$$Z_N(\omega) = 1 + \Gamma_N Z_S(\omega)/D_S(\omega) + \Gamma_1(\omega)Z_N(\omega)/D_N(\omega) \tag{4.4d}$$

where

$$D_I(\omega) = \left[\tilde{\Delta}_I^2(\omega) - \omega^2 Z_I^2(\omega)\right]^{1/2}, \quad I = N \text{ or } S. \tag{4.4e}$$

The square root in (4.4e) must always be chosen to have a positive real part.

The scattering rates Γ_S and Γ_N are defined by

$$\Gamma_S = \pi A T^2 d_N N_{NO} = \frac{1}{2\tau_S} \tag{4.5a}$$

and

$$\Gamma_N = \pi A T^2 d_S N_{SO} = \frac{1}{2\tau_N}. \tag{4.5b}$$

which clearly satisfy

$$\frac{\Gamma_S}{\Gamma_N} = \frac{d_N N_{NO}}{d_S N_{SO}}. \tag{4.6}$$

The relaxation time is estimated by McMillan[11] to be

$$\tau_N = L_N/(v_{FN}\sigma) \tag{4.7}$$

where L_N is the average path length traveled between collisions with

the barrier, and σ is the barrier penetration probability. This gives

$$\Gamma_N = \frac{v_{FN}\sigma}{4Bd_N} \quad . \tag{4.8}$$

where $2Bd_N$ represents the average distance traveled between collisions with the barrier, with B taken to be a constant of order two for relatively clean films. These results imply that $\Gamma_{N(S)}$ is inversely proportional to $d_{N(S)}$. These parameters are usually fixed by matching the experimentally observed depression of T_c with varying thicknesses, while keeping the ratio Γ_S/Γ_N constant as indicated by (4.6).

The frequency dependent impurity scattering contributions Γ_1 and Γ_2 are given by

$$\Gamma_1(\omega) = \frac{\pi}{2\pi N_{NO}} \sum_{\ell=1}^{\infty} (2\ell+1)(1-\eta_\ell\epsilon_\ell)\frac{\omega^2 Z_N^2(\omega)-\tilde{\Delta}_N^2(\omega)}{\omega^2 Z_N^2(\omega)-\tilde{\Delta}_N^2(\omega)\epsilon_\ell^2} \quad . \tag{4.9a}$$

$$\Gamma_2(\omega) = \frac{\pi}{2\pi N_{NO}} \sum_{\ell=1}^{\infty} (2\ell+1)(\epsilon_\ell-\eta_\ell)\epsilon_\ell \frac{\omega^2 Z_N^2(\omega)-\tilde{\Delta}_N^2(\omega)}{\omega^2 Z_N^2(\omega)-\tilde{\Delta}_N^2(\omega)\epsilon_\ell^2} \quad . \tag{4.9b}$$

where the scattering parameters as defined in Chapter II are

$$\epsilon_\ell = \cos(\delta_\ell^+ - \delta_\ell^-) \quad . \tag{4.10a}$$

and

$$\eta_\ell = \cos(\delta_\ell^+ + \delta_\ell^-) \quad . \tag{4.10b}$$

Recall that the parameter η_ℓ indicates the strength of the normal (non-exchange) scattering from the SR impurities, and is most often taken to be unity (pure exchange scattering) as most superconducting propterties are independent of normal scattering. There are, however, cases where the normal state electronic mean free path is important, as is the case for the electromagnetic coherence length and the experimentally more important upper critical magnetic field H_{c2}. In this thesis η_ℓ will be assumed to be unity unless otherwise specified.

The quantity Δ_{Ph} introduced in (4.4a) is the superconducting order parameter, which satisfies the usual BCS self-consistency equation

$$\Delta_{Ph} = N_{SO}V \int_0^{\omega_D} d\omega \; \mathrm{Re}\left[\frac{\tilde{\Delta}_S(\omega)}{[\omega^2 Z_S^2(\omega)-\tilde{\Delta}_S^2]^{1/2}}\right] \tanh(\beta\omega/2) \qquad (4.11)$$

Two of the equations (4.4) may be eliminated by using the definitions

$$\Delta_I(\omega)=\tilde{\Delta}_I(\omega)/Z_I(\omega), \quad I=N,S \; , \qquad (4.12)$$

which results in

$$\Delta_N(\omega) = \frac{\Gamma_N \Delta_S(\omega)}{[\Delta_S^2(\omega)-\omega^2]^{1/2}}\left[1+\frac{\Gamma_N}{[\Delta_S^2(\omega)-\omega^2]^{1/2}}+\frac{\Gamma(\omega)}{[\Delta_N^2(\omega)-\omega^2]^{1/2}}\right]^{-1} \qquad (4.13a)$$

and

$$\Delta_S(\omega) = \left[\Delta_{Ph}+\frac{\Gamma_S \Delta_N(\omega)}{[\Delta_N^2(\omega)-\omega^2]^{1/2}}\right]\left[1+\frac{\Gamma_S}{[\Delta_N^2(\omega)-\omega^2]^{1/2}}\right]^{-1} . \qquad (4.13b)$$

The frequency dependent pair-breaking parameter in (4.13a) is given by

$$\Gamma(\omega) = \Gamma_1(\omega) - \Gamma_2(\omega)$$

$$= \frac{n}{2\pi N_{NO}} \sum_{\ell=1}^{\infty} (2\ell+1)(1-\epsilon_\ell^2) \frac{\omega^2 - \Delta_N^2(\omega)}{\omega^2 - \Delta_N^2(\omega)\epsilon_\ell^2} \qquad (4.14)$$

In the AG limit $\epsilon_0 \to 1$, in which case Γ is frequency independent.

The pair of equations (4.13), together with the order parameter equation (4.11) written in terms of $\Delta_S(\omega)$, may be solved numerically for Δ_{Ph} and the functions $\Delta_S(\omega)$ and $\Delta_N(\omega)$ by first assuming a value for Δ_{Ph}, solving for $\Delta_N(\omega)$ and $\Delta_S(\omega)$ at various frequencies, and then integrating (4.11) to arrive at a new value for Δ_{Ph}. The entire procedure is then repeated until Δ_{Ph} has converged to a stationary value. However, in this case the original set of four coupled equations (4.4) were chosen for numerical solution, rather than the pair (4.13). Although this approach requires slightly more computational time, one appealing feature is that in (4.4) all square roots may always be chosen in one consistent manner, namely to have a positive imaginary part; in the case of (4.13) one must choose that square root which is consistent with the convention in (4.4).

In either case a further complicating factor is that although well behaved at most frequencies, in the neighborhood of any gap edge where the gap functions $\Delta_I(\omega)$ change from being real to complex valued functions, the sets of equations (4.4) or (4.13) do not iterate to

convergence. Following McMillan[11], this problem was circumvented by deriving a set of first order differential equations (by differentiating the equations with respect to frequency), which could then be integrated through the troublesome region using the Runge-Kutta[91] method. The accuracy of this procedure is confirmed following each use by checking for the convergence of the functions at the endpoint of the integration region: if the functions are not consistent with the true converged values to within some reasonably small error, then the entire procedure is begun again with a smaller step size in the Runge-Kutta integration. As an aside here one might mention that this problem is most apparent in the SR model with a small impurity concentration, where the number of "gap edges" may be as large as $2n+1$, where n is the number of scattering parameters included. This results in the computer code, as it currently stands, being most efficient for larger concentrations.

Note that the result for the superconducting critical temperature derived by Kaiser and Zuckermann[85] also applies in this case, with only trivial modification. The imaginary axis version of equations (4.13) are expanded in powers of Δ_S and Δ_N, keeping only the linear terms. The result is

$$\ln\left[\frac{T_c^0}{T_c}\right] - \frac{\Gamma_S}{A_+ - A_-}\left[\left(1-\frac{\alpha}{A_+}\right)\psi\left(\frac{A_+}{2\pi T_c}+\frac{1}{2}\right)-\left(1-\frac{\alpha}{A_-}\right)\psi\left(\frac{A_-}{2\pi T_c}+\frac{1}{2}\right)\right]-\psi\left(\frac{1}{2}\right) \quad . \quad (4.15a)$$

where

$$A_{\pm} = \frac{1}{2}\left[\alpha+\Gamma_N+\Gamma_S\right] \pm \frac{1}{2}\left[\left[\alpha+\Gamma_N+\Gamma_S\right]^2 - 4\alpha\Gamma_S\right]^{1/2} . \qquad (4.15b)$$

and

$$\alpha = \frac{n}{2\pi N_{NO}} \sum_{\ell=1}^{\infty} (2\ell+1)(1-\epsilon_\ell^2) . \qquad (4.15c)$$

The only difference between this result and the AG limit of Kaiser and Zuckermann[85] is in the pair-breaking parameter α defined in (4.15c).

Critical parameters, which reduce T_c to zero, may also be found exactly as done by KZ by taking the limit T_c goes to zero in (4.15a). The critical parameters are then given by

$$\left[\frac{A_+ - A_-}{\Gamma_S}\right] ln(\Delta_0/2) = \left[1-\frac{\alpha_c}{A_+}\right] lnA_+ - \left[1-\frac{\alpha_c}{A_-}\right] lnA_- . \qquad (4.16)$$

where the critical value of the pair-breaking parameter α_c must in general be determined numerically, as $A_\pm$ also depend on α_c, so that (4.16) cannot be solved explicitly for α_c. As pointed out by KZ, (4.16) has no solution unless d_S is less than or equal to some critical thickness given by $\Gamma_S \geq \frac{\Delta_0}{2}$. For very thick S films ($\Gamma_S << \Delta_0$) the model predicts the critical temperature to be only very weakly dependent on the thickness of the N film or on any magnetic properties of the N film.

4.2 The Free Energy Difference

The reduction of the critical temperature of a thin superconducting film by a normal metal film through the proximity effect is only one part of a general modification of the thermodynamic properties. For example, the jump in the specific heat at the critical temperature is also reduced, as pointed out by Fulde and Moorman[92] within Ginzburg-Landau theory and Mohabir and Nagi[93] within the McMillan model, and as observed experimentally in eutectic alloys[94] (bulk material composed of alternating planes of two different metals). Although the composite materials examined up to now probably do not satisfy the condition of layers thinner than a coherence length as assumed in the McMillan model, it may still be of some interest to examine the predictions of this model for thermodynamic properties in general.

The approach taken here to calculating the free energy difference between normal and superconducting states of a proximity effect bilayer will be to generalize the strong-coupling calculation of Bardeen and Stephen[31] (BS) to include the proximity effect within the McMillan model. This involves using a modified form of the free energy functional used by BS, although most of the succeeding steps are then conventional. It is demonstrated in Appendix B that the total free energy difference for the bilayer may be found by applying the conventional Bardeen-Stephen[31] formula for the free energy difference of a superconductor to each side, with the input being the gap and renormalization functions calculated within the McMillan model, and

then adding the two contributions with the proper weighting. It should be stressed that only the total free energy difference is given correctly by this procedure; the contributions from the two sides have no significance taken independently. In fact, if one insists on examining these contributions separately (although the division is not unique, there is a "natural" division which may be intuitively appealing) then a correction term to the BS formula must be added for each side. Although this correction is not small, it gives an equal correction to the two sides, with the final result that in calculating the total free energy difference no correction is required to the BS formula. The total free energy difference per unit volume will then be given by

$$\Delta F = v_S \Delta F_S + v_N \Delta F_N \quad (4.17)$$

where v_I, I=N or S, is the volume fraction of a given material, and ΔF_I is the free energy difference per unit volume in material I. The fractional volumes must obviously satisfy

$$\frac{v_S}{v_N} = \frac{d_S}{d_N} \quad (4.18)$$

since the two films are assumed to share a common surface area A. Recalling the relationship between r_S and r_N given by (4.6), (4.17) may be expressed as

$$\frac{\Delta F}{N_{S0}} = \left[\frac{1}{1+d_N/d_S}\right]\left[f_S+\frac{r_S}{r_N}f_N\right] . \qquad (4.19)$$

where

$$f_I=\frac{\Delta F_I}{N_{I0}} , \quad I=N,S . \qquad (4.20)$$

The values of f_S and f_N required in (4.19) may be calculated using the Bardeen-Stephen[31] formula for the free energy difference, which may be written in the form (A.25)

$$f_I^{BS}=-2\pi T \sum_{n\geq 0}\left[\left[\left[\tilde{\omega}_I^2(n)+\tilde{\Delta}_I^2(n)\right]^{1/2}-\tilde{\omega}_I(n)\right]\left[1-\frac{\tilde{\omega}_I^0(n)}{\left[\tilde{\omega}_I^2(n)+\tilde{\Delta}_I^2(n)\right]^{1/2}}\right]\right] . \qquad (4.21)$$

Here f_I^{BS} is the free energy difference per unit volume between superconducting and normal states divided by the appropriate one-electron density of states N_{I0}. I=N or S. The function $i\tilde{\omega}_I(n) = i\omega_n Z_I(i\omega_n)$ is the renormalized Matsubara frequency, and $i\tilde{\omega}_I^0(n)$ is the normal state ($\Delta\to 0$) limit of this. The functions $Z_I(i\omega_n)$ and $\tilde{\Delta}_I(n) = \tilde{\Delta}_I(i\omega_n)$ are the imaginary axis renormalization and pairing functions for the material I=S or N. In our model these would be given by the imaginary axis equivalent of (4.4).

In the case of a pure superconductor in proximity with a pure normal metal (no magnetic impurities) the expression (4.21) or the real axis equivalent may simply be evaluated twice, once with the functions Z_S and Δ_S, and then once again with the functions Z_N and Δ_N. However if the normal side of the proximity junction contains magnetic impurities described by the SR model, then for the N side of the

junction a correction term must be added to (4.21). This SR correction has been calculated by Yamamoto and Nagi[29], and has the form

$$f_N^{SR}=-2\pi T\sum_{n\geq 0}\sum_{\ell=1}^{\infty}(2\ell+1)\alpha_\ell\left[(1-\epsilon_\ell)\frac{\tilde{\Delta}_N^2(n)}{\tilde{\Delta}_N^2(n)\epsilon_\ell^2+\tilde{\omega}_N^2(n)}\left[\frac{\tilde{\omega}_N(n)}{[\tilde{\omega}_N^2(n)+\tilde{\Delta}_N^2(n)]^{1/2}}-1\right]\right.$$
$$\left.+\frac{\tilde{\Delta}_N^2(n)}{\tilde{\Delta}_N^2(n)\epsilon_\ell^2+\tilde{\omega}_N^2(n)}+\ell n\left[\frac{\tilde{\Delta}_N^2(n)\epsilon_\ell^2+\tilde{\omega}_N^2(n)}{\tilde{\Delta}_N^2(n)+\tilde{\omega}_N^2(n)}\right]\right]. \qquad (4.22)$$

where

$$\alpha_\ell = \frac{n}{2\pi N_{NO}}(1-\epsilon_\ell^2) \qquad (4.23)$$

as defined in (2.57b).

The free energy difference therefore becomes

$$f_S = f_S^{BS} \qquad (4.24a)$$

for the superconducting side, and

$$f_N = f_N^{BS} + f_N^{SR} \qquad (4.24b)$$

for the normal side of the junction. In the AG limit ($\epsilon_0 \to 1$) the SR correction term goes to zero and is not required.

One further step remains before the presentation of some results, that being the representation of the Matsubara frequency sums in equations (4.21-22) in terms of real frequency axis integrals, as the gap equations (4.4) are being solved for this case. Using the

standard techniques[16], that is by first representing the sums as contour integrals and then deforming the contours, one obtains

$$f_I^{BS} = -\mathrm{Im}\int_0^\infty d\omega \left[\left[\left[\tilde{\Delta}_I^2(\omega)-\tilde{\omega}_I^2(\omega)\right]^{1/2}+i\tilde{\omega}_I(\omega)\right] \times \left[1+\frac{i\tilde{\omega}_I^0(\omega)}{\left[\tilde{\Delta}_I^2(\omega)-\tilde{\omega}_I^2(\omega)\right]^{1/2}}\right]\right]\tanh\left[\frac{\beta\omega}{2}\right]. \tag{4.25}$$

where the functions $\tilde{\Delta}_I(\omega)$ and $\tilde{\omega}_I(\omega) = \omega Z_I(\omega)$ are given by the solution of (4.4), and the square roots are taken with a positive real part. The functions $i\tilde{\omega}_I^0(\omega) = i\omega Z_I^0(\omega)$ are the normal state ($\Delta\to 0$) limits of the renormalized frequencies. From (4.4) these are

$$Z_N^0(\omega) = 1 + i\frac{\Gamma_N+\Gamma_1^0}{\omega}, \tag{4.26a}$$

and

$$Z_S^0(\omega) = 1 + \frac{i\Gamma_S}{\omega}, \tag{4.26b}$$

for $\omega > 0$. The scattering rate Γ_1^0 in (4.26a) is the normal state limit of the function $\Gamma_1(\omega)$ defined in (4.9), and is given by

$$\Gamma_1^0 = \frac{n}{2\pi N_{N0}} \sum_{\ell=1}^{\infty} (2\ell+1)(1-\eta_\ell\epsilon_\ell). \tag{4.27}$$

First consider the case of pure proximity junctions, that is the McMillan model without any paramagnetic impurities. In this case

there are two parameters which may be varied, Γ_S and Γ_N. From (4.19) it is obvious that the total free energy difference normalized to that of the pure superconductor may be expressed as a function of Γ_S and Γ_N, with the ratio d_N/d_S coming in explicitly only in an overall normalization factor, $\frac{1}{1+d_N/d_S}$. It will therfore suffice to present results for the total free energy difference with this normalization factor $\frac{1}{1+d_N/d_S}$ calculated with the assumption $N_{S0}=N_{N0}$, which implies that $\frac{1}{1+d_N/d_S} = \frac{1}{1+\Gamma_S/\Gamma_N}$. If a particular junction composition is desired, then the ratio of thicknesses and Γ's must of course be consistent with (4.6), which relates the Γ's to the densities of states and thicknesses. The total free energy or specific heat could then easily be calculated by multiplying the result calculated assuming $N_{S0}=N_{N0}$ by the ratio $[1+\Gamma_S/\Gamma_N]/[1+d_N/d_S]$.

First consider the dependence of the total free energy difference on the parameters Γ_S and Γ_N. Figure 4.1(a) shows, not surprisingly, that the magnitude of the free energy difference per unit volume at low temperatures decreases with increasing normal film thickness, or with decreasing superconducting film thickness. Of more interest, however, may be the actual shape of the temperature dependence, which is most graphically displayed by the deviation function D(t) shown in Fig 4.1(b). Recall that D(t), as previously discussed in Section 2.5, for a pure BCS superconductor reaches a minimum value of approximately -0.037 at $t^2=0.5$, and that strong coupling superconductors such as lead or mercury have positive D(t) curves, which may be approximately attributed to the increase of the

ratio $2\Delta_0/T_c$ for these materials compared to the BCS prediction of 3.53. Within this proximity effect model, for a given r_N, as r_S varies from small values (large d_S) to larger ones (small d_S), the minimum of D(t) becomes more negative, and also moves to lower reduced temperature $t=T/T_c$. This behavior may be understood qualitatively in terms of the proximity effect system being an extra-weak coupling superconductor, with an "effective gap" which satisfies $2\Delta_{eff}/T_c<3.53$.

Another property which might be considered here is the difference in specific heats between the normal and superconducting states of the junction. This is given, as usual, by

$$\Delta C = -T \frac{d^2 \Delta F}{dT^2} \tag{4.28}$$

Figure 4.2(a) shows some examples of the predicted temperature dependence of the specific heat difference for the same parameters as in Fig. 4.1. Note first of all that the jump at T_c is strongly suppressed by decreasing superconducting film thickness. Secondly, the specific heat difference at low temperatures, $0.05 \lesssim T/T_c \lesssim 0.5$, is enhanced (becoming smaller in absolute value) for decreasing r_S (increasing d_S). Figure 4.3 shows that f_N, the contribution from (4.25) for the N side, has a small peak at low temperature $T/T_c \simeq 0.1$, while the contribution from the supconducting side f_S (not shown) is always a monotonic function of temperature and is qualitatively the same as the total shown in Fig. 4.1. When the two contributions are properly conbined the total free energy difference is also monontonic.

but the structure in f_N may show up in the temperature derivatives of the total.

Figure 4.4 shows the dependence of the free energy difference and D(t) on temperature for one set of proximity effect parameters and several paramagnetic impurity concentrations with $\epsilon_0=0$. As in the non-proximity case, the minimum of D(t) increases with increasing impurity concentration in the gapless region.

The temperature dependence of the specific heat difference for the same parameters is shown in Fig. 4.5, where a small structure at t≈0.1 is seen to disappear with increasing impurity concentration. This is consistent with the behavior of the N side contribution to the free enregy difference, Fig. 4.6, where the peak at t≈0.1 disappears with increasing impurity concentration.

Please note once more that the function f_N plotted in Figs. 4.3 and 4.6 was calculated using only the BS formula, (4.25), and does not include the correction given by (B.21). As previously mentioned, within the present model the two contributions to the total free energy difference have no physical significance when taken separately. The function f_N is shown merely to indicate the source of the large curvature of the specific heat difference at t≈0.1.

At this point it is useful to reconsider the jump in the specific heat at the critical temperature, as this may be calculated analytically. This serves two purposes: first, and primarily, it is a very good check of the accuracy of the previous numerical real axis calculation, and second this allows the dependence of the jump on the relevant parameters to be examined with only a trivial amount of

numerical computation, which is more efficient than the numerical procedure which must be used at arbitrary temperatures. This also will allow the present aproach to be compared with the previous calculation of the specific heat jump of pure proximity effect junctions by Mohabir and Nagi[93]. Although the McMillan model of the proximity effect was used, their calculation of the specific heat jump was very different from the present approach; Mohabir and Nagi[93] performed an integration over the coupling constant directly, which is accomplished in the present approach through the use of the result of Luttinger and Ward[95]. The results will be compared after the discussion of the present calculation.

Recall first the Bardeen-Stephen[31] free energy formula on the imaginary frequency axis, (4.21) or (B.25)

$$f_I^{BS} = -2\pi T \sum_{n\geq 0} \left[\left[[\tilde{\omega}_I^2(n)+\tilde{\Delta}_I^2(n)]^{1/2} - \tilde{\omega}_I(n) \right] \left[1 - \frac{\tilde{\omega}_I^0(n)}{[\tilde{\omega}_I^2(n)+\tilde{\Delta}_I^2(n)]^{1/2}} \right] \right] . \quad (4.29)$$

For temperatures approaching T_c the pairing function $\tilde{\Delta}$ goes to zero; (4.29) as well as the gap equations may therefore be expanded in powers of this function. To order Δ^4 the summand in (4.29) (call it $h_I(n)$), becomes

$$h_I(n) = \left[[\tilde{\omega}_I^2(n)+\tilde{\Delta}_I^2(n)]^{1/2} - \tilde{\omega}_I(n) \right] \left[1 - \frac{\tilde{\omega}_I^0(n)}{[\tilde{\omega}_I^2(n)+\tilde{\Delta}_I^2(n)]^{1/2}} \right]$$

$$= \frac{1}{2u_I^2(n)}\left[\tilde{\omega}_I(n)-\tilde{\omega}_I^0(n)\right] - \frac{1}{8u_I^4(n)}\left[\tilde{\omega}_I(n)-3\tilde{\omega}_I^0(n)\right] . \qquad (4.30)$$

In (4.30) the function $u_I(n)=\dfrac{\tilde{\omega}_I(n)}{\tilde{\Delta}_I(n)}$ is inversely proportional to Δ_I, so that in order to find $h_I(n)$ to order Δ^4 one must insert $\tilde{\omega}_I(n)-\tilde{\omega}_I^0(n)$ to order Δ^2, and $\tilde{\omega}_I(n)-3\tilde{\omega}_I^0(n)$ to zeroth order in Δ. This may easily be done by expanding the gap equations in powers of the Δ's. The imaginary frequency axis version of the set of equations (4.13) is given by the limit $\omega \to -i\omega_n$, which gives

$$\tilde{\Delta}_S(n) = \Delta_{Ph} + \Gamma_S\tilde{\Delta}_N(n)/D_N(n) , \qquad (4.31a)$$

$$\tilde{\omega}_S(n) = \omega_n + \Gamma_S\tilde{\omega}_N(n)/D_N(n) , \qquad (4.31b)$$

$$\tilde{\Delta}_N(n) = \Gamma_N\tilde{\Delta}_S(n)/D_S(n) + \Gamma_2(n)\tilde{\Delta}_N(n)/D_N(n) , \qquad (4.31c)$$

$$\tilde{\omega}_N(n) = \omega_n + \Gamma_N\tilde{\omega}_S(n)/D_S(n) + \Gamma_1(n)\tilde{\omega}_N(n)/D_N(n) , \qquad (4.31d)$$

where

$$D_I(n) = \left[\tilde{\Delta}_I^2(n)+\tilde{\omega}_I^2(n)\right]^{1/2} , \quad I=N \text{ or } S. \qquad (4.31e)$$

The frequency dependent impurity scattering contributions Γ_1 and Γ_2 are given by

$$\Gamma_1(n) = \tau \sum_{\ell=1}^{\infty} (2\ell+1)(1-\eta_\ell\epsilon_\ell)\frac{\tilde{\omega}_N^2(n)+\tilde{\Delta}_N^2(n)}{\tilde{\omega}_N^2(n)+\tilde{\Delta}_N^2(n)\epsilon_\ell^2} \qquad (4.32a)$$

$$\Gamma_2^{\sim}(n) = \gamma \sum_{\ell=1}^{\infty} (2\ell+1)(\epsilon_\ell - \eta_\ell)\epsilon_\ell \frac{\tilde{\omega}_N^2(n)+\tilde{\Delta}_N^2(n)}{\tilde{\omega}_N^2(n)+\tilde{\Delta}_N^2(n)\epsilon_\ell^2} . \qquad (4.32b)$$

with $\gamma = \frac{n}{2\pi N_{NO}}$.

To order Δ^2 the renormalized frequencies from (4.31) are

$$\tilde{\omega}_S(n) = \omega_n + \Gamma_S\left[1 - \frac{1}{2u_N^2(n)}\right] \qquad (4.33a)$$

and

$$\tilde{\omega}_N(n) = \omega_n + \Gamma_N\left[1 - \frac{1}{2u_S^2(n)}\right] + \gamma(1-\epsilon_0)\left[1 + \frac{1}{u_N^2(n)}\left[[1-\epsilon_0^2] - \frac{1}{2}\right]\right] . \qquad (4.33b)$$

where the limit of only a single scattering parameter ϵ_0, and no normal scattering ($\eta_0=1$, this cancels out of the final result in any event) has been taken for simplicity.

Upon substituting the results (4.33) into (4.30) and retaining terms to fourth order in Δ, the summands for the free energy difference become

$$h_S(n) = \frac{\omega_n+\Gamma_S}{4u_S^4(n)} - \frac{\Gamma_S}{4u_S^2(n)u_N^2(n)} . \qquad (4.34a)$$

and

$$h_N(n) = \frac{\omega_n+\Gamma_N}{4u_N^4(n)} - \frac{\Gamma_N}{4u_S^2(n)u_N^2(n)} + \frac{\gamma(1-\epsilon_0)(1-\epsilon_0^2)}{2u_N^4(n)} . \qquad (4.34b)$$

At this point the other contribution to the free energy difference on

the normal side of the junction should also be considered, that is the SR correction of Yamamoto and Nagi[29], which has the form (4.22)

$$f_N^{SR}=-2\pi T\sum_{n\geq 0}\sum_{\ell=0}^{\infty}(2\ell+1)\alpha_\ell\left[(1-\epsilon_\ell)\frac{\tilde{\Delta}_N^2(n)}{\tilde{\Delta}_N^2(n)\epsilon_\ell^2+\tilde{\omega}_N^2(n)}\left[\frac{\tilde{\omega}_N(n)}{[\tilde{\omega}_N^2(n)+\tilde{\Delta}_N^2(n)]^{1/2}}-1\right]\right.$$
$$\left.+\frac{\tilde{\Delta}_N^2(n)}{\tilde{\Delta}_N^2(n)\epsilon_\ell^2+\tilde{\omega}_N^2(n)}+\ell n\left[\frac{\tilde{\Delta}_N^2(n)\epsilon_\ell^2+\tilde{\omega}_N^2(n)}{\tilde{\Delta}_N^2(n)+\tilde{\omega}_N^2(n)}\right]\right]. \qquad (4.35)$$

where $\alpha_\ell=\gamma(1-\epsilon_\ell^2)$.

Proceeding exactly as in the previous case by expanding to fourth order in Δ, (4.35) becomes

$$f_N^{SR}=-2\pi T\sum_{n\geq 0}\gamma\left[\frac{-(1-\epsilon_0)(1-\epsilon_0^2)+(1-\epsilon_0^2)^2}{2u_N^4(n)}\right]. \qquad (4.36)$$

When the above result is combined with the normal side Bardeen-Stephen term f_N^{BS} given by (4.29), (4.30) and (4.34b) one finds

$$f_N=f_N^{BS}+f_N^{SR}=-2\pi T\sum_{n\geq 0}\left[\frac{\omega_n+\Gamma_N}{4u_N^4(n)}-\frac{\Gamma_N}{4u_S^2(n)u_N^2(n)}+\frac{\alpha(1-\epsilon_0^2)}{2u_N^4(n)}\right] \qquad (4.37a)$$

where $\alpha=\gamma(1-\epsilon_0^2)$ is the pair-breaking parameter when only S-wave scattering is included, and

$$f_S - f_S^{BS} = -2\pi T \sum_{n\geq 0} \left[\frac{\omega_n + \Gamma_S}{4u_S^4(n)} - \frac{\Gamma_S}{4u_S^2(n)u_N^2(n)} \right] . \qquad (4.37b)$$

Note that in the limit of no paramagnetic impurities ($\alpha \to 0$) the two expressions (4.37) differ only by the interchange of N and S, as would be expected. Also, in the AG limit of $\epsilon_0 \to 1$ the SR correction term in f_N explicitly goes to zero.

Now that the free energy difference near T_c has been expressed in terms of these sums, the remaining major steps are to determine the functional forms of $u_S(n)$ and $u_N(n)$ as explicit functions of the Matsubara frequencies $i\omega_n$, and then the evaluation of the sums. The first of these is very simple; the gap equations (4.31) may be linearized in the Δ's near T_c, allowing the self-consistent pair of equations

$$\Delta_N(n) = \Gamma_N \Delta_S(n) \left[\omega_n + \Gamma_N + \alpha \right]^{-1} \qquad (4.38a)$$

and

$$\Delta_S(\omega) = \left[\Delta_{Ph}\omega_n + \Gamma_S \Delta_N(n) \right] \left[\omega_n + \Gamma_S \right]^{-1} \qquad (4.38b)$$

to be solved analytically. Substituting (4.38b) into (4.38a) gives

$$u_N(n)^{-1} = \frac{\Delta_N(n)}{\omega_n} = \Gamma_N \Delta_{Ph} \left[[\omega_n + \Gamma_N + \alpha][\omega_n + \Gamma_S] - \Gamma_S \Gamma_N \right]^{-1} \qquad (4.39)$$

which may then be inserted into (4.38b) to obtain

$$u_S(n)^{-1}=\frac{\Delta_S(n)}{\omega_n}=\Delta_{Ph}\left[\omega_n+\Gamma_N+\alpha\right]\left[\left[\omega_n+\Gamma_N+\alpha\right]\left[\omega_n+\Gamma_S\right]-\Gamma_S\Gamma_N\right]^{-1}. \qquad (4.40)$$

The next step is not quite as easy as the previous one; frequency sums of terms of the form

$$U(T)\Delta_{Ph}^4 = 2\pi T\sum_{n\geq 0}\left[\frac{\omega_n+\Gamma_S}{u_S^4(n)}\right], \qquad (4.41a)$$

$$V(T)\Delta_{Ph}^4 = 2\pi T\sum_{n\geq 0}\left[\frac{\omega_n+\Gamma_N}{u_N^4(n)}\right], \qquad (4.41b)$$

$$W(T)\Delta_{Ph}^4 = 2\pi T\sum_{n\geq 0}\left[\frac{1}{u_S^2(n)u_N^2(n)}\right], \qquad (4.41c)$$

and

$$Y(T)\Delta_{Ph}^4 = 2\pi T\sum_{n\geq 0}\left[\frac{1}{u_N^4(n)}\right], \qquad (4.41d)$$

must be performed, where the functions $u_N(n)$ and $u_S(n)$ are given by (4.39-40). These sums may be performed analytically in terms of polygamma functions[96], which involves first expanding the summands in terms of partial fractions. The results may be expressed in terms of the variables

$$A_\pm = \frac{1}{2}\left[\alpha+\Gamma_N+\Gamma_S\right] \pm \frac{1}{2}\left[\left[\alpha+\Gamma_N+\Gamma_S\right]^2-4\alpha\Gamma_S\right]^{1/2}. \qquad (4.42)$$

previously introduced in the T_c equation (4.15), and in terms of the new auxiliary functions

$$E_{\pm} = \left[\left\{\alpha+\Gamma_N+\Gamma_S\right\}^2 - 4\alpha\Gamma_S\right]^{-1/2}\left\{\Gamma_N+\alpha-\Lambda_{\pm}\right\}. \qquad (4.43)$$

The results may then be written in the form:

$$\begin{aligned} U(T) = & -\frac{E_-^4(\Gamma_S-\Lambda_-)}{6(2\pi T)^3}\psi^{(3)}(\bar{\Lambda}_-) + \frac{E_+^4(\Gamma_S-\Lambda_-)}{6(2\pi T)^3}\psi^{(3)}(\bar{\Lambda}_+) \\ & - \frac{E_-^3}{2(2\pi T)^2}\left\{E_- - \frac{4E_+(\Gamma_S-\Lambda_-)}{\Lambda_+-\Lambda_-}\right\}\psi^{(2)}(\bar{\Lambda}_-) - \frac{E_+^3}{2(2\pi T)^2}\left\{E_+ - \frac{4E_-(\Gamma_S-\Lambda_+)}{\Lambda_--\Lambda_+}\right\}\psi^{(2)}(\bar{\Lambda}_+) \\ & + \frac{2E_-^2E_+}{2\pi T(\Lambda_+-\Lambda_-)}\left\{-2E_- - (2E_-+3E_+)\frac{(\Gamma_S-\Lambda_-)}{(\Lambda_+-\Lambda_-)}\right\}\psi^{(1)}(\bar{\Lambda}_-) \\ & + \frac{2E_+^2E_-}{2\pi T(\Lambda_--\Lambda_+)}\left\{-2E_+ - (2E_++3E_-)\frac{(\Gamma_S-\Lambda_+)}{(\Lambda_--\Lambda_+)}\right\}\psi^{(1)}(\bar{\Lambda}_+) \\ & - \frac{2E_-E_+(\Gamma_S-\Gamma_N-\alpha)}{(\Lambda_+-\Lambda_-)^3}\left[1 - \frac{\Gamma_S\Gamma_N}{(\Lambda_+-\Lambda_-)^2} + \left\{\frac{\Gamma_S-\Gamma_N-\alpha}{\Lambda_+-\Lambda_-}\right\}^2\right]\left\{\psi(\bar{\Lambda}_-)-\psi(\bar{\Lambda}_+)\right\}. \qquad (4.44a) \end{aligned}$$

$$\begin{aligned} V(T) = & \left\{\frac{\Gamma_N}{\Lambda_+-\Lambda_-}\right\}^4\left\{\frac{\Gamma_N-\Lambda_-}{6(2\pi T)^3}\psi^{(3)}(\bar{\Lambda}_-) + \frac{\Gamma_N-\Lambda_+}{6(2\pi T)^3}\psi^{(3)}(\bar{\Lambda}_+)\right. \\ & - \frac{1}{2(2\pi T)^2}\left\{1 - \frac{4(\Gamma_N-\Lambda_-)}{\Lambda_+-\Lambda_-}\right\}\psi^{(2)}(\bar{\Lambda}_-) - \frac{1}{2(2\pi T)^2}\left\{1 - \frac{4(\Gamma_N-\Lambda_+)}{\Lambda_--\Lambda_+}\right\}\psi^{(2)}(\bar{\Lambda}_+) \\ & - \frac{2}{2\pi T(\Lambda_+-\Lambda_-)}\left\{2-5\frac{(\Gamma_N-\Lambda_-)}{(\Lambda_+-\Lambda_-)}\right\}\psi^{(1)}(\bar{\Lambda}_-) - \frac{2}{2\pi T(\Lambda_--\Lambda_+)}\left\{2-5\frac{(\Gamma_N-\Lambda_+)}{(\Lambda_--\Lambda_+)}\right\}\psi^{(1)}(\bar{\Lambda}_+) \\ & \left. + \frac{10(\Gamma_N-\Gamma_S-\alpha)}{(\Lambda_+-\Lambda_-)^3}\left\{\psi(\bar{\Lambda}_-)-\psi(\bar{\Lambda}_+)\right\}\right\}. \qquad (4.44b) \end{aligned}$$

$$W(T) = \left\{\frac{\Gamma_N}{A_+ - A_-}\right\}^2 \left\{ \frac{E_-^2}{6(2\pi T)^3}\,\psi^{(3)}(\bar{A}_-) + \frac{E_+^2}{6(2\pi T)^3}\,\psi^{(3)}(\bar{A}_+) \right.$$
$$+ \frac{1}{(2\pi T)^2}\left[\frac{E_-^2+E_+E_-}{A_+ - A_-}\right]\psi^{(2)}(\bar{A}_-) + \frac{1}{(2\pi T)^2}\left[\frac{E_+^2+E_-E_+}{A_- - A_+}\right]\psi^{(2)}(\bar{A}_+)$$
$$+ \frac{3E_-^2+E_+^2+6E_-E_+}{2\pi T(A_+ - A_-)^2}\,\psi^{(1)}(\bar{A}_-) + \frac{3E_+^2+E_-^2+6E_-E_+}{2\pi T(A_+ - A_-)^2}\,\psi^{(1)}(\bar{A}_+)$$
$$\left. + \frac{4(E_-^2+E_+^2+3E_-E_+)}{(A_+ - A_-)^3}\left[\psi(\bar{A}_-) - \psi(\bar{A}_+)\right]\right\}. \qquad (4.44c)$$

and

$$Y(T) = \left\{\frac{\Gamma_N}{A_+ - A_-}\right\}^4 \left\{\frac{1}{6(2\pi T)^3}\left[\psi^{(3)}(\bar{A}_-) + \psi^{(3)}(\bar{A}_+)\right]\right.$$
$$+ \frac{2}{(2\pi T)^2}\left[\left[\frac{1}{A_+ - A_-}\right]\psi^{(2)}(\bar{A}_-) + \left[\frac{1}{A_- - A_+}\right]\psi^{(2)}(\bar{A}_+)\right]$$
$$\left. + \frac{10}{2\pi T(A_+ - A_-)^2}\left[\psi^{(1)}(\bar{A}_-) + \psi^{(1)}(\bar{A}_+)\right] + \frac{20}{(A_+ - A_-)^3}\left[\psi(\bar{A}_-) - \psi(\bar{A}_+)\right]\right\}. \qquad (4.44d)$$

The functions $\psi^{(n)}(\bar{A}_\pm)$ are polygamma[96] functions and the arguments are defined by $\bar{A}_\pm = \frac{A_\pm}{2\pi T} + \frac{1}{2}$.

Recalling the definitions of these functions (4.41), the result (4.37) for the free energy difference becomes

$$f_S - f_S^{BS} = -2\pi T \sum_{n\geq 0}\left[\frac{\omega_n + \Gamma_S}{4u_S^4(n)} - \frac{\Gamma_S}{4u_S^2(n)u_N^2(n)}\right] -$$
$$- \frac{(\Delta_{Ph})^4}{4}\left[U(T) - \Gamma_S W(T)\right], \qquad (4.45a)$$

and

$$f_N - f_N^{BS} + f_N^{SR} = -2\pi T \sum_{n\geq 0} \left[\frac{\omega_n + \Gamma_N}{4u_N^4(n)} - \frac{\Gamma_N}{4u_S^2(n)u_N^2(n)} + \frac{\alpha(1-\epsilon_0^2)}{2u_N^4(n)} \right]$$

$$- - \frac{(\Delta_{Ph})^4}{4} \left[V(T) - \Gamma_N W(T) + 2\alpha(1-\epsilon_0^2) Y(T) \right] . \qquad (4.45b)$$

The next step leading toward the calculation of the jump in the specific heat is the determination of the temperature dependence of the order parameter Δ_{Ph} near T_c. This is most easily accomplished starting from the imaginary axis representation of the gap equation (4.11), which is

$$\Delta_{Ph} = N_{S0} V \, 2\pi T \sum_{n=0}^{N_c} \frac{\Delta_S(n)}{\{\omega_n^2 + \Delta_S^2(n)\}^{1/2}} . \qquad (4.46)$$

where the cutoff on the sum is given by $(2n+1)\pi T \leq \omega_D$. Now (4.46) may be expanded in powers of Δ_S near T_c, resulting in

$$\frac{1}{N_{S0} V} = 2\pi T \sum_{n=0}^{N_c} \left[S_n - \tfrac{1}{2}(\Delta_{Ph})^2 S_n^3 \right] + O(\Delta_{Ph}^4) . \qquad (4.47)$$

where the function S_n is given by

$$S_n = \frac{1}{\Delta_{Ph} u_S(n)} = \frac{\omega_n + \Gamma_N + \alpha}{(\omega_n + \Gamma_N - \alpha)(\omega_n + \Gamma_S) - \Gamma_S \Gamma_N} . \qquad (4.48)$$

Now note that with the definitions

$$R(T) = 2\pi T \sum_{n=0}^{N_c} S_n - \frac{1}{N_{SO} V} \quad . \tag{4.49a}$$

and

$$P(T) = \pi T \sum_{n=0}^{N_c} S_n^3 \quad . \tag{4.49b}$$

(4.47) may be solved for the order parameter to get

$$\Delta_{Ph}^2(T) = R(T)/P(T) \quad . \tag{4.50}$$

The functions R(T) and P(T) may be evaluated in terms of polygamma functions just as in the previous cases, resulting in

$$R(T) = \ell n\left[\frac{T_c^0}{T}\right] + \Psi(1/2) - E_- \Psi(\bar{A}_-) + E_+ \Psi(\bar{A}_+) \tag{4.51a}$$

and

$$P(T) = \frac{1}{4(2\pi T)^2}\left[-E_- \Psi^{(2)}(\bar{A}_-) + E_+ \Psi^{(2)}(\bar{A}_+)\right]$$

$$+ \frac{3E_- E_+}{4\pi T(A_- - A_+)}\left[E_- \Psi^{(1)}(\bar{A}_-) - E_+ \Psi^{(1)}(\bar{A}_+)\right]$$

$$- \frac{3E_- E_+ (E_- + E_+)}{2(A_- - A_+)^2}\left[\Psi(\bar{A}_-) - \Psi(\bar{A}_+)\right] \quad . \tag{4.51b}$$

Also note that the function R(T) is actually the equation which determines T_c through $R(T_c)=0$. This is important to recognize as it

greatly simplifies the determination of the jump in the specific heat at T_c. That is, recalling that the difference in specific heat is related to the free energy difference by

$$\Delta C = -T_c \left[\frac{d^2 \Delta F}{dT^2}\right]_{T=T_c} \tag{4.52}$$

and that the free energy difference is proportional to $\Delta_{Ph}^4(T)$, one realizes that the only term which survives after twice differentiating is that which is proportional to $\left[R'(T_c)\right]^2$ (using $R(T_c)=0$). Using (4.45) and (4.50-52) the specific heat difference becomes

$$\frac{\Delta C_S}{N_{S0}} = (T_c/2)\left[\frac{R'(T_c)}{P(T_c)}\right]^2 \left[U(T_c) - \Gamma_S W(T_c)\right] \tag{4.53a}$$

and

$$\frac{\Delta C_N}{N_{N0}} = (T_c/2)\left[\frac{R'(T_c)}{P(T_c)}\right]^2 \left[V(T_c) - \Gamma_N W(T_c) + 2\alpha(1-\epsilon_0^2) Y(T_c)\right] \tag{4.53b}$$

where the derivative of R is given by

$$R'(T) = -\frac{1}{T} + \frac{E_- A_-}{2\pi T^2}\psi^{(1)}(\bar{A}_-) - \frac{E_+ A_+}{2\pi T^2}\psi^{(1)}(\bar{A}_+) \tag{4.54}$$

This essentially completes the calculation of the specific heat jump. Taking the limit $\Gamma_S \to 0$, $\Gamma_N \to \infty$, and $\alpha \to 0$ of (4.53) the result for the jump of a pure BCS superconductor

$$\Delta C_0 = -N_0 \frac{16\pi^2 T_c^0}{\zeta^{(2)}_{(1/2)}} \simeq 1.43\ \gamma T_c^0 \qquad (4.55)$$

is recovered, where $\gamma = \left[\frac{2\pi^2}{3} N_0\right]$ is the coefficient of the linear term in the electronic specific heat of the normal state. It will be convenient to normalize the calculated values in the proximity effect case by dividing by this amount. The normalized specific heat jump is therefore

$$\frac{\Delta C}{\Delta C_0} = \left[1+d_N/d_S\right]^{-1}\left[\frac{\Delta C_S}{N_{S0}}(\Gamma_S/\Gamma_N)\frac{\Delta C_N}{N_{N0}}\right] \qquad (4.56)$$

with the contributions from the two sides of the junction given by (4.53), and of course the results (4.47) needed in the evaluation of these expressions.

Figure 4.7 shows the dependence of the specific heat jump at T_c on Γ_S for various values of Γ_N. This may be compared directly with Fig. 3a of Mohabir and Nagi[93], as the identical parameters have been employed. Although the results are qualitatively in agreement, they differ significantly in a quantitative sense. For small Γ_N the present results show a much greater suppression of the specific heat jump for a given Γ_S than the results of Mohabir and Nagi[93]. A small peak in the jump very near the critical value of Γ_S in Fig. 3a of reference 93 is also absent in the results presented here.

The source of these discrepencies may be found at the starting point of the calculation of Mohabir and Nagi[93], their equation (28)

$$(\delta F)_S = \int_0^{\Gamma_S} \delta(1/\Gamma_S)\ \Delta_S^2 \ . \qquad (4.57)$$

together with the same expression with S replaced by N for the normal side. This ansatz immediately implies that if the pairing interaction on the normal side of the junction is zero ($\Gamma_N \to 0$), the normal side will make no explicit contribution to the free energy difference or the specific heat jump. The error in this procedure is that the two sides of the junction are being treated as if they were entirely independent systems, and not strongly coupled by the fact that they share a common pool of conduction electrons. The difference between the present results and those of Mohabir and Nagi[93] may to a good approximation be attributed to their method's incorrect handling of the normal side in the limit of no pairing interaction, as is shown in Fig. 4.8, where the specific heat jumps for the two sides are plotted for the same parameters as in Fig. 4.7. The contributions from the N side are always negative, resulting in a decrease in the size of the jump. Note that the contribution from the superconducting side shown in Fig. 4.8 is very close to the total jump predicted by Mohabir and Nagi[93], including the small peak near the critical value of Γ_S. This peak cancels with a peak from the normal side when the total jump, the only value with any physical significance, is calculated.

Figure 4.9(a) shows the predicted behavior for the specific heat jump as a function of Γ_N for various values of Γ_S, with no paramagnetic impurities. Also shown for reference purposes in Fig.

4.9(b) is the reduced critical temperature T_c/T_c^0, as well as in Fig. 4.9(c) the ratio $\left[\frac{\Delta C}{\Delta C_0}\right]\left[\frac{T_c^0}{T_c}\right]$, which would be predicted to be equal to unity by the law of corresponding states for non-proximity superconductors. The fact that the jump is reduced by a larger amount than is T_c (as indicated by the curves in Fig. 4.9(c) always being less than or equal to one) is in disagreement with the prediction of Zaitlin[97] for the Cooper limit (film thickness much less than the coherence length). Zaitlin[97] has solved the Bogoliubov equation for the excitation spectrum of a bilayer within certain approximations, and has found the jump in this limit to be given by the BCS form, with the replacement of the energy gap Δ by a parameter Δ_{eff}. Zaitlin assumes, however, that the ratio $\frac{2\Delta_{eff}}{T_c} = 3.53$, the BCS value, without any real justification. Zaitlin also does not allow for the existence of superconductivity in the normal metal region, which is not a good approximation in this extreme thin film limit. The present results raise some doubts about the conclusions arrived at by Zaitlin[97] for this extreme limit.

Examining Fig. 4.9 closely, one might notice that the results may be divided into two categories: the two curves for thick superconducting films (Γ_S/T_c^0=0.1 and 0.8) are qualitatively different from those for Γ_S/T_c^0>1.0 (the actual division is at $\Gamma_S = \Delta_0/2 \simeq T_c^0/1.13$). The source of this qualitative difference is that within the McMillan model for $\Gamma_S<\Delta_0/2$ T_c is finite for all values of Γ_N, while there is a critical value of Γ_N for larger values of Γ_S. As shown in

Fig. 4.9(c), the corresponding states prediction of $\left[\frac{\Delta C}{\Delta C_0}\right]\left[\frac{T_c^0}{T_c}\right]=1$ holds only in the limits $T_c \to 0$ or $T_c \to T_c^0$ ($\Gamma_N \to \infty$).

Turning now to the influence of paramagnetic impurities on the specific heat jump, there will again be two regimes with qualitatively different behavior: $\Gamma_S < \Delta_0/2$, where T_c is always finite, and $\Gamma_S > \Delta_0/2$, where T_c goes to zero for some combination of Γ_N and α. The behavior predicted in the first case is shown in Fig. 4.10, where the jump, reduced critical temperature, and the ratio of the two are plotted as a function of α (for $\epsilon_0 \to 0$) for $\Gamma_S = T_c^0/2.0$, and various Γ_N. Note that in this case the influence of the paramagnetic impurities is not very great, with a large concentration being required to suppress either T_c or the specific heat jump appreciably.

The case of a thin superconducting film with $\Gamma_S = T_c^0 = 1.5$ is shown in Fig. 4.11. In this case the specific heat jump is again more strongly suppressed than the critical temperature, although both go to zero at a critical concentration α_c. Figure 4.12 shows that all of these results depend only very weakly on the SR scattering parameter ϵ_0, as the cases $\epsilon_0 \to 0$ and $\epsilon_0 \to 1$ are nearly identical.

4.3 The Electromagnetic Penetration Depth

One notable feature of the superconducting state is the almost complete screening of electromagnetic fields from the interior of bulk samples by surface supercurrents. For example, to a good approximation

an applied weak magnetic field decays exponentially in magnitude with distance into the superconductor, with a characteristic length λ which is called the electromagnetic penetration depth. For conventional bulk superconductors λ is only very weakly temperature dependent at low temperatures, with a rapid increase near the critical temperature where λ diverges. The general form of this temperature dependence is reasonably well described by the simple dependence predicted by the two fluid model, $\lambda \propto [1-(T/T_c)^4]^{-1}$, so that the deviation of the temperature dependence from this form is often plotted. Recently, however, Kresin[98] has found that the penetration depth of the "normal" side of a proximity effect junction displays a rapid increase at low temperatures, in good agreement with experiment[99].

The approach taken by Kresin[98] is to restrict the temperature range considered to only very low temperatures, where the penetration depth may be small compared to the coherence length and the film thickness d_N. Furthermore, the McMillan[11] model is used in the description of the proximity effect, requiring that the coherence length ξ be greater than the film thickness d_N. In this situation Kresin finds that the standard result for the non-local (Pippard) limit penetration depth still holds, with the only concession to the proximity effect being the replacement of the BCS gap function by the gap function calculated within the McMillan[11] model. Consistent with this approach paramagnetic impurities may be included on the normal side of the junction by including the appropriate self-energy contribution. It may then readily be verified that Kresin's[98] final result (his equations (16-19)) is unchanged, with

$$\lambda_N = \kappa\phi^{-1/3} \tag{4.58a}$$

where

$$\kappa = 4(3^{-3/2})\left[\frac{m^* v_{FN}}{12\pi^2 n e^2}\right]^{1/3} \tag{4.58b}$$

and

$$\phi = \pi T \sum_{m\geq 0} \frac{\Delta_N^2(m)}{\omega_m^2+\Delta_N^2(m)} \tag{4.58c}$$

In (4.58b) m^* and n are the effective mass and electron concentration in the film N, v_{FN} is the Fermi velocity in N, e is the electronic charge, and the gap function $\Delta_N(m)$ is given by (4.4) and (4.12).

One further step required in the evaluation of the penetration depth is the familiar recasting of (4.58c) into the form of a real frequency axis integral, as my existing computer code solves for the function $\Delta_N(\omega)$ rather than the thermodynamic function $\Delta_N(m)$. Using the standard methods[16] one finds

$$\phi = \frac{1}{2}\,\mathrm{Im}\int_0^\infty d\omega\, \frac{\Delta_N^2(\omega)}{\Delta_N^2(\omega)-\omega^2}\tanh(\beta\omega/2) \tag{4.59}$$

Now (4.58-59), together with the gap equations (4.4), may be used to calculate the penetration depth of the normal side of the junction including the effects of SR model impurities.

Kresin[98] has found that the zero temperature penetration depth $\lambda(0)$ is an increasing function of the normal film thickness for a

given superconducting film thickness, which is a result of the decrease of the strength of the superconducting correlations.

Considering the dependence of $\lambda(0)$ on paramagnetic impurity concentration, as in the case of the specific heat jump, one finds that the results may be divided into two qualitatively different groups: in the one case $\Gamma_S < \Delta_0/2$, T_c and $\lambda(0)$ are finite for all values of Γ_N and α, and in the second case $\Gamma_S > \Delta_0/2$, critical values of Γ_N and α exist, for which T_c goes to zero and $\lambda(0)$ diverges. Some results for the first case are shown in Fig. 4.13(a), where the inverse penetration depth is plotted as a function of the pair-breaking parameter α (with the scattering parameter $\epsilon_0 = 0$) for a few different values of Γ_N. The inverse of the penetration depth is plotted to avoid the divergence of $\lambda(0)$ which occurs at the critical concentration, and which shows up in the second case, Fig. 4.13(b), as the inverse penetration depth going to zero. Of course long before this point is reached the penetration depth will have increased to the point where it is of the order of the film thickness, which violates one of the basic assumptions made at the outset. The large impurity concentration region is therefore not of interest within this model, although just what is "large" can only be decided after estimating the various parameters for a particular junction composition.

The dependence of $\lambda(0)$ on the Shiba-Rusinov scattering parameter ϵ_0 is explored in Fig. 4.14, where it is shown that as ϵ_0 increases $\lambda(0)$ decreases, with the amount of variation being larger for thin superconducting films (Γ_S large) and for larger impurity concentrations.

Next consider the temperature dependence of the penetration depth, some examples of which are shown in Fig. 4.15(a), where the penetration depth, normalized to the zero temperature value $\lambda(0)$, is plotted as a function of reduced temperature T/T_c. Note that with increasing impurity concentration the rapid rise in λ at low temperature found in the pure case is suppressed. The mechanism for this may be better understood by examining Fig. 4.15(b), where the same results are replotted with a different normalization, that is with all values normalized to $\lambda_0(0)$, the penetration depth of the pure junction at zero temperature, rather than to $\lambda(0)$, the penetration depth at zero temperature for the given set of material parameters. When all curves are normalized by the same value the actual shape of the curves at higher temperatures ($T/T_c \simeq 0.3$-0.4) is not greatly affected by increasing α; to a good approximation in this region the curves simply shift up by a constant amount. At lower temperatures the shape of the curves is altered slightly, with the increase in $\lambda(T)/\lambda_0(0)$ with α being largest at zero temperature. The marked decrease in slope of the curves in Fig. 4.15(a) at higher temperatures with increasing α simply reflects the fact that the low temperature penetration depth increases more rapidly than that at higher temperatures.

The usefulness of the above pictorial display becomes most evident upon consideration of the dependence of these results on the scattering parameter ϵ_0, an example of which is shown in Fig. 4.16. Although the curves for $\epsilon_0 = 0$ and for $\epsilon_0 = 1.0$ differ markedly in Fig. 4.16(a) at all temperatures, the results plotted in Fig. 4.16(b) show that in absolute terms only at the very lowest temperatures does the

value of ϵ_0 have any effect. This is reassuring, as for the parameters considered here the parameter ϵ_0 affects only the very low frequency region of the gap function, so that one would expect only the very low temperature region to be influenced by this parameter.

In summary, the low temperature penetration depth of the normal side of a proximity effect junction has been found to be very sensitive to the introduction of paramagnetic impurities. The rapid rise of penetration depth with temperature reported by Kresin[98] for the case of a pure proximity junction is found to be suppressed by paramagnetic impurities, an effect which results from λ in the very low temperature region being more strongly enhanced than at higher temperatures. Furthermore, this low temperature enhancement is quite sensitive to the nature of the impurity scattering as described by the parameter ϵ_0.

4.4 Optical Absorption

The frequency dependence of the absorption of electromagnetic radiation by a superconductor is determined by the structure of the quasiparticle density of states, and as pointed out in the discussion of intrinsic superconductors with paramagnetic impurities in Section 2.6, optical experiments may be very useful in cases where the construction of good tunneling junctions is difficult for a particular material.

In this section the optical absorption of proximity effect induced superconductors will be considered. Within the present

approximation of the McMillan model for the proximity effect, this may be calculated in exactly the same manner as for the case of intrinsic superconductors, with of course the usual replacement of the gap function by the appropriate one. The optical absorption of the normal side (N) of a proximity junction is then given by (2.65-66),

$$\frac{\sigma_1(\omega)}{\sigma_N} = \frac{1}{\omega}\int_{\omega_g-\omega}^{\omega_g} d\nu\ [n(\nu)n(\omega+\nu)+p(\nu)p(\omega+\nu)]\ \tanh\left\{\frac{\beta}{2}(\omega+\nu)\right\}$$

$$+\frac{1}{\omega}\int_{\omega_g}^{\infty} d\nu\ [n(\nu)n(\omega+\nu)+p(\nu)p(\omega+\nu)]\ \left[\tanh\left\{\frac{\beta}{2}(\omega+\nu)\right\} - \tanh\left\{\frac{\beta\nu}{2}\right\}\right]. \quad (4.60)$$

Here

$$n(\nu) = \mathrm{Re}\left[\frac{\nu}{\{\nu^2-\Delta_N^2(\nu)\}^{1/2}}\right] \quad (4.61a)$$

is the single particle density of states, and

$$p(\nu) = \mathrm{Re}\left[\frac{\Delta_N(\nu)}{\{\nu^2-\Delta_N^2(\nu)\}^{1/2}}\right] \quad (4.61b)$$

is the pair density of states. Note that the notation here is slightly different from that used in (2.65-66), with $u(\nu)=\nu/\Delta(\nu)$ providing the necessary connection. As before, σ_N is the normal state conductivity, and is assumed to be frequency independent in the frequency range of interest. The frequency ω_g is the lowest frequency where the density of states becomes non-zero. Equation (4.60) may now be integrated

numerically, using the solution of the gap equations (4.4) as input.

First considering the variation of the absorption with normal film thickness without paramagnetic impurities, one might expect this to be very much like that of a BCS superconductor, with a gap edge that decreases with increasing normal film thickness d_N. This is indeed the case to a reasonably good approximation, as shown in Fig. 4.17(a), although there is a small "kink" in the curves at a frequency which depends on the film thickness. This feature is associated with the two-peaked structure of the density of states, shown in Fig. 4.17(b) (the densities of states on the superconducting side are shown in Fig. 4.18 for the sake of completeness). In the two extreme limits of Γ_N going to zero or infinity the two peaked structure disappears, in the one case because the density of states becomes identical to that of the normal state, and in the other case because the two peaks merge together into a single one. The structure is most evident in the intermediate thickness cases of Fig. 4.17(a). Although this structure is easily seen in some of the calculated curves, it is questionable as to whether or not it might be seen experimentally. The densities of states calculated within the present model represent an idealized version of what is observed experimentally, where structures are generally not as sharp as the calculated ones. This might well result in this feature becoming unobservably small for real systems.

Turning now to the question of including paramagnetic impurities in the normal side of the junction, it has previously been pointed out by Kaiser[89] for the model of Müller-Hartmann and Zittartz[21], which is very similar to that of Shiba[8] and Rusinov[9],

that the location of states within the energy gap is quite well described by the non-proximity results, with the replacement of the order parameter by an effective gap given by the location of the peak in the density of states in the absense of impurities. In light of this, it should not be surprising to see that the low frequency region of the optical absorption is very similar to that of the intrinsic case considered in Section 2.6. Figures 4.17-18 show a comparison of results for the scattering parameters ϵ_0=0.0, 0.5, and 1.0 for two different exchange scattering rates α. Note that the existence of a band of states in the gap leads to two peaks in the optical absorption, just as in the intrinsic case. The absorption at higher frequencies is not very sensitive to small amounts of paramagnetic impurities.

In conclusion, just as in the case of intrinsic superconductors, optical absorption is a very sensitive probe of the density of states of induced superconductors, and as such may be a useful tool in the probing of the interactions between magnetic impurities and conduction electrons in metals in general.

4.5 Proximity Effect Induced Superconducting Spin-Glasses

4.5.i Introduction

One great advantage of the proximity effect is that it allows the superconducting electrons to be used to probe some fundamental properties of non-superconducting metals. For example, the tunneling

characteristics of some well known Kondo alloys which are not intrinsic superconductors have been examined by Dumoulin, Guyon, and Nedellec[100], something which is not possible without the proximity effect. Another example, and the one which is of most interest here, is the examination of the tunneling characteristics of Ag-Mn spin-glass alloys by Schuller, Orbach and Chaikin[101]. Silver is not a superconductor, but Ag-Mn is one of the prototypical spin-glass systems, which has often been studied in the normal state. The sensitivity of superconductivity to the details of magnetic scattering should provide useful information about the spin-glass state.

Schuller *et al.*[101] were able to conclude that the exchange scattering rate of conduction electrons below the spin-glass freezing temperature is suppressed by approximately 5 percent compared to that above the freezing temperature, but did not compare their results to a detailed calculation. Nass, Levin, and Grest[60] performed a fully dynamic calculation of the exchange scattering rate of a spin-glass within a hydrodynamic model, but once again the proximity effect was not included. It is therefore of interest to reanalyze the results of Schuller *et al.*[101] using the McMillan model for the proximity effect, and including the spin-glass effects using the simplified static limit of the theory of Nass *et al.*[60], which has previously been discussed in Chapter III for the case of intrinsic spin-glass superconductors.

4.5.ii Calculations

The gap equations for a spin-glass in proximity with a

superconductor are, within the present approximations, merely trivially different in structure from those previously considered for the case of paramagnetic impurities. The required result may be found by replacing the exchange scattering rate α in the SR limit equations (4.4) by a temperature dependent scattering rate $\alpha(T)$, and of course taking the limit of ϵ_0 going to one, corresponding to the weak scattering limit. The result is

$$\tilde{\Delta}_S(\omega) = \Delta_{Ph} + \Gamma_S\tilde{\Delta}_N(\omega)/D_N(\omega) \tag{4.62a}$$

$$Z_S(\omega) = 1 + \Gamma_S Z_N(\omega)/D_N(\omega) \tag{4.62b}$$

$$\tilde{\Delta}_N(\omega) = \Gamma_N\tilde{\Delta}_S(\omega)/D_S(\omega) + \Gamma_2(T)\tilde{\Delta}_N(\omega)/D_N(\omega) \tag{4.62c}$$

$$Z_N(\omega) = 1 + \Gamma_N Z_S(\omega)/D_S(\omega) + \Gamma_1(T)Z_N(\omega)/D_N(\omega). \tag{4.62d}$$

where

$$D_I(\omega) = \left[\tilde{\Delta}_I^2(\omega)-\omega^2 Z_I^2(\omega)\right]^{1/2}, \quad I=N \text{ or } S. \tag{4.62e}$$

This is exactly the same form as in the paramagnetic impurity case, with the replacement of the functions $\Gamma_{1(2)}(\omega)$ by the frequency independent, but temperature dependent values given by

$$\Gamma_1(T) = -\Gamma_2(T) - \alpha(T)/2 . \tag{4.63}$$

where the scattering rate $\alpha(T)$ is given by (3.24),

$$\alpha(T) = 2\pi n_I N_{NO} J^2 [T\chi(T)+\tilde{Q}(T)] . \qquad (4.64)$$

This temperature dependent scattering rate has previously been discussed in Section 3.3

The experiment of Schuller *et al.*[101] involved the measurement of the tunneling conductance of junctions composed of a normal metal, an insulating barrier and thin (approximately 200 to 800 Å thick) Ag-Mn films, which were in proximity with 3000 Å thick Pb films. One factor which should be kept in mind is that this thickness of Pb is several times the coherence length of bulk Pb, so that the applicability of the McMillan model might be doubtful. It has been found[86], however, that the critical temperature depression and tunneling conductance of films of this thickness are just as well (or badly) described by the McMillan model as are these properties for thinner films, so that this model is often applied in circumstances where the approximations made in the derivation may not be valid.

The tunneling conductance is defined as the derivative with respect to voltage of the current versus voltage curve, and when normalized to the normal state value is given by[89]

$$\sigma(V) = \frac{1}{4T} \int_0^\infty d\omega \, n_N(\omega) \left[\mathrm{sech}^2\left[\frac{\omega+eV}{2T}\right] + \mathrm{sech}^2\left[\frac{-\omega+eV}{2T}\right] \right] . \qquad (4.65)$$

where the density of states on the normal side (normalized to the

normal state value) is given as usual by

$$n_N(\omega) = \mathrm{Re}\left[\frac{\omega}{\{\omega^2-\Delta_N^2(\omega)\}^{1/2}}\right] . \qquad (4.66)$$

and V is the applied voltage. The conductance is easily calculated numerically given the gap function as calculated from (4.62).

To end this section, it will be useful to derive an approximate analytic expression for the zero frequency density of states $n_N(0)$ in the gapless region. This allows the zero frequency conductance to be estimated very quickly, and may help in understanding the numerical results. Equations (4.62) may be rewritten in terms of the gap functions $\Delta_I(\omega)=\phi_I(\omega)/Z_I(\omega)$, I=N or S, in the form

$$\Delta_N(\omega) = \frac{\Gamma_N\ \Delta_S(\omega)}{[\Delta_S^2(\omega)-\omega^2]^{1/2}}\left[1+\frac{\Gamma_N}{[\Delta_S^2(\omega)-\omega^2]^{1/2}}+\frac{\alpha(T)}{[\Delta_N^2(\omega)-\omega^2]^{1/2}}\right]^{-1} \qquad (4.67a)$$

and

$$\Delta_S(\omega) = \left[\Delta_{Ph}+\frac{\Gamma_S\ \Delta_N(\omega)}{[\Delta_N^2(\omega)-\omega^2]^{1/2}}\right]\left[1+\frac{\Gamma_S}{[\Delta_N^2(\omega)-\omega^2]^{1/2}}\right]^{-1} . \qquad (4.67b)$$

To take the zero frequency limit of (4.67), which is required in order to calculate the zero frequency density of states, it is helpful to introduce the functions $u_I(\omega)=\omega/\Delta_I(\omega)$, which are finite in the zero frequency limit. Equations (4.67) become

$$u_N = \frac{(1-u_S^2)^{1/2}}{\Gamma_N} \left[\frac{\Gamma_N u_S}{(1-u_S^2)^{1/2}} - \frac{\alpha(T) u_N}{(1-u_N^2)^{1/2}} \right] . \qquad (4.68a)$$

and

$$u_S = u_N \left[1 + \frac{\Delta_{Ph}}{\Gamma_S}(1-u_N^2)^{1/2} \right]^{-1} . \qquad (4.68b)$$

Note that in (4.68) the functions u_S and u_N are understood to have frequency arguments equal to zero. An equation for u_N may be obtained by substituting u_S from (4.68b) into (4.68a), resulting in

$$\frac{\Delta_{Ph}}{\Gamma_S}(1-u_N^2) = - \frac{\alpha(T)}{\Gamma_N} \left[\left\{ 1 + \frac{\Delta_{Ph}}{\Gamma_S}(1-u_N^2)^{1/2} \right\}^2 - u_N^2 \right]^{1/2} . \qquad (4.69)$$

Defining the new variable

$$z = (1-u_N^2)^{1/2} , \qquad (4.70)$$

(4.69) may be rewritten in the form

$$z^3 - \left[\frac{\alpha(T)}{\Gamma_N} \right]^2 \left[1 + \left[\frac{\Gamma_S}{\Delta_{Ph}} \right]^2 \right] z - \frac{2\Gamma_S}{\Delta_{Ph}} \left[\frac{\alpha(T)}{\Gamma_N} \right]^2 = 0 . \qquad (4.71)$$

The parameter range of interest is $\Gamma_S < \Delta_{Ph}$, $\alpha > \Gamma_N$ in order for the junction to be gapless, in which case this cubic has three distinct real roots, which may be written in the form[96]

$$z_1 = S+T . \qquad (4.72a)$$

$$z_2 = -\frac{1}{2}(S+T) + i\frac{3^{1/2}}{2}(S-T) \quad . \tag{4.72b}$$

$$z_3 = -\frac{1}{2}(S+T) - i\frac{3^{1/2}}{2}(S-T) \quad . \tag{4.72c}$$

where

$$S = \left[R+(Q^3+R^2)^{1/2}\right]^{1/3} \quad . \tag{4.73a}$$

$$T = \left[R-(Q^3+R^2)^{1/2}\right]^{1/3} \quad . \tag{4.73b}$$

$$Q = -\frac{1}{3}\left[\frac{\alpha(T)}{\Gamma_N}\right]^2\left[1 + \left[\frac{\Gamma_S}{\Delta_{Ph}}\right]^2\right] \quad . \tag{4.73c}$$

and

$$R = \frac{\Gamma_S}{\Delta_{Ph}}\left[\frac{\alpha(T)}{\Gamma_N}\right]^2 \quad . \tag{4.73d}$$

Using the fact that S and T are complex conjugates, the roots given in (4.72) may be written in the form

$$z_1 = 2(-Q)^{1/2}\cos[\theta/3] \quad . \tag{4.74a}$$

$$z_2 = -2(-Q)^{1/2}\cos[(\theta-\pi)/3] \quad . \tag{4.74b}$$

$$z_3 = -2(-Q)^{1/2}\cos[(\theta+\pi)/3] \quad . \tag{4.74c}$$

where

$$\tan\theta = (|Q^3+R^2|)^{1/2}/R^{-1} \qquad (4.74d)$$

The appropriate root (n=1, 2, or 3) must be chosen so that the density of states given by (4.66) is positive; this may easily be found to be the case for n=1 if the density of states is rewritten in the form

$$n_N(0) = \mathrm{Re}\left[\frac{u_N}{(u_N^2-1)^{1/2}}\right] = \mathrm{Im}\left[\frac{u_N}{(1-u_N^2)^{1/2}}\right]$$

$$= \frac{(z^2-1)^{1/2}}{z} \qquad (4.75)$$

Equation (4.75), together with the knowledge that $\mathrm{Im}(u_N)>0$ for ω near zero, shows that z must be positive, which is only satisfied for z_1 for the parameter range of interest.

At this point the zero frequency density of states has been found, but the result is quite cumbersome and unenlightening. It is therefore useful to expand the result in powers of the parameter $\frac{\Gamma_S}{\Delta_{Ph}}$, which is much less than one for thick superconducting films. Equation (4.74a) then takes the form

$$z_1 = \frac{\alpha(T)}{\Gamma_N} + \frac{\Gamma_S}{\Delta_{Ph}} + \mathcal{O}[(\Gamma_S/\Delta_{Ph})^2] \qquad (4.76)$$

and the final result (4.75) becomes

$$n_N(0) = \left[1-\left[\frac{\Gamma_N}{\alpha(T)}\right]^2\right]^{1/2} + \frac{\Gamma_S}{\Delta_{Ph}}\left[\frac{\Gamma_N}{\alpha(T)}\right]^3\left[1-\left[\frac{\Gamma_N}{\alpha(T)}\right]^2\right]^{-1/2} + O[(\Gamma_S/\Delta_{Ph})^2]. \quad (4.77)$$

To a very good approximation for small Γ_S the value of Δ_{Ph} may be replaced by the gap of the pure bulk superocnductor Δ_0, so that (4.77) may be used to very quickly calculate the zero frequency density of states for a given choice of parameters. It is interesting to note that even with the replacement of Γ_N by an effective gap Δ_{eff}, the leading term of (4.77) does not become exactly the form used by Schuller *et al.*[101] in their analysis.

$$n_N(0) \approx [1-\tfrac{1}{2}(\Delta_{eff}/\Gamma_S)^2]. \quad (4.78)$$

which is the result for intrinsic superconductors in the gapless region. Although the two forms are not identical, the difference in the predicted dependence of $n_N(0)$ on $\Gamma_S/\alpha(T)$ is quite small for a wide range of parameters.

4.5iii Results

In order to compare the predictions of this model with the experimental results of Schuller *et al.*[101] the various parameters needed must be estimiated. There are a number of restrictions on the choice of parameters: the ratio Γ_S/Γ_N is in principle fixed by the experimental film thicknesses and the normal state specific heat coefficients γ_1. It is often found[100], however, that in order to fit

the observed dependence of critical temperature on thickness this value must be varied significantly from the nominal one. This restriction is therefore not as strong as it might appear to be at first glance. Another constraint is of course the fitting of the observed critical temperatures, along with matching the observed low temperature zero bias conductances. When taken all together, these constraints serve to narrow the choice of values for Γ_S, Γ_N and $\alpha(0)$ significantly, although there is of course still room for variation due to the commonly observed violation of the first constraint.

To begin with, the ratio of Γ_S to Γ_N might be chosen to satisfy

$$\Gamma_S/\Gamma_N = \frac{\gamma_N d_N}{\gamma_S d_S} \quad (4.79)$$

where the coefficients of the low temperature linear specific heat γ_I satisfy $\frac{\gamma_S}{\gamma_N} \simeq 2.67$ [102]. This will be taken as a guide only, the actual ratio will be varied to explore the consequences. To achieve a critical temperature of approximately 6.4 K as is the case for the 400 Å and 600 Å AgMn films of figure 2 of Schuller *et al.*, compared to a critical temperature of approximately 7.2 K for pure Pb, the value of Γ_S must be of the order of 0.1 meV (or roughly 1.2 K). The amount of pair-breaking may then be fixed by adjusting $\alpha(0)$ to yield the observed low temperature zero bias conductance $\sigma(0)$, which is the same as the zero frequency density of states.

Some results for the predicted temperature dependence of the zero bias conductance are shown in Fig. 4.21 for a wide range of

parameters, along with a few experimental points from the 400 Å film in Fig. 2 of Schuller *et al*[101]. Although there is significant variation among the curves, the outstanding feature is that the Abrikosov-Gor'Kov (AG) curve is very different from both the experimental data and the model spin-glass results. As mentioned by Schuller *et al.*[101], with a temperature independent exchange scattering rate as in the AG model, the zero bias tunneling conductance is essentially independent of temperature for temperatures less than approximately 3 K. This result is also only very weakly affected by variations of the proximity effect parameters Γ_S and Γ_N.

Figure 4.22, however, shows that the apparent agreement of the model spin glass conductance with the Ag-Mn experiment may be misleading. In this figure the procedure used by Schuller *et al.*[101] is applied to some of the results from Fig. 4.21: the zero temperature density of states is used to calculate a thermally smeared conductance called σ_T (dashed lines), which may be compared with the results of the full calculation (solid lines) and with the corresponding experimental results. For temperatures less than or equal to 2 K the experimental conductance is identical with the thermally smeared value, only at higher temperatures does the measured conductance increase more rapidly, which is an indication of an increasing exchange scattering rate. The model spin-glass results on the other hand, show significant differences at much lower temperatures. The main point brought out by this figure, however, is that the effects of thermal smearing may be very different for the calculated conductances and the experimental ones. This results from the fact that the low temperature conductance

is very sensitive to the low frequency region of the density of states; a seemingly small difference in the shape of the density of states may result in significantly different temperature variation of the conductance. As it is well known[86] that even for non-magnetic systems the McMillan[11] model does not perfectly reproduce the structure of the density of states, a direct comparison of the calculated conductance with the experimental measurements does not necessarily give useful information about the temperature dependence of the exchange scattering rate. This problem may be circumvented by following the lead of Schuller *et al.* and comparing the difference between the calculated conductance and the thermally smeared value $\sigma_T(T)$ with the same quantity as determined experimentally. This procedure should remove a large part of the error introduced by the imperfect match of experimental and theoretical densities of states. A similar comparison between the conductance and the thermally smeared value σ_T for the 800 Å sample of Fig. 3 of Schuller *et al.*[101] and some model calculations is shown in Fig. 4.23. The 600 Å sample of Fig. 2[101] had the same nominal Mn concentration as the 400 Å film, and with the appropriate change of Γ_N, results calculated for the two consistently show the same type of agreement (or disagreement) with experiment, so this sample will not be considered further here.

Figure 4.24 shows some examples of the difference between the conductance $\sigma(T)$ and the thermally smeared value $\sigma_T(T)$ as a function of temperature for the 400 Å sample. One feature worth noting here is that all of the results for the spin-glass model $\bar{D}(T_f)=1.0$, $\tilde{Q}(t)=S^2(1-t^2)$ show an increase in conductance at a much lower

temperature than is experimentally observed; moreover the size of the increase is significantly larger than the experimentally observed scale of variation. The model $\bar{D}(1)=2.0$, $\tilde{Q}(t)=S^2(1-t)$ is in better agreement with experiment, although there is still much room for improvement. Finally, the solid line is a curve calculated using the conclusions of Schuller *et al.*[101] as a guide; for this curve the function $\alpha(T)$ was constant for $T<0.8T_f$, constant at a value 5 percent larger for $T>1.2T_f$, and linearly joining these two points in the region between $0.8T_f$ and $1.2T_f$. This model gives reasonably good agreement with experiment, although some discrepancies remain at the highest temperatures considered. As a whole, these results comfirm the original conclusions of Schuller *et al.*[101] for this sample; that is there seems to be a roughly 5 percent change in the exchange scattering rate in the vicinity of the freezing temperature T_f. Note that for S=5/2 for Mn in Ag the scale of variation of the scattering rate is predicted by the model of Nass *et al.*[60] to be given by the ratio $\frac{S^2}{S(S+1)} \simeq 0.71$, which implies roughly 30 percent variation of $\alpha(T)$.

The situation is made even more interesting by examining the results for the 800 Å sample shown in Fig. 4.25. In this case the $\bar{D}(1)=1.0$ model again shows too rapid an increase at low temperatures, while the model with $\bar{D}(1)=2.0$ and $\tilde{Q}_1(\bar{t})=S^2(1-\bar{t})$ seems to give a reasonable fit. The simple triangle model with 5 percent variation of $\alpha(T)$ does not give nearly enough pair-breaking at high temperatures to be in agreement with the experimental points.

This analysis indicates that the 400 and 800 Å samples may have

had significantly different temperature variations of the exchange scattering rate: in the first case the increase from zero temperature to approximately twice the freezing temperature is roughly 5 percent, while in the second case it is significantly larger, of the order of 20 percent difference between zero and twice the freezing temperature. Recalling that the experimental conductance difference $[\sigma(T)-\sigma_T(T)]/\sigma(0)$ of the 600 Å sample is virtually identical to that of the 400 Å sample, and that the two had the same Mn concentration of 0.35-at.%, compared to 0.1-at.% for the 800 Å sample, it is tempting to attribute this significant difference to spin-glass effects, and not to any proximity effect complications. From this point of view the essential difference between these samples was the Mn concentration, which differed by a factor of 3.5. One very important fact is that the ratio of freezing temperatures is only approximately 2.6, compared to this concentration ratio of 3.5, so that for concentrations of 0.35-at.% the thin film Ag-Mn spin glass is already in the nonscaling regime. Stated briefly, in the very low concentration region where the freezing temperature is directly proportional to magnetic ion concentration, metallic spin-glasses such as Ag-Mn are found to obey very simple scaling relationships[55]. These may be expressed in the form

$$\frac{P}{n} = \mathcal{P}(T/n, H/n) \qquad (4.80)$$

where P is some thermodynamic property, n is the magnetic ion concentration, and T and H are temperature and magnetic field

respectively. This scaling behavior is understood theoretically to arise from the $1/r^3$ decay of the RKKY interaction with distance. If applied to this particular case, scaling would predict that the relative change in exchange scattering rate should be a universal function of T/T_f, with the overall normalization varying linearly with concentration. Note that to this point scaling has been implicitly assumed, with my $\alpha(T)$ curves being universal functions of T/T_f.

With the above factors in mind, the deviation of the freezing temperature from scaling may be an indication that nonscaling behavior would also be expected for the exchange scattering rate, consistent with the observed difference in conductance. Finally, although these concentrations of Mn in Ag would normally be expected to be within the scaling regime, the fact that these were thin films rather than bulk samples may have resulted in deviations from scaling for concentrations where scaling is commonly obeyed.

Fig. 4.1 a) The free energy difference per unit volume of a proximity junction normalized to the free energy difference per unit volume of the bulk superconductor versus reduced temperature, $t=T/T_c$, for the proximity effect parameters:

$\Gamma_S/T_c^0=0.10$, $\Gamma_N/T_c^0=0.72$ (————),

$\Gamma_S/T_c^0=0.72$, $\Gamma_N/T_c^0=1.50$ (.....),

$\Gamma_S/T_c^0=0.72$, $\Gamma_N/T_c^0=0.72$ (-------),

$\Gamma_S/T_c^0=0.72$, $\Gamma_N/T_c^0=0.10$ (-.-.-.-).

b) The deviation function, $D(t) = \frac{H_c(t)}{H_c(0)} - (1-t^2)$, as a function of t^2 for the same parameters as in a).

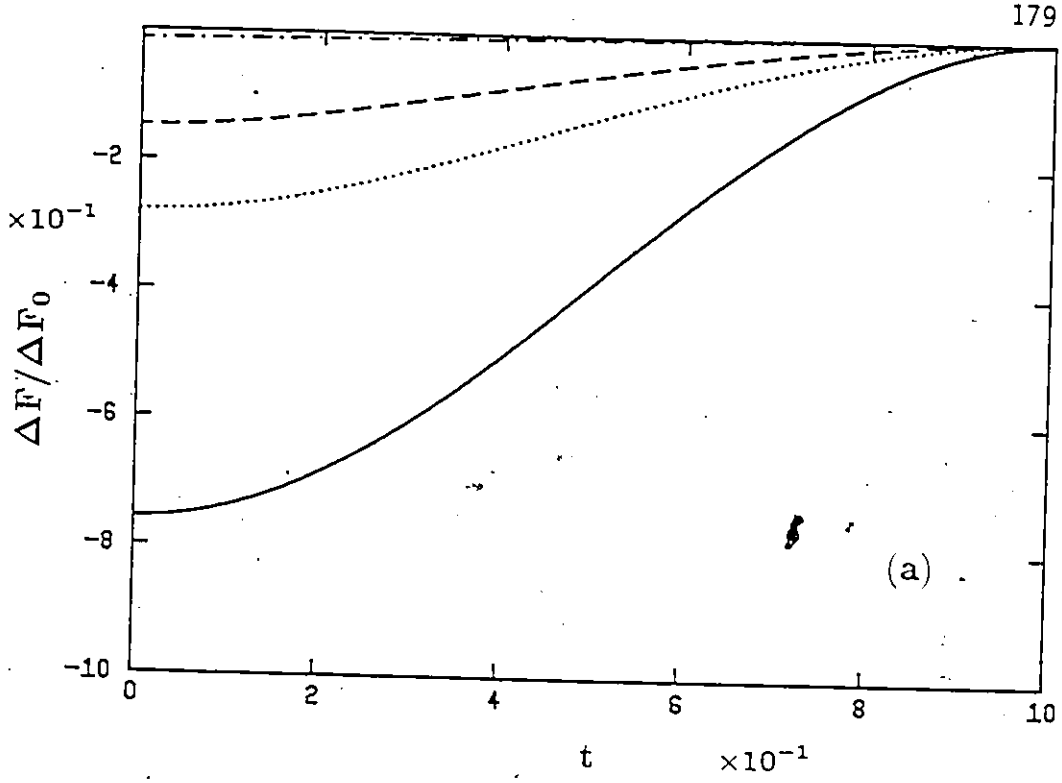
-2
×10⁻¹
-4
-6
-8
-10
ΔF/ΔF₀
0
2
4
6
8
10
t
×10⁻¹
(a)

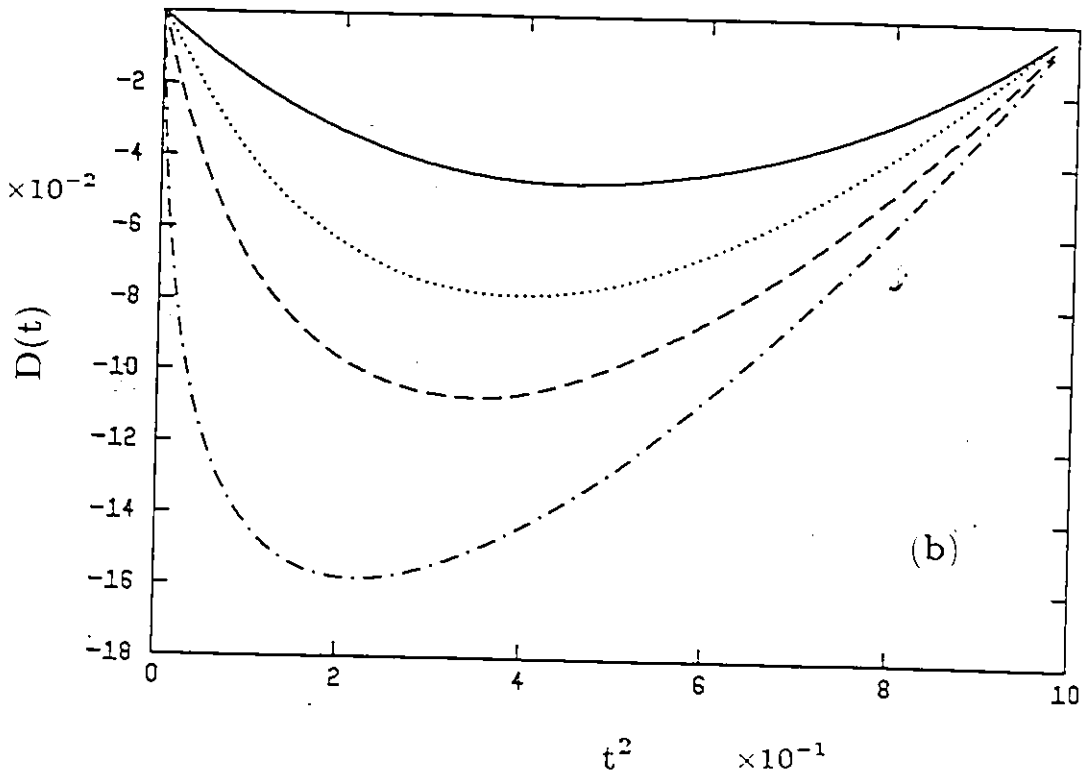
-2
-4
×10⁻²
-6
-8
-10
-12
-14
-16
-18
D(t)
0
2
4
6
8
10
t²
×10⁻¹
(b)

Fig. 4.2 The specific heat difference $\frac{\Delta C}{\Delta C_0}$ versus reduced temperature $t=T/T_c$ for a proximity effect junction. The specific heat difference has been normalized to the specific heat differ- at T_c for the pure superconductor ΔC_0. The proximity effect parameters are the same as in Fig. 4.1.

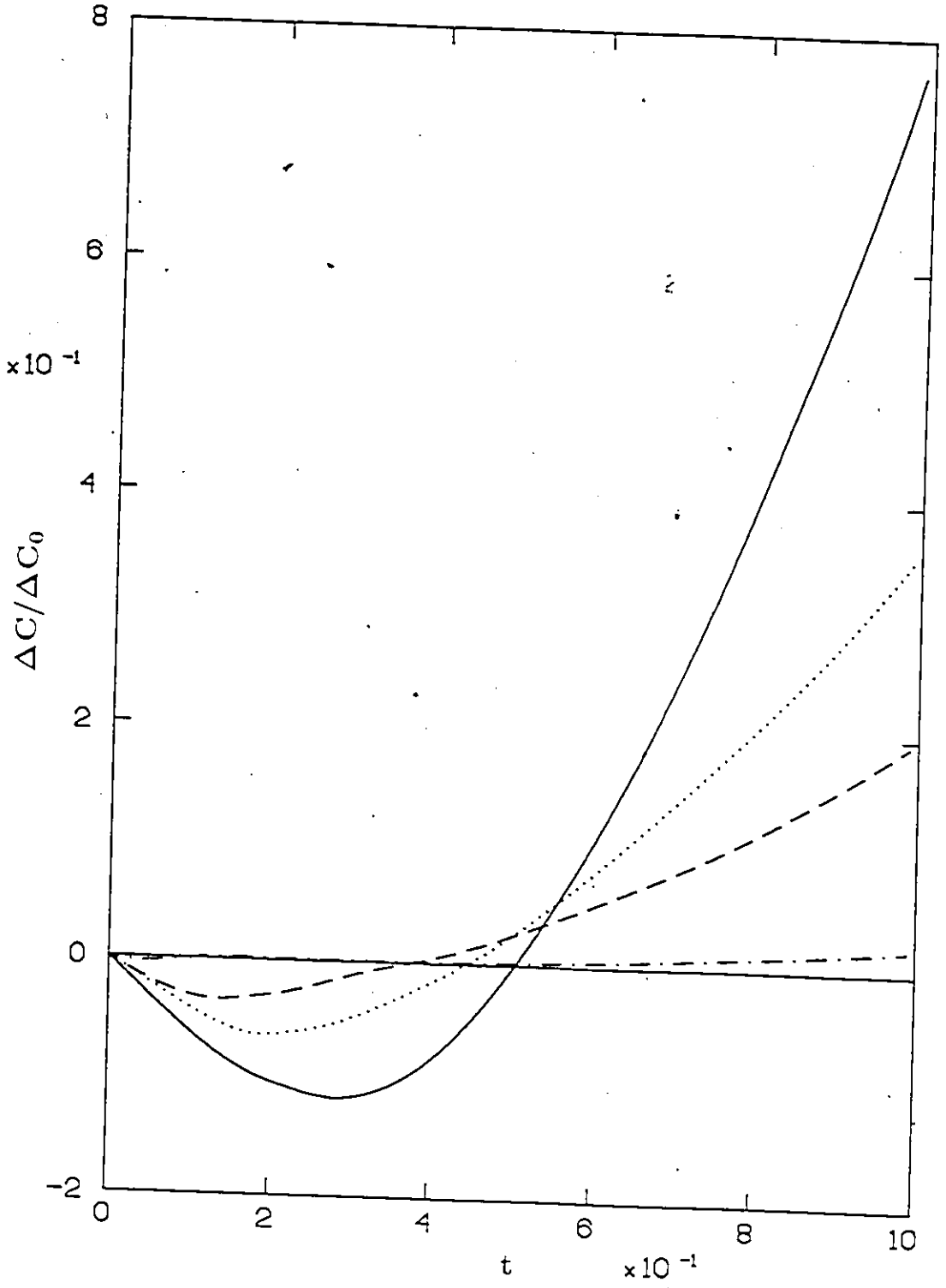
8
6
x10 -1
4
ΔC/ΔC0
2
0
-2
0
2
4
6
8
10
t
x10 -1

Fig. 4.3 The temperature dependence of the contribution of the normal side of a proximity effect junction to the total free energy difference. The proximity effect parameters are the same as in Figs. 4.1 and 4.2.

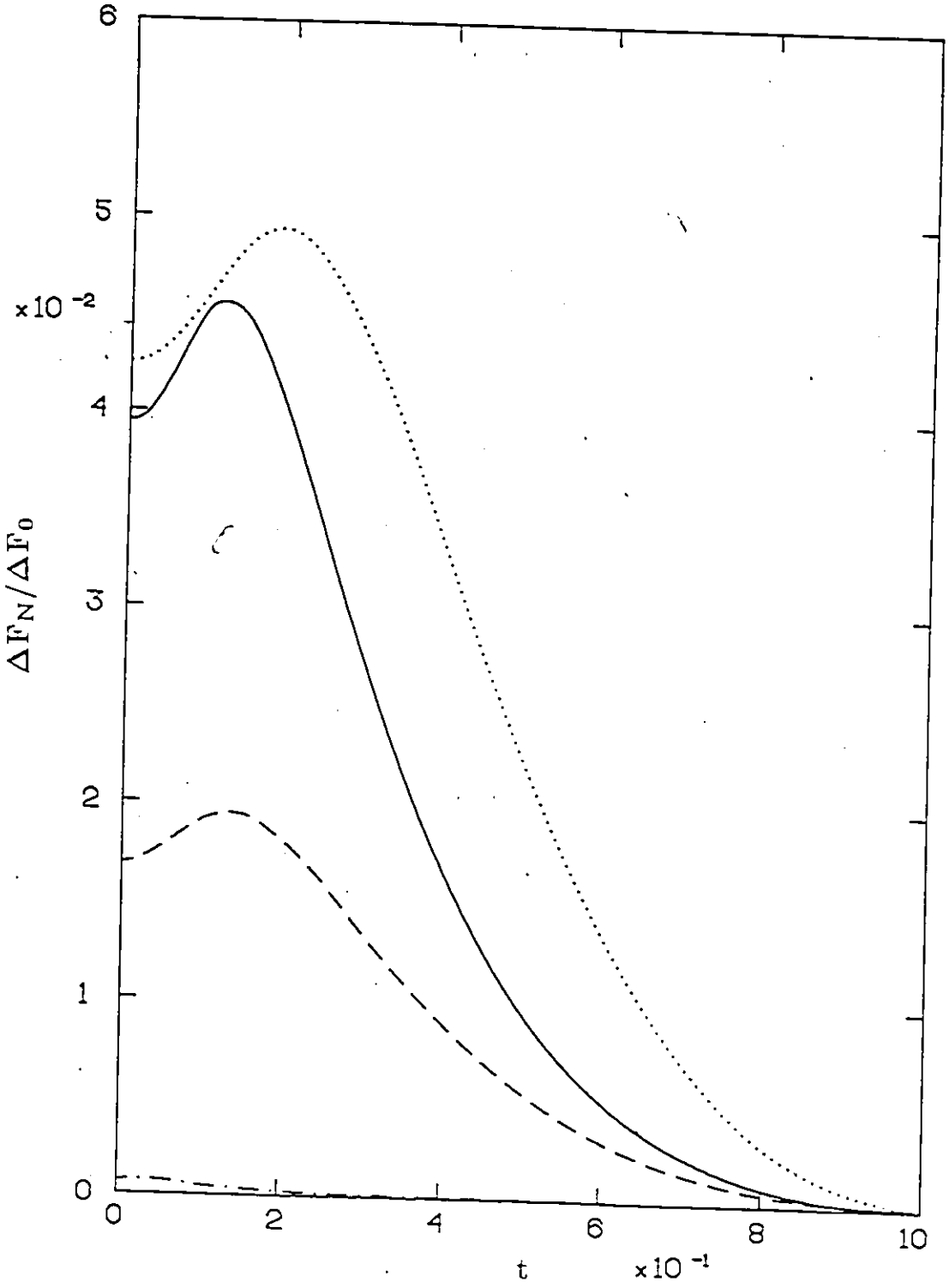
6
5
x10 -2
4
3
2
1
0
ΔF_N/ΔF_0
0
2
4
6
8
10
t
x10 -1

Fig. 4.4 a) The temperature dependence of the total free energy difference of a proximity effect junction containing paramagnetic impurities on the normal side. The proximity effect parameters are $\Gamma_S = \Gamma_N = 0.36T_c^0$, with $\epsilon_0=0$, and:

$\alpha=0.01T_c^0$ (————),

$\alpha=0.10T_c^0$ (.....),

$\alpha=0.36T_c^0$ (-------),

$\alpha=1.00T_c^0$ (-.-.-.-).

b) The deviation function D(t) as a function of the square of the reduced temperature, $t=T/T_c$, for the same parameters as in a).

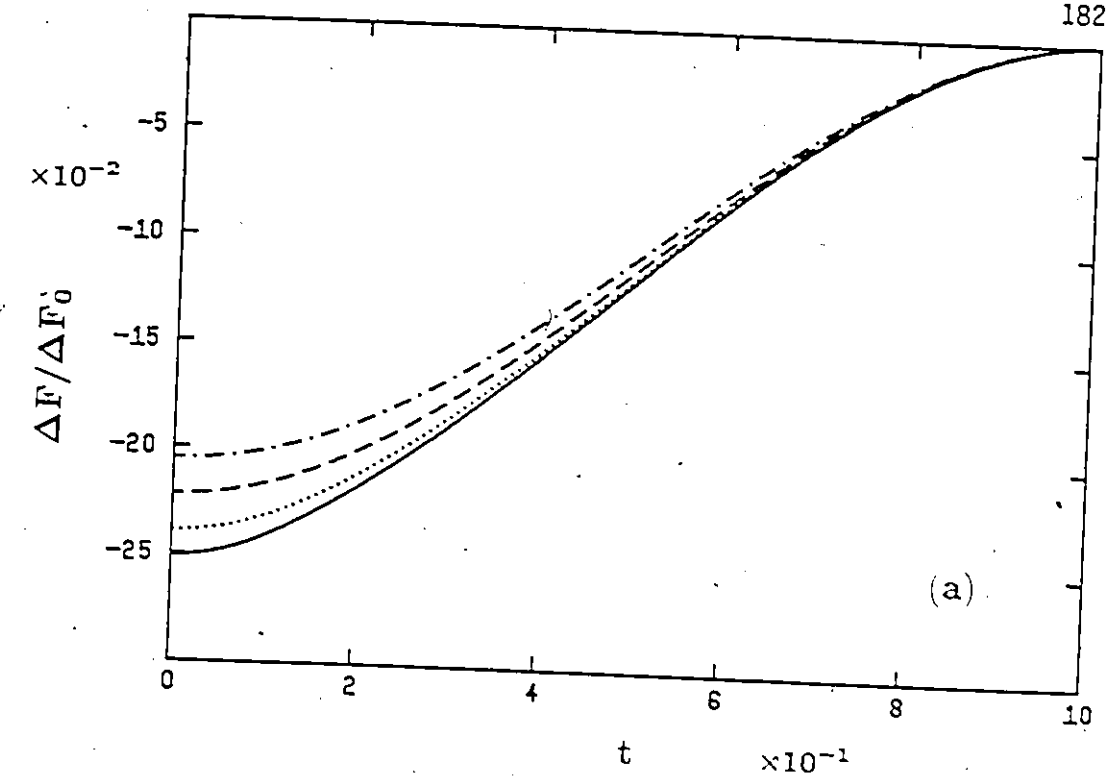
-5
$\times 10^{-2}$
-10
-15
$\Delta F/\Delta F_0'$
-20
-25
(a)
0
2
4
6
8
10
t
$\times 10^{-1}$

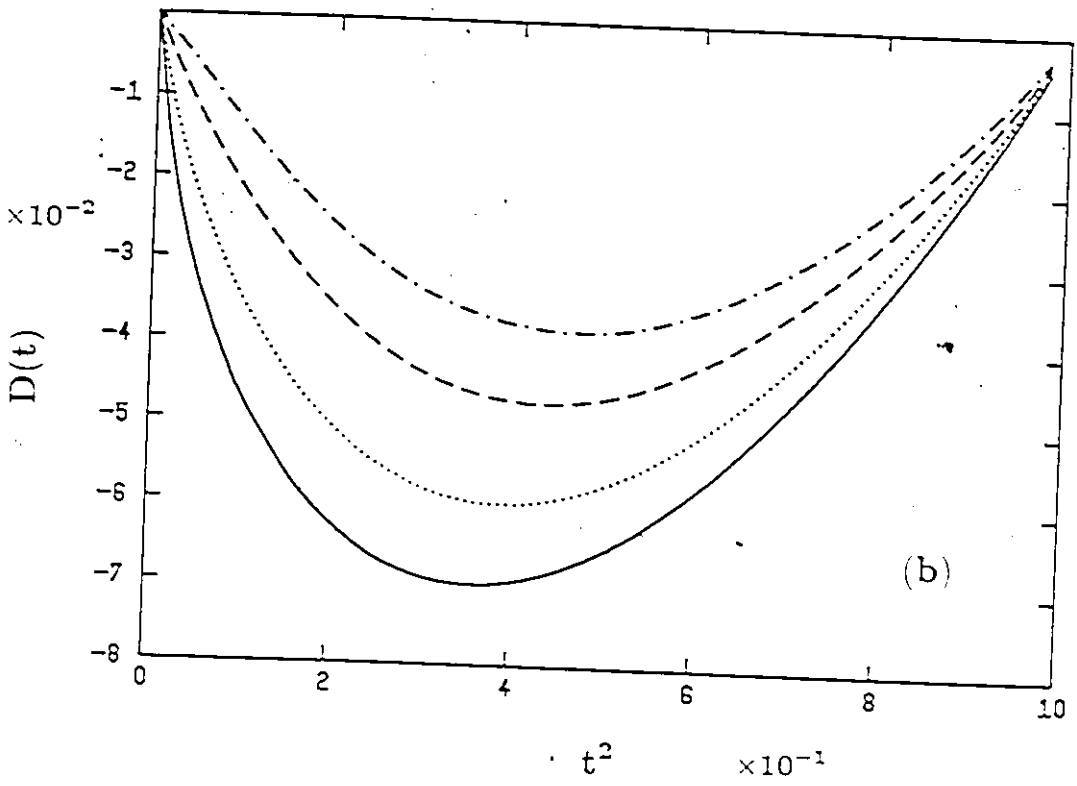
-1
-2
$\times 10^{-2}$
-3
-4
D(t)
-5
-6
-7
-8
(b)
0
2
4
6
8
10
t^2
$\times 10^{-1}$

Fig. 4.5 The teperature dependence of the normalized specific heat difference of a proximity effect junction containing SR model paramagnetic impurities. The parameters are as given in Fig. 4.4.

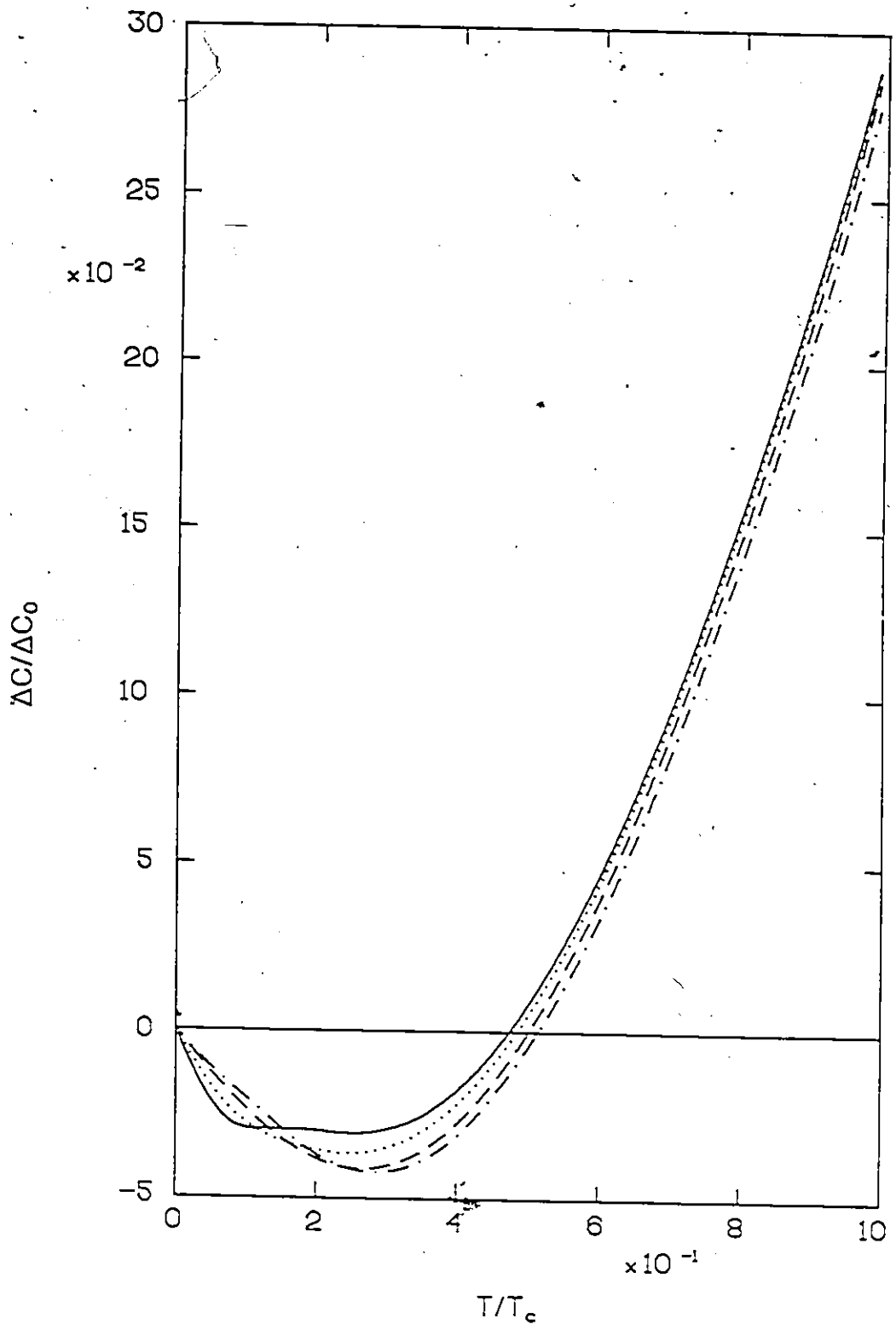
30
25
x10 -2
20
15
10
5
0
-5
ΔC/ΔC0
0
2
4
6
8
10
x10 -1
T/Tc

Fig. 4.6 The temperature dependence of the contribution of the normal side of a proximity effect junction containing paramagnetic impurities to the total free energy difference. The curves correspond to varying impurity concentrations, with parameters as in Figs. 4.4 and 4.5.

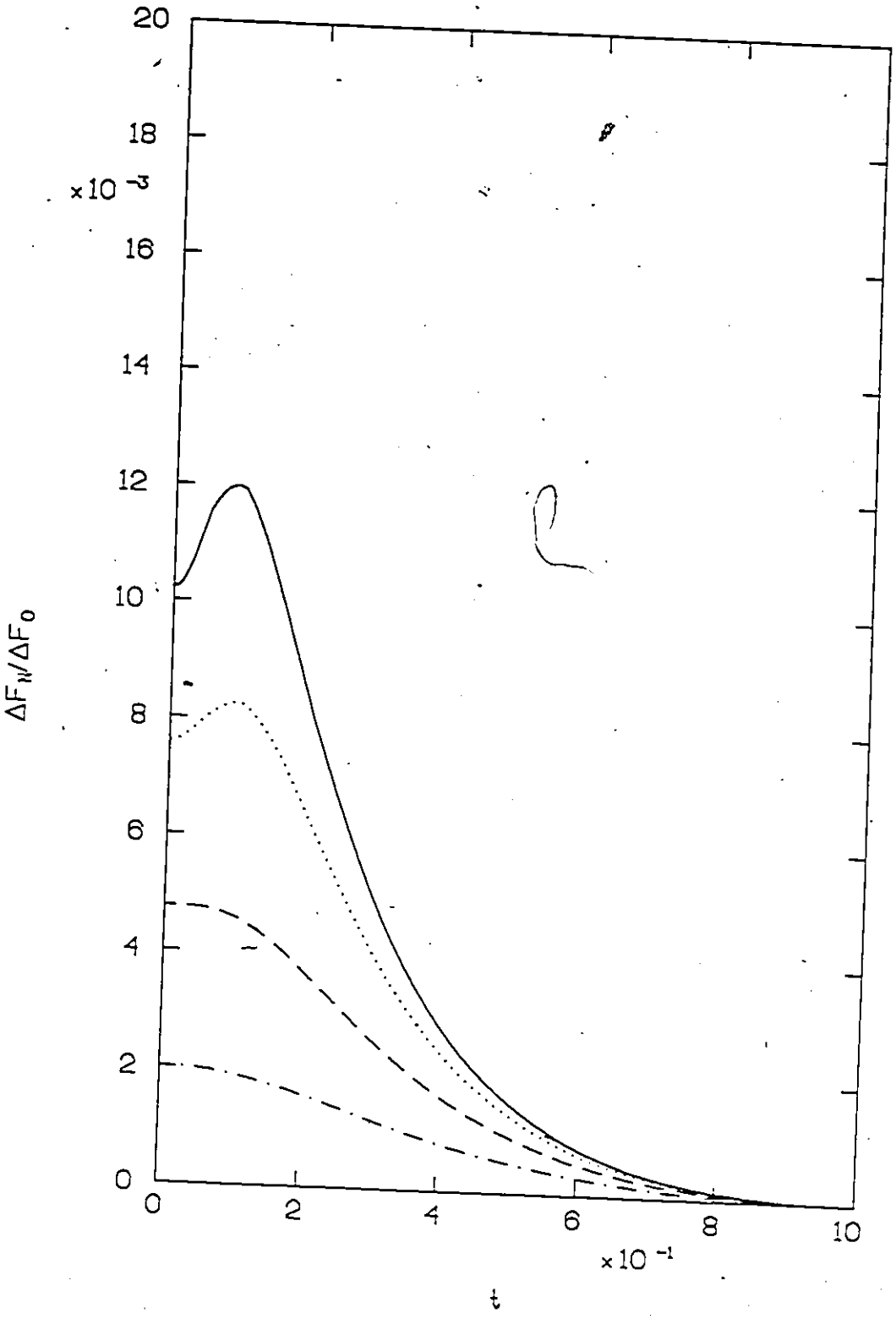
20
18
x10 -3
16
14
12
10
8
6
4
2
0
0
2
4
6
8
10
x10 -1
t
ΔF_N/ΔF_0

Fig. 4.7 The specific heat jump at T_c as a function of Γ_S for a pure proximity effect junction with:

Γ_N/T_c^0=5.0 (————),

Γ_N/T_c^0=1.0 (.....),

Γ_N/T_c^0=0.5 (-------),

Γ_N/T_c^0=0.1 (-.-.-.-),

Γ_N/T_c^0=0.01 (-.-.-.-).

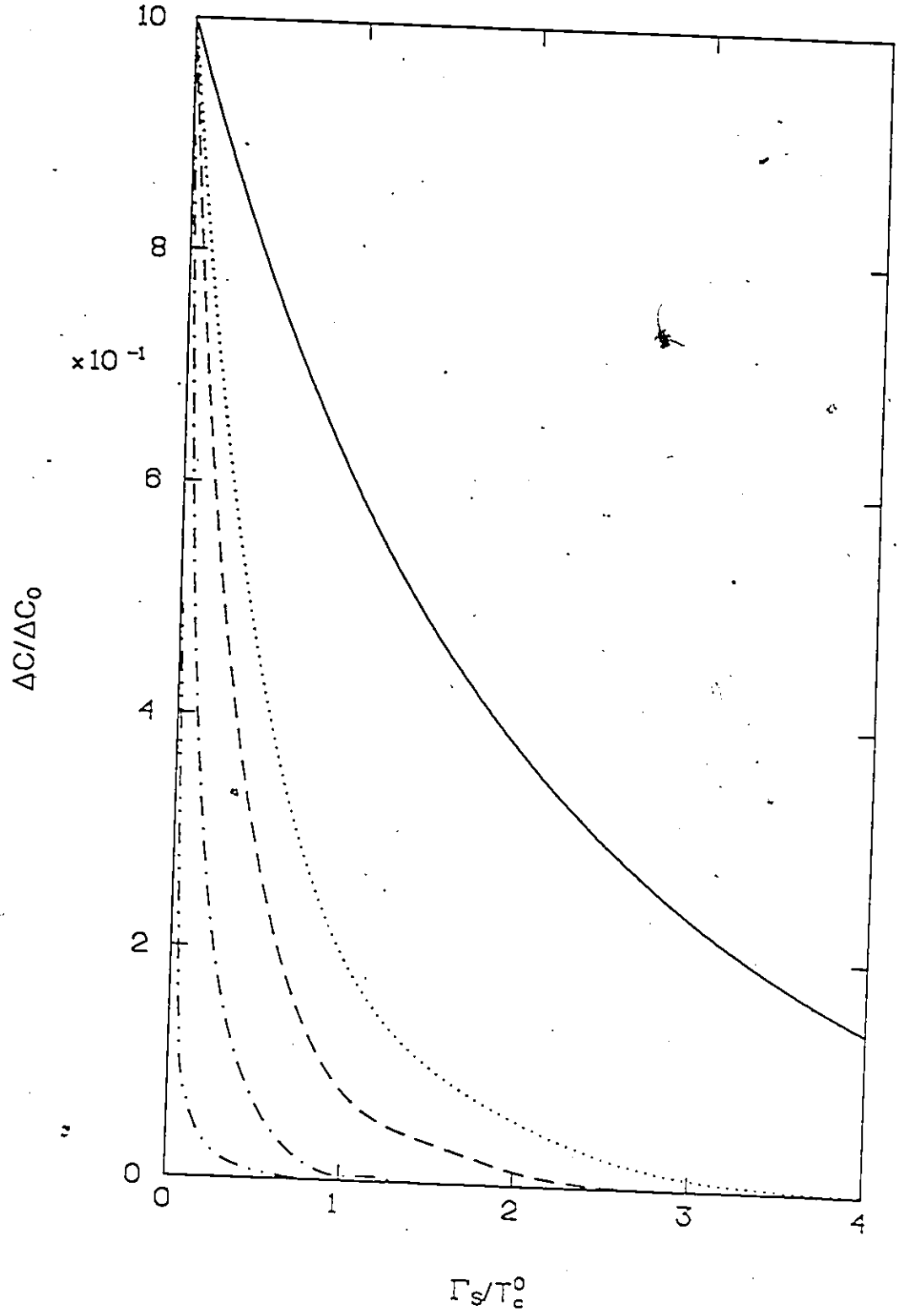
10
8
x10 -1
6
4
2
0
0
1
2
3
4
ΔC/ΔC₀
Γs/Tc°

Fig. 4.8 The contributions to the specific heat jump from the two sides of a proximity effect junction as a function of Γ_S for a pure proximity effect junction with the same parameters as in Fig. 4.7:

$\Gamma_N/T_c^0=5.0$ (————),

$\Gamma_N/T_c^0=1.0$ (. . . . .),

$\Gamma_N/T_c^0=0.5$ (- - - - - - -),

$\Gamma_N/T_c^0=0.1$ (- - - - - - -),

$\Gamma_N/T_c^0=0.01$ (- - - - - - -).

The contributions from the S side are positive, while the contributions from the N side for the same parameters are given by the same type of line for negative ΔC. Note that the final three curves for the N side are indistinguishable from the axis $\Delta C = 0$ on this scale. Also note that when the two contributions are combined to find the total jump they must be added with the correct weighting for their relative volumes.

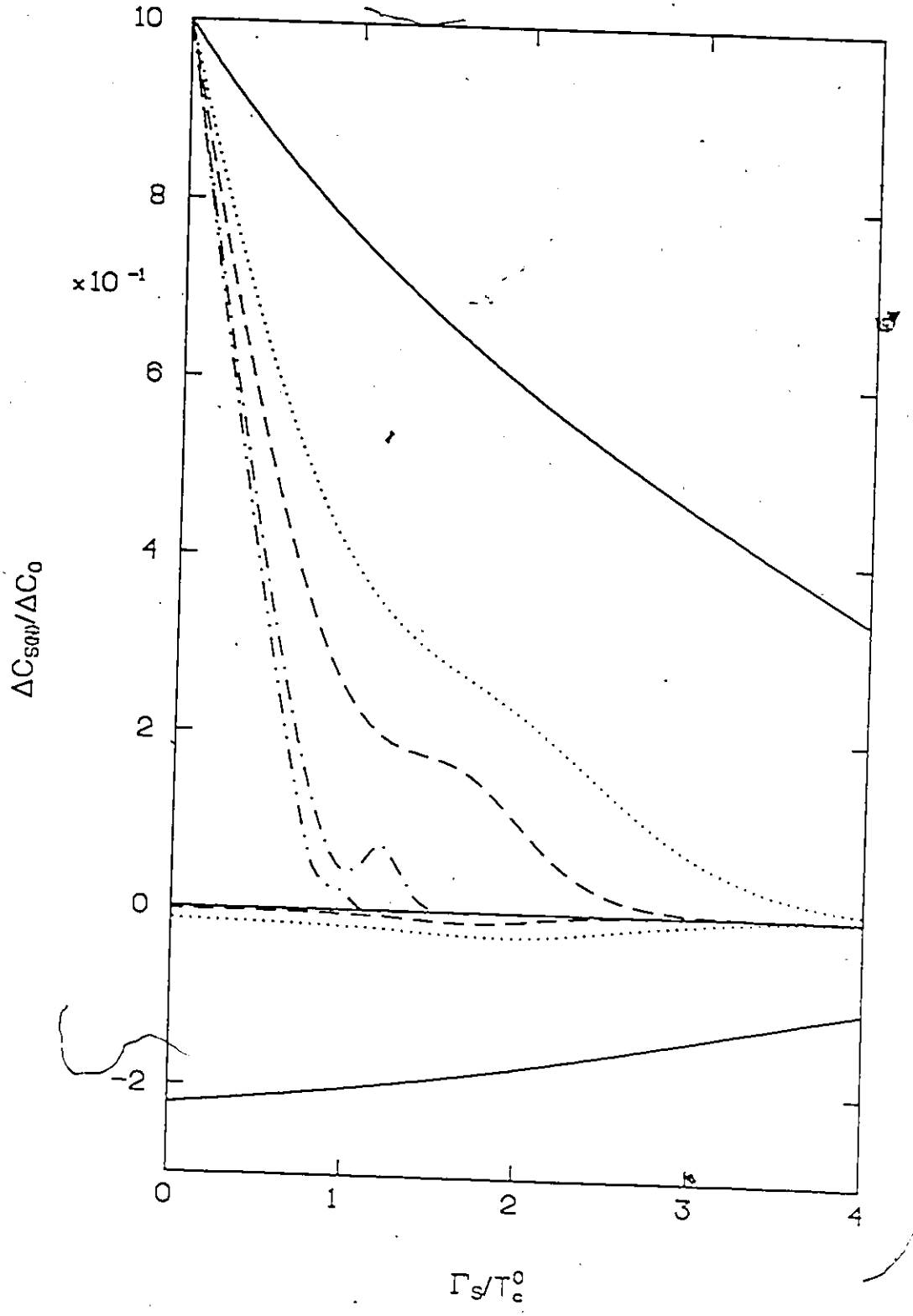
10
8
x10 -1
6
4
2
0
-2
0
1
2
3
4
ΔC_sat/ΔC_o
Γ_s/T_c^o

Fig. 4.9 a) The specific heat jump at T_c as a function of Γ_N for a pure proximity effect junction with:

$\Gamma_S/T_c^0=0.1$ (————),

$\Gamma_S/T_c^0=0.8$ (.....),

$\Gamma_S/T_c^0=1.4$ (-------),

$\Gamma_S/T_c^0=2.0$ (-.-.-.-),

$\Gamma_S/T_c^0=4.0$ (-.....-).

b) The reduced critical temperature for the same parameters as in a).

c) The function $(\Delta C/T_c)/(\Delta C^0/T_c^0)$ versus Γ_N for the same parameters as in a) and b).

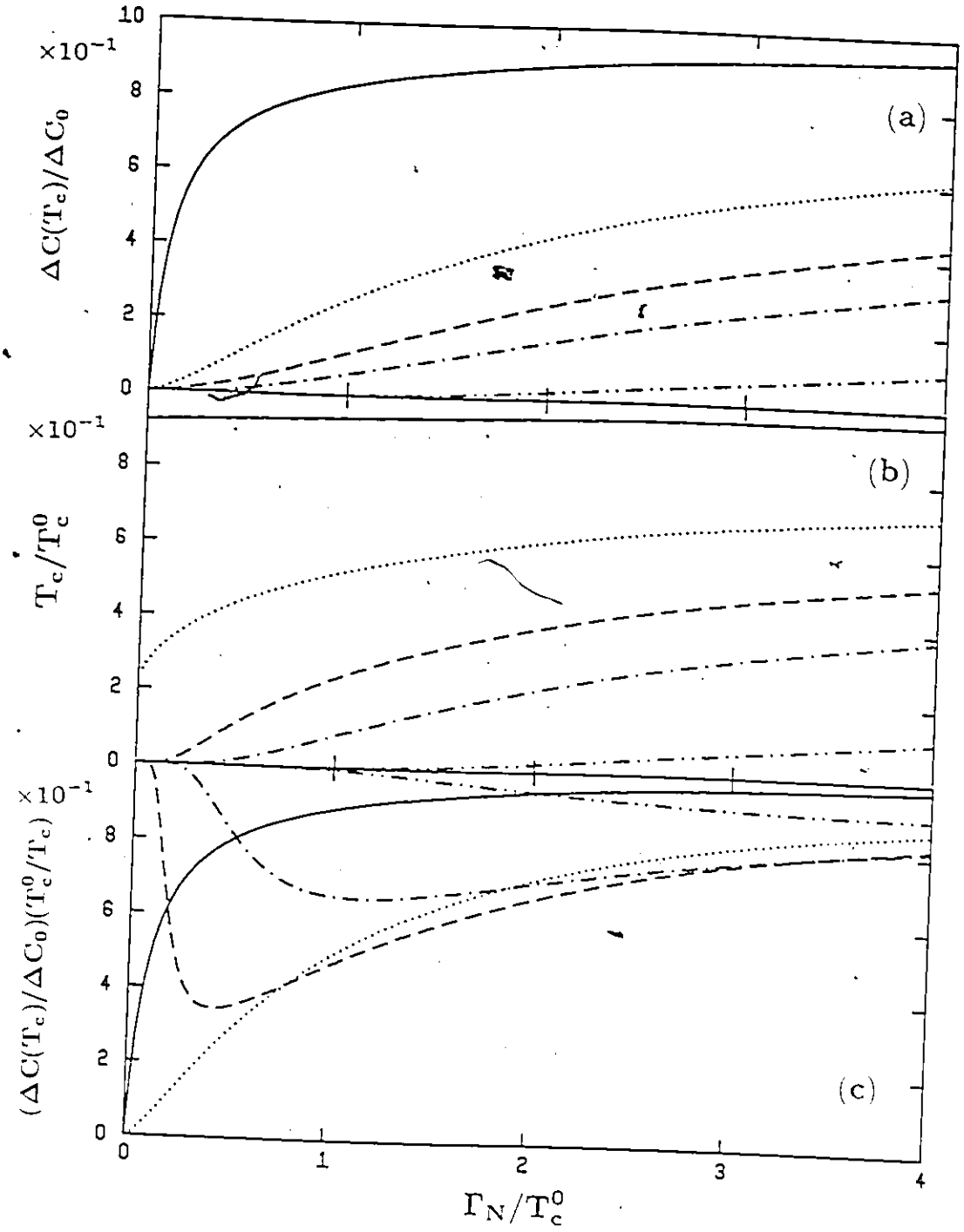
(a)
(b)
(c)
$\times 10^{-1}$
$\Delta C(T_c)/\Delta C_0$
T_c/T_c^0
$(\Delta C(T_c)/\Delta C_0)(T_c^0/T_c)$
Γ_N/T_c^0
0
1
2
3
4
0
2
4
6
8
10

Fig. 4.10 a) The specific heat jump at T_c as a function of paramagnetic impurity concentration for a proximity effect junction with $\Gamma_S/T_c^0=0.5$. SR impurity scattering parameter $\epsilon_0=0$. and with the following:

$\Gamma_N/T_c^0=0.1$ (————),

$\Gamma_N/T_c^0=0.8$ (.....),

$\Gamma_N/T_c^0=1.4$ (-------),

$\Gamma_N/T_c^0=2.0$ (-.-.-.-),

$\Gamma_N/T_c^0=4.0$ (-.-.-.-).

b) The reduced critical temperature for the same parameters as in a).

c) The function $(\Delta C/T_c)/(\Delta C^0/T_c^0)$ versus impurity concentration for the same parameters as in a) and b).

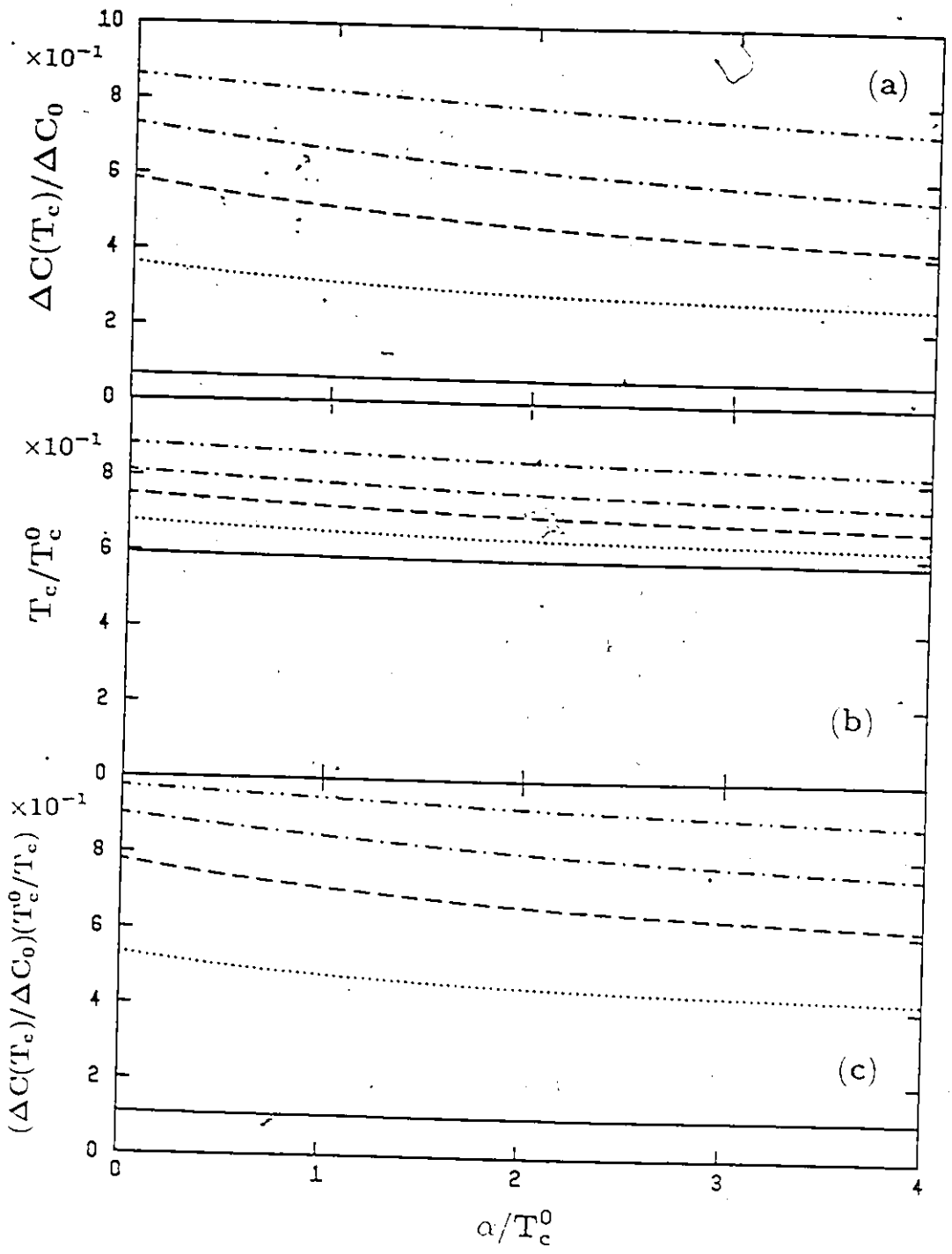
10
×10⁻¹
8
6
4
2
0
ΔC(Tc)/ΔC0
(a)
×10⁻¹
8
6
4
2
0
Tc/Tc0
(b)
×10⁻¹
8
6
4
2
0
(ΔC(Tc)/ΔC0)(Tc0/Tc)
(c)
0
1
2
3
4
α/Tc0

Fig. 4.11 a) The specific heat jump at T_c as a function of paramagnetic impurity concentration for a proximity effect junction with $\Gamma_S/T_c^0=1.5$. SR impurity scattering parameter $\epsilon_0=0$, and with the following:

$\Gamma_N/T_c^0=0.8$ (————),

$\Gamma_N/T_c^0=1.5$ (.....),

$\Gamma_N/T_c^0=3.0$ (-------),

$\Gamma_N/T_c^0=5.0$ (-·-·-·-),

$\Gamma_N/T_c^0=10.0$ (-·-·-·-).

b) The reduced critical temperature for the same parameters as in a).

c) The function $(\Delta C/T_c)/(\Delta C^0/T_c^0)$ versus impurity concentration for the same parameters as in a) and b).

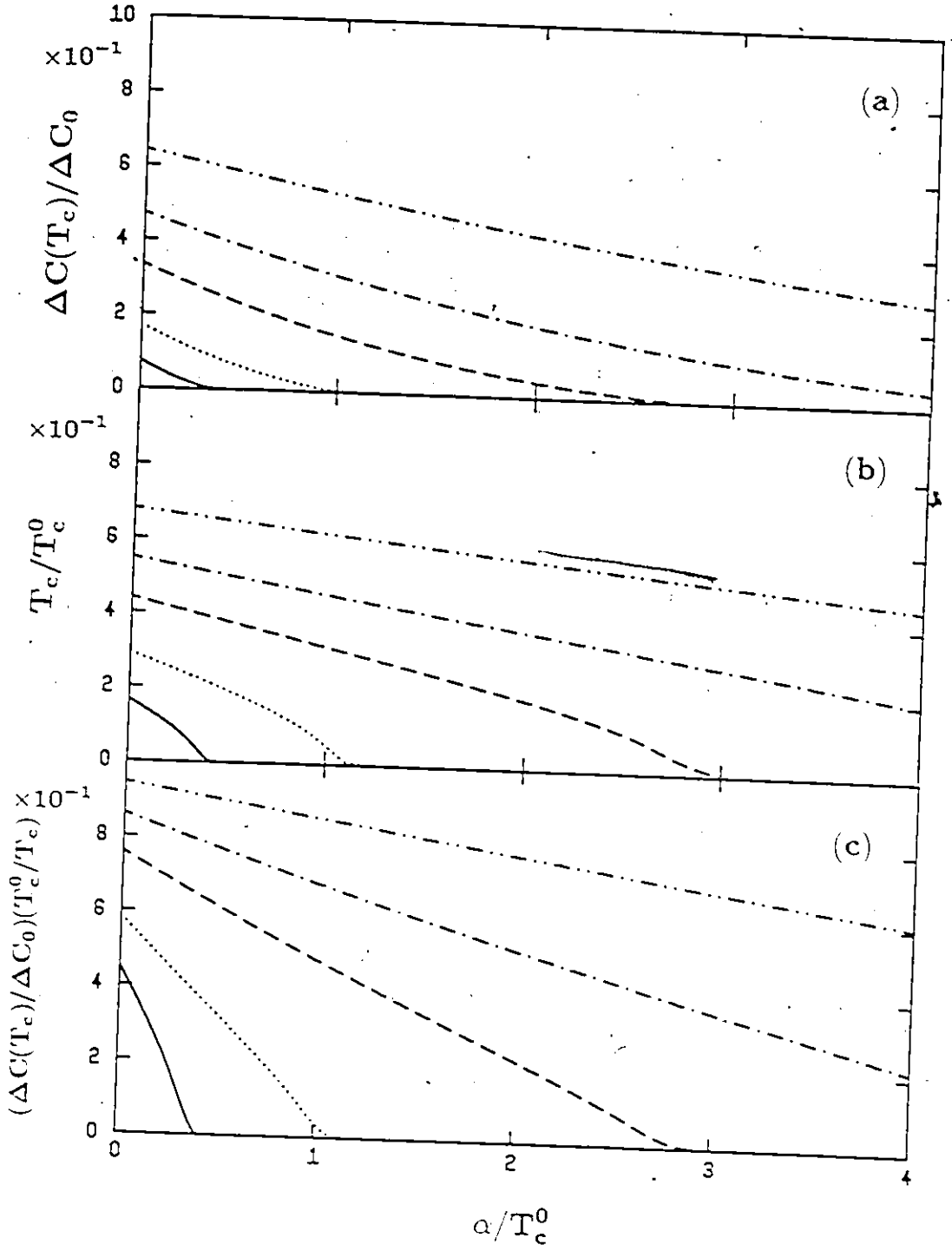
(a)
(b)
(c)
$\Delta C(T_c)/\Delta C_0$
T_c/T_c^0
$(\Delta C(T_c)/\Delta C_0)(T_c^0/T_c)$
$\times 10^{-1}$
α/T_c^0
0
1
2
3
4
0
2
4
6
8
10

Fig. 4.12 a) The specific heat jump of an proximity effect junction as a function of SR impurity concentration for the parameters:

$\Gamma_S/T_c^0=1.5$, $\Gamma_N/T_c^0=3.0$, $\epsilon_0=0.0$ (————).

$\Gamma_S/T_c^0=1.5$, $\Gamma_N/T_c^0=3.0$, $\epsilon_0=1.0$ (.....).

$\Gamma_S/T_c^0=1.5$, $\Gamma_N/T_c^0=10.0$, $\epsilon_0=0.0$ (-------).

$\Gamma_S/T_c^0=1.5$, $\Gamma_N/T_c^0=10.0$, $\epsilon_0=1.0$ (-.-.-.-).

b) The reduced critical temperature for the same parameters as in a).

c) The function $(\Delta C/T_c)/(\Delta C^0/T_c^0)$ versus impurity concentration for the same parameters as in a) and b).

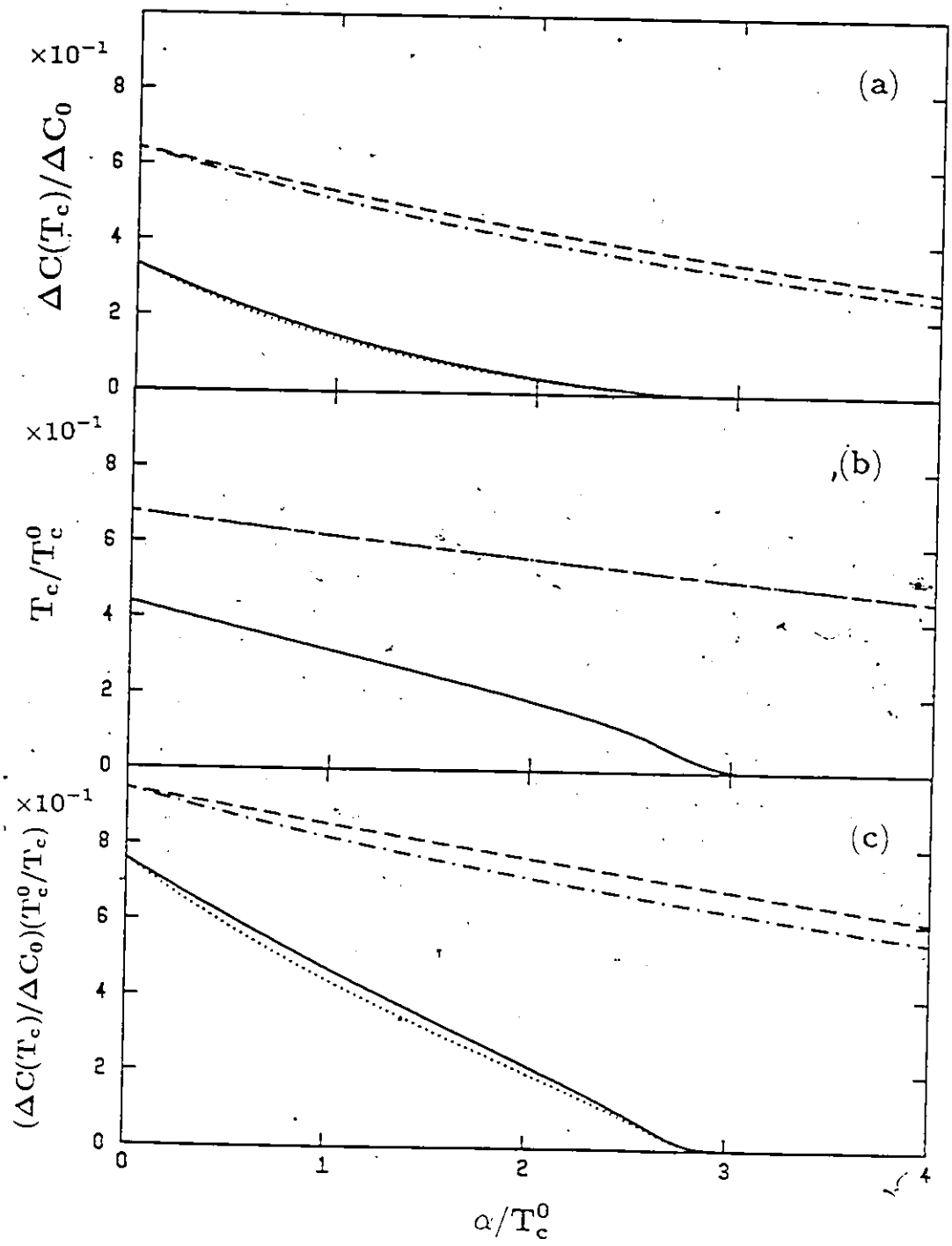
(a)
(b)
(c)
$\times 10^{-1}$
$\Delta C(T_c)/\Delta C_0$
T_c/T_c^0
$(\Delta C(T_c)/\Delta C_0)(T_c^0/T_c)$
α/T_c^0
0
1
2
3
4
0
2
4
6
8

Fig. 4.13 The inverse electromagnetic penetration depth at zero temperature of the normal side of a proximity effect junction as a function of paramagnetic impurity concentration in the SR model with $\epsilon_0=0$.

a) "Thick" superconducting film $\Gamma_S/T_c^0=0.36$ and:

$\Gamma_N/T_c^0=0.10$ (————).

$\Gamma_N/T_c^0=0.72$ (.....).

$\Gamma_N/T_c^0=1.50$ (-------).

b) "Thin" superconducting film $\Gamma_S/T_c^0=1.5$ and:

$\Gamma_N/T_c^0=0.36$ (————).

$\Gamma_N/T_c^0=0.72$ (.....).

$\Gamma_N/T_c^0=1.50$ (-------).

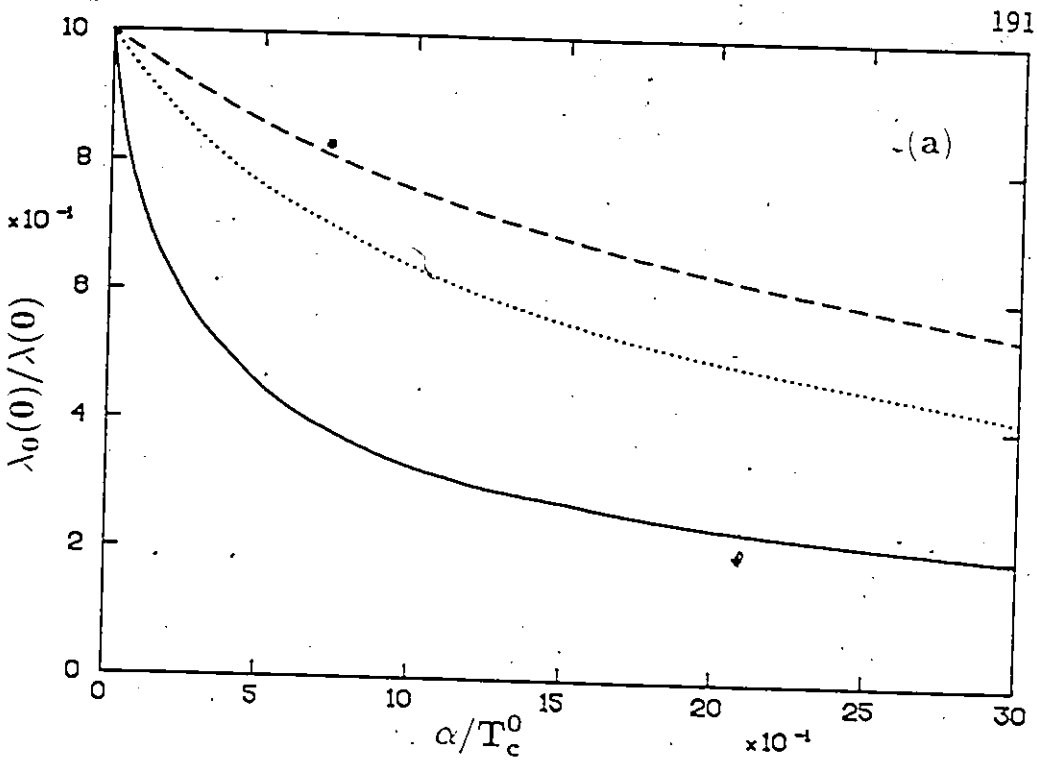
(a)
$\lambda_0(0)/\lambda(0)$
α/T_c^0
x10⁻¹
0
2
4
6
8
10
0
5
10
15
20
25
30

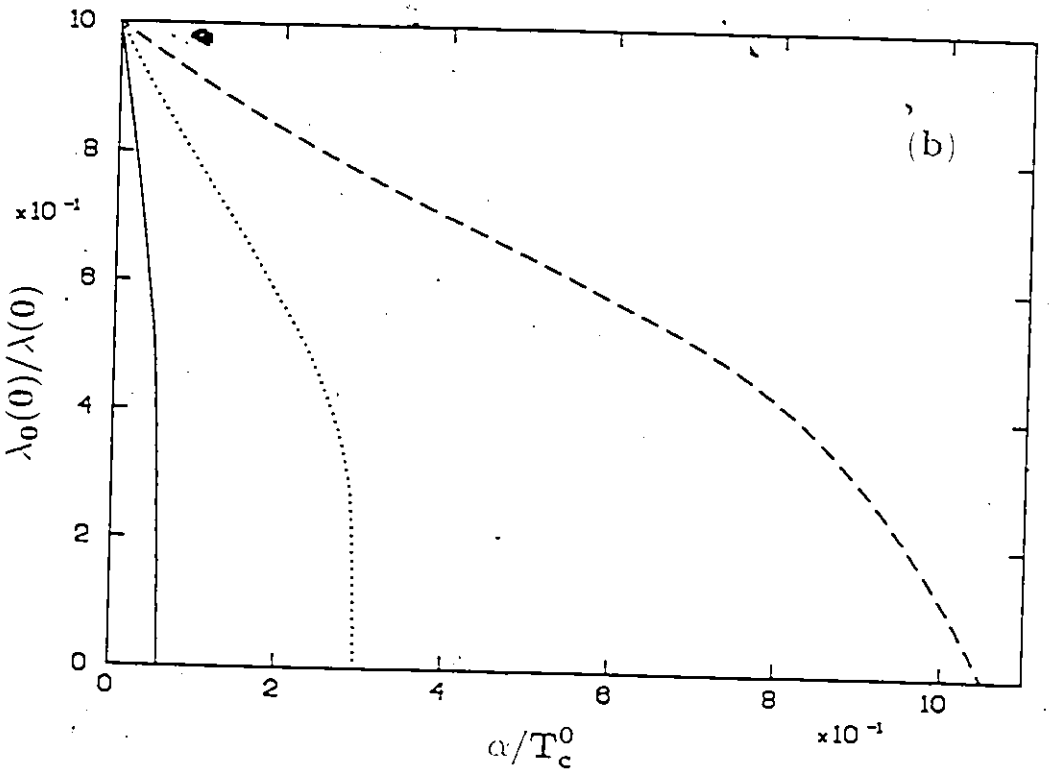
(b)
$\lambda_0(0)/\lambda(0)$
α/T_c^0
x10⁻¹
0
2
4
6
8
10

Fig. 4.14 The dependence of the zero temperature penetration depth of the normal side of a proximity effect junction on the SR scattering parameter ϵ_0 for the parameters $\Gamma_N/T_c^0=0.72$ and:
$\Gamma_S/T_c^0=1.5$ and $\alpha/T_c^0=0.01$ (————).
$\Gamma_S/T_c^0=1.5$ and $\alpha/T_c^0=0.20$ (.....).
$\Gamma_S/T_c^0=0.36$ and $\alpha/T_c^0=0.10$ (-------).
$\Gamma_S/T_c^0=0.36$ and $\alpha/T_c^0=0.72$ (-.-.-.-).

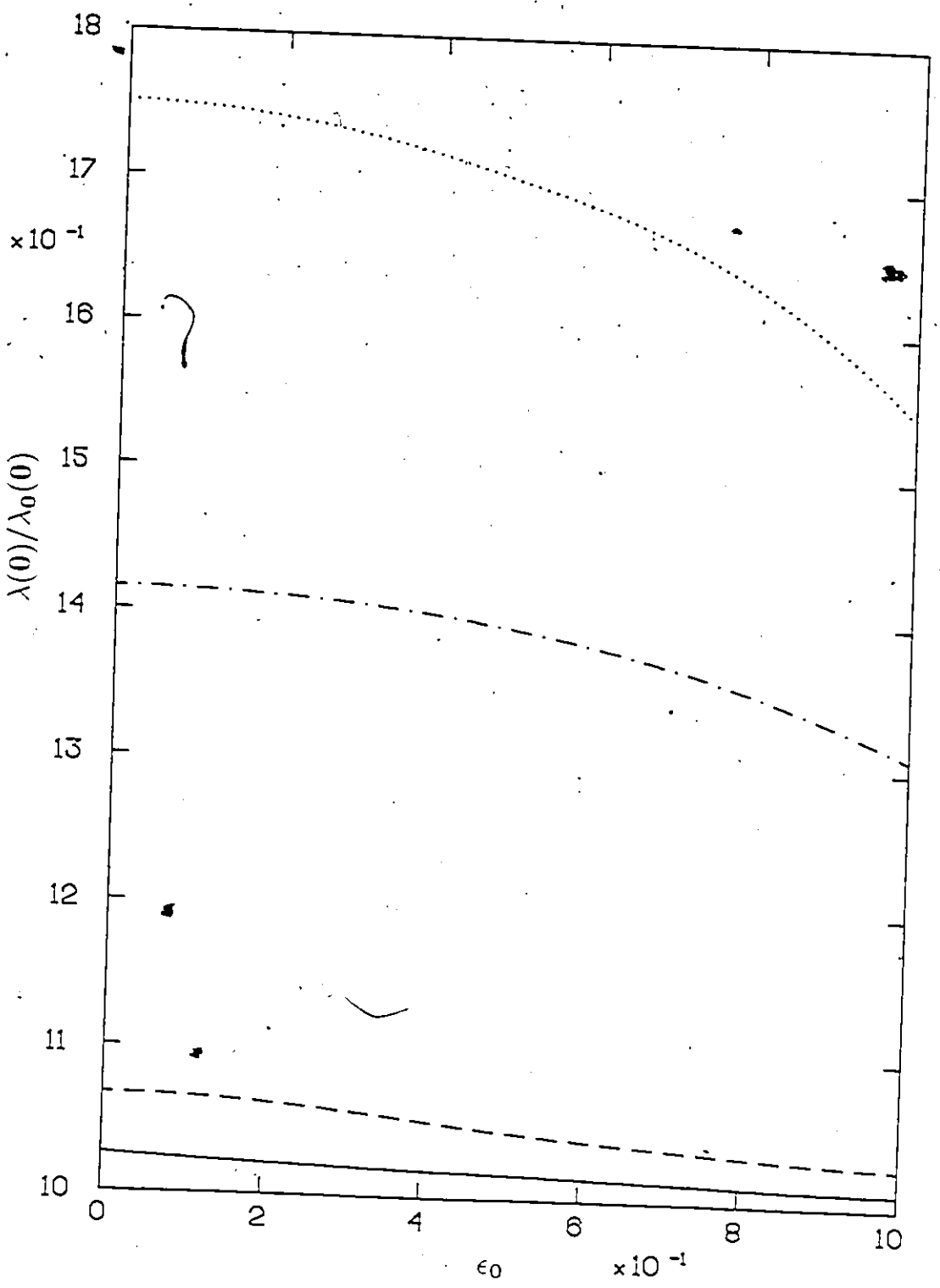
18
17
16
15
14
13
12
11
10
$\times 10^{-1}$
$\lambda(0)/\lambda_0(0)$
0
2
4
6
8
10
ϵ_0
$\times 10^{-1}$

Fig. 4.15 The temperature dependence of the electromagnetic penetration depth of the normal side of a proximity effect junction containing SR model paramagnetic impurities.

a) The penetration depth $\lambda(T)$, normalized to the zero temperature value $\lambda(0)$ for the same material, with paramters $\Gamma_S/T_c^0=0.36$, $\Gamma_N/T_c^0=0.72$, $\epsilon_0=0$ and:

$\alpha/T_c=0$ (————),

$\alpha/T_c=0.01$ (.....),

$\alpha/T_c=0.10$ (-------),

$\alpha/T_c=0.72$ (-·-·-·-).

b) The penetration depth $\lambda(T)$ normalized to the zero temperature value of the junction without paramagnetic impurities $\lambda_0(0)$ for the same parameters as in a).

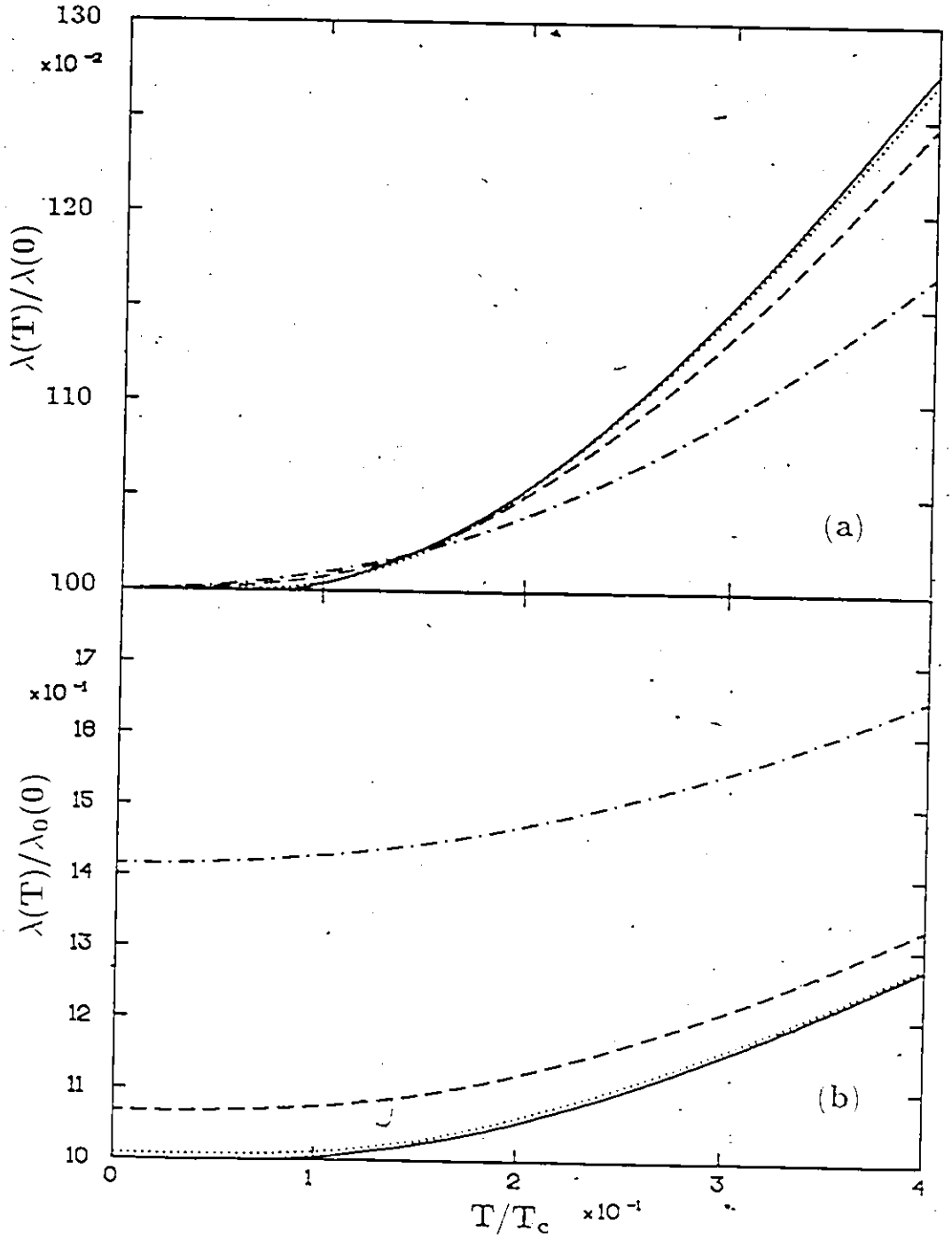
130
x10⁻²
120
110
100
λ(T)/λ(0)
(a)
17
x10⁻¹
16
15
14
13
12
11
10
λ(T)/λ₀(0)
(b)
0
1
2
3
4
T/T_c
x10⁻¹

Fig. 4.16 The temperature dependence of the electromagnetic penetration depth of the normal side of a proximity effect junction containing SR model paramagnetic impurities.

a) The penetration depth $\lambda(T)$, normalized to the zero temperature value $\lambda(0)$ for the same material, with paramters $\Gamma_S/T_c^0=0.36$, $\Gamma_N/T_c^0=0.10$, and:

$\alpha/T_c=0$ (————),

$\alpha/T_c=0.01$ and $\epsilon_0=0$ (.....),

$\alpha/T_c=0.10$ and $\epsilon_0=0$ (-------),

$\alpha/T_c=0.10$ and $\epsilon_0=1.0$ (-·-·-·-).

b) The penetration depth $\lambda(T)$ normalized to the zero temperature value of the junction without paramagnetic impurities $\lambda_0(0)$ for the same parameters as in a).

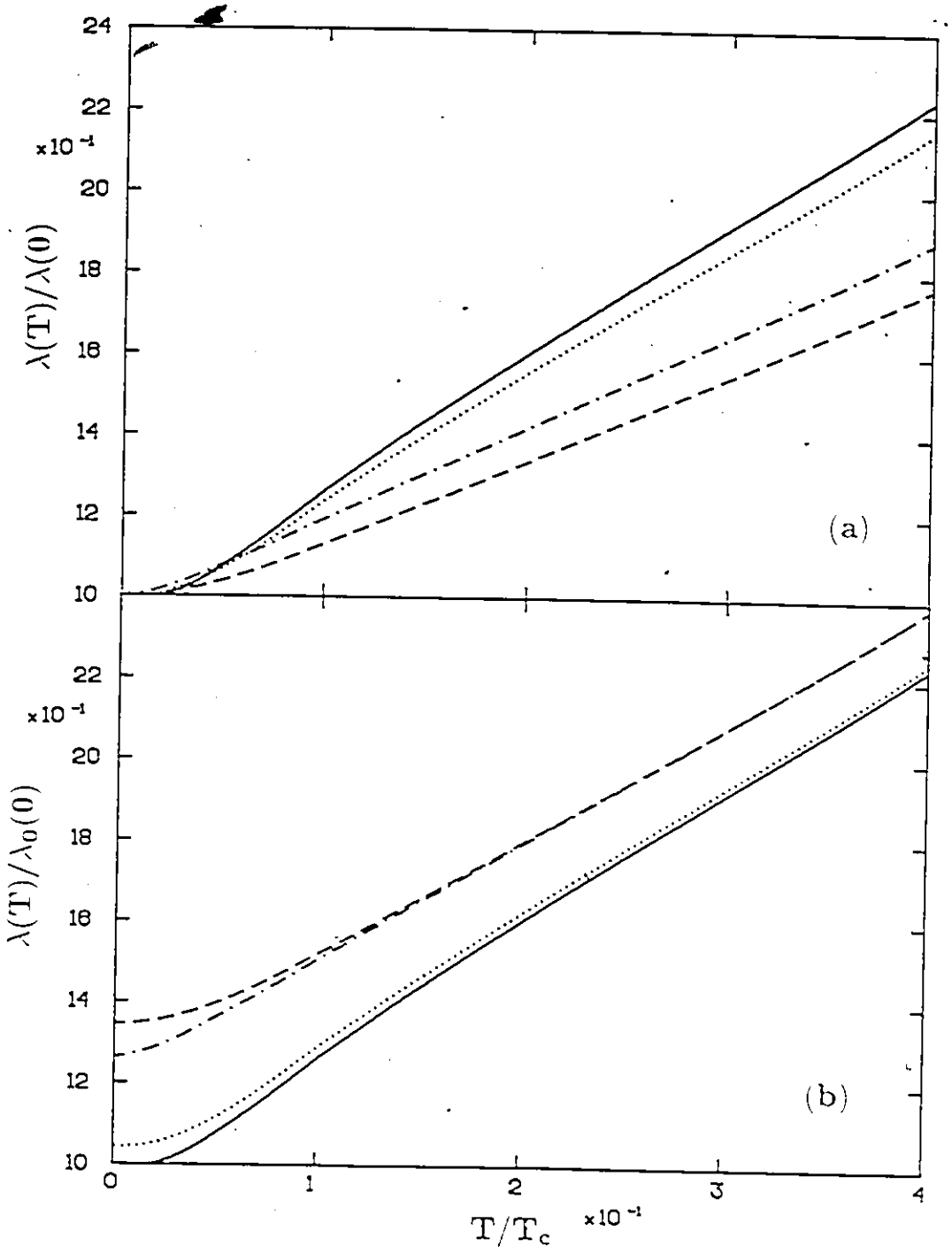
24
22
x10⁻¹
20
18
16
14
12
10
λ(T)/λ(0)
(a)
22
x10⁻¹
20
18
16
14
12
10
λ(T)/λ₀(0)
(b)
0
1
2
3
4
T/Tc
x10⁻¹

Fig. 4.17 a) The frequency dependence of the optical absorption of the normal side of a pure proximity effect junction with a thick superconducting film $\Gamma_S/T_c^0=0.1$ and for:

$\Gamma_N/T_c^0=0.10$ (———).

$\Gamma_N/T_c^0=0.36$ (.....).

$\Gamma_N/T_c^0=0.72$ (– – – –).

$\Gamma_N/T_c^0=1.50$ (– · – · –).

$\Gamma_N/T_c^0=4.00$ (– · · – · · –).

b) The density of states of the normal side of a junction $N_N(\omega)/N_{NO}$ for the same parameters as in a).

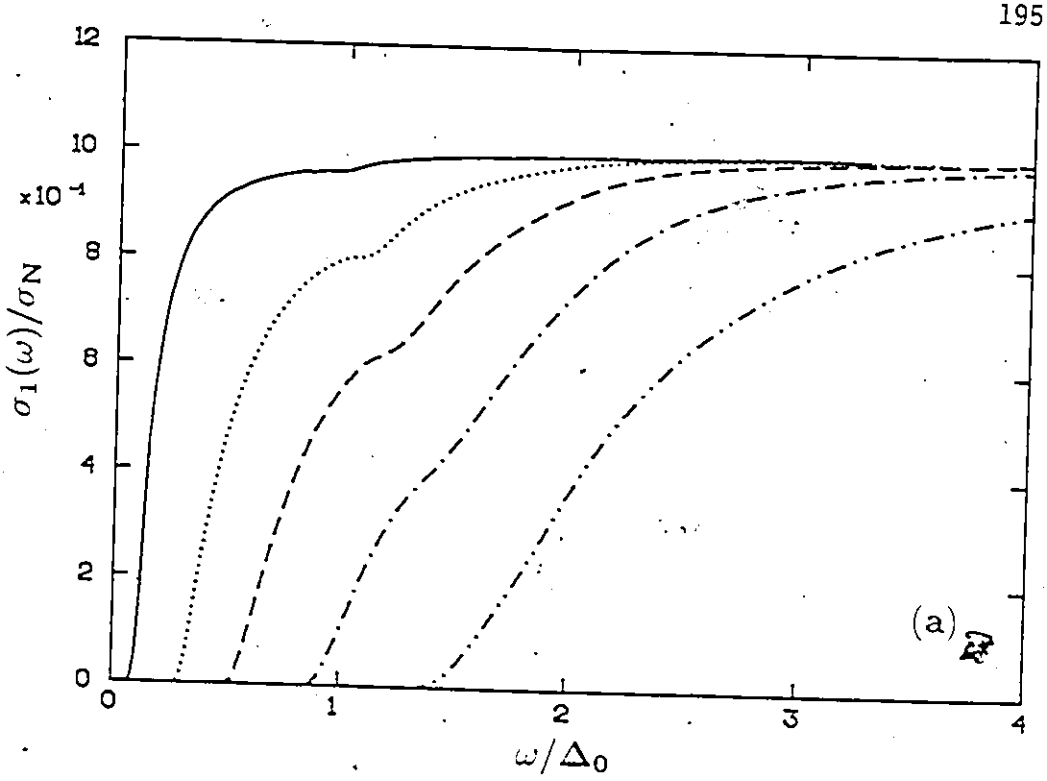
12
10
×10⁻⁴
8
6
4
2
0
0
1
2
3
4
$\sigma_1(\omega)/\sigma_N$
ω/Δ_0
(a)

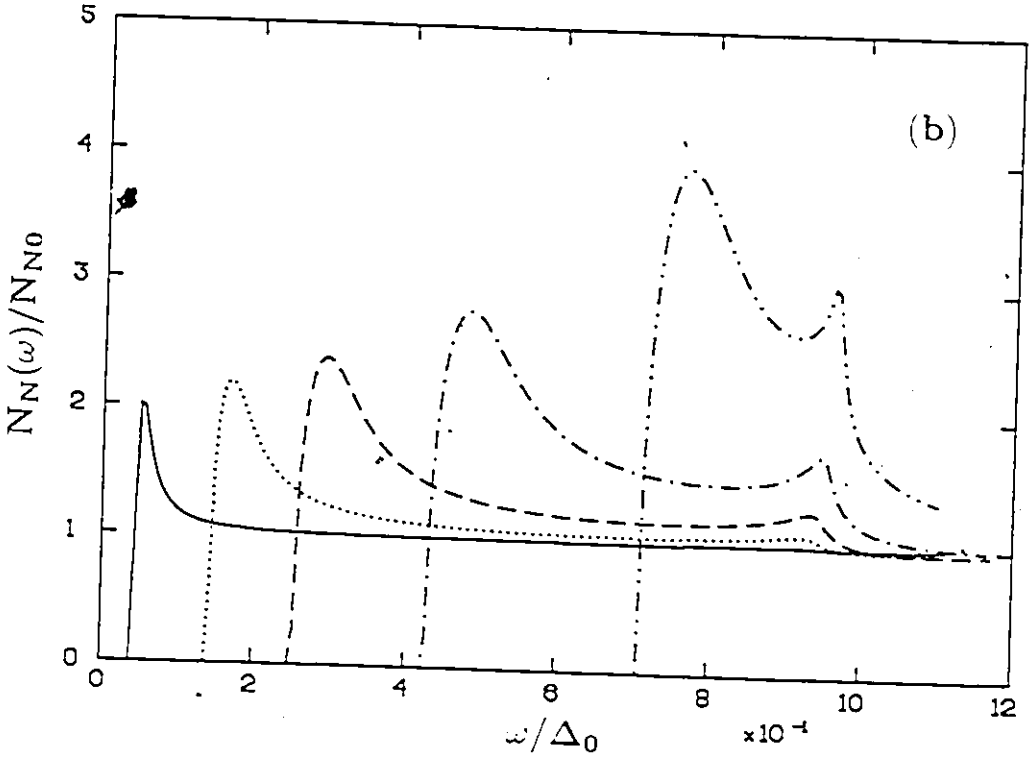
5
4
3
2
1
0
0
2
4
6
8
10
12
×10⁻⁴
$N_N(\omega)/N_{N0}$
ω/Δ_0
(b)

Fig. 4.18 The density of states of the superconducting side of a proximity effect junction for the same parameters as in Fig. 4.15.

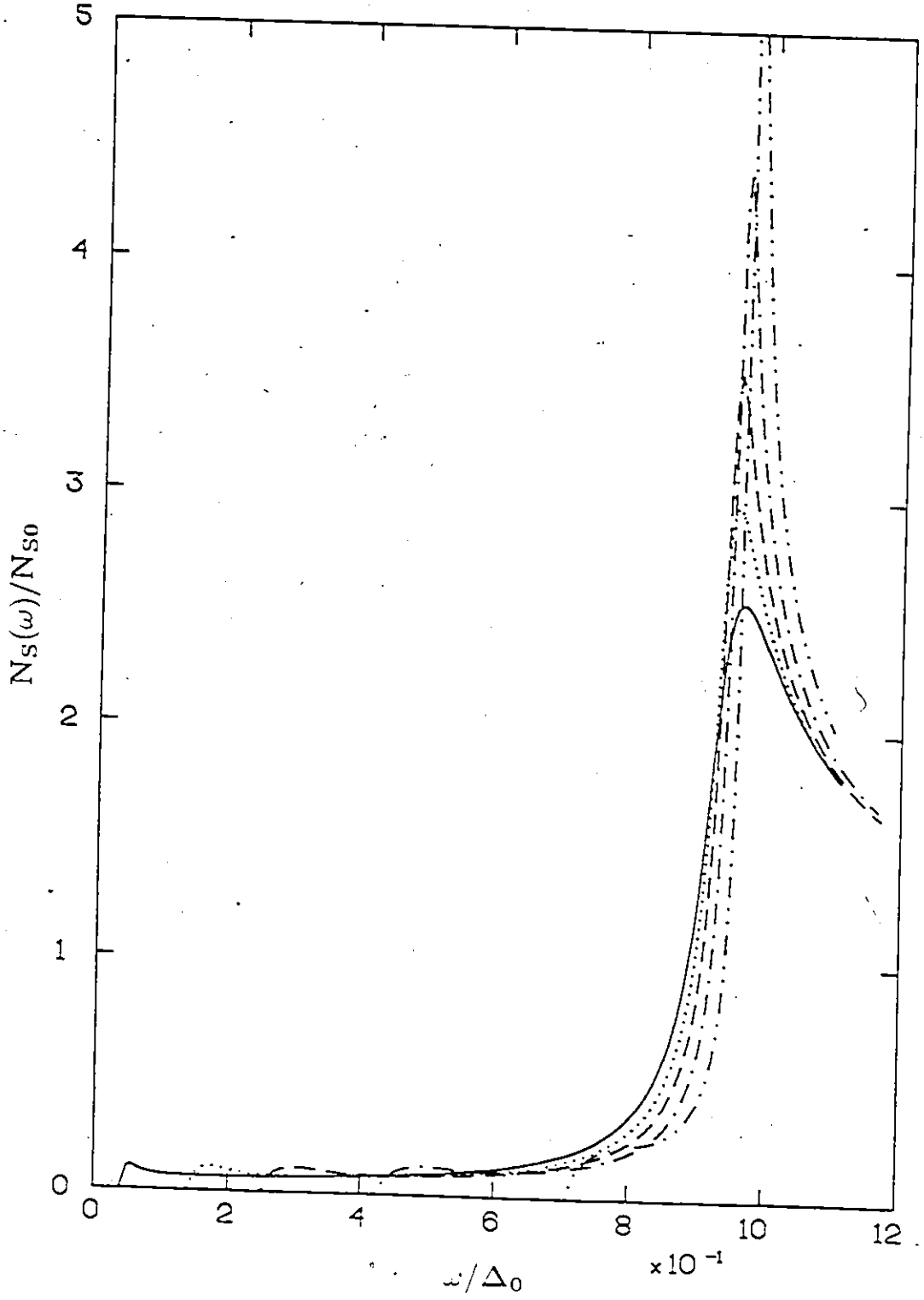
5
4
3
2
1
0
0
2
4
6
8
10
12
$N_S(\omega)/N_{S0}$
ω/Δ_0
$\times 10^{-1}$

Fig. 4.19 a) The frequency dependence of the optical absorption of the normal side of a proximity effect junction containing a small amount of SR paramagnetic impurities, $\alpha/T_c^0=0.01$, for $\Gamma_S = \Gamma_N = 0.36T_c^0$ and:

$\epsilon_0=1.0$ (.....),

$\epsilon_0=0.5$ (-------),

$\epsilon_0=0.0$ (-.-.-.-),

Also included is the pure case $\alpha=0$ (————).

b) The density of states on the normal side of the junction for the same parameters as in a).

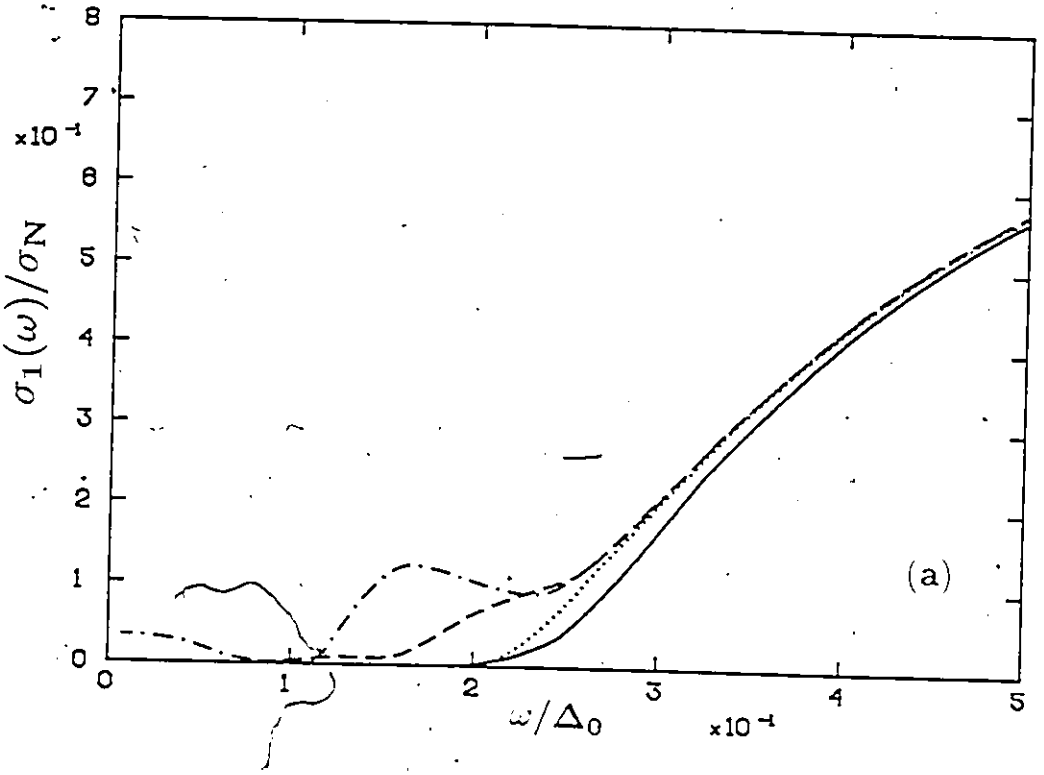
$\sigma_1(\omega)/\sigma_N$
x10⁻¹
0
1
2
3
4
5
6
7
8
ω/Δ_0
x10⁻¹
(a)

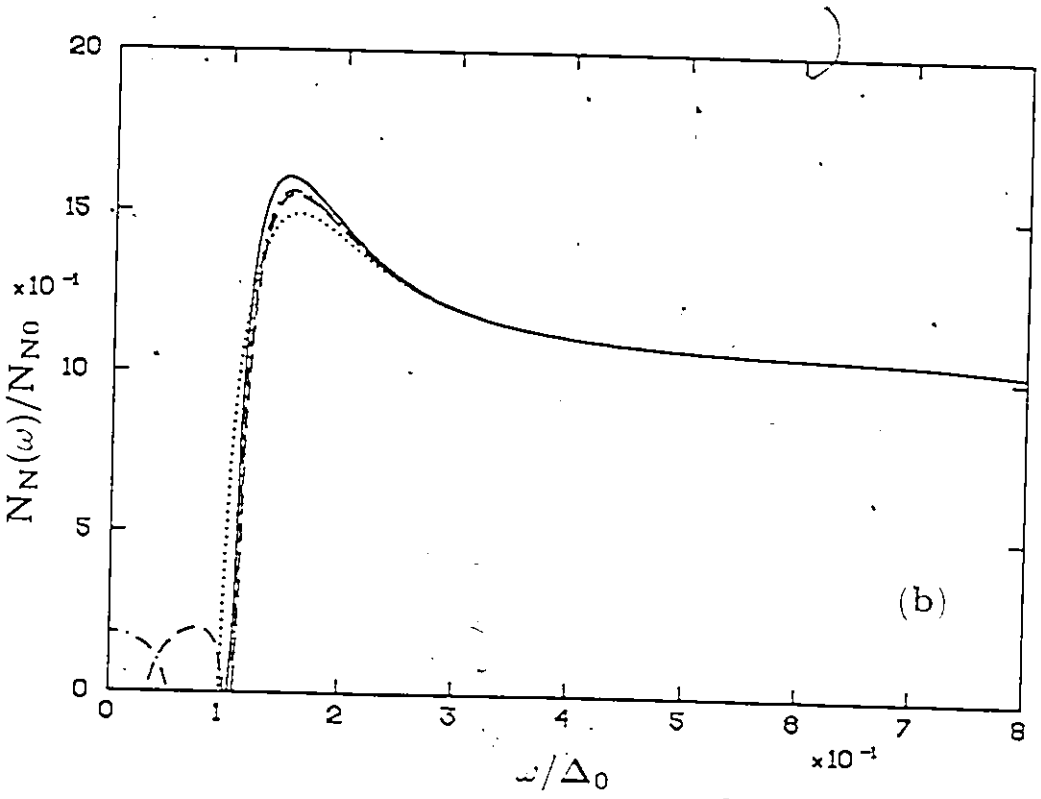
$N_N(\omega)/N_{N0}$
x10⁻¹
0
5
10
15
20
1
2
3
4
5
6
7
8
ω/Δ_0
x10⁻¹
(b)

Fig. 4.20 a) The frequency dependence of the optical absorption of the normal side of a proximity effect junction containing a small amount of SR paramagnetic impurities, $\alpha/T_c^0=0.1$, for $\Gamma_S = \Gamma_N = 0.36T_c^0$ and:

$\epsilon_0=1.0$ (.....),

$\epsilon_0=0.5$ (-------),

$\epsilon_0=0.0$ (-.-.-.-),

Also included is the pure case $\alpha=0$ (————).

b) The density of states on the normal side of the junction for the same parameters as in a).

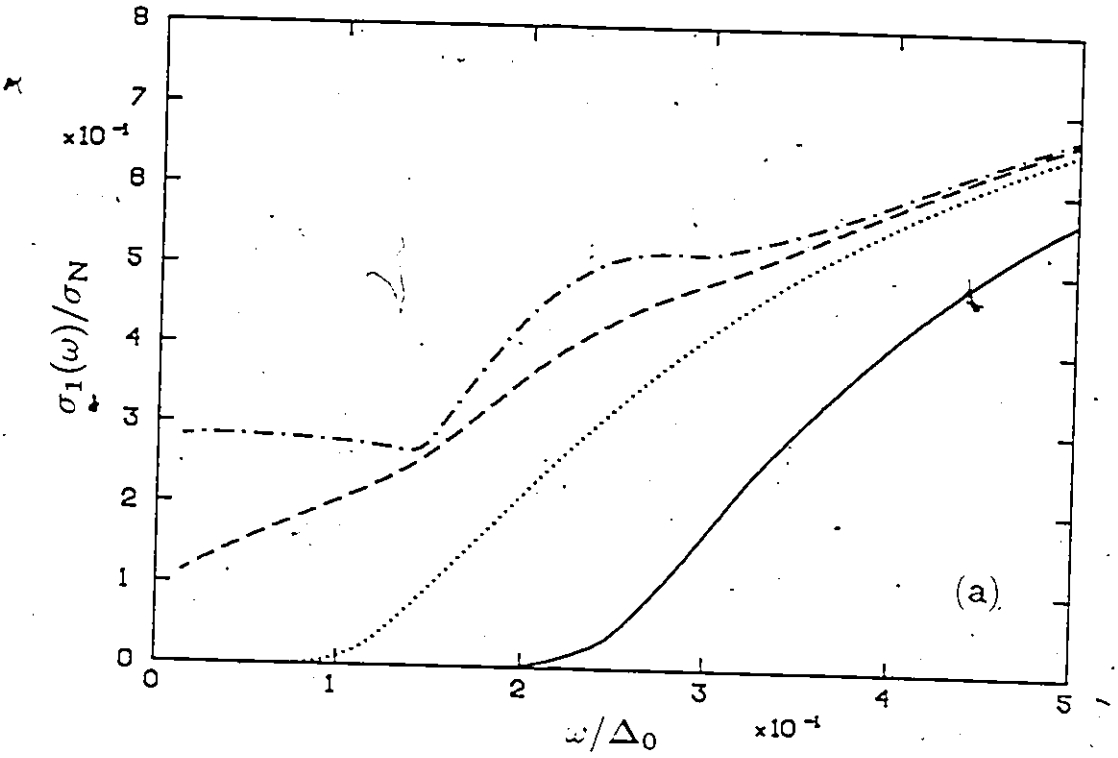
8
7
×10⁻¹
8
5
4
3
2
1
0
σ1(ω)/σN
0
1
2
3
4
5
ω/Δ0
×10⁻¹
(a)

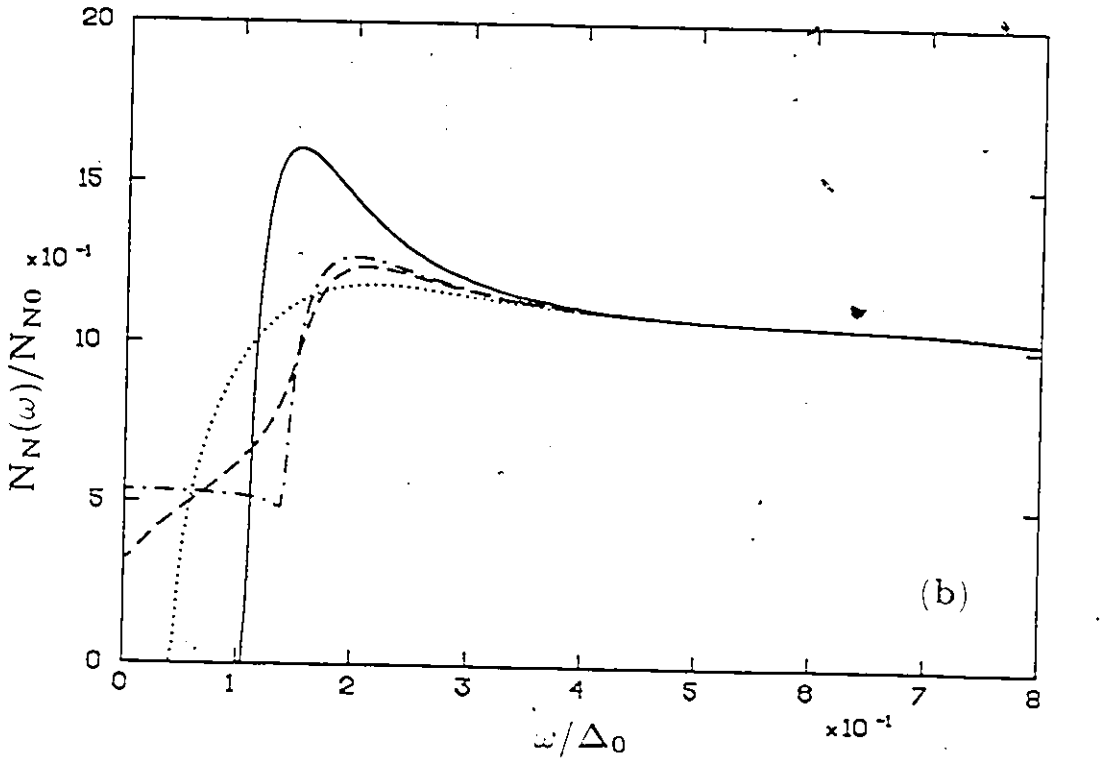
20
15
×10⁻¹
10
5
0
NN(ω)/NN0
0
1
2
3
4
5
8
7
8
ω/Δ0
×10⁻¹
(b)

Fig. 4.21 The zero bias conductance $\sigma(T)/\sigma_N$ of a proximity effect induced superconducting spin-glass as a function of temperature. The parameters are:

Γ_S=0.09 meV, Γ_N=2.263 meV, and $\alpha(\infty)$=8.91 meV with the spin-glass model SG I, $\bar{D}(1)$=1.0, $\bar{\tau}$=0.2, and $\tilde{Q}(\bar{t})=S^2(1-\bar{t}^2)$ (———).

Γ_S=0.03922 meV, Γ_N=1.0 meV, and $\alpha(\infty)$=4.10 meV with the spin-glass model SG I, $\bar{D}(1)$=1.0, $\bar{\tau}$=0.2, and $\tilde{Q}(\bar{t})=S^2(1-\bar{t}^2)$ (.....).

Γ_S=0.03922 meV, Γ_N=0.8 meV, and $\alpha(\infty)$=3.15 meV with the spin-glass model SG II, $\bar{D}(1)$=2.0, $\bar{\tau}$=0.2, and $\tilde{Q}(\bar{t})=S^2(1-\bar{t}^2)$ (------).

Also included is an AG curve: Γ_S=0.09 meV, Γ_N=2.263, and α=8.5 meV (-·-·-·).

The experimental points are from the 400 Å sample of Fig 2 of Ref 99.

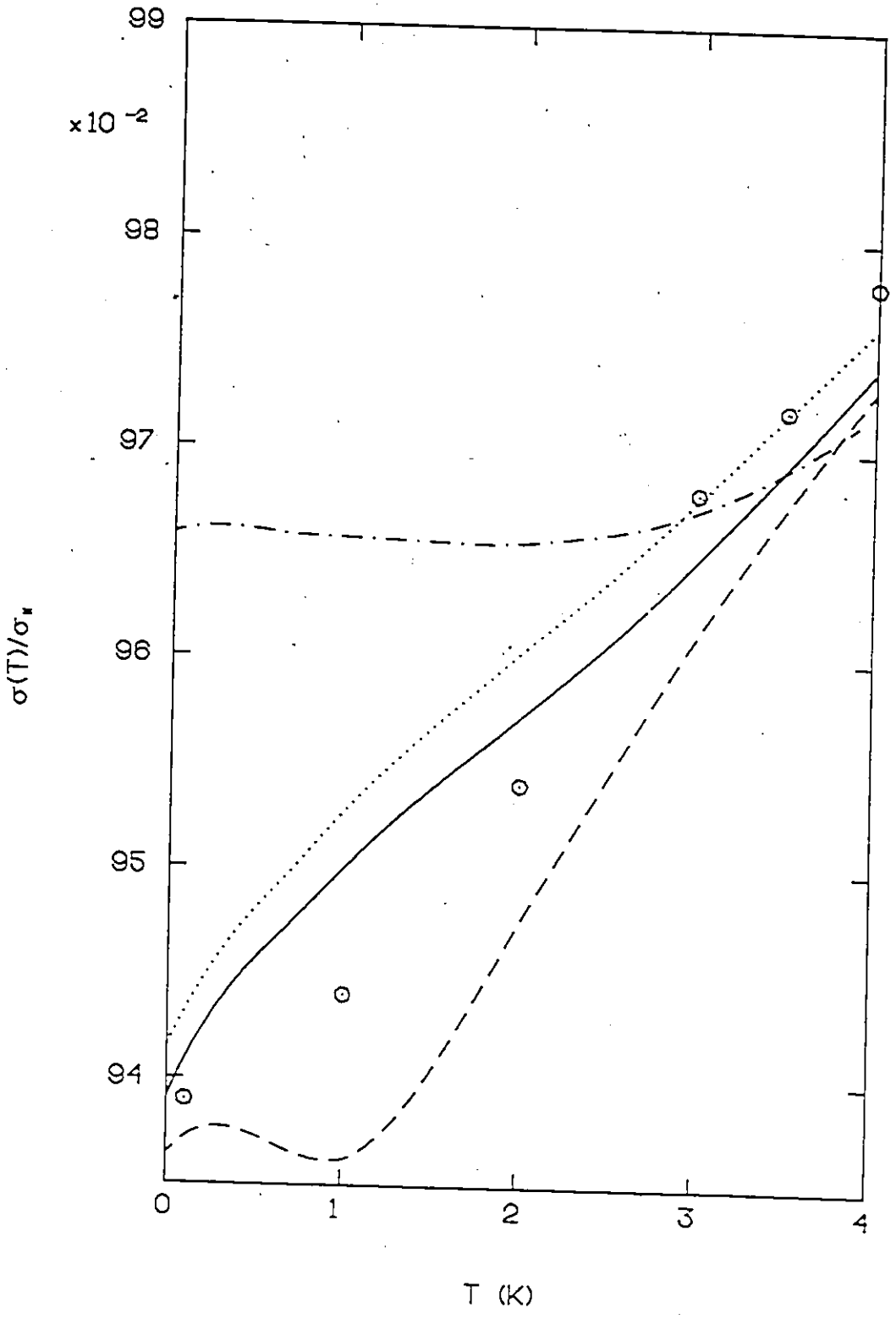
99
x10 -2
98
97
96
95
94
σ(T)/σ*
0
1
2
3
4
T (K)

Fig. 4.22 Comparison of the temperature dependence of the zero bias conductance (———) and the thermally smeared conductance σ_T (------) for an induced superconducting spin-glass. The curves labeled 1 were calculated using Γ_S=0.09 meV, Γ_N=2.263 meV and $\alpha(\infty)$=8.91 meV with the spin-glass model SG I. The curves labeled 2 were calculated with Γ_S=0.03922 meV, Γ_N= 0.8 meV, and $\alpha(\infty)$=8.91 meV, with the spin-glass model SG II. The circled data points are experimental points, and the squares are the thermally smeared values for the 400 Å sample of Fig. 2 of Ref 99.

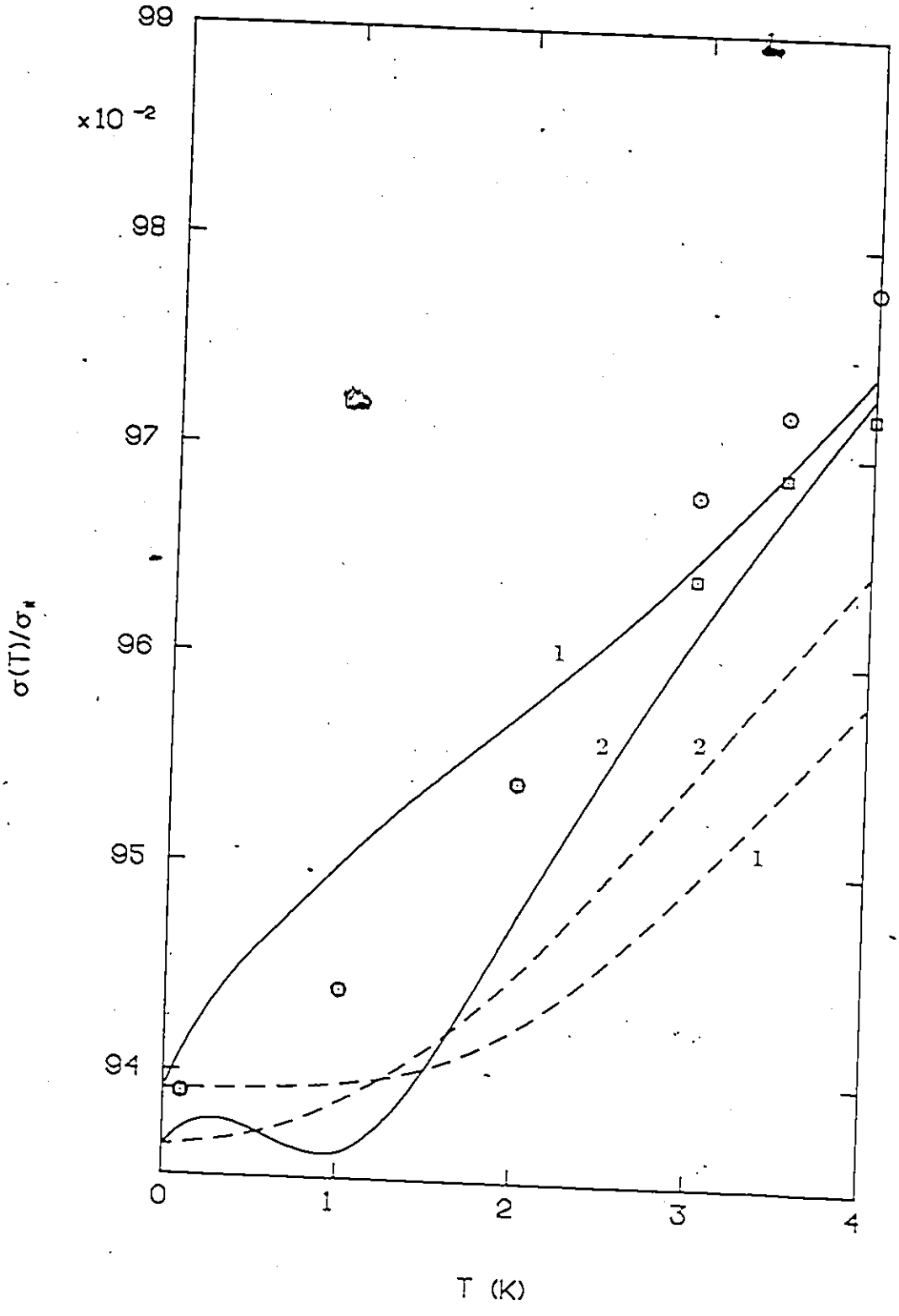
99
x10 -2
98
97
96
95
94
σ(T)/σ
0
1
2
3
4
T (K)
1
2
2
1

Fig. 4.23 Comparison of the temperature dependence of the zero bias conductance (———) and the thermally smeared conductance σ_T (------) for an induced superconducting spin-glass. The curves labeled 1 were calculated using Γ_S=0.09 meV, Γ_N=1.29 meV and $\alpha(\infty)$=2.45 meV with the spin-glass model SG I. The curves labeled 2 were calculated with Γ_S=0.09 meV, Γ_N= 1.29 meV, and $\alpha(\infty)$=2.45 meV, with the spin-glass model SG II. The circled data points are experimental points, and the squares are the thermally smeared values for the 800 Å sample of Fig. 3 of Ref 99.

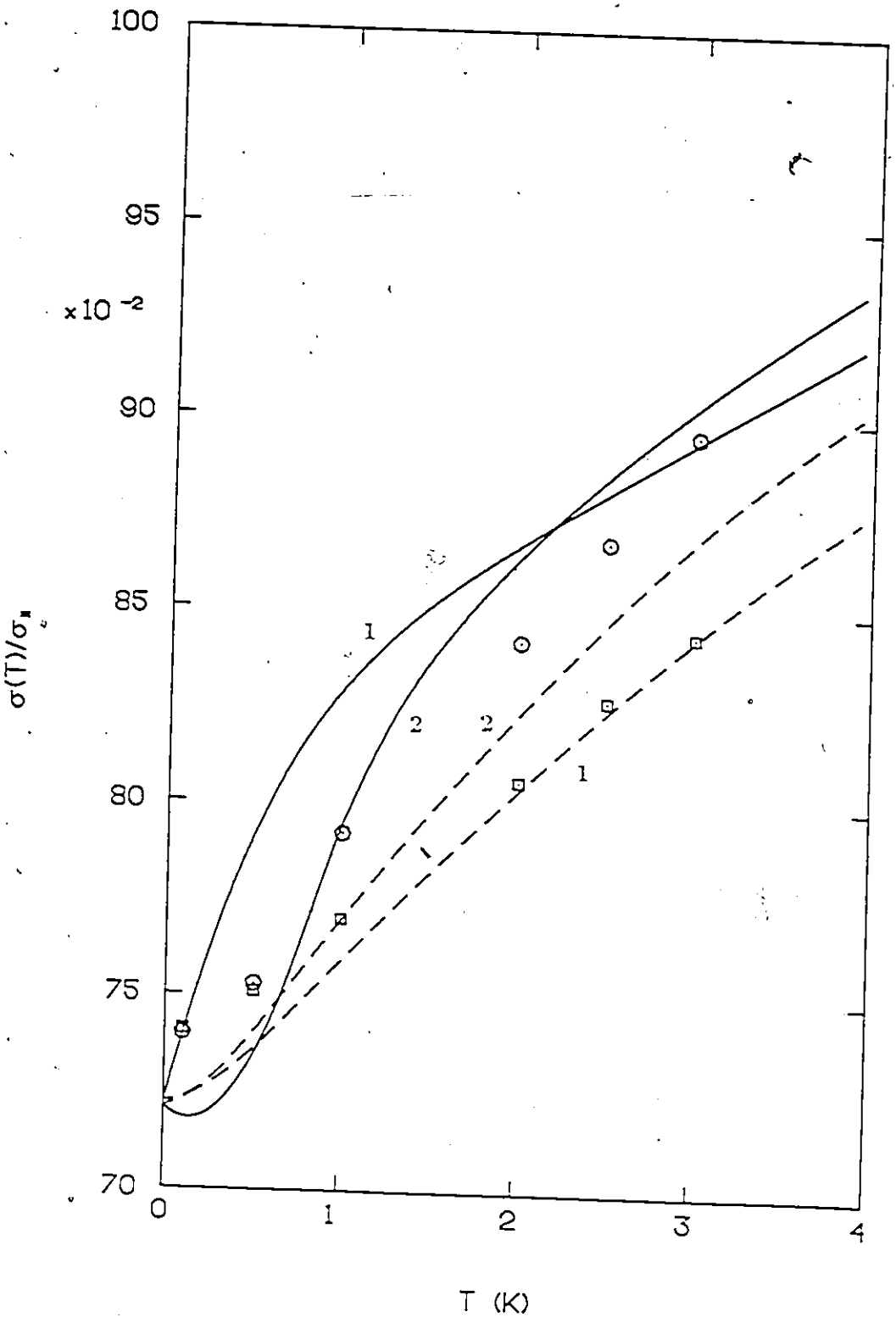
100
95
x10 -2
90
85
80
75
70
σ(T)/σ
0
1
2
3
4
T (K)
1
2
2
1

Fig. 4.24 The difference between the zero bias conductance and the thermally smeared conductance as a function of temperature for several spin-glass models:

Γ_S=0.09 meV, Γ_N=2.263 meV and $\alpha(\infty)$=8.91 meV for the spin-glass model with 5 percent increase in $\alpha(\bar{t})$ between $\bar{t}$=0.8 and $\bar{t}$=1.2 as described in the text (———).

Γ_S=0.09 meV, Γ_N=2.263 meV and $\alpha(\infty)$=8.91 meV for the spin-glass model SG I (.....).

Γ_S=0.03922 meV, Γ_N=1.0 meV and $\alpha(\infty)$=4.1 meV for the spin-glass model SG I (------).

Γ_S=0.2 meV, Γ_N=4.0 meV and $\alpha(\infty)$=15.9 meV for the spin-glass model SG I (-·-·-·).

Γ_S=0.03922 meV, Γ_N=0.8 meV and $\alpha(\infty)$=3.15 meV for the spin-glass model SG II (-·-·-·).

The experimental points are from the 400 Å Ag-Mn sample of Fig. 2 of Ref. 99.

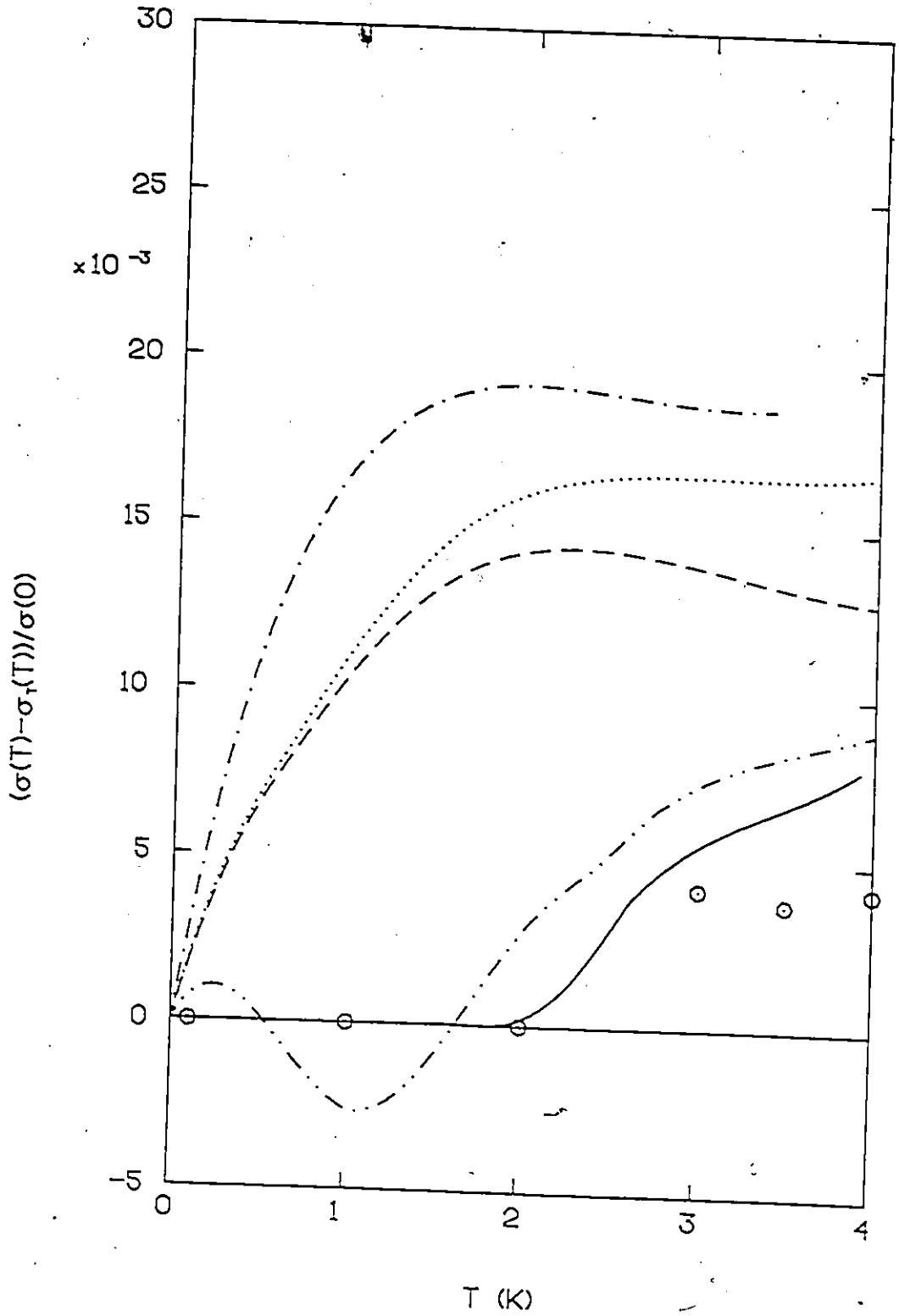
30
25
x10 -3
20
15
10
5
0
-5
0
1
2
3
4
T (K)
(σ(T)-σr(T))/σ(0)

Fig. 4.25 The difference between the zero bias conductance and the thermally smeared conductance as a function of temperature for several spin-glass models of the 800 Å Ag-Mn sample of Ref. 99:

Γ_S=0.09 meV, Γ_N=1.29 meV and $\alpha(\infty)$=2.45 meV for the spin-glass model SG I (———),

Γ_S=0.09 meV, Γ_N=0.566 meV and $\alpha(\infty)$=0.974 meV for the spin-glass model SG I (.....),

Γ_S=0.09 meV, Γ_N=1.132 meV and $\alpha(\infty)$=1.68 meV for the AG model (------),

Γ_S=0.09 meV, Γ_N=1.29 meV and $\alpha(\infty)$=1.75 meV for the spin-glass model with 5 percent increase in $\alpha(\bar{t})$ between $\bar{t}$=0.8 and $\bar{t}$=1.2 as described in the text (-·-·-·),

Γ_S=0.09 meV, Γ_N=1.132 meV and $\alpha(\infty)$=1.95 meV for the spin-glass model SG I (-··-··),

Γ_S=0.09 meV, Γ_N=1.29 meV and $\alpha(\infty)$=2.45 meV for the spin-glass model SG II (-·-·-).

The experimental points are from the 800 Å Ag-Mn sample of Fig. 3 of Ref. 99.

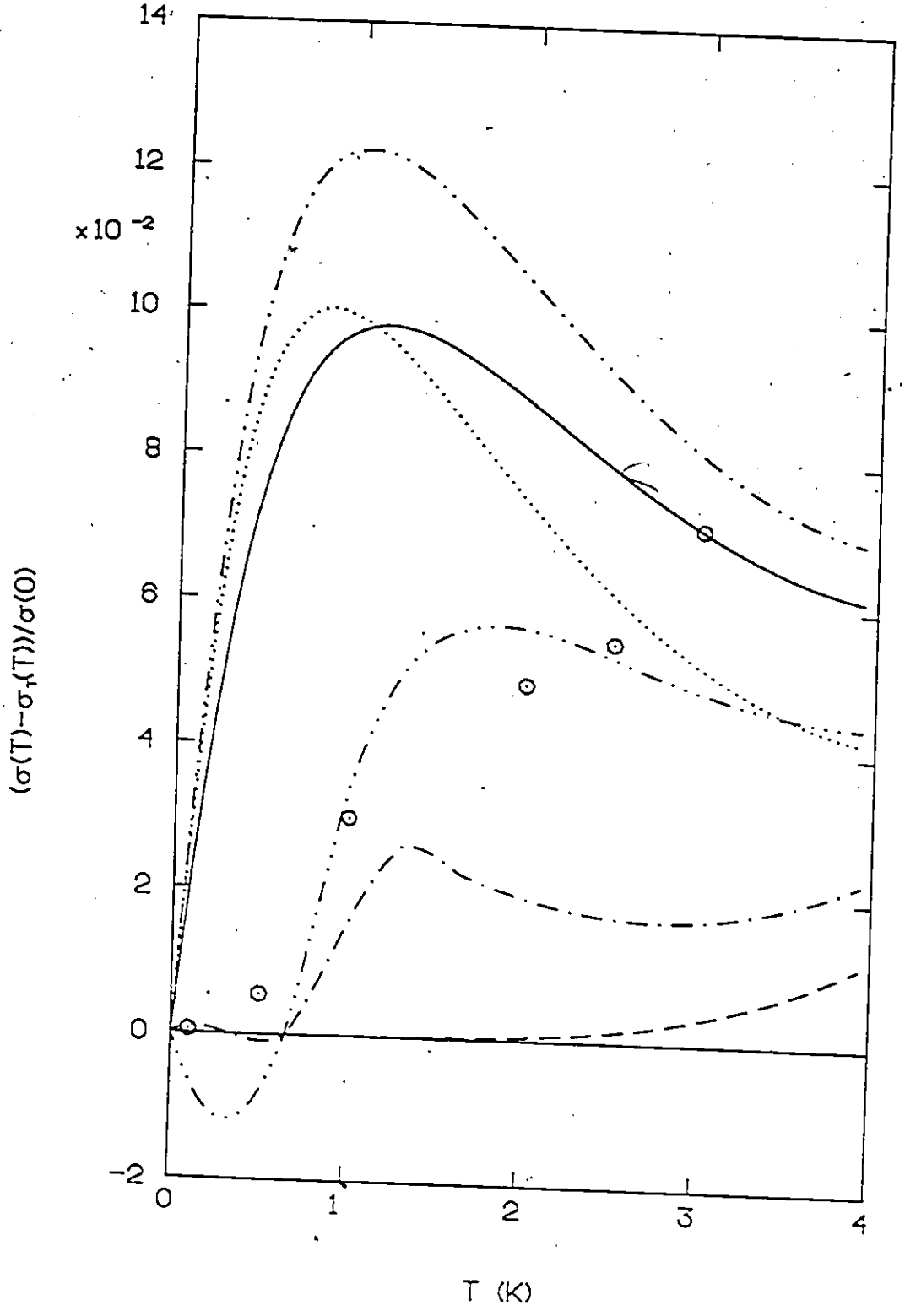
14
12
x10 -2
10
8
6
4
2
0
-2
0
1
2
3
4
T (K)
(σ(T)−σr(T))/σ(0)

CHAPTER V

SUMMARY AND CONCLUSIONS

In the first part of this thesis some of the consequences of the theory of Shiba[8] and Rusinov[9] for the effects of paramagnetic impurities in superconductors were examined. The temperature dependence of the critical magnetic field as described by the deviation function was shown to be very sensitive to the existence of quasiparticle states within the energy gap, and the behavior of D(t) was found to be correlated with the zero frequency density of states. The variation of D(t) with impurity concentration for Zn-Mn[25] was shown to be much better described by SR theory with either of the two sets of scattering parameters considered than is the case with AG theory.

Of the various sets of parameters considered, the optical absorption experiments for Pb-Mn[6] were shown to be best described by the parameters due to Bauriedl *et al.*[35]. A small structure associated with the bands in the gap predicted by SR theory is also predicted to occur at finite temperature.

The variation of the electromagnetic coherence length with the SR scattering parameter ϵ_0 was found to be different from the behavior previously reported by Lemberger *et al.*[39]. This may be attributed to the non-standard gap equations used in the previous work[39], where the

exchange scattering contributions from the SR impurities to the two channels (ω and Δ) were not as given by SR, but were motivated by the AG theory.

It has also been found that while there is evidence for deviations from AG behavior in the thermal conductivity of superconductors containing transition metal impurities, the existing experimental measurements often do not extend reliably to low enough temperatures to distinguish between a wide variety of scattering parameters.

The spin-glass model calculations of Chapter III show that systems such as $Gd_xCe_{1-x}Ru_2$, which exhibit significant deviations from the AG prediction for the reduction of the critical temperature with impurity concentration, are also expected to exhibit significant deviations from AG behavior for a variety of physical properties. It would be of great interest to see experimental measurements of the low temperature magnetic penetration depth, the critical magnetic field or perhaps the temperature dependence of the optical absorption at low temperature (the calculations for the latter are not included in this thesis but will be forthcoming) for a material such as $Gd_xCe_{1-x}Ru_2$.

The model of Lee[54] for reentrant ferromagnetic superconductors was shown to be only in qualitative agreement with the temperature dependence of the free energy difference determined experimentally[75] for $ErRh_4B_4$. Similarly, the temperature dependence of the thermal conductivity displays qualitative agreement with experiment[81], but in both cases the model predicts a more sudden increase in pair-breaking as the reentrant temperature is approached

than is observed experimentally. Finally, within this model the measured peak in ultrasonic attenuation[82] at higher temperature cannot be understood at all.

In Chapter IV a variety of properties of proximity effect junctions have been considered within the McMillan[11] model. The free energy difference is found to be given by applying the standard Bardeen-Stephen[31] result to both sides of the junction and adding the contributions weighted with the appropriate volume fraction. The temperature dependence of the free energy difference is found to differ significantly from that of a BCS superconductor, with the deviation function becoming much more negative than the BCS prediction. In disagreement with a previous calculation[93], the jump in the specific heat at T_c is predicted to have a significant (negative) contribution from the normal side of the junction, resulting in a more rapid depression of the jump with increasing normal film thickness than previously predicted[93]. Both the free energy difference and the specific heat jump are suppressed by the addition of paramagnetic impurities, although these properties are relatively insensitive to the details of scattering as described by the SR scattering parameter ϵ_0.

The optical absorption of the normal side of a proximity effect junction is found to have a small structure associated with the two peaked structure of the density of states predicted by the McMillan model, although this may not be observable experimentally. The addition of SR model paramagnetic impurities to the normal side of a proximity effect junction results in optical absorption which is qualitatively the same as that of the intrinsic case. The

electromagnetic penetration depth at low temperature is found to be quite sensitive to the addition of paramagnetic impurities, with the rapid rise with increasing temperature found by Kresin[98] in the pure case being suppressed with increasing pair-breaking. The low temperature penetration depth is also shown to be sensitive at very low temperatures to the location of the states in the gap determined by the SR scattering parameter ϵ_0.

Finally, the determination of the suppression of the exchange scattering rate of the spin-glass Ag-Mn below the freezing temperature as measured experimentally by Schuller *et al.*[101] and previously analysed without including the proximity effect by Nass *et al.*[60], is found to be qualitatively unchanged when the proximity effect is included within the McMillan model. There is little doubt that the exchange scattering rate is suppressed at low temperature, although the amount of suppression and the details of the temperature dependence are more model dependent. Within the present model, the explanation of the temperature dependence of the tunneling conductance of the Ag-Mn samples with differing Mn concentrations requires the use of different model parameters. This is necessary in order to generate temperature dependent exchange scattering rates which are different functions of the reduced temperature $\tilde{t}=T/T_f$. The fact that the temperature scale on which the exchange scattering rate varies does not scale linearly with the freezing temperature may be due to the thin film spin glass already being out of the low concentration scaling regime, which is consistent with the non-scaling behavior of the freezing temperature.

The confirmation of the qualitative aspects of the spin-glass

model by the experiment on the proximity effect induced superconducting spin-glass Ag-Mn indicates once more the desirability of further experiments on intrinsic spin-glass superconductors such as $Gd_xCe_{1-x}Ru_2$. Without the complications of the proximity effect there are less parameters which may be varied, and the chance for a quantitative comparison between theory and experiment is greatly improved.

APPENDIX A

THE INTEGRAL FOR λ

The integral appearing in (3.23) may be written in the form

$$I = \int_{-\infty}^{\infty} d\bar{\omega} \int_0^1 \frac{dx\ x^3}{\bar{\omega}^2 + (\bar{D}x^2 - \bar{\omega}^2\bar{\tau})^2} \tag{A.1}$$

Defining $\Omega = \bar{\omega}\bar{\tau}$ and $b = \bar{D}\bar{\tau}$, (A.1) may be rewritten in the form

$$I = \bar{\tau} \int_0^1 dx\ x^3\ I_\Omega \tag{A.2}$$

where

$$I_\Omega = \int_{-\infty}^{\infty} \frac{d\Omega}{\Omega^2 + (bx^2 - \Omega^2)^2} \tag{A.3}$$

The roots of the denominator of the integrand in (A.3) are

$$\Omega^2 = E_\pm = \left[bx^2 - \frac{1}{2}\right] \pm \left[\frac{1}{4} - bx^2\right]^{1/2} \tag{A.4}$$

so that

$$I_\Omega = \frac{1}{E_+ - E_-} \int_{-\infty}^{\infty} d\Omega \left[\frac{1}{\Omega^2 - E_+} - \frac{1}{\Omega^2 - E_-}\right] \tag{A.5}$$

The integral in (A.5) is readily performed by closing the integration contour at infinity in the upper-half plane of the variable Ω, and applying the method of residues, resulting in

$$I_{\Omega} = \frac{i\pi}{E_+ - E_-}\left[E_+^{-1/2} - E_-^{-1/2}\right] . \qquad (A.6)$$

Because the poles of the integrand in (A.5) were enclosed in the upper half plane, the square roots of $E_\pm$ in (A.6) must be chosen with a positive imaginary part.

The remaining integral may be performed by introducing a new variable

$$y = \left[\frac{1}{4} - bx^2\right]^{1/2} , \qquad (A.7)$$

so that (A.4) becomes

$$E_\pm = -y^2 \pm y = \frac{1}{4} - (y \mp \tfrac{1}{2})^2 . \qquad (A.8)$$

Consider first the case $b < \frac{1}{4}$ for simplicity. In this case the variable y is real and positive for all x in the region of integration, and using (A.7-8) one finds

$$E_+^{1/2} = i\left[\frac{1}{2} - y\right] , \qquad (A.9a)$$

and

$$E_-^{1/2} = i\left[y + \frac{1}{2}\right] . \qquad (A.9b)$$

The choice of the phases of the square roots in (A.9) was made by invoking the previously mentioned condition that the imaginary part must be positive.

Equation (A.6) may now be written as

$$I_{\Omega} = \frac{\pi}{bx^2} \qquad (A.10)$$

which together with (A.2-3) readily gives the required result.

$$I = \frac{\pi\bar{\tau}}{2b} = \frac{\pi}{2\bar{D}} \qquad (A.11)$$

In the case $b > \frac{1}{4}$ the variable y is complex for part of the path of integration over x, and it becomes necessary to consider the two regions $bx^2 \lessgtr \frac{1}{4}$ separately in order to ensure that the imaginary parts of $E_{\pm}^{1/2}$ are always positive. After just slightly more work than in the previous case, the final result is identical to (A.11).

Appendix B

FREE ENERGY DIFFERENCE OF A PROXIMITY JUNCTION

The free energy difference between the superconducting and normal states of a strong-coupling superconductor was cast into a very useful form by Bardeen and Stephens[31] (BS), who generalized the work of Eliashberg[103] and Luttinger and Ward[95] to this particular case. The work of BS has likewise been generalized to include further complications. For example, Mitrović and Carbotte[104] have derived an analogous result for cases where the normal state electronic density of states has structure on a frequency scale of the order of the Debye frequency. Yamamoto and Nagi[29] have found that a correction term is necessary when paramagnetic impurities in the model of Shiba[8] and Rusinov[9] are included. Following the spirit of the calculation of Yamamoto and Nagi[29], it will be shown in in this appendix that the conventional BS[31] equations may be used to calculate the free energy difference of a proximity bilayer within the McMillan[11] model, with "correction" terms canceling exactly to zero. This calculation will exclude SR model impurities for the sake of brevity; the generalization required to include this effect follows exactly the calculation of Yamamoto and Nagi[29].

The starting point of the calculation will be the free energy functional

$$\Omega = \frac{-1}{2\beta}\sum_{\underline{k},n} \mathrm{Tr}\left[ln\left[\mathcal{G}_S^{-1}(\underline{k},n)\right]+\Sigma_S(\underline{k},n)\mathcal{G}_S(\underline{k},n)\right]$$

$$- \frac{1}{2\beta}\sum_{\underline{k},n} \mathrm{Tr}\left[ln\left[\mathcal{G}_N^{-1}(\underline{k},n)\right]+\Sigma_N(\underline{k},n)\mathcal{G}_N(\underline{k},n)\right]$$

$$+ \frac{1}{4\beta^2}\sum_{\substack{\underline{k},n\\ \underline{q},m}} V_{\underline{k}\underline{q}}\mathrm{Tr}\left[\rho_3\mathcal{G}_S(\underline{k},n)\rho_3\mathcal{G}_S(\underline{q},m)\right]$$

$$+ \frac{1}{2\beta}\sum_{\substack{\underline{k},n\\ \underline{q}}} T^2_{\underline{k}\underline{q}}\mathrm{Tr}\left[\rho_3\mathcal{G}_S(\underline{k},n)\rho_3\mathcal{G}_N(\underline{q},n)\right] . \qquad (B.1)$$

The functions $\mathcal{G}_S(\underline{k},n)$, $\mathcal{G}_N(\underline{k},n)$, $\Sigma_S(\underline{k},n)$ and $\Sigma_N(\underline{k},n)$ are the matrix Green's functions and self-energies introduced in Chapter II, where the subscripts S and N refer to the superconducting and normal sides of the junction respectively, and by Tr the trace of the matrix is meant. Note that the pairing interaction has been used in the BCS form, so that phonon contributions need not be considered. By construction this functional Ω is stationary with respect to variations of the self-energies about their true values, and reduces to the functional of BS in the non-proximity limit. These are the necessary and sufficient conditions of Luttinger and Ward[95] for this functional to yield the correct free energy, within of course the approximation that only these most important self-energy contributions are being retained.

Explicitly, using Dyson's equation (2.48)

$$\mathcal{G}_I^{-1}(\underline{k},n)=\mathcal{G}_I^{0\,-1}(\underline{k},n)-\Sigma_I(\underline{k},n),\quad I=N \text{ or } S, \tag{B.2}$$

it is easily verified that requiring the first order variation of the functional (B.1) be zero ($\delta\Omega=0$) results in exactly the self-energies

$$\Sigma_S(k,n)=\frac{1}{\beta}\sum_{\underline{q},m} V_{\underline{k}\underline{q}}\rho_3\mathcal{G}_S(\underline{q},m)\rho_3 + T^2\sum_{\underline{q}}\rho_3\mathcal{G}_N(\underline{q},n)\rho_3$$

$$=\Sigma_S^{BCS}(\underline{k},n)+\Sigma_S^T(\underline{k},n) \tag{B.3a}$$

and

$$\Sigma_N(k,n)= T^2\sum_{\underline{q}}\rho_3\mathcal{G}_S(\underline{q},n)\rho_3 = \Sigma_N^T(\underline{k},n)\ . \tag{B.3b}$$

which are the self energies of the pure McMillan model, (4.2).

To begin with, use the identity

$$\mathrm{Tr}[\ell n\mathcal{A}] = \ell n[\mathrm{Det}(\mathcal{A})]\ . \tag{B.4}$$

for $\mathcal{A}$ any Hermitian matrix, with Det signifying the determinant of the matrix (this is trivially true for $\mathcal{A}$ diagonal, and in the general case $\mathcal{A}$ may be diagonalized by a unitary transformation), in order to rewrite one contribution to (B.1) in the form

$$\mathrm{Tr}[\ell n\mathcal{G}_I^{-1}(\underline{k},n)] = \ell n\left[\mathrm{Det}[\mathcal{G}_I^{-1}(\underline{k},n)]\right]. \tag{B.5}$$

Recalling the general form for the inverse of the matrix Green's function (2.46)

$$\mathcal{G}_I^{-1}(\underline{k},n) = i\omega_n Z_I(\underline{k},n) - (\epsilon_{\underline{k}}+x_{\underline{k}})\rho_3 - \phi_I(\underline{k},n)\rho_2\sigma_2 \ . \qquad (B.6)$$

(with small notational changes: $\epsilon_{\underline{k}}+x_{\underline{k}} \to \tilde{\epsilon}_{\underline{k}}$, and $\phi_I(\underline{k},n) \to \tilde{\Delta}(\underline{k},n)$) and introducing the functions

$$G_I(\underline{k},n) = [\mathcal{G}_I(\underline{k},n)]_{11} = -\frac{i\omega_n Z_I(n)+(\epsilon_k+x_k)}{N_I(\underline{k},n)} \ . \qquad (B.7a)$$

and

$$F_I(\underline{k},n) = [\mathcal{G}_I(\underline{k},n)]_{14} = -\frac{\phi_I(\underline{k},n)}{N_I(\underline{k},n)} \ . \qquad (B.7b)$$

where

$$N_I(\underline{k},n) = \omega_n^2 Z_I^2(\underline{k},n)+(\epsilon_{\underline{k}}+x_{\underline{k}})^2+\phi_I^2(\underline{k},n) \ . \qquad (B.8)$$

together with the definitions

$$\Sigma_{1I}(\underline{k},n) = [\Sigma_I(\underline{k},n)]_{11} \qquad (B.9a)$$

and

$$\Sigma_{2I}(\underline{k},n) = [\Sigma_I(\underline{k},n)]_{14} \ . \qquad (B.9b)$$

one may write

$$\mathrm{Det}[\mathcal{G}_I^{-1}(k,n)] = \phi_I^2(\underline{k},n) \ . \qquad (B.10)$$

with

$$\phi_I(\underline{k},n) = \left\{[i\omega_n-\epsilon_{\underline{k}}-\Sigma_{1I}(k,n)][i\omega_n+\epsilon_{\underline{k}}+\Sigma_{1I}^*(k,n)]-\Sigma_{2I}^2(\underline{k},n)\right\} . \qquad (B.11)$$

Equation (B.10) immediately gives

$$\ell n\left[\mathrm{Det}[\mathcal{G}_I^{-1}(\underline{k},n)]\right] = 2\ell n\phi_I(k,n) \quad . \tag{B.12}$$

Using the above definitions once more, and the fact that the Pauli matrices are traceless, the traces of the other terms which are needed in the evaluation of the functional Ω are readily evaluated. For example,

$$\mathrm{Tr}\left[\Sigma_I(\underline{k},n)\mathcal{G}_I(\underline{k},n)\right] = \frac{-1}{N_I(\underline{k},n)}\mathrm{Tr}\left[\left[i\omega_n[1-Z_I(\underline{k},n)]+x_{\underline{k}}\rho_3+\phi_I(\underline{k},n)\rho_2\sigma_2\right]\right.$$
$$\left.\left[i\omega_n Z_I(\underline{k},n)+[\epsilon_{\underline{k}}+x_{\underline{k}}]\rho_3+\phi_I(\underline{k},n)\rho_2\sigma_2\right]\right]$$

$$= \frac{-4}{N_I(\underline{k},n)}\left[i\omega_n Z_I(\underline{k},n)i\omega_n[1-Z_I(\underline{k},n)] + (\epsilon_{\underline{k}}+x_{\underline{k}})x_{\underline{k}} + \phi_I^2(k,n)\right]$$

$$= 4\left[\mathrm{Re}[G_I(\underline{k},n)\Sigma_{1I}(\underline{k},n)] - F_I(\underline{k},n)\Sigma_{2I}(\underline{k},n)\right] \quad . \tag{B.13}$$

Note that the band structure renormalization $x_{\underline{k}}$ is to a good approximation equal to zero, and in the conventional approximations (which will also be made here) is set to zero. In this case it is not really necessary to take the real part (Re) of $G_I\Sigma_I$ as is done in (B.13), as this quaintity is real for $x_{\underline{k}} = 0$.

In a similar fashion one finds

$$\mathrm{Tr}\left[\rho_3\mathcal{G}_I(\underline{k},n)\rho_3\mathcal{G}_J(\underline{q},m)\right] = 4\left[\mathrm{Re}\left[G_I(\underline{k},n)G_J(\underline{q},m)\right]-F_I(\underline{k},n)F_J(\underline{q},m)\right]. \tag{B.14}$$

where I and J may be N or S as required. Using the results (B.12-14), the free energy functional (B.1) may be written in the form

$$\Omega = -\frac{1}{\beta}\sum_{\underline{k},n}\left[\ell n\left[\Phi_S(\underline{k},n)\right]+2\left[\mathrm{Re}[\Sigma_{1S}(\underline{k},n)G_S(\underline{k},n)]-\Sigma_{2S}(\underline{k},n)F_S(\underline{k},n)\right]\right]$$

$$-\frac{1}{\beta}\sum_{\underline{k},n}\left[\ell n\left[\Phi_N(\underline{k},n)\right]+2\left[\mathrm{Re}[\Sigma_{1N}(\underline{k},n)G_N(\underline{k},n)]-\Sigma_{2N}(\underline{k},n)F_N(\underline{k},n)\right]\right]$$

$$+\frac{1}{\beta^2}\sum_{\substack{\underline{k},n\\ \underline{q},m}} V_{\underline{k}\underline{q}}\left[\mathrm{Re}\left[G_S(\underline{k},n)G_S(\underline{q},m)\right]-F_S(\underline{k},n)F_S(\underline{q},m)\right]$$

$$+\frac{2}{\beta}\sum_{\substack{\underline{k},n\\ \underline{q}}} T^2_{\underline{k}\underline{q}}\left[\mathrm{Re}\left[G_S(\underline{k},n)G_N(\underline{k},m)\right]-F_S(\underline{k},n)F_N(\underline{k},m)\right]. \qquad (B.15)$$

The momentum sums in (B.15) could now in principle be evaluated, but as there is a significant amount of cancellation among the terms which may be easily seen at this point, it is useful to first manipulate (B.15) slightly. Recalling the self-energies (B.3), (B.15) becomes

$$\Omega = -\frac{1}{\beta}\sum_{\underline{k},n}\left[\ell n\left[\Phi_S(\underline{k},n)\right]+2\left[\mathrm{Re}[\Sigma_{1S}(\underline{k},n)G_S(\underline{k},n)]-\Sigma_{2S}(\underline{k},n)F_S(\underline{k},n)\right]\right]$$

$$-\frac{1}{\beta}\sum_{\underline{k},n}\left[\ell n\left[\Phi_N(\underline{k},n)\right]+2\left[\mathrm{Re}[\Sigma_{1N}(\underline{k},n)G_N(\underline{k},n)]-\Sigma_{2N}(\underline{k},n)F_N(\underline{k},n)\right]\right]$$

$$+\frac{1}{\beta}\sum_{\underline{k},n}\left[\mathrm{Re}\left[G_S(\underline{k},n)\Sigma^{BCS}_{1S}(\underline{k},n)\right]-F_S(\underline{k},n)\Sigma^{BCS}_{2S}(\underline{k},n)\right]$$

$$+\frac{1}{\beta}\sum_{\underline{k},n}\left[\mathrm{Re}\left[G_S(\underline{k},n)\Sigma^{T}_{1S}(\underline{k},n)\right]-F_S(\underline{k},n)\Sigma^{T}_{2S}(\underline{k},n)\right.$$

$$\mathrm{Re}\left[G_N(\underline{k},n)\Sigma^T_{1N}(\underline{k},n)\right]-F_N(\underline{k},n)\Sigma^T_{2N}(\underline{k},n)\Big]. \qquad (B.16)$$

In (B.16) the terms on the last three lines combine exactly to cancel out one half of the terms of the form $2\left[\mathrm{Re}G_I\Sigma_{1I}-F_I\Sigma_{2I}\right]$ in the first two lines, resulting in the functional

$$\Omega = -\frac{1}{\beta}\sum_{\underline{k},n}\left[\ell n\left[\phi_S(\underline{k},n)\right]+\mathrm{Re}[\Sigma_{1S}(\underline{k},n)G_S(\underline{k},n)]-\Sigma_{2S}(\underline{k},n)F_S(\underline{k},n)\right]$$

$$-\frac{1}{\beta}\sum_{\underline{k},n}\left[\ell n\left[\phi_N(\underline{k},n)\right]+\mathrm{Re}[\Sigma_{1N}(\underline{k},n)G_N(\underline{k},n)]-\Sigma_{2N}(\underline{k},n)F_N(\underline{k},n)\right]. \qquad (B.17)$$

At this point the conventional approximation[31] for evaluating the normal state limit of (B.17) may be made by taking the limit of F_I and Σ_{2I} going to zero, without, however, replacing the diagonal Green's function G_I by its' true normal state value. That is, if one denotes the normal state limits by a superscript ^{0}, G^0_I is approximated by simply taking the limit $\phi_I\to 0$. This is reasonable because of the stationary property of the free energy functional; a small error in G^0_I will induce only higher order errors in the free energy difference. The difference in free energies between the superconducting and normal states of the junction in the form them takes the form

$$\Omega-\Omega^0=$$

$$=-\frac{1}{\beta}\sum_{\underline{k},n}\left[\ell n\left[\frac{\phi_S(\underline{k},n)}{\phi^0_S(\underline{k},n)}\right]+\mathrm{Re}[\Sigma_{1S}(\underline{k},n)G_S(\underline{k},n)-\Sigma^0_{1S}(\underline{k},n)G^0_S(\underline{k},n)]-\Sigma_{2S}(\underline{k},n)F_S(\underline{k},n)\right]$$

$$\frac{1}{\beta}\sum_{\underline{k},n}\left[\ell n\left[\frac{\Phi_N(\underline{k},n)}{\Phi_N^0(\underline{k},n)}\right]+\mathrm{Re}[\Sigma_{1N}(\underline{k},n)G_N(\underline{k},n)-\Sigma_{1N}^0(\underline{k},n)G_N^0(\underline{k},n)]-\Sigma_{2N}(\underline{k},n)F_N(\underline{k},n)\right].$$

(B.18)

At this point (B.18) appears to be simply the BS result, repeated for the two sides of the junction N and S. There is, however, a significant difference. The terms involving $\Sigma_{1I}G_I$ and the normal state limits of this may be written in the form

$$\Sigma_{1I}G_I-\Sigma_{1I}^0G_I^0 - [G_I+G_I^0][\Sigma_{1I}-\Sigma_{1I}] + C_I \qquad (B.19)$$

where

$$C_I = G_I'\Sigma_I^0 - G_I^0\Sigma_I' \qquad (B.20)$$

and the arguments $(\underline{k},n)$ of all functions in (B.19-20) have been suppressed. In the non-proximity case the correction C_I may easily be shown to be zero after performance of the momentum sum by using the equations for the self-energy in terms of the Green's function. In the proximity case however, these become

$$C_S = T^2\sum_{\underline{q}}\left[\mathrm{Re}[G_S(\underline{k},n)G_N^0(\underline{q},n)-G_S^0(\underline{k},n)G_N(\underline{q},n)]\right] \neq 0 \qquad (B.21a)$$

and

$$C_N = T^2\sum_{\underline{q}}\left[\mathrm{Re}[G_N(\underline{k},n)G_S^0(\underline{q},n)-G_N^0(\underline{k},n)G_S(\underline{q},n)]\right]. \qquad (B.21b)$$

Taken separately, neither C_S nor C_N are zero after summation over $\underline{k}$, but they are equal and opposite and therefore cancel exactly. In the numerical evaluation of the free energy difference it is obviously useful to take advantage of this cancellation from the outset, which amounts to using the BS functional with no corrections. The only caveat is that without the inclusion of these corrections the separate contributions to the total free energy difference from the two sides have no physical significance at all, only the total has meaning. With the inclusion of the corrections, one might consider examining the separate contributions from N and S sides, although on very general grounds it could also be argued that this division is not at all unique. In general, the energies of the components of an interacting system can only be defined in an arbitrary manner.

Using (B.18-19) the free energy difference may be written in the form

$$\Omega-\Omega^0 = -\frac{1}{\beta}\sum_{\underline{k},n}\left[ln\left[\frac{\phi_S(\underline{k},n)}{\phi_S^0(\underline{k},n)}\right]\right.$$

$$\left.+Re[\{G_S(\underline{k},n)+G_S^0(\underline{k},n)\}(\Sigma_{1S}(\underline{k},n)-\Sigma_{1S}^0(\underline{k},n)\}]-\Sigma_{2S}(\underline{k},n)F_S(\underline{k},n)\right]$$

$$-\frac{1}{\beta}\sum_{\underline{k},n}\left[ln\left[\frac{\phi_N(\underline{k},n)}{\phi_N^0(\underline{k},n)}\right]\right.$$

$$\left.+Re[\{G_N(\underline{k},n)+G_N^0(\underline{k},n)\}(\Sigma_{1N}(\underline{k},n)-\Sigma_{1N}^0(\underline{k},n)\}]-\Sigma_{2N}(\underline{k},n)F_N(\underline{k},n)\right] . \qquad (B.22)$$

Now the functions (B.7-9) may be substituted into (B.22) and the integrals

$$\int_{-\infty}^{\infty} d\epsilon \, \frac{1}{\epsilon^2+A^2} = \frac{\pi}{A} \qquad [\mathrm{Re}(A)>0] \qquad \text{(B.23a)}$$

and

$$\int_{-\infty}^{\infty} d\epsilon \, \ln\left[\frac{\epsilon^2+A^2}{\epsilon^2+B^2}\right] = \pi(A-B) \qquad [\mathrm{Re}(A,B)>0] \qquad \text{(B.23b)}$$

used, in order to rewrite the free energy difference (B.22) in the form

$$\begin{aligned}\Omega-\Omega^0 = &-\frac{\pi}{\beta} N_{0S} d_S A \sum_n \left[2\left\{ [\tilde{\omega}_S^2(n)+\phi_S^2(n)]^{1/2} - |\tilde{\omega}_S(n)| \right\} \right. \\ &\left. - \left\{ \frac{\tilde{\omega}_S(n)}{[\tilde{\omega}_S^2(n)+\phi_S^2(n)]^{1/2}} - \mathrm{sn}(\omega_n) \right\} \left\{ \tilde{\omega}_S - \tilde{\omega}_S^0 \right\} - \frac{\phi_S^2(n)}{[\tilde{\omega}_S^2(n)+\phi_S^2(n)]^{1/2}} \right] \\ &-\frac{\pi}{\beta} N_{0N} d_N A \sum_n \left[2\left\{ [\tilde{\omega}_N^2(n)+\phi_N^2(n)]^{1/2} - |\tilde{\omega}_N(n)| \right\} \right. \\ &\left. - \left\{ \frac{\tilde{\omega}_N(n)}{[\tilde{\omega}_N^2(n)+\phi_N^2(n)]^{1/2}} - \mathrm{sn}(\omega_n) \right\} \left\{ \tilde{\omega}_N - \tilde{\omega}_N^0 \right\} - \frac{\phi_N^2(n)}{[\tilde{\omega}_N^2(n)+\phi_N^2(n)]^{1/2}} \right]. \qquad \text{(B.24)}\end{aligned}$$

The notation $\tilde{\omega}_I(n)=\omega_n Z_I(n)$ and $\tilde{\omega}_I^0(n)=\omega_n Z_I^0(n)$ has been introduced in (B.24), as well as the function $\mathrm{sn}(\omega_n)$, which is 1 if $\omega_n>0$, and -1 if $\omega_n<0$. This result may be further rearranged to the form

$$\begin{aligned}\Omega-\Omega^0 = &-\frac{2\pi}{\beta} N_{0S} d_S A \sum_{n\geq 0} \left[\left\{ [\tilde{\omega}_S^2(n)+\phi_S^2(n)]^{1/2} - |\tilde{\omega}_S(n)| \right\} \left\{ 1 - \frac{\tilde{\omega}_S^0(n)}{[\tilde{\omega}_S^2(n)+\phi_S^2(n)]^{1/2}} \right\} \right] \\ &-\frac{2\pi}{\beta} N_{0N} d_N A \sum_{n\leq 0} \left[\left\{ [\tilde{\omega}_N^2(n)+\phi_N^2(n)]^{1/2} - |\tilde{\omega}_N(n)| \right\} \left\{ 1 - \frac{\tilde{\omega}_N^0(n)}{[\tilde{\omega}_N^2(n)+\phi_N^2(n)]^{1/2}} \right\} \right]. \qquad \text{(B.25)}\end{aligned}$$

which is the form required in Chapter IV. The extension of the above work to include paramagnetic impurities within the SR model on the normal side of the junction may, upon examination of the calculation of Yamamoto and Nagi[29], be performed by adding the correction, their equation (27) ,(4.22) here, to the above result.

REFERENCES

(1) J. Bardeen, L.N. Cooper, and J.R. Schrieffer, *Phys. Rev.* 106, 162 (1957); 108, 1175 (1957).

(2) B.T. Matthias, H. Suhl, and E. Corenzwit, *Phys. Rev. Lett.* 1, 92 (1959).

(3) A.A. Abrikosov and L.P. Gor'kov, *Zh. Eksp. Teor. Fiz.* 39, 1781 (1960) [English Translation: *Sov. Phys. - JETP* 12, 1243 (1961)].

(4) R.M. White, *Quantum Theory of Magnetism*, (Springer-Verlag, Berlin, 1983).

(5) M.B. Maple, in *Magnetism* , edited by G.T. Rado and H. Suhl, (Academic Press, New York, 1973), Vol. 5, p.289

(6) J.G. Dick and F. Reif, *Phys. Rev.* 181, 774 (1969).

(7) M.A. Woolf and F. Reif, *Phys. Rev.* 137, A557 (1965).

(8) H. Shiba, *Prog. Theor. Phys.* 40, 435 (1968).

(9) A.I. Rusinov, *Zh. Eksp. Teor. Fiz.* 56, 2043 (1969) [English Translation: *Sov. Phys. - JETP* 29, 1101 (1969)].

(10) C.A.M. Mulder, A.J. van Duyneveldt, and J.A. Mydosh, *Phys. Rev.* B23, 1384 (1981).

(11) W.L. McMillan, *Phys. Rev.* 175, 537 (1968).

(12) Y. Nambu, *Phys. Rev.* 117, 648 (1960).

(13) V. Ambegaokar and A. Griffin, *Phys. Rev.* 137, A1151 (1961).

(14) S.V. Vonsovsky, Yu. A. Izyumov, and E.Z. Kurmaev, *Superconductivity of Transition Metals*, translated by E.H. Brandt and A.P. Zavarnitsyn, (Springer-Verlag, Berlin, 1982).

(15) L.P. Gor'kov, *Zh. Eksp. Teor. Fiz.* 34, 735 (1958) [English Translation: *Sov. Phys. - JETP* 34, 505 (1959)].

(16) J. Schrieffer, *Theory of Superconductivity*, (W.A. Benjamin, New York, 1964).

(17) L.S. Rodberg and R.M. Thaler, *Introduction to the Quantum Theory of Scattering* (Academic Press, New York, 1967)

(18) A.I. Larkin and Yu. N. Ovchinnikov, *Zh. Eksp. Teor. Fiz.* 55, 2262 (1968) [English Translation: *Sov. Phys. - JETP* 28, 1200 (1969)].

(19) G. Arfken, Chapter 12 of *Mathematical Methods for Physicists* (Academic Press, New York, 1970) p. 534.

(20) S. Doniach and E.H. Sondheimer, *Green's Functions for Solid State Physicists*, (W.A. Benjamin, Massauchsetts, 1974).

(21) J. Zittartz and E. Müller-Hartmann, *Z. Physik* 232, 11 (1970).

E. Müller-Hartmann and J. Zittartz, *Z. Physik* 234, 58 (1970).

J. Zittartz, *Z. Physik* 237, 419 (1970).

(22) Y. Nagaoka, *Phys. Rev.* 138, A1112 (1965).

(23) W. Stephan and J.P. Carbotte, *Phys. Rev.* B31, 2952, (1985).

(24) W.R. Decker and D.K. Finnemore, *Phys. Rev.* 172, 430 (1968).

(25) F. W. Smith, *J. Low Temp. Phys.* 5, 683 (1971).

(26) A.N. Chaba and A.D.S. Nagi, *Can J. Phys.* 50, 1736 (1972).

(27) H. Shiba, *Prog. Theor. Phys.* 50, 50 (1973).

(28) H.G. Zarate and J.P. Carbotte, *Solid State Comm.* 52, 445 (1984).

(29) H. Yamamoto and A.D.S. Nagi, *Phys. Rev.* B30, 1573 (1984).

(30) S. Skalski, O. Betbeder-Matibet, and P.R. Weiss, *Phys. Rev.* 136, A1500 (1964).

(31) J. Bardeen and M. Stephen, *Phys. Rev.* B6, 1485 (1964).

(32) B.D. Terris and D.M. Ginsberg, *Phys. Rev.* B29, 2503 (1984).

(33) A.B. Kunz and D.M. Ginsberg, *Phys. Rev.* B22, 3165 (1980).

(34) W. Stephan and J.P. Carbotte, *Phys. Rev.* B33, 4615 (1986). Erratum: *Phys. Rev.* B34, 4897 (1986).

(35) W. Bauriedl, P. Ziemann, and W. Buckel, *Phys. Rev. Lett.* 47, 1163 (1981).

(36) K. Machida, *Prog. Theor. Phys.* 54, 1251 (1975).

(37) S.B. Nam, *Phys. Rev.* 156, 487 (1967).

(38) M. Tinkham, *Introduction to Superconductivity* (McGraw-Hill, New York, 1975)

(39) T.R. Lemberger, D.M. Ginsberg and G. Rickayzen, *Phys. Rev.* B18, 6057 (1978).

(40) B. Leon and A.D.S. Nagi, *J. Phys. F: Metal Phys.* 5, 1533 (1975).

(41) D.H. Sanchez, *J. Low Temp. Phys.* 17, 101, (1974).

(42) T.R. Lemberger and D.M. Ginsberg, *Phys. Rev.* B14, 1785 (1976).

(43) K. Matsui and Y. Masuda, *J. Phys. Soc. Japan*, 46, 144 (1979).

(44) J. Kondo, *Prog. Theor. Phys.* 32, 37 (1964)

(45) N.W. Ashcroft and N.D. Mermin, *Solid State Physics*, (Holt, Rinehart and Winston, Philadelphia, 1976).

(46) J.X. Przybysz and D.M. Ginsberg, *Phys. Rev.* B14, 1039 (1976).

(47) J.X. Przybysz and D.M. Ginsberg, *Phys. Rev.* B15, 2835 (1977).

(48) B.D. Terris and D.M. Ginsberg, *Phys. Rev.* B25, 3132 (1982).

(49) M.B. Maple and O. Fischer, in *Superconductivity in Ternary Compounds II*, edited by M.B Maple and O. Fischer (Springer-Verlag, Berlin, 1982)

(50) W.A. Fertig, D.C. Johnston, L.E. DeLong, R.W. McCallum, M.B. Maple, B.T. Matthias, *Phys. Rev. Lett.* 38, 387 (1977).

(51) M. Ishahawa, O. Fischer, *Solid State Comm.* 23, 37 (1977).

(52) J.W. Lynn, A. Ragazoni, R. Pynn, and J. Jaffrin, *J. Phys. Lett. (Paris)* 42, L45 (1981).

J.W. Lynn, G. Shirane, W. Thomlinson, R.N. Shelton, and D.E. Moncton, *Phys. Rev.* B24, 3817 (1981).

J.W. Lynn, G. Shirane, W. Thomlinson, and R.N. Shelton, *Phys. Rev. Lett.* 46, 368 (1981).

D.E. Moncton, D.B. McWhan, P.H. Schmidt, G. Shirane, W. Thomlinson, M.B. Maple, H.B. McKay, L.D. Woolf, Z. Fisk, and D.C. Johnston, *Phys. Rev. Lett.* 45, 2060 (1981).

S.K. Sinha, H.A. Mook, D.G. Hinks, G.WW. Crabtree. *Phys. Rev. Lett.* 48, 950 (1982).

(53) P.W. Anderson and H. Suhl, *Phys. Rev.* 116, 898 (1959).

(54) T-K. Lee, *Solid State Comm.* 34, 9 (1980).

(55) K. Binder and A.P. Young, *Rev. Mod. Phys.* 58, 801 (1986).

(56) K.H. Fischer, *Phys. Stat. Sol.* (B) 116, 357 (1983)

(57) K. Moorjani and J.M.D. Coey, *Magnetic Glasses*, (Elsevier, Amsterdam, 1984).

(58) D. Davidov, K. Baberschke, J.A. Mydosh, aand G.J. Nieuwenhuys, *J. Phys. F: Metal Phys.* 7, L47 (1977).

(59) S.F. Edwards and P.W. Anderson, *J. Phys. F: Metal Phys.* 5, 965 (1975)

(60) M.J. Nass, K. Levin, and G.S. Grest, *Phys. Rev.* B23, 1111 (1981).

(61) J. Keller and R. Benda, *J. Low Temp. Phys.* 2, 141 (1970).

(62) S. Maekawa and M. Tachiki, *Phys. Rev.* B18, 4688 (1978).

(63) J. Keller, in *Ternary Superconductors*, edited by G.K. Shenoy, B.D. Dunlap, and F.Y. Fradin (Elsevier-North Holland, New York, 1981).

(64) I.E. Dzyaloshinskii and G.E. Volovik, *Jour. de Phys.* 39, 693 (1978).

(65) K.H. Fischer, *Z. Phys.* B34, 45 (1979).

(66) H.S. Bennett and P.C. Martin, *Phys. Rev.* 13B, A608 (1965).

(67) B.I. Halperin and P.C. Hohenberg, *Phys. Rev.* 188, 898 (1969).

(68) D. Forster, *Hydrodynamic Fluctuations, Broken Symmetry, and Correlation Functions* (W.A. Benjamin, Reading, Massachusetts, 1975).

(69) C.M. Skoukoulis and G.S. Grest, *Phys. Rev.* B21, 5119 (1980).

(70) W.A. Roshen and J. Ruvalds, *Phys. Rev.* B31, 2929 (1985).

(71) K.H. Bennemann, *Phys. Rev. Lett.* 17, 438 (1966).

(72) T.E. Jones, J.F. Kwak, E.P. Chock and P.M. Chaikin, *Solid State Comm.* 27, 209 (1978).

(73) R.C. Shukla and A.D.S. Nagi, *J. Phys. F: Metal Phys.* 6, 1765 (1976).

(74) J.W. Thomasson and D.M. Ginsberg, *Phys. Rev.* B15, 4270 (1977).

(75) F. Behroozi, G.W. Crabtree, S.A. Campbell, D.R. Snider, S. Schneider and M. Levy, *J. Low Temp. Phys.* 49, 73 (1982).

(76) M. Schossmann and J.P. Carbotte, *Phys. Rev.* B35, 7 (1987)

(77) W. Dupont, E. Ziemniak, and K.D. Usadel, *J. Low Temp. Phys.* 52 41 (1983).

(78) L.D. Woolf, D.C. Johnston, H.B. McKay, R.W. McCallum, and M.B. Maple, *J. Low Temp. Phys.* 35, 651 (1979).

(79) L. Coffey, K. Levin, and G.S. Grest, *Phys. Rev.* B27, 2740 (1983).

(80) P. Fulde and I. Peschel, *Adv. in Phys.* 21, 1 (1972).

(81) W. Odoni and H.R. Ott, *Phys. Lett.* 70A, 480 (1979).

(82) S.C. Schneider, M. Levy, R. Chen, M. Tachiki, D.C. Johnston and B.T. Matthias, *Solid State Comm.* 40, 61 (1981).

S.C. Schneider, M. Levy, M. Tachiki, and D.C. Johnston, *Physica* 108B, 807 (1981).

(83) M. Tachiki, T. Koyama, H. Matsumoto, and H. Umezawa, *Solid State Comm.* 34, 269 (1980).

(84) G. Deutscher and P.G. de Gennes, in *Superconductivity*, edited by R.D. Parks (Marcel Dekker, New York,1964), Vol. 2, p. 1005.

(85) A.B. Kaiser and M.J. Zuckermann, *Phys. Rev.* B1, 229 (1970).

(86) P.W. Wyatt, R.C. Barker and A. Yelon, *Phys. Rev.* B6, 4169 (1966).

(87) P.W. Anderson, *J. Phys. Chem. Solids* 11, 26 (1959).

(88) K. Machida, *J. Low Temp. Phys* 27, 737 (1977).

K. Machida and L. Dumoulin, *J. Low Temp. Phys.* 31, 143 (1978).

(89) A.B. Kaiser, *Phys. Rev.* B22, 2323 (1980).

(90) N. Mori, *J. Low Temp. Phys.* 40, 275 (1980); 43, 107 (1981).

(91) F.B. Hildebrand, *Introduction to Numerical Analysis* (McGraw-Hill, New York, 1956).

(92) P. Fulde and W. Moormann, *Phys. Kondens. Materie* 6, 403 (1967).

(93) S. Mohabir and A.D.S. Nagi, *J. Low Temp. Phys.* 36, 307 (1979).

(94) J. Lechevet, J.E. Neighbor and C.A. Shiffman, *J. Low Temp. Phys.* 27, 407 (1977).

(95) J.M. Luttinger and J.C. Ward, *Phys. Rev.* 118, 1418 (1960).

(96) P.J. Davis, *in Handbook of Mathematical Functions*, edited by M. Abramowitz and I.A. Stegun, (Dover, New York, 1965) p. 253.

(97) M.P. Zaitlin, *Phys. Rev.* B25, 5729 (1982).

(98) V. Kresin, *Phys. Rev* B32, 145 (1985).

(99) R. Simon and P. Chaikin, *Phys. Rev.* B23, 4463 (1981); B30, 3750 (1984).

R. Simon, P. Chaikin, and S. Wolf, *Bull. Amer. Phys. Soc.* 27, 205 (1982).

A. Mota, D. Marek and J. Weber, *Helv. Phys. Acta* 55, 647 (1982); in *Proceedings of LT17*, edited by U. Eckern, A. Schmid, W. Weber and H. Wuhl (North-Holland, Amsterdam, 1984), p. 1023.

(100) L. Dumoulin, E. Guyon and P. Nedellec, *Phys. Rev. Lett.* 34, 264 (1975); *Phys. Rev.* B16, 1086 (1977).

(101) I. Schuller, R. Orbach and P.M. Chaikin, *Phys. Rev. Lett.* 41, 1413 (1978).

(102) *CRC Handbook of Chemistry and Physics - 62nd Edition*, edited by R.C. West and M.J. Astle (CRC Press, Boca Rolton, Fla., 1981) p. D-159.

(103) G.M. Eliashberg, *Zh. Eksperim. i Teor. Fiz.* 43, 1005 (1962) [English transl.: *Soviet Phys.-JETP* 16, 780 (1963)].

(104) B. Mitrović and J.P. Carbotte, Can. J. Phys. 61, 872 (1983).